Characterization of the immune response in elastase-induced AAA progression using scRNA-sequencing techniques

Inaugural-Dissertation

zur Erlangung des Doktorgrades
der Mathematisch-Naturwissenschaftlichen Fakultät
der Heinrich-Heine-Universität Düsseldorf

vorgelegt von

Christin Elster

aus Bottrop

Düsseldorf, Mai 2025

Aus der Klinik für Kardiologie, Pneumologie und Angiologie
der Heinrich-Heine-Universität Düsseldorf
Klinikdirektor: Univ.-Prof. Dr. med. Malte Kelm

Gedruckt mit der Genehmigung der Mathematisch-Naturwissenschaftlichen Fakultät der
Heinrich-Heine-Universität Düsseldorf

Berichterstatter:

1. Prof. Dr. rer. nat. Norbert Gerdes
2. Prof. Dr. rer. nat. Martin Lercher

Tag der mündlichen Prüfung: 04.12.2025

Parts of this dissertation were already published as paper:

Elster et al. “Application and challenges of TCR and BCR sequencing to investigate T- and B-cell clonality in elastase-induced experimental murine abdominal aortic aneurysm”, Front. Cardiovasc. Med., 14 November 2023, https://doi.org/10.3389/fcvm.2023.1221620

Parts of this dissertation were already presented as poster or presentation on a scientific conference:

Elster, Christin (2022), *“Identification of CD40-expressing IFNICs in AAA”*
Poster at the 3rd international TRR259 Symposium on new mechanistic insights into aortic diseases (Bonn, Germany)

Elster, Christin (2023), *“scRNA- and CITE-seq-based identification and characterization of immune cell types involved in elastase-induced aneurysm progression”*
Science at a Glance (SaaG) presentation at the 91st EAS Congress (Mannheim, Germany)

Elster, Christin (2023), *“Deciphering immune cell heterogeneity in experimental aneurysm using scRNA- and CITE-sequencing”*
Presentation at the 15th BMFZ Retreat (Bergisch-Gladbach, Germany)

Elster, Christin (2024), *“Comprehensive and parallel analysis of different cardiovascular diseases using CITE-sequencing”*
Presentation in the “Young Investigator Session” at the 6th Vascular Medicine and Atherosclerosis Congress (Augsburg, Germany)

Elster, Christin (2025), *“Characterization of IFNIC macrophages as potential therapeutic target in aortic aneurysm using scRNA- and CITE-sequencing”*
Presentation in the “Young Investigator Session” at the 7th Vascular Medicine and Atherosclerosis Congress (Essen, Germany)

Abstract

Background: Cardiovascular diseases (CVDs) are the leading cause of death worldwide and inflammatory processes play a crucial role in their pathogeneses. Abdominal aortic aneurysm (AAA) is a multifactorial and progressive disease with high mortality rate due to rupture. Immune cell infiltration and inflammation contribute strongly to AAA development. The co-stimulatory molecules CD40 and CD40L play a key role in mediating the immune response and were previously shown to be involved in AAA formation. However, insights into the specific role of different immune cell types and pathophysiologic processes in AAA are scarce and pharmacologic treatment options are lacking.

Aim: The overall aim of this study was to explore and characterize the immune cell heterogeneity in experimental elastase-induced AAA progression to identify key players, genes and signaling pathways. This included a broad comparison of AAA pathology with inflammatory processes involved in the related CVDs atherosclerosis and myocardial infarction (MI), a detailed characterization of immune cell types and dynamics involved in AAA progression, investigation of the role of CD40 signaling in AAA, and examination of T and B cell clonality in AAA.

Methods: Different single-cell RNA sequencing (scRNA-seq) techniques, as well as flow cytometry and immunofluorescence stainings were used to study various aspects of the immune response in AAA progression. ScRNA-seq and scRNA-seq of T and B cell receptors were performed at day 3, 7, 14 and 28 of elastase-induced AAA formation in mice. Saline-perfused aortae at day 3 and 28 and aortae from non-operated mice served as controls. For a comprehensive comparison of AAA with atherosclerosis and MI, atherosclerotic aortae from aged apolipoprotein E-deficient (*Apoe*$^{-/-}$) mice, elastase-induced AAA at day 3, 7 and 14, as well as hearts at day 1 and 5 post reperfused MI were subjected to Cellular Indexing of Transcriptomes and Epitopes by sequencing (CITE-seq). In addition, CITE-seq was used to determine the correlation between RNA and protein expression. CD40-deficient mice were used to investigate the contribution of CD40 signaling to angiotensin II-induced AAA formation, progression and rupture. In addition, expression patterns of CD40 and CD40L were examined using flow cytometry, immunofluorescence staining, and scRNA-seq.

Results: CITE-seq revealed that immune cell proportions varied across the three CVDs, with T cells predominating in atherosclerosis and macrophages and neutrophils in AAA and MI. Moreover, specific immune cell subsets and pathways were identified for each disease. In addition, CITE-seq proved as powerful tool for characterizing subpopulations at the protein

level, especially since the observed correlation between protein expression and mRNA expression was low. In AAA, the highest immune cell infiltration and the strongest intercellular communication were observed 7 days after elastase-perfusion. Neutrophils, macrophages, dendritic cells, NK, T and B cells, were detected at day 3, 7, 14 and 28 after elastase-perfusion, but differed in their proportion during AAA progression. Overall, macrophages were the predominant immune cells in AAA. In total, 30 distinct immune cell subsets were identified in AAA, including 7 neutrophil subtypes, 4 dendritic cell populations, 10 macrophage subsets and 9 lymphocyte clusters. Of all these subtypes, interferon-inducible cells (IFNIC) macrophages were identified as potential key player in AAA formation and progression, as they were highly inflammatory, accounted for the largest macrophage subset at day 7 and 14 after elastase-induced AAA formation, and were barely present in controls. IFNIC macrophages exhibited a type-I interferon gene signature, were responsive to IFN-β and showed a strong upregulation of the JAK-STAT-signaling pathway. Based on protein markers obtained from CITE-seq data, a flow cytometry panel for the detection and isolation of IFNIC macrophages was established to enable further investigations of these cells. CD40 and CD40L expression was observed at all studied time points of elastase-induced AAA progression. CD40-deficient mice had a significantly lower AAA incidence, significantly reduced abdominal aortic diameter and an improved survival 28 days after angiotensin II infusion compared to control mice. IFNIC macrophages and $CD4^+$ T cells were identified as key players in CD40 signaling 7 days after AAA formation. ScRNA-seq of T and B cell receptors showed a clonal expansion of T cells, but not of B cells, in experimental elastase-induced AAA. For T cells several clones were identified in 11 of 16 AAA samples and 1 of 8 control samples. Only a few clones were shared between the individual AAA samples.

Conclusion: This study provides the first in-depth analysis of immune cell subtypes and inflammatory processes involved in elastase-induced AAA progression using scRNA-seq, CITE-seq and scRNA-seq of T and B cells receptors. Overall, this study indicates day 7 as critical time point in experimental AAA development, highlights the crucial role of inflammation in the development of AAA and offers several options for new therapeutic approaches. In particular, IFNIC macrophages, type-I interferon signaling and CD40 signaling represent promising therapeutical targets in AAA. The observation of clonal expanded T cells, supports the notion that specific antigen-driven T cells play a role in AAA formation.

Zusammenfassung

Hintergrund: Kardiovaskuläre Erkrankungen (CVD) sind weltweit die häufigste Todesursache, und Entzündungsprozesse spielen eine entscheidende Rolle bei ihrer Entwicklung. Das Bauchaortenaneurysma (AAA) ist eine multifaktorielle und fortschreitende Erkrankung mit einer hohen Sterblichkeitsrate aufgrund von Rupturen. Die Infiltration von Immunzellen und Entzündungsprozesse tragen wesentlich zur Entstehung des AAA bei. Die ko-stimulatorischen Moleküle CD40 und CD40L spielen eine Schlüsselrolle bei der Vermittlung der Immunreaktion und sind nachweislich an der Entstehung des AAA beteiligt. Es fehlt jedoch an Erkenntnissen über die spezifische Rolle verschiedener Immunzellarten und –prozesse in der AAA-Pathologie und an pharmakologischen Behandlungsmöglichkeiten.

Ziel: Das übergeordnete Ziel dieser Studie war es, die Heterogenität der Immunzellen bei der experimentellen Elastase-induzierten AAA-Progression zu erforschen und zu charakterisieren, um wichtige Faktoren, Gene und Signalwege zu identifizieren. Dies beinhaltete einen groben Vergleich der AAA-Pathologie mit Entzündungsprozessen, die bei den verwandten CVDs Atherosklerose und Myokardinfarkt (MI) auftreten, eine detaillierte Charakterisierung der Immunzelltypen und –dynamik, die an der AAA-Progression beteiligt sind, die Untersuchung der Rolle der CD40-Signalübertragung und der T- und B-Zell-Klonalität im AAA.

Methoden: Verschiedene Einzelzell-RNA-Sequenzierungstechniken (scRNA-seq) sowie Durchflusszytometrie und Immunofluoreszenzfärbungen wurden verwendet, um verschiedene Aspekte der Immunantwort bei der AAA-Progression zu untersuchen. ScRNA-seq und scRNA-seq von T- und B-Zellrezeptoren wurden an Tag 3, 7, 14 und 28 der Elastase-induzierten AAA-Bildung bei Mäusen durchgeführt. Mit Kochsalzlösung perfundierte Aorten an Tag 3 und 28 sowie Aorten von nicht operierten Mäusen dienten als Kontrollen. Für einen umfassenden Vergleich von AAA mit Atherosklerose und MI wurden atherosklerotische Aorten von gealterten *Apoe*$^{-/-}$ Mäusen, Elastase-induzierte AAA an Tag 3, 7 und 14 sowie Herzen an Tag 1 und 5 nach reperfundiertem MI einer zellulären Indexierung von Transkriptomen und Epitopen durch Sequenzierung (CITE-seq) unterzogen. CITE-seq wurde zusätzlich verwendet, um die Korrelation zwischen mRNA- und Proteinexpression zu analysieren. CD40-defiziente Mäuse wurden verwendet, um die Rolle der CD40-Signalübertragung bei Angiotensin-II induzierter AAA-Bildung, -Progression und -Ruptur zu untersuchen. Darüber hinaus wurden die Expressionsmuster von CD40 und CD40L mittels Durchflusszytometrie, Immunfluoreszenzfärbung und scRNA-seq untersucht.

Ergebnisse: CITE-seq zeigte, dass die Verteilung der Immunzellen bei den drei CVDs verschieden war, wobei T-Zellen in Atherosklerose und Makrophagen und Neutrophile in AAA und MI überwiegten. Außerdem wurden für jede Erkrankung spezifische Untergruppen von Immunzellen und bestimmte Signalwege identifiziert. Zusätzlich erwies sich CITE-seq als effizientes Mittel zur Charakterisierung von Subpopulationen auf Proteinebene, insbesondere da die beobachtete Korrelation zwischen Proteinexpression und mRNA-Expression gering war. Bei AAA wurde an Tag 7 nach Elastase-Perfusion die stärkste Immunzellinfiltration und interzelluläre Kommunikation beobachtet. Neutrophile, Makrophagen, dendritische Zellen, NK-, T- und B-Zellen wurden an Tag 3, 7, 14 und 28 nach Elastase-Perfusion nachgewiesen, unterschieden sich jedoch in ihrem Anteil während des Fortschreitens des AAA. Makrophagen waren die vorherrschenden Immunzellen im AAA. Insgesamt wurden im AAA 30 verschiedene Untergruppen von Immunzellen identifiziert, darunter 7 Neutrophil-Subtypen, 4 dendritische Zellpopulationen, 10 Makrophagen-Untergruppen und 9 Lymphozyten-Subpopulationen. Von all diesen Subtypen wurden IFNIC-Makrophagen als potenzielle Schlüsselakteure bei der Entstehung und dem Fortschreiten des AAA identifiziert, da sie hochentzündlich waren, an Tag 7 und 14 nach Elastase-induzierten AAA-Bildung die größte Makrophagen-Subpopulation darstellten und in den Kontrollen kaum vorhanden waren. IFNIC-Makrophagen wiesen eine Typ-I-Interferon-Gensignatur auf, reagierten auf IFN-β und zeigten eine starke Hochregulierung des JAK-STAT-Signalweges. Basierend auf Proteinmarkern, die aus CITE-seq-Daten gewonnen wurden, wurde ein Durchflusszytometrie-Panel zum Nachweis und zur Isolierung von IFNIC-Makrophagen erstellt, um weitere Untersuchungen dieser Zellen zu ermöglichen. Die Expression von CD40 und CD40L wurde zu allen untersuchten Zeitpunkten der Elastase-induzierten AAA-Progression nachgewiesen. CD40-defiziente Mäuse zeigten eine signifikant niedrigere AAA-Inzidenz, einen signifikant reduzierten abdominalen Aortendurchmesser und eine verbesserte Überlebensrate 28 Tage nach Angiotensin-II-Infusion im Vergleich zu Kontrollmäusen. IFNIC Makrophagen und $CD4^+$ T-Zellen wurden als zentrale Akteure der CD40-Signalübertragung 7 Tage nach AAA-Bildung identifiziert. ScRNA-seq von T- und B-Zell-Rezeptoren zeigte eine klonale Expansion von T-Zellen, aber nicht von B-Zellen, im experimentellen Elastase-induzierten AAA. Für T-Zellen wurden in 11 von 16 AAA-Proben und in 1 von 8 Kontrollproben mehrere Klone identifiziert. Einige wenige Klone wurden in mehreren verschiedenen AAA Proben gefunden.

Schlussfolgerung: Diese Studie ist die erste umfassende Analyse von Immunzellsubtypen und Entzündungsprozessen, die an der Elastase-induzierten AAA Progression beteiligt sind, die scRNA-seq, CITE-seq und scRNA-seq von T- und B-Zellrezeptoren verwendet.

Insgesamt zeigt diese Studie, dass Tag 7 einen kritischen Zeitpunkt in der experimentellen AAA-Entwicklung darstellt, verdeutlicht die wesentliche Rolle von Immunzellen bei AAA und bietet mehrere Ansatzpunkte für neue therapeutische Strategien. Insbesondere IFNIC-Makrophagen, der Typ-I-Interferon-Signalweg und die CD40-Signalübertragung stellen vielversprechende therapeutische Ziele dar. Des Weiteren unterstützt die Beobachtung klonal expandierter T-Zellen die Theorie, dass spezifisch antigengesteuerte T-Zellen eine Rolle bei der AAA-Bildung spielen.

Graphical abstract

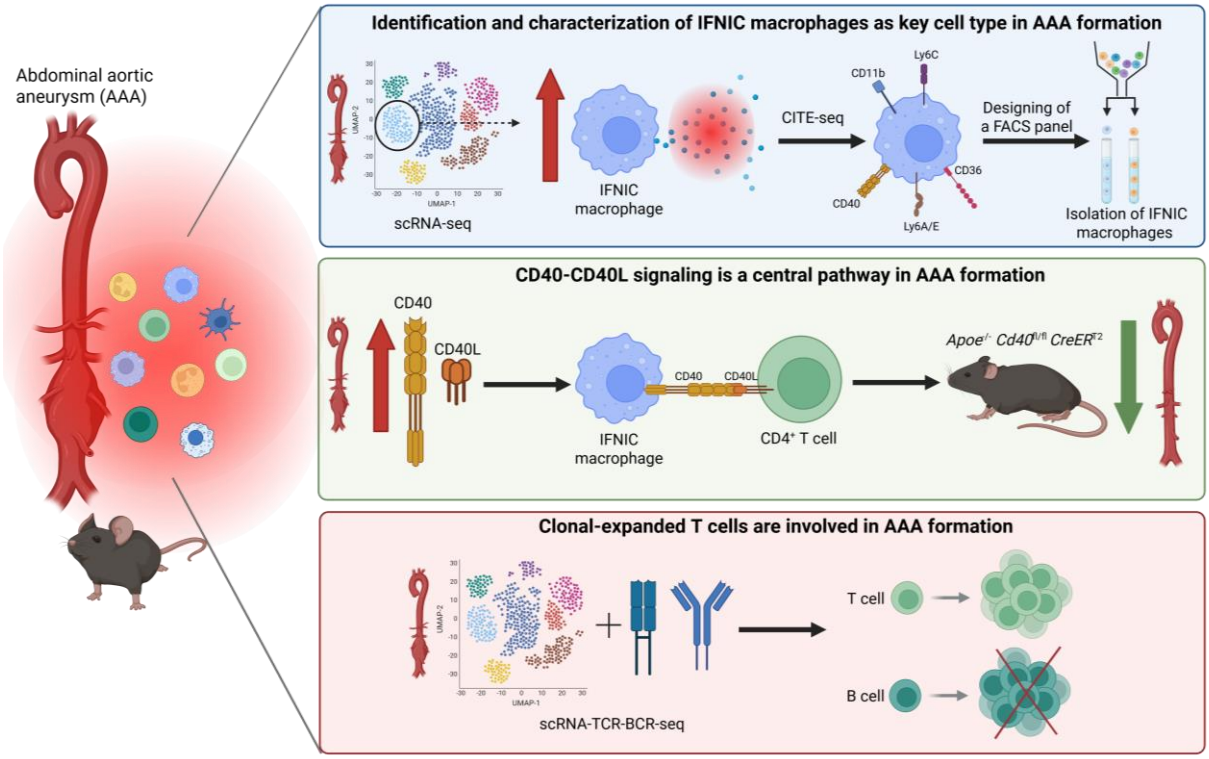

Figure 1: Graphical Abstract of the thesis. The overall aim of this work was to decipher the immune cell heterogeneity in experimental AAA progression and to identify key players, genes or signaling pathways. **Identification and characterization of IFNIC macrophages as key player in AAA formation:** Within the different immune cell types detected in AAA by scRNA-seq, IFNIC macrophages were characterized as highly inflammatory and identified as potential key players in the formation and progression of AAA. Therefore, CITE-seq was used to further investigate IFNIC macrophages at the protein level. Based on that, a flow cytometry panel was designed to detect and isolate IFNIC macrophages. **CD40-CD40L signaling is a central pathway in AAA formation:** The co-stimulatory molecules CD40 and CD40L are highly expressed in all stages of AAA progression. Bioinformatic analysis of cell-cell communication predicted IFNIC macrophages as main receiver and $CD4^+$ T cells as dominant sender of CD40 signaling. CD40 deficiency protected mice from AAA formation. **Clonal expanded T cells are involved in AAA formation:** scRNA-TCR-BCR-seq showed a clonal expansion of T cells, but not B cells, in experimental elastase-induced AAA, supporting the notion that specific antigen-driven T cells play a role in AAA formation.

Table of contents

Table of figures

Table of tables

Abbreviations

AAA ..... Abdominal Aortic Aneurysm
AIRR ..... Adaptive Immune Receptor Repertoire
AngII ..... Angiotensin II
ANOVA ..... Analysis of Variance
APC ..... Antigen-Presenting Cell
Apoe$^{-/-}$ ..... Apolipoprotein E Deficient
BCR ..... B Cell Receptor
bw ..... Body Weight
CD40 ..... Cluster of Differentiation 40
CD40L ..... CD40 Ligand
cDC ..... Conventional Dendritic Cell
CDR ..... Complementarity Determining Region
cGas ..... Cyclic GMP-AMP Synthase
CITE-seq ..... Cellular Indexing of Transcriptomes and Epitopes by Sequencing
CMO ..... Cell Multiplexing Oligo
CVDs ..... Cardiovascular Diseases
DAPI ..... 4′,6-Diamidin-2-phenylindol
DC ..... Dendritic Cell
DEG ..... Differentially-expressed Gene
dsDNA ..... Double-stranded DNA
ECG ..... Electrocardiogram
ECM ..... Extracellular Matrix
ePPE ..... external peri-adventitial Porcine Pancreatic Elastase Application
FOXP3 ..... Forkhead Box Protein 3
GO ..... Gene Ontology
HLA ..... Human Leukocyte Antigen
i.p. ..... Intraperitoneally
i.v. ..... Intravenously
I/R ..... Ischemia Reperfusion
IFNAR1 ..... Interferon-Alpha/Beta Receptor Subunit 1
IFNIC ..... Interferon-inducible Cell
IFN ..... Interferon
IFNβ ..... Interferon beta
IFNγ ..... Interferon gamma

Ig .....Immunoglobulin
IgH..... Immunoglobulin Heavy Chain
IgK ..... Immunoglobulin Kappa Light Chain
IgL ..... Immunoglobulin Lambda Light Chain
IL ..... Interleukin
ILC..... Innate Lymphoid Cell
IRF3 ..... Interferon Regulatory Factor 3
ISG ..... Interferon-stimulated Genes
iNKT ..... Type I Natural Killer T Cell
iNOS ..... Inducible Nitric Oxide Synthase
JAK3 .....Janus Family Kinase 3
LAD .....Left Anterior Descending Coronary Artery
LDL .....Low-Density Lipoprotein
LTL..... Leading to Leading Edge
MAPK.....Mitogen-activated Protein Kinase
MDA5 ..... Melanoma Differentiation-associated Protein 5
MFI..... Mean Fluorescence Intensity
MHC..... Major Histocompatibility Complex
MI .....Myocardial Infarction
MMP..... Matrix Metalloproteinases
NETs .....Neutrophil Extracellular Traps
NFκB .....Nuclear Factor κB
NK cell..... Natural Killer Cell
NKT cell..... Natural Killer T Cell
PCA.....Principal Component Analysis
pDC.....Plasmacytoid Dendritic Cell
PI3K .....Phosphoinositide 3-Kinase
PLCγ..... Phospholipase Cγ
PPE..... Porcine Pancreatic Elastase
qPCR .....Quantitative Polymerase Chain Reaction
RIG-I ..... Retinoic Acid Inducible Gene I
ROS .....Reactive Oxygen Species
RT .....Room Temperature
s.c. ..... Subcutaneously
sCD40L .....Soluble CD40L
scRNA-seq ..... Single-Cell RNA Sequencing

scRNA-TCR-BCR-seq ..... scRNA Sequencing of TCRs and BCRs
SD ..... Standard Deviation
STAT ..... Signal Transducer and Activator of Transcription
STING ..... Stimulator of Interferon Genes
TAA ..... Thoracic Aortic Aneurysm
TAM ..... Tamoxifen
TCR ..... T Cell Receptor
Th ..... T Helper
TLR ..... Toll-like Receptor
TNFR ..... Tumor Necrosis Factor Receptor
TNFα ..... Tumor Necrosis Factor Alpha
TRA ..... TCR Alpha Chain
TRAF ..... Tumor Necrosis Factor Receptor-associated Factor
TRAV ..... TCR Alpha Chain V Gene
TRB ..... TCR Beta Chain
TRBV ..... TCR Beta Chain V Gene
Treg ..... Regulatory T Cell
UMAP ..... Uniform Manifold Approximation and Projection
VDJ ..... Variable, Diversity, and Joining
VSMC ..... Vascular Smooth Muscle Cell
WT ..... Wild-Type

1 Introduction

1.1 Cardiovascular diseases

Cardiovascular diseases (CVDs) encompass disorders of the heart and blood vessels, including atherosclerosis, coronary heart diseases, myocardial infarction (MI) and aortic diseases such as aortic aneurysms and discetions.[1, 2] CVDs are the leading cause of death worldwide accounting for approximately 17.9 million deaths per year.[1] According to the WHO, approximately 12.1 million people died from CVDs in 2019.[3] Within 3 years, the number of deaths related to CVDs worldwide has continued to rise sharply, reaching 20.5 million in 2021.[3] CVDs are caused by a combination of environmental influences, genetic predisposition and lifestyle factors. Main risk factors for CVDs include hypertension, smoking, elevated cholesterol levels, diabetes, obesity, air pollution, physical inactivity and an unhealthy diet.[1-3] The risk of CVDs increases with age, with men being more likely to develop CVDs than women.[2]

1.2 Atherosclerosis

Atherosclerosis is a complex, degenerative disease of the arteries and the main underlying pathology of other CVDs.[4, 5] It is characterized by a pathological deposition of lipids in the inner wall layer of arteries and chronic inflammation. Atherosclerotic plaque formation develops usually asymptomatic over a period of many years and leads to the blockage of arteries, which can result in MI or stroke.[4, 5] Furthermore, atherosclerosis can promote the formation of aortic aneurysms.[6]

The development of an atherosclerotic plaque starts with the infiltration and deposition of low-density lipoprotein (LDL) and other lipids in the inner layer of the artery wall (Figure 2).[4, 5, 7] Inside the artery wall, LDL is oxidized by reactive oxygen species (ROS). Macrophages are recruited, that take up oxidized LDL and transform into foam cells. This leads to increasing inflammatory processes in the vessel wall and more immune cells, including T and B cells are attracted. Foam cells undergo apoptosis and necrosis building a necrotic core inside the plaque. The continued accumulation of lipids and immune cells, along with the formation of a fibrous cap composed of collagens, elastin and fibronectin produced by vascular smooth muscle cells (VSMCs), forms the plaque. Rupture or erosion of the fibrous cap leads to spontaneous interaction with systemic blood cells, which triggers thrombus formation and results in blockage of the artery.[4, 7]

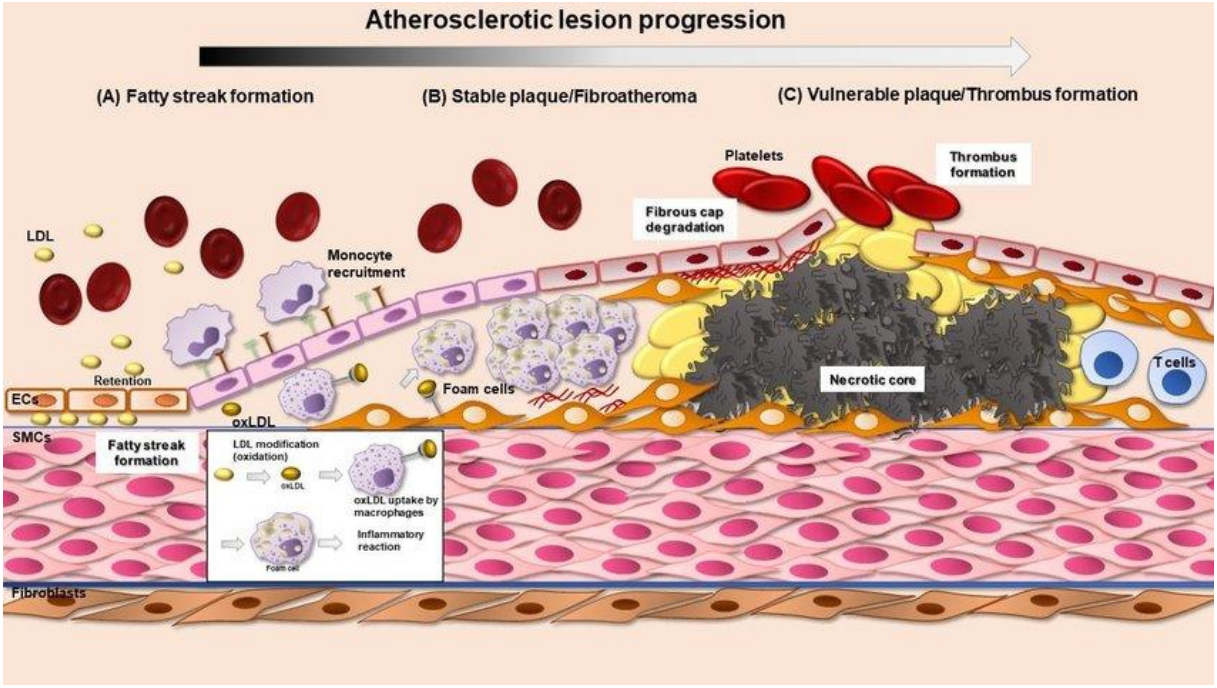

Figure 2: Atherosclerotic plaque formation and rupture. (A) Deposition and oxidation of low-density lipoprotein (LDL) in the inner wall layer of the artery leads to monocyte recruitment. Monocytes differentiate to macrophages, take up oxidized LDL and transform into foam cells that trigger an inflammatory reaction. (B) A stable plaque is formed of a lipid core and a fibrous cap. Vascular smooth muscle cells (VSMCs) produce collagen, elastin, fibronectin and other extracellular matrix molecules that form the fibrous cap. (C) The accumulation of necrotic foam cells builds a necrotic core. A thin fibrous cap results in a vulnerable plaque that can rupture and initiate thrombus formation resulting in the blockage of the artery. Figure from Charla et al.[8]

1.3 Myocardial infarction (MI)

Thrombus formation caused by rupture or erosion of an atherosclerotic plaque in one of the coronary arteries of the heart, is the predominant cause of MI (Figure 3).[9, 10] MI is defined as myocardial cell death due to sustained ischemia that restricts oxygen supply to the myocardium.[9] The death of cardiac cells initiates an acute inflammatory response including immune cell recruitment and clearing of damaged and dead cells.[11, 12] This is followed by a reparative phase that is associated with fibrotic scar formation and neovascularization. Inflammation plays a crucial role in cardiac repair, but prolonged or exaggerated inflammation can have adverse effects leading to improper healing and heart failure.[12, 13]

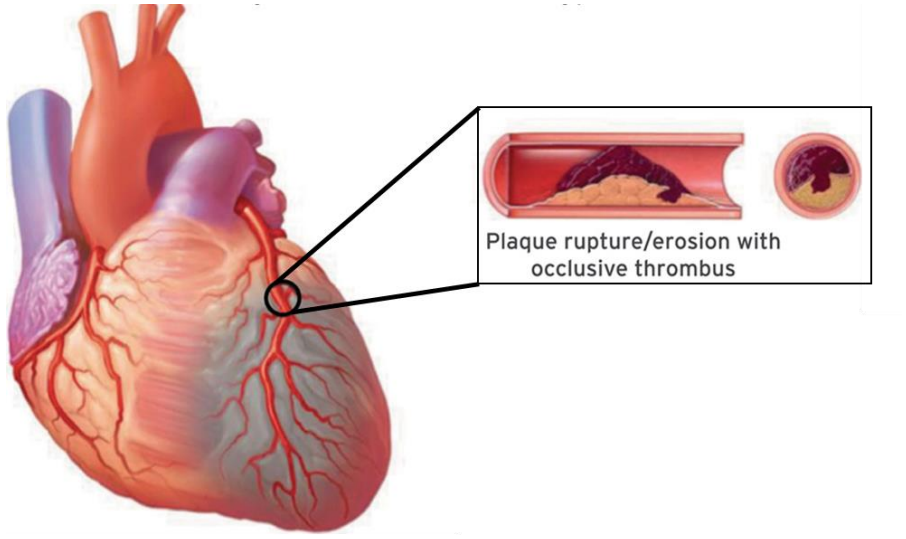

Figure 3: Myocardial infarction caused by rupture of an atherosclerotic plaque with subsequent thrombus formation in one of the coronary arteries of the heart. Figure modified from Thygesen et al.[14]

1.4 Abdominal aortic aneurysm (AAA)

Abdominal aortic aneurysm (AAA) is one of the most common aortic diseases and characterized by a permanent dilation of the abdominal aorta greater than 50% or 3 cm.[15, 16] The aorta is the largest blood vessel carrying blood from the heart to the rest of the body and was classified as separate organ in 2024.[16] AAA is a multifactorial and progressive disease. Genetic factors and inflammation strongly contribute to AAA development.[17] The prevalence of AAA is approximately four times higher in men than in women and increases with age in both genders.[18, 19] In 2019, the global prevalence of AAA in men older than 60 years was 2.45% and 0.59% in women of the same age.[18] AAAs are usually asymptomatic and grow fusiform, meaning that they expand in all directions of the vessel. Most AAAs develop in the infrarenal region of the aorta between the renal veins and the aortic bifurcation.[15] Rupture of AAA is associated with a high mortality rate, as the severe blood loss is fatal within a few minutes. According to the Global Burden of Disease Study 2020, 150,000 deaths worldwide are attributed to aortic aneurysms each year.[19] Thus, early detection of AAA is of great importance. The primary screening method for detection of AAA and further monitoring of AAA expansion is ultrasonography.[20] To date, there is no effective drug treatment and the only therapeutic option is surgery.[21] According to current guidelines, open surgical or endovascular treatment should only be performed if the risk of intervention is lower than the risk of rupture, which would lead to death if left untreated. Surgical repair of asymptomatic AAA is recommended when the diameter exceeds 5 cm in women and 5.5 cm in men, or if the AAA growth exceeds 1 cm per year.[16]

The aorta consists of three layers that are all effected by the dilation in AAA pathology.[15] The intima is the inner layer of the aorta and is composed of a single layer of endothelial cells.[22] The middle layer, the media, comprises VSMCs, elastic fibers and collagen. The adventitia is the outer layer of the aorta and consists of fibroblast and collagen fibers.[22] Pathophysiological hallmarks of AAA formation are infiltration of inflammatory cells, extracellular matrix (ECM) degradation, VSMC phenotype switching and apoptosis, production of cytokines, matrix metalloproteinases (MMP) and ROS, and often thrombus formation (Figure 4).[15, 23, 24] All these processes lead to vascular remodeling and weakening of the aortic wall. Cells of both, the innate and the adaptive immune response, including neutrophils, macrophages, dendritic cells (DCs), natural killer (NK) cells, T and B cells, play a role in aortic wall inflammation and contribute to AAA formation.[25]

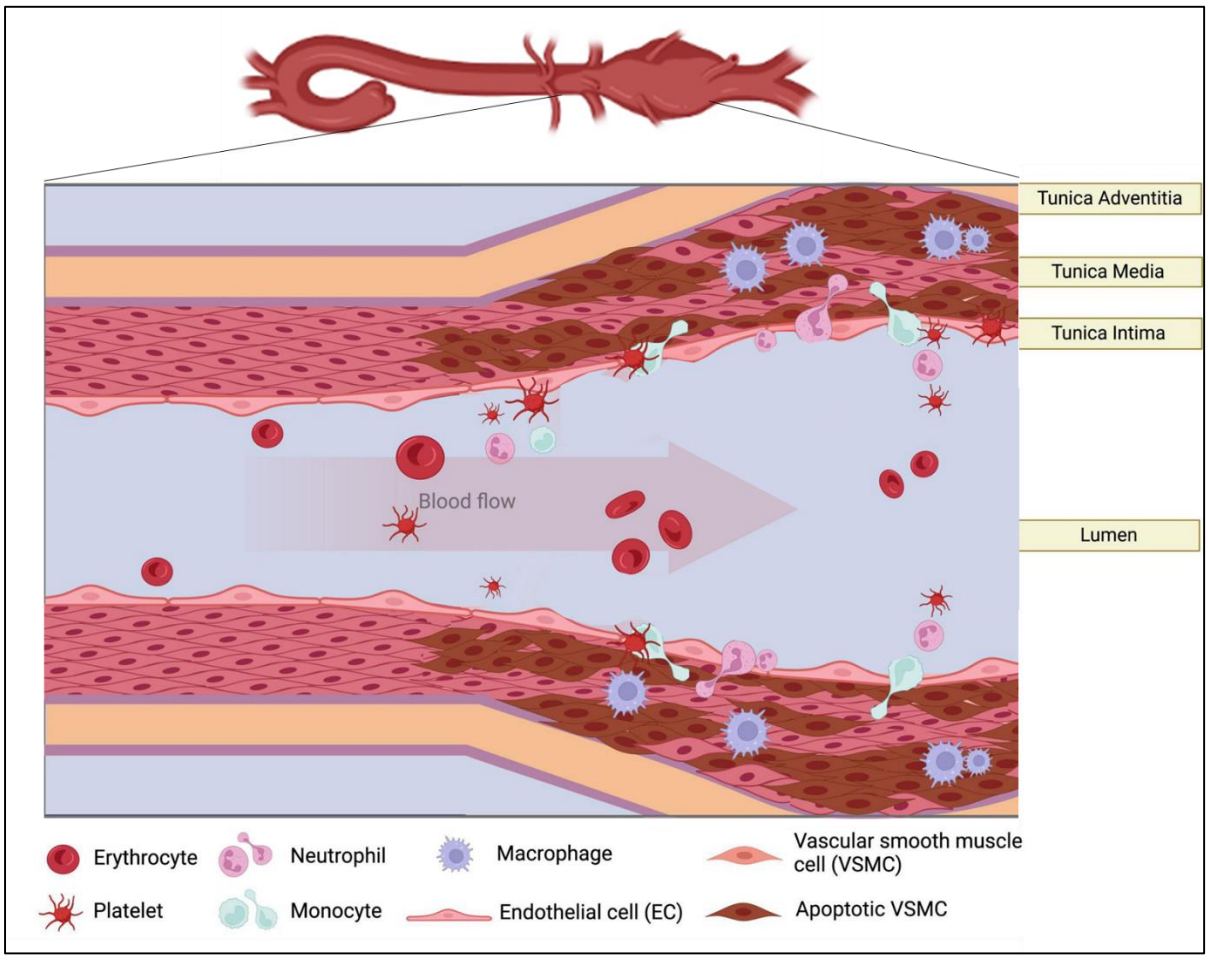

Figure 4: Pathogenesis of AAA formation. The healthy aorta is composed of the intimal, medial, and adventitial layer. The inner layer of the aorta, the intima, consists of a single layer of endothelial cells. The media is the middle layer of the aorta and comprises VSMCs, elastic fibers and collagen. The adventitia consists of fibroblast and collagen fibers. AAA pathology is characterized by inflammatory cell infiltration, such as neutrophils, monocytes and macrophages, extracellular matrix (ECM) degradation and VSMC apoptosis. Platelet activation and accumulation is also often associated with AAA. Figure modified from Lowis et al.[26]

1.4.1 Innate immune cells in AAA pathology

Innate immunity is characterized by rapid recruitment of immune cells to sites of injury and inflammation through the production of cytokines and chemokines, as well as the activation of the adaptive immune response. This first line of defense against pathogens includes neutrophils, macrophages, DCs, NK cells, and innate lymphoid cells (ILCs).[27]

Well studied is, that neutrophils are the first responders to infections and tissue damage.[28] They are the most abundant cell type in human blood and are constantly produced in the bone marrow. Their antimicrobial functions are phagocytosis, degranulation and formation of neutrophil extracellular traps (NETs).[28, 29] In addition, they are involved in degradation of the ECM and regulation of the immune response by producing MMPs, cytokines and other inflammatory factors.[28, 30] Although neutrophils were originally considered a homogeneous cell population, distinct subsets of neutrophils with different functions have been described.[31] Several studies showed that neutrophils play a role in AAA formation. Elevated neutrophil counts in blood of patients was associated with AAA formation and plasma levels of the neutrophil markers myeloperoxidase, MMP-9, α-defensin and neutrophil elastase were increased in AAA patients compared to healthy individuals.[32, 33] In addition, depletion of neutrophils in mice protects from elastase-induced AAA formation.[34] In other studies, reduced AAA formation was also attributed to a decreased neutrophil recruitment.[35, 36] Furthermore, there is evidence that NET formation could play a crucial role in AAA development as high levels of NET-associated markers were found in mouse models and AAA patients.[37-39]

DCs are antigen-presenting cells (APC) and activate the adaptive immune response by presenting antigens on their cell surface to T cells.[40] Depletion of DCs in mice was shown to limit AAA growth, reduce the number of effector T cells as well as B cells in the blood, and decrease the activity of neutrophil elastase in the plasma.[41] DCs are generally divided in conventional/classical DCs (cDCs), migratory DCs, plasmacytoid DCs (pDCs) and monocyte-derived DCs. Migratory DCs are present in non-lymphoid tissue, including the aorta, and encompass, among others, $CD103^+$ DCs that have been reported to be atheroprotective.[40, 42] pDCs are known to produce type-I interferons (IFN) and promote inflammation.[40] Yan et al. showed that NET formation by neutrophils leads to the recruitment of pDCs in AAA.[38] Depletion of pDCs and blocking of type-I IFNs reduced experimental AAA formation.[38] Monocyte-derived DCs arise under inflammatory conditions and produce tumor necrosis

factor alpha (TNFα) and inducible nitric oxide synthase (iNOS).[40, 43] Their role in AAA has not been described, yet.

Macrophages play a central role in tissue homeostasis and inflammation.[44] Their main function is to engulf and digest pathogens and present antigens to T cells. Besides increasing inflammation and stimulating the immune system, macrophages also play an important anti-inflammatory role and can reduce immune reactions by releasing cytokines.[44] In context of AAA, macrophages are involved in ECM remodeling, promotion and resolution of inflammation, and in tissue healing and repair.[45] Macrophages have been detected in human AAA and experimental AAA models and represent the most common cell type in media and adventitia of aneurysmal tissue.[45-47] Macrophages can be tissue resident, meaning they originate from embryonic precursors and are self-maintained during adulthood, or arise from peripheral blood monocytes.[44, 45] Both types are involved in AAA pathology, but the majority of macrophages are monocyte-derived macrophages.[45, 48] This is consistent with the findings that monocyte depletion in mice lead to decreased macrophage accumulation in the aortic wall and reduced Angiotensin II (AngII)-induced AAA formation.[48] Furthermore, Hans et al. showed that reduced AngII-induced AAA formation by inhibition of Notch1 signaling was accompanied with reduced macrophage recruitment[49], suggesting an important role for macrophages in AAA formation. Several strategies targeting macrophage recruitment, accumulation, and activation in AAA were studied, such as inhibition of chemokine axes, targeting specific macrophage-related cytokines, and modulation of macrophage phenotype.[45] Blocking of CXCL12/CXCR4, CCL2/CCR2 or CXCL4/CCL5 signaling was shown to reduce macrophage infiltration and protect against experimental AAA formation.[50-52] A proper ratio of pro- and anti-inflammatory cells is important for tissue homeostasis, but in AAA, pro-inflammatory macrophages are known to dominate against anti-inflammatory macrophages.[53] Thus, modulating this ratio by increasing anti-inflammatory macrophage polarization was found to inhibit AAA formation.[53, 54] Originally, macrophages were only divided into pro-inflammatory classical activated M1 and anti-inflammatory alternative activated M2 macrophages.[44] However, this classification in only two types is too simplified and does not represent the heterogeneity of macrophages in vivo.[55] The emerge of single-cell RNA sequencing (scRNA-seq) techniques led to the identification of many more different macrophage subtypes, such as inflammatory macrophages, TREM2^{high} macrophages, interferon-inducible (IFNIC) macrophages, proliferative macrophages, aorta intima-resident macrophages, cavity macrophages and SMC-derived macrophages.[55-57] Overall, macrophages play a critical role in AAA development, but roles and functions of

distinct subsets are still unclear and treatments specifically targeting macrophage subsets are lacking.

ILCs are lymphocytes that lack adaptive antigen receptors and represent the innate counterpart of T cells.[58] ILCs are primary tissue resident cells. They are present in lymphoid and non-lymphoid tissue and rarely in the blood. Their functions include tissue homeostasis, tissue remodeling, cytokine production and regulation of both innate and adaptive immune cells. ILCs are classified in three types based on their similarity to T helper (Th) cell subsets.[58, 59] ILC1s mirror Th1 cells and respond to intracellular pathogens. ILC2s are similar to Th2 cells and react to large extracellular parasites and allergens. ILC3s are the counterpart to Th17 cells and involved in the response to extracellular bacteria and fungi. It is known that ILCs play a crucial role in allergy, asthma and autoimmune diseases.[59] However to date, not much is known about their role in CVDs. There is evidence for both a protective and a detrimental role.[60] In context of AAA, Zhang et al. showed that ILC2s release interleukin (IL) 5 and 13, that inhibit apoptosis of VSMCs and promotes their proliferation, resulting in protection against experimental AAA formation in mice.[61]

NK cells belong to the group of ILC1s and are the innate counterpart to cytotoxic T cells.[62] In contrast to other immune cells, they can recognize and kill virus-infected cells, stressed cells and pathogens without prior antigen sensitization. NK cells release several different cytokines, particularly interferon gamma (IFNγ) and TNFα. Cytokine production of NK cells recruits and activates cells of the innate and the adaptive immune response.[62] NK cells could be detected in human AAA samples and the percentage of circulating NK cells was shown to be upregulated in the blood of AAA patients compared to controls.[63-65] Furthermore, there is evidence that the NK cell mediated cytotoxicity pathway is activated in human AAA.[66]

Natural killer T (NKT) cells share characteristics of NK cells and T cells.[67] Their function is similar to that of NK cells, but they differ in their lineage development, as NKT cells are a subgroup of T cells. CD1d-dependent type I NKT cells (iNKT) promote aneurysm progression by secreting cytokines that lead to increased production of matrix-degrading enzymes by VSMC and macrophages.[68] Lack of iNKT cells resulted in reduced AngII-induced AAA formation.[68] Vice versa, activation of iNKT with α-galactosylceramide led to increased AAA incidence and inflammatory cell infiltration into the aneurysmal tissue in the AngII mouse model.[67] In contrast, Saito et al. that also used α-galactosylceramide in the AngII model, but in obese mice, showed less AAA formation and reduced inflammatory cell infiltration after iNKT activation.[69]

1.4.2 Adaptive immune cells in AAA pathology

The second line of defense in the immune response is adaptive immunity, which acts antigen-specific and includes lymphocytes such as T and B cells.[27] It depends on APCs of the innate immunity that present antigens to T and B cells. The main functions of adaptive immunity are the recognition of specific antigens and their differentiation from self-antigens, as well as the development of an immunological memory that enables a rapid and effective immune response in case of a second infection with the same pathogen.[27] A dysfunctional reaction of the adaptive immune system, which leads to the attack against healthy cells in the body, is the underlying cause of autoimmune diseases.[27, 70] T and B cells are among the predominant infiltrating immune cells in human AAA tissue[71-73] and their presence was confirmed in several experimental mouse models of AAA.[74-78] Moreover, multiple studies have revealed that autoimmunity may contribute to the pathogenesis of AAA.[71, 72, 79, 80]

T cells express T cell receptors (TCR) and recognize antigens that are presented by APCs via major histocompatibility complex (MHC), also known as human leukocyte antigen (HLA).[81] After activation, T cells undergo clonal expansion and differentiation to execute their effector functions. They are generally divided in $CD4^+$ T helper cells and $CD8^+$ cytotoxic T cells.[25] T helper cells activate other cells including B cells, cytotoxic T cells and macrophages, and are further distinguished in Th1 cells, Th2 cells, Th17 cells and regulatory T cells (Treg).[81] Cytotoxic T cells directly kill virus-infected and tumor cells, and are divided into effector cells and memory cells.[25, 81] Xiong et al. suggested a key role of $CD4^+$ T helper cells in AAA as they showed that absence of $CD4^+$ T cells prevented AAA formation in mice.[82] Th1 and Th2 cells were found to be present in various stages of AAA development.[83] Th1-derived IFNγ, TNF and CD40 ligand (CD40L) are associated with macrophage activation, regulation of VSMC apoptosis, and aortic wall remodeling.[25, 83, 84] Th2 cells release inflammatory mediators and cytokines such as IL-4, -5, -9, -10, and -13 and Fas ligand that may contribute to aortic wall degradation and the regulation of AAA progression.[25, 83, 85] IL-17, that is primarily secreted by Th17 cells, is elevated in AAA and elastase-induced AAA formation was attenuated in IL-17-deficient mice.[86] Tregs express forkhead box protein 3 (FOXP3) and are essential for limiting chronic inflammation, sustaining peripheral tolerance and preventing autoimmunity.[87] In the context of AAA, Tregs were shown to have a protective role.[88, 89] It was shown that $CD8^+$ cytotoxic T cells infiltrate the aneurysmal wall and release IFNγ, which promotes cellular apoptosis and recruitment of MMP-producing macrophages.[90]

The main function of B cells is the presentation of antigens to T cells and the production of antibodies.[91] They further mediate the immune response by secretion of cytokines. B cells are mainly divided into B1 and B2 cells.[91] B1 cells derive from the fetal liver and respond to self and T cell-independent antigens by producing natural immunoglobulin (Ig) M antibodies.[91] B2 cells derive from the bone marrow and represent the majority of B cells in adults.[91] They include marginal zone B cells and conventional follicular B cells. Marginal zone B cells can rapidly respond to blood borne antigens via IgM in a T cell-independent or T cell-dependent manner.[91] Follicular B cells undergo isotype switching in response to T cell-dependent antigens and differentiate into memory B cells or antibody-secreting plasma cells that can secrete all Ig isotypes.[91] The role of B cells in AAA is controversially discussed. B cell-derived immunoglobulins, such as IgM and IgG, accumulate in AAA tissue, where they contribute to inflammation and tissue degradation.[74, 92] B cell depletion has been shown to prevent AAA growth in experimental models. Schaheen et al. demonstrated that B cell depletion with an anti-CD20 antibody reduced AAA growth in both AngII-induced and elastase-induced AAA.[93] Another study observed significantly smaller AAAs in B cell-deficient muMT mice compared to wild-type (WT) mice following periaortic application of $CaCl_2$.[74] Injection of polyclonal IgG antibodies into muMT mice resulted in AAAs of similar size to those in WT mice, suggesting that IgG alone is sufficient to promote AAA development.[74] In contrast, Meher et al. found no differences in experimental AAA formation between muMT mice and WT mice, and showed that adoptive transfer of B2 cells suppressed AAA formation and reduced the infiltration of mononuclear cells into aneurysmal tissue.[75]

Clonality and diversity analysis of the adaptive immune receptor repertoire (AIRR), which is the union of all B and T cell receptors of one individual, provide insights into disease mechanisms. The AIRR can change greatly with the onset and progression of diseases and AIRR sequencing is increasingly used to investigate clonal expansion and diversity of T and B cells in pathological contexts such as autoimmune diseases, sterile inflammatory diseases, infections, and cancer.[94, 95] The TCR repertoire is estimated to comprise 10^7 unique receptors in humans and 10^6 in mice.[96] The B cell repertoire is even larger, with an estimated size of 10^{18} in humans and 10^{13} in mice.[97, 98] TCRs and B cell receptors (BCRs) are highly diverse heterodimers that recognize an immense variety of antigens.[95] BCRs consist of a combination of heavy and light chains, while TCRs are built by a combination of α/β or γ/δ chains (Figure 5 A). Most TCRs consist of a combination of α and β chains. These receptors are generated through variable, diversity, and joining (VDJ) recombination, which involves the rearrangement of the V-, D-, and J-gene segments (Figure 5 B). For the formation of TCR α chains and BCR light chains, only V- and J-genes are involved in the recombination

process. Additional diversity is achieved by the random addition or deletion of nucleotides at the junction sites between the gene segments and through chain pairing. Somatic hypermutation further contributes to a greater diversity of BCRs. Each receptor chain contains three hypervariable loops termed complementarity determining regions (CDR) that are essential for antigen binding. CDR3 is commonly used as a region of interest to identify T and B cell clones due to its high diversity and key role in antigen binding.[95, 99-102] A clone is defined as a set of cells that express identical immune receptors, which implies that the receptors consist of the same V-, D-, and J-genes and encode the identical CDR3 nucleotide sequence.[102]

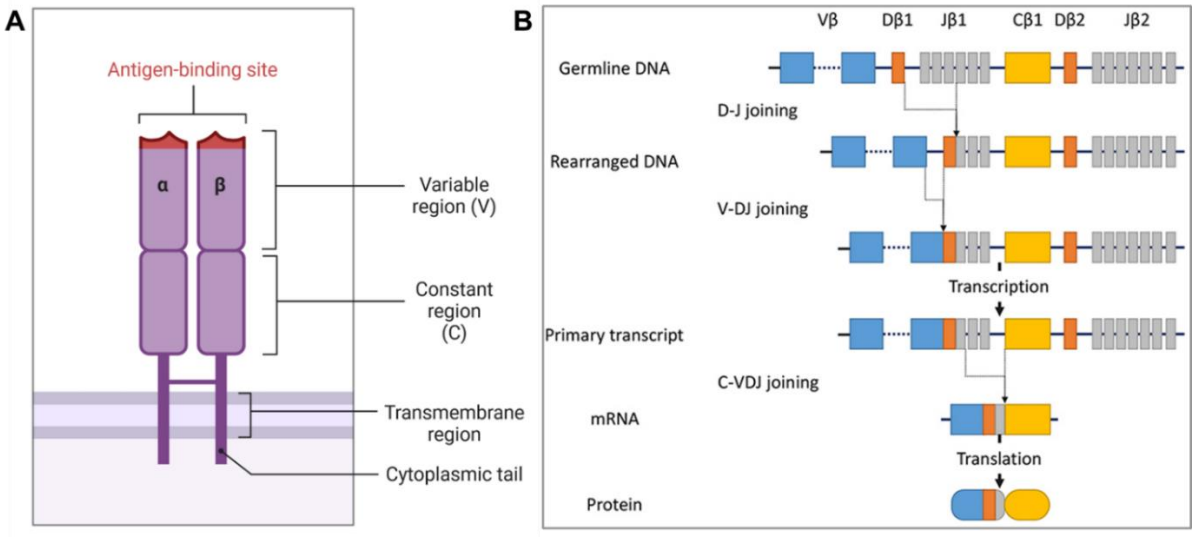

Figure 5: Structure of a TCR and schematic illustration of VDJ recombination of the TCRβ gene respectively. A: The TCR consists of two polypeptide chains, in most cases one alpha and one beta chain. TCRs are defined by three regions: the variable (v), constant (c) and transmembrane regions. The variable region (v) contains the antibody binding site. **B:** The somatic recombination of the TCRβ gene begins with D-J recombination, followed by V-DJ joining. This random recombination of the different segments generates TCR diversity. After transcription, the intervening sequences are spliced, producing the TCRβ chain transcript, which includes the V, D, J, and C region segments. Then, the transcript is translated into protein. Figure created with Biorender and modified from Fujii et al.[103]

Autoimmune responses are characterized by the presence of self-reactive T cells, autoantibodies and inflammation.[70] Investigation of the TCR-MHC complex provided evidence that AAA pathology involves a specific antigen-driven T cell response.[71, 79] Different studies detected a clonal expansion of T cells in AAA lesions, associated AAA with MHC class I and II types, and identified self- or non-self-antigens that may be related to AAA.[71, 80, 104-107] The presence of clonally expanded TCRs in aneurysmal lesions of patients with AAA or thoracic aortic aneurysms (TAA) was shown by several studies[106-108], supporting the assumption that AAA may be promoted by specific antigen-driven T cells. In addition, clonal expansion of Tregs was found in experimental elastase-induced AAA formation in mice.[109] There is also evidence that an autoimmune reaction directed against self-antigens present in

the aortic wall plays a role in AAA pathogenesis. Zhou et al. identified a natural IgG antibody against fibrinogen in aortic tissues of elastase-induced AAA that contributes to AAA formation by activating the complement lectin pathway.[104] Another study indicates that a collagen-associated 80-kDA protein present in the aneurysm wall may be a potential target of the autoimmune response in AAA.[105] They showed that 8 of 10 IgG antibodies, including autoantibodies, isolated from the aortic wall of AAA patients reacted with an 80-kDa protein from aortic microfibrillar extracts. This protein was located in the adventitial connective tissue matrix.[105] Further investigation of the role of T cells, B cells, and Ig involved in AAA in context of an autoimmune response can be useful to improve the understanding of AAA pathology.

1.5 The co-stimulatory molecules CD40 and CD40L

Co-stimulatory molecules play a crucial role in adaptive immunity and in mediating inflammation. Cluster of differentiation 40 (CD40) and its ligand CD40 ligand (CD40L) are co-stimulatory molecules that amplify the immune response by providing a second signal after the interaction of MHC and TCR to properly activate T cells (Figure 6).[110] CD40 and CD40L are type I and II transmembrane proteins that belong to the tumor necrosis factor receptor (TNFR) family.[110, 111] CD40 is expressed on a wide range of cells. It was initially identified on B cells[112], but is also found on other APCs such as neutrophils, monocytes, DCs and macrophages.[110, 111] Additionally, CD40 is expressed on endothelial cells, fibroblasts and epithelial cells. CD40L is predominantly expressed by T cells, but can also be detected on platelets, activated B cells and endothelial cells. In addition, there is a soluble form of CD40L (sCD40L). Under inflammatory conditions, CD40L expression has been observed on mast cells, monocytes, NK cells and basophils.[110, 111]

Binding of CD40L to CD40 leads to the recruitment of TNFR-associated factors (TRAFs).[113] TRAF1, TRAF2, TRAF3, TRAF5, and TRAF6 can bind to CD40. Depending on the bound TRAF protein, different pathways are activated, including the nuclear factor κB (NFκB)-signaling pathway, the mitogen-activated protein kinase (MAPK) pathway, phosphoinositide 3-kinase (PI3K) pathway and the phospholipase Cγ (PLCγ) pathway (Figure 6).[110, 113] Independent of TRAFs, Janus family kinase 3 (JAK3) can bind directly to the cytoplasmic domain of CD40 and activates the signal transducer and activator of transcription (STAT) pathway.[114] Activation of these different pathways results in transcription of various genes that mediate humoral and cellular immune response.[110, 113]

CD40-CD40L signaling has a distinct impact on different cell types. In T cells, CD40L co-stimulation leads to cytokine production and promotes differentiation into T helper cells, that

support B cell-mediated antibody responses and memory formation.[110, 115] In B cells, CD40-CD40L engagement promotes survival, proliferation, isotype switching, immunoglobulin production, and cytokine secretion that mediate immune cell recruitment and inflammation.[110] In addition, CD40-CD40L signaling influences B cell differentiation towards memory B cells rather than plasma cells.[116] In other APCs, like monocytes and DCs, CD40-CD40L interaction enhances survival, cytokine production, nitric oxide synthesis, and antigen cross-presentation.[110] Overall, CD40 signaling leads to full maturation of DCs to effectively induce activation and differentiation of T cells.

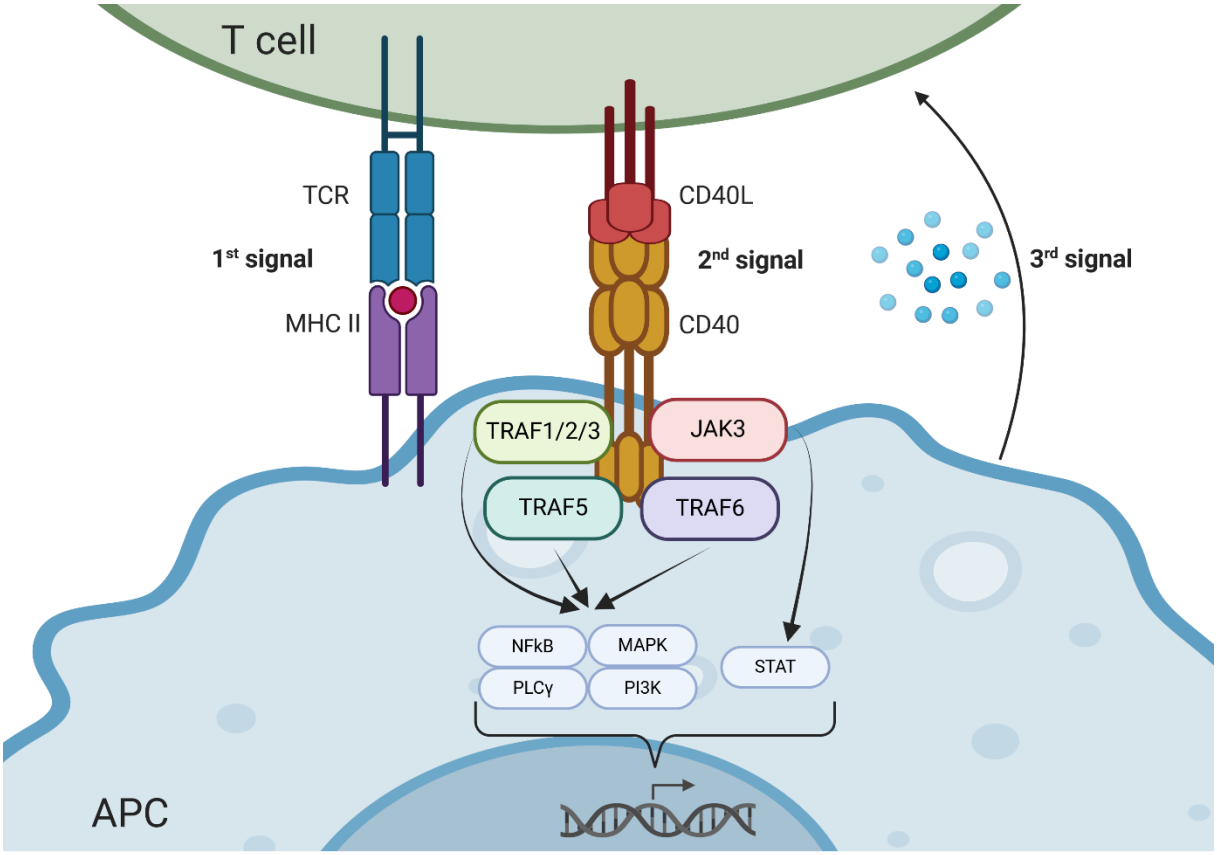

Figure 6: CD40/CD40L signaling. An antigen-presenting cell (APC) presents a bound antigen via its major histocompatibility complex (MHC) to the T cell receptor (TCR) of a T cell, which is the first signal for activation of the T cell. Simultaneously, CD40, expressed on the APC, binds to its ligand CD40L, expressed on the T cell, and provides a second signal. This leads to the release of cytokines, which enhance the response and provide the third signal. After binding of CD40L to CD40 TRAF proteins are recruited that activate different pathways including NFκB, MAPK, PI3K and PLCγ. JAK3 can bind to CD40 independent of TRAF proteins and activates the STAT pathway. Activation of these pathways results in transcription of various genes and the release of cytokines that enhance the immune response. Created with Biorender based on Strohm et al.[117]

1.6 The role of CD40-CD40L signaling in CVDs

Since CD40-CD40L signaling regulates inflammation by mediating cell differentiation and inducing secretion of several pro-inflammatory cytokines and chemokines, it plays an important role in CVDs. Multiple studies found elevated sCD40L plasma levels in patients

with CVDs and healthy individuals that were associated with an increased risk of recurrent and future cardiovascular events.[118-121] Thus, sCD40L can be used as risk marker for CVDs. In atherosclerosis, CD40 signaling is involved in plaque initiation, immune cell recruitment, as well as plaque destabilization and rupture.[122] Inhibition of CD40 signaling using an anti-CD40L antibody in hyperlipidemic mice resulted in smaller atherosclerotic lesions with reduced lipid content and less inflammatory cells.[123] However, treatment with anti-CD40L antibody, caused thromboembolic complications in non-human primates and patients.[124, 125] Inhibition of CD40-TRAF6 signaling led also to a reduction of atherosclerotic lesions and a more stable, anti-inflammatory plaque phenotype in apolipoprotein E deficient (*Apoe*$^{-/-}$) mice, while specifically blocking of CD40-TRAF2/3/5 signaling had no beneficial effects on atherosclerosis.[126, 127] Since atherosclerosis is the main underlying cause for MI, CD40 signaling also plays a crucial role in MI. Our working group showed that activation of CD40 signaling via an agonistic CD40 antibody in mice resulted in larger infarct sizes and impaired cardiac function after ischemia reperfusion.[128] Vice versa, blocking of CD40-TRAF6 signaling showed beneficial cardiac function by reducing scar size. In a mouse model of non-ischemic heart failure, inhibition of CD40-TRAF6 signaling resulted in an improved cardiac function due to reduced fibrosis and immune cell recruitment.[129] In context of AAA, CD40L-deficiency and pharmacological blocking of downstream CD40 signaling via TRAF6 was shown to protect against AAA formation and rupture.[84, 130] Thus, CD40 and CD40L are promising therapeutic targets and their role in CVDs, especially in AAA requires further investigation.

1.7 scRNA-sequencing techniques

ScRNA-seq has become the state-of-the-art technology to uncover the composition of different cell types and functions in complex tissues by deciphering the complexity and heterogeneity of RNA transcripts in single cells.[131] Since Tang et al. developed the first approach of scRNA-seq in 2009[132], an increasing number of modified and improved scRNA-seq technologies were developed, including Cellular Indexing of Transcriptomes and Epitopes by Sequencing[133] (CITE-seq) and scRNA sequencing of TCRs and BCRs (scRNA-TCR-BCR-seq).[134] CITE-seq enables the simultaneous analysis of protein and transcriptome measurements using oligonucleotide-labeled antibodies that can be subjected to sequencing.[133] scRNA-TCR-BCR-seq is a powerful tool to investigate T and B cell clonality, AIRR overlap between individuals, V-gene usage, and diversity.[102] In contrast to bulk RNA sequencing of TCRs and BCRs, scRNA-TCR-BCR-seq provides information on TCR chain pairing, has a higher resolution and is more suitable for investigating the TCR specificity for an antigen of interest.[134]

2 Objectives of the study

AAA is a complex, multifactorial and life-threatening disease associated with SMC apoptosis, ECM degradation, extensive immune cell infiltration and inflammation. Although the major cell types involved in AAA are known, a detailed characterization of the cell types and their specific function in AAA is lacking and appropriate targets for drug therapy have not yet been identified. Specific antigen-driven T cells and CD40-CD40L signaling were shown to play a crucial role in AAA development and represent potential therapeutic targets. The use of scRNA-seq techniques enables a comprehensive and unbiased characterization of the cell types and genes involved in AAA development. Deeper analysis of the appearance of cell types, diverse functional states of the cells as well as changes in their molecular profile with progression of AAA, is essential to understand the underlying pathological mechanisms involved in the development and progression of AAA and to identify potential targets for therapeutic intervention. The overall aim of this work was to decipher the immune cell heterogeneity in experimental AAA progression and to identify key players, genes or signaling pathways. CD40-CD40L signaling was hypothesized to play a crucial role in AAA pathology and was specifically investigated. In addition, the hypothesis that AAA exhibits features of an autoimmune response and is driven by antigen-specific T cells was examined. Thus, this thesis is divided into the following three parts:

1) **Characterization of immune cell heterogeneity in experimental AAA progression and identification of potential therapeutic targets**
   A comprehensive analysis of immune cell subsets involved at different stages of elastase-induced AAA progression was performed using flow cytometry, immunofluorescence stainings, scRNA-seq and CITE-seq. CITE-seq was furthermore utilized to compare the immune cell responses in AAA with those observed in atherosclerosis and MI to identify common or unique immune signatures across these CVDs and to examine the correlation between RNA and protein expression.

2) **Investigation of the role of CD40-CD40L signaling in AAA**
   CD40-deficient mice were used to investigate the contribution of CD40 signaling to AngII-induced AAA formation, progression and rupture. Flow cytometry, immunofluorescence staining and scRNA-seq was performed to examine CD40 and CD40L expression in AAA and to identify cell types that are involved in CD40-CD40L signaling.

3) **Examination of T and B cell clonality in experimental AAA**
   scRNA-TCR-BCR-seq was performed to analyze T and B cell clonality in elastase-induced AAA progression to explore potential antigen-driven immune responses and their relevance to AAA pathology.

These objectives aim to provide a detailed understanding of the immune landscape in AAA and to potentially identify novel therapeutic targets for this disease.

3 Material and Methods

3.1 Mice

Male C57BL/6J mice aged 10-11 weeks were purchased from Janvier Labs (Saint-Berthevin, France). *Apoe*$^{-/-}$ mice were purchased from Jackson Laboratories (JAX, Bar Harbor, Maine, USA). Some studies were performed on tamoxifen (TAM)-inducible, global CD40-deficient mice with *Apoe*$^{-/-}$ background (*Apoe*$^{-/-}$ *Cd40*$^{fl/fl}$ *CreER*^{T2} and their Cre negative (*Cre*^{wt}) littermates previously generated by us.[135] Genotypes were confirmed using polymerase chain reaction that was performed by Transnetyx (Cordova, USA). Mice were housed under standard laboratory conditions with a 12 h light/dark cycle in the central facility premises for animal research and scientific animal protection tasks (ZETT) at the Heinrich-Heine-University Düsseldorf. Mice had *ad libitum* access to drinking water and standard chow. All animal studies were performed according to Animal Research: Reporting of *In Vivo* Experiments (ARRIVE II) guidelines[136] and approved by the regional authority (LANUV; North-Rhine-Westphalia State Agency for Nature, Environment and Consumer Protection; license approval number AZ 81-02.04.2018.A408, 2024-419-Grundantrag and 81-02.04.2020.A225.) in accordance with the European Convention for the protection of vertebrate animals used for experimental and other scientific purposes.

3.2 Porcine pancreatic elastase (PPE) perfusion model to induce AAA formation

To induce AAA in male C57BL/6J mice, the PPE perfusion model was used as previously described by Pyo et al.[137] Briefly, the mice received analgesics by injecting 0.1 mg/kg body weight (bw) buprenorphine (Temgesic©; Indivior Europe, Dublin, Irleand) subcutaneously (s.c.) 30 min prior to surgery. The mice were anesthetized with isoflurane (initial 3%, then 1.5%) and oxygenated air and were placed on a heated pad at 37°C. After absence of the toe reflexes, laparotomy was performed, and the proximal and distal infrarenal aorta was isolated and temporarily ligated. The aorta was punctured, a catheter was inserted, and the infrarenal part was perfused with sterile isotonic saline containing type I PPE (2.5–3 U/ml cat#E1250 Merck, Darmstadt, Germany) or 0.9% sodium chloride (NaCl, sham surgery) under 120 mmHG for 5 min. Elastase concentrations ranged from 2.5 to 3 U/ml depending on the batch number, as different concentrations were necessary to trigger the same AAA incidence and size. After perfusion, the aortic puncture was sutured, the ligations were removed, and the abdomen was closed. Afterwards, mice received Metamizol (Zentiva, Prag,

Czech Republic, 1.33 mg/ml, sweetened) via the drinking water for three days. If required, mice additionally received buprenorphine (0.1 mg/kg bw, s.c.) in the first eight hours. The mice were monitored regularly until the end of the experiment. The surgeries to induce AAA were performed by the technical assistants Julia Odendahl and Stefanie Becher.

3.3 Angiotensin II (AngII) model to induce AAA formation in CD40 deficient mice

The AngII model was used to induce AAA formation in the TAM-inducible global CD40 KO-model (*Apoe*$^{-/-}$ *Cd40*$^{fl/fl}$ *CreER*^{T2} mice strain). Two weeks prior AngII-pump implantation, *Apoe*$^{-/-}$ *Cd40*$^{fl/fl}$ *CreER*^{T2} mice were injected intraperitoneally (i.p.) with 100 µl TAM (cat# T5648, Merck, 1 mg/injection) solved in peanut oil (cat#P2144, Merck) to induce a global CD40 deficiency. TAM injections were repeated daily for 5 consecutive days. *Cre*^{wt} littermates, that served as controls, received TAM injections at the same time.

Apoe$^{-/-}$ *Cd40*$^{fl/fl}$ *CreER*^{T2} mice and *Apoe*$^{-/-}$ *Cd40*$^{fl/fl}$ *Cre*^{wt} littermates were continuously infused with AngII via osmotic pumps (model 1004, Alzet, Cupertino, USA) at a rate of 1 µg/kg/min for 28 days, as described by Daugherty et al.[138] One day prior to implantation, osmotic pumps were filled with AngII (cat#A9525, Merck) and primed by incubating them in 0.9% sodium chloride (NaCl; cat#B101153, Fresenius Kabi, Bad Homburg, Germany) at 37°C. Mice received analgesics by injecting buprenorphine (0.1 mg/kg bw, s.c.) 30 minutes before surgery. Anesthesia was induced with 3% isoflurane and maintained at 1.5%, with mice placed on a heated pad at 37°C. After absence of toe reflexes, a subcutaneous pocket was created over the right shoulder of the mouse. The pump was inserted with the moderator head directed caudally and the incision was sutured. Postoperative analgesia was provided by administering Metamizol (1.33 mg/ml, sweetened) in the drinking water for a minimum of two days. Mice were monitored regularly until the end of the experiment.

If mice died prior to the experimental endpoint, an autopsy was performed to determine the cause of death. Mice that died from rupture of an aneurysm were included in the analysis of AAA incidence.

3.4 Ischemia reperfusion (I/R) model to induce MI

The I/R model was used to induce reperfused MI in male C57BL/6J mice. Shortly before surgery, mice were injected with buprenorphine (0.1 mg/kg bw, s.c.). After 30 min, they were briefly anesthetized with 3% isoflurane in an inhalation chamber and then intubated using a

venous cannula (Vasofix Safety Kanüle 20 G 1,1x25 mm, B. Braun, Melsungen, Germany). Mice were placed on a heated surgery table and anesthesia was maintained with isoflurane (2%) and oxygenated air (30% oxygen) at a respiratory volume of 0.2 to 0.25 mL and a respiratory rate of 140 breaths per minute. Electrocardiogram (ECG) and body temperature (37°C) were constantly monitored. To induce MI, the left anterior descending coronary artery (LAD) was occluded for 45 min using a 7-0 prolene thread as previously described.[139] MI induction was verified by ECG (ST-segment elevation) and an optical control (heart discolors brightly below the thread). After 45 min, the suture was reopened to allow reperfusion of the LAD. Mice received buprenorphine every 4 h (0.1 mg/kg body weight, s.c.) during the day. At night, they received buprenorphine in their drinking water for 3 days and were monitored regularly until the end of the experiment. The surgical procedures were performed by the technical assistant Stefanie Becher.

3.5 Aortic diameter measurement

Non-invasive ultrasound imaging was used to measure the aortic diameter prior to surgery (baseline) and AAA development and progression was monitored weekly. The Vevo 3100 high-resolution *in vivo* imaging system with a 25–55 MHz transducer (MX550D, VisualSonics Inc., FUJIFILM, Toronto, Canada) was used for imaging. Mice were anesthetized with isoflurane (initially 3%, then 1.5%) and placed on a heated pad at 37°C. Aspiration rate ECG, and body temperature were monitored during the entire time of imaging. To assess the aortic diameter, longitudinal B-mode images of the infrarenal aorta were acquired. The aortic diameter was analyzed from leading to leading edge (LTL, Figure 7) in three cardiac cycles at end-diastole using the Vevo LAB 5.6.0 software. AAA incidence was defined as an increase in aortic diameter of at least 1.5-fold.

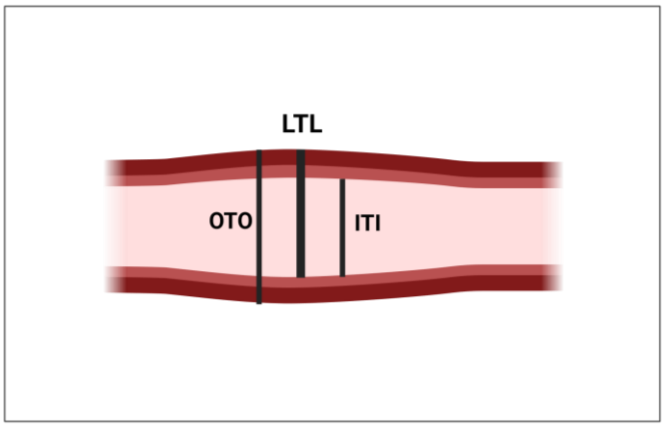

Figure 7: Scheme of different methods to determine the aortic diameter in ultrasound images. The vessel diameter can be measured from the anterior external wall to the posterior internal wall, which is referred to as the leading to leading (LTL) edge. The outer to outer (OTO) method measures the external aortic diameter and the inner to inner (ITI) method measures the internal aortic diameter. Figure created with Biorender.

3.6 Organ harvesting

Mice were sacrificed at day 3, 7, 14 and 28 post PPE or sham surgery and at day 1 and 5 after I/R surgery. For scRNA-seq experiments, 10 min prior to organ harvesting mice were injected intravenously (i.v.) with 100 µl CD45-FITC antibody (cat#553079, dilution 1:1000 BioLegend, San Diego, California, USA) to label circulating leukocytes. Mice were weighted, anesthetized and received analgesia with ketamine (100 mg/kg bw; Ketaset, Zoetis, Pasippany, New Jersey, USA) and xylazine (10 mg/kg bw; Rompun, Bayer, Leverkusen, Germany). After the absence of toe reflexes, blood was collected from the heart with a heparinized syringe. Thorax and abdomen were opened, the vena cava was cut, and the cardiovascular system was perfused with cold DPBS (cat#D8537, Merck) through the left ventricle of the heart. The infrarenal part of the aorta was isolated by carefully removing all fatty tissue, collected, and stored in DPBS on ice until further processing.

3.7 Preparation of single cell suspensions

For further analysis of aortic and cardiac cells by flow-cytometry, scRNA-seq and CITE-seq, single cell suspensions were prepared according to the following protocols.

3.7.1 Digestion of aortic tissue into single cells

The isolated infrarenal aortae were digested into single cells based on the protocol from Hu et al.[140] Briefly, aortic tissue was cut into 1-2 mm pieces and transferred into an enzyme mix containing 400 U/ml collagenase I (cat#C0130-100MG, Merck), 120 U/ml collagenase XI (cat#C7657-25MG, Merck), 60 U/ml hyaluronidase I-S (cat#H3506-100MG, Merck), and 60 U/ml Dnase I (cat#11285932001, Merck) in DPBS supplemented with calcium and magnesium ($DPBS^{++}$, cat#D8662, Merck) and 20 mM HEPES (cat#15630106, Thermo Fisher Scientific, Waltham, Massachusetts, USA). The aortae were incubated in the enzyme mix for 50 min on a shaker (600 rpm) at 37°C. The cell suspension was filtered through a 100 µm cell strainer (cat#43-50100-50, pluriSelect Life Science, Leipzig, Germany). The remaining aortic tissue was mashed with a syringe plunger through the cell strainer, which was rinsed several times with DPBS. After centrifugation (10 min, 450 × g, 4°C), the cells were resuspended in cold DPBS until further processing.

For flow cytometric analysis, cells were subsequently resuspended in RPMI-1640 (cat#R7388, Merck) supplemented with 10% fetal calf serum (cat#F9665, Merck) and incubated on a shaker (600 rpm, 12 min, 37°C). Finally, cells were centrifuged (10 min, 450 × g, 4°C), resuspended in DPBS and stored on ice.

3.7.2 Digestion of cardiac tissue into single cells

Hearts were cut into small pieces and digested with an enzyme mix containing the enzymes A, D and R from the Tissue Dissociation Kit 1 (cat#130-110-201, Miltenyi Biotec, Bergisch Gladbach, Germany) in RPMI-1640 for 15-20 min at 37°C with shaking. Next, the cell suspension was passed through a 100 µm strainer and subsequently filtered through a 40 µm stainer (cat#43-50040-51, pluriSelect Life Science). The strainer was washed with RPMI-1640, the filtered cells were centrifuged for 5 min at 450 x g at 4°C and the supernatant was removed. The cell pellet was resupended in red blood cell lysis buffer containing 8.29 mg/ml ammoniochloride, 1 mg/ml potassium bicarbonate and 0.0375 mg/ml sodium-ethylenediaminetetraacetic acid (Na-EDTA) in water (pH 7.4; central pharmacy, university hospital Düsseldorf, Germany) and incubated for 5 min. Cells were centrifuged for 5 min at 450 x g at 4°C. and supernatant was discarded. The pellet was resuspended in 3 ml of cold DPBS. To remove debris, 1 ml of debris removal solution (#cat130-109-398, Miltenyi Biotec) was added and carefully overlaid with 4 ml of cold DPBS. Samples were centrifuged for 10 min at 3000 x g at 4°C leading to the formation of three phases. The upper two phases containing DPBS and debris were removed. Remaining cells in the lowest phase were resuspended in cold DPBS and again centrifuged for 10 min at 3000 x g at 4°C. After discarding the supernatant, cells were resuspended in 1 ml of cold DPBS and stored on ice.

3.8 Sequencing experiments

Three different sequencing techniques were used in this work. scRNA-seq and CITE-seq were performed to investigate the cell heterogeneity in AAA progression. scRNA-TCR-BCR-seq was used to analyze T and B cell clonality in AAA. CITE-seq was additional used to compare the immune response in MI, atherosclerosis and AAA, and to examine mRNA-protein-correlation. Aortae of C57BL/6J mice harvested at day 3, 7, 14 and 28 after PPE surgery and at day 3 and 28 after sham surgery were subjected to scRNA-seq as well as scRNA-TCR-BCR-seq. Pooled non-perfused aortae of non-operated mice served as additional controls. (Table 1). For CITE-seq, aneurysms were harvested at day 3, 7 and 14 after PPE surgery, aortae with atherosclerotic lesions were harvested from old *ApoE*$^{-/-}$ mice and hearts were removed at day 1 and 5 after I/R surgery (Table 2).

3.8.1 Staining and sorting of single cells for scRNA-seq and TCR-BCR-seq

Cell suspensions of aortae were transferred to a 96-well plate and centrifuged for 5 min at 500 × g and 4°C. Cells were stained with a staining mix containing Fc receptor blocker

(cat#101320, TruStain FcX™, BioLegend, 1:100), viability stain (cat#423102, Zombie Aqua™ Fixable Viability Kit, BioLegend, 1:500), CD45-APC/cyanine 7 (#cat103116, BioLegend, clone 30-F11, 1:200), TER-119-FITC (#cat116206 , BioLegend, clone TER-119, 1:200), and C0443 CD41 (cat#133943, BioLegend, Barcode Sequence ACTTGGATGGACACT, 1:1400) in DPBS. In addition, an individual TotalSeq Hashtag antibody (BioLegend, TotalSeq™-C) was added to the single-cell suspension of each aortic tissue (Table 1). The hashtag antibodies allow the combination of several samples in the same 10X sequencing run and are needed to demultiplex cells from individual samples. Ten samples were labeled with an antibody from the TotalSeq™-C series. Two additional hashtag antibodies were built by combining the antibodies MHC I-biotin (BioLegend, clone 28-8-6) and CD45-biotin (BioLegend, clone 30-F11) with the streptavidin-conjugated barcodes TotalSeq™ C971 or C972 (Table 1). The samples were stained with the staining mix and hashtag antibodies for 15 min at room temperature (RT) in the dark. After centrifugation (5 min, 500 × g, 4°C), the supernatant was discarded, and cells were resuspended in MACS buffer (cat#130-091-221, Miltenyi Biotec) for following cell sorting. Cell sorting was performed on a MoFlo XDP (Beckman Coulter, Krefeld, Germany) with assistance from Dr. Katarina Raba at the Core Flow Cytometry Facility at the Institute for Transplantation Diagnostics and Cell Therapeutics of the university hospital Düsseldorf. From each aortic suspension, up to 3000 living $CD45^+$ cells and 3000 living $CD45^-$ cells were collected. If the corresponding cell count from one suspension was not reached, this was compensated by collecting more cells from another suspension (Table 1). All collected cells were combined into one reaction tube and centrifuged for 5 min at 500 × g at RT. The supernatant was removed, and cells were resuspended in MACS buffer (#cat130-091-221, Miltenyi Biotec). Viability and number of cells was examined using the BD Rhapsody™ Scanner (DC, Becton Dickinson GmbH, Heidelberg, Germany). Recounting of the cells confirmed approximately 60000 living cells that were subjected to scRNA-seq and TCR-BCR-seq.

Table 1: Overview of mice used for scRNA-seq and TCR-BCR-seq. For each mouse the time point, the used hashtag antibody, the sequencing run and the number of collected immune ($CD45^+$) and non-immune ($CD45^-$) cells are listed.

Mouse	Time point	Hashtag antibody	Sequencing run	Number of $CD45^+$ cells	Number of $CD45^-$ cells
#1	sham d28	C0301 cat# 155861	1	747	3000
#2	sham d28	C0302 cat# 155863	1	2211	3000
#3	d28	C0303 cat# 155865	1	3000	3000
#4	d28	C0304 cat# 155867	1	3450	3000

#5	d14	C0305 cat# 155869	1	3450	3000
#6	d14	C0306 cat# 155871	1	3450	3000
#7	d7	C0307 cat# 155873	1	3450	3000
#8	d7	C0308 cat# 155875	1	3450	3000
#9	d3	C0309 cat# 155877	1	3450	3000
#10	d3	C0310 cat# 155879	1	3450	3000
#11	sham d3	C0971 cat# 405271 MHC I-Biotin cat# 114603 CD45-Biotin cat# 103103	1	3000	3000
#12	sham d3	C0972 cat# 405273 MHC I-Biotin cat# 114603 CD45-Biotin cat# 103103	1	3000	3000
#13	sham d28	C0301 cat# 155861	2	2	55
#14	non-perfused	C0302 cat# 155863	2	139	2515
#15	d28	C0303 cat# 155865	2	2150	1886
#16	d28	C0304 cat# 155867	2	2240	2450
#17	d7	C0305 cat# 155869	2	8500	6800
#18	d7	C0306 cat# 155871	2	8500	6800
#19	d7	C0307 cat# 155873	2	8500	6800
#20	d3	C0308 cat# 155875	2	5170	818
#21	d3	C0309 cat# 155877	2	1325	246
#22	d3	C0310 cat# 155879	2	5170	1270
#23	sham d3	C0971 cat# 405271 MHC I-Biotin cat# 114603 CD45-Biotin cat#103103	2	365	478
#24	non-perfused	C0972 cat#405273 MHC I-Biotin cat#114603 CD45-Biotin cat#103103	2	149	2670

3.8.2 Staining and sorting of single cells for CITE-seq

For CITE-seq cells were stained with a staining mix containing Fc receptor blocker (cat#101320, TruStain FcX™, BioLegend, 1:100), CD45-APC/cyanine 7 (cat#103116, BioLegend, clone 30-F11, 1:200) and TotalSeq™-A Mouse Universal Cocktail, V1.0 (cat#199901, BioLegend, 1:1200). The TotalSeq™-A Mouse Universal Cocktail, V1.0

contains 119 antibodies against cell surface antigens of immune cells and 9 isotype control antibodies (supplementary table 1). An individual TotalSeq^{TM}-B hashtag antibody (BioLegend) or a cell multiplexing oligo (CMO) sequence (10X Genomics) was added to each sample for multiplexing (Table 2). Samples were stained with the staining mix and hashtag antibodies for 15 min at RT in the dark. After centrifugation (5 min, 500 × g, 4°C), the supernatant was discarded and the cells were resuspended in MACS buffer (#cat130-091-221, Miltenyi Biotec). 4′,6-Diamidin-2-phenylindol (DAPI, cat#62248, Thermo Fisher Scientific, 1 ng/ml) was added to the cells and cells were sorted using a MoFlo XDP. Cell sorting was performed with assistance from Katarina Raba at the Core Flow Cytometry Facility at the Institute for Transplantation Diagnostics and Cell Therapeutics of the university hospital Düsseldorf. For each sample approximately 6700 CD45$^+$ cells were collected to reach a total number of approximately 60,000 cells. All cells were combined into one reaction tube and centrifuged for 5 min at 500 × g at RT. The supernatant was removed, and the cells were resuspended in MACS buffer (#cat130-091-221, Miltenyi Biotec). Viability and number of cells was examined using the BD Rhapsody-System. Approximately 40,000 cells were loaded on the 10X chip for CITE-seq.

Table 2: Overview of mice used for CITE-sequencing. For each mouse the condition, the used hashtag antibody and the number of collectec CD45$^+$ immune cells are listed.

Mouse	Condition	Hashtag antibody	Number of CD45$^+$ cells
#1 #2	AAA d3	B0305 cat# 155839	6700
#3 #4	AAA d7	B0304 cat#155837	6700
#5 #6	AAA d14	B0301 cat#155831	6700
#7 #8	I/R d1	CMO311 cat#2000317	6700
#9 #10	I/R d5	B0309 cat#155847	6700
#11 #12	*Apoe*$^{-/-}$	CMO310 cat#2000316	6700
#13 #14	*Apoe*$^{-/-}$	B0306 cat#155841	6700

3.8.3 Generation of single-cell library

Single-cell libraries were generated with the 10X Chromium Controller system utilizing the Chromium Next GEM Single Cell 5′ Kit v2 (cat#CG000331, 10X Genomics, Pleasanton, CA, USA) according to the instructions of the manufacturer. Sequencing was carried out on a NextSeq 550 system (Illumina Inc. San Diego, CA, USA) with a mean sequencing depth of ~50,000 reads/cell for gene expression and ~20,000 reads/cell for the TotalSeq-ADT library. The T cell and B cell libraries and the hashtag libraries were sequenced at ~5000 reads/cells. Library generation was performed by Dr. Tobias Lautwein at the Genomics & Transcriptomics Laboratory in Düsseldorf.

3.8.4 Processing of 10X genomics single-cell data

Raw sequencing data was processed using the 10X Genomics CellRanger software (v6.0.2). Raw BCL files were demultiplexed and processed to Fastq files using the CellRanger mkfastq pipeline. Alignment of reads to the mm10 genome and the corresponding VDJ gene references and UMI counting was performed via the CellRanger multi pipeline to generate a gene–barcode matrix.

3.8.5 Preprocessing of scRNA- and CITE-seq data

Data was analyzed using the R package Seurat v4.[141] First, the hashtag library was added as assay to the metadata of the RNA library. For CITE-seq, the ADT library, which contains the protein expression data, was additional added as assays to the metadata of the RNA library. Cells with less than 200 RNA counts or more than 30% mitochondrial RNA were excluded. Data were normalized with the function *NormalizeData()* with the normalization method *LogNormalize* and a factor of 10,000. In this normalization step feature counts for each cell were divided by the total counts for that cell multiplied by the scale.factor (10000) and then natural-log transformed using log1p. *ScaleData()* was used to scale the expression level for each feature by dividing the centered feature expression levels by their standard deviations. Principal component analysis (PCA, 75 dimensions), variable gene finding, cell clustering, and uniform manifold approximation and projection (UMAP) dimensional reduction (30 dimensions) were performed. Doublets were removed with DoubletFinder v2.0[142] and cells with positivity for more than one hashtag were also excluded.

3.8.6 Identification of cell clusters by scRNA- and CITE-seq

Immune cell clusters present in the CITE-seq dataset were assigned based on mRNA and protein expression (Table 3). False-positive antibody bindings were identified and excluded using nine isotype controls. Neutrophils, macrophages, DCs, NK cells, T cells and B cells were identified in the CITE-seq data (Table 3).

In the scRNA-seq dataset immune cells were identified by expression of *Ptprc* (encoding for CD45) and non-immune cells by absence of *Ptprc* expression. Based on the expression of specific mRNAs, *Ptprc*-negative cells were identified as endothelial cells, VSMCs, fibroblasts and myofibroblasts (Table 3). The obtained immune cell clusters were assigned as neutrophils, macrophages, DCs, B cells, T cells and NK cells (Table 3). Next, neutrophils, macrophages/DCs and T/B/NK cells were bioinformatically selected and separately reclustered (30 dimensions) to obtain a more detailed cluster resolution. *FindAllMarkers()* was used to find differentially expressed genes for each subcluster. Clusters that accounted for less than 0.5% of all immune cells were excluded from further analysis.

To detect the identified subpopulations also in the CITE-seq data, a label transfer from the scRNA-seq dataset to the CITE-seq dataset was performed to annotate the cells. *FindTransferAnchors()* was used to find a set of anchors between both datasets, which were used to transfer the cell annotations. During the label transfer each cell received a prediction score, which was used to validate the accuracy of the label transfer.

The *Seurat* functions *VlnPlot(), FeaturePlot(), RidgePlot()* and *DotPlot()* were used to visualize the normalized and log-transformed expression of genes and proteins.

Table 3: mRNAs and proteins that were used to identify different cell types by scRNA- and CITE-seq

Cell type	mRNA	protein
Neutrophils	*S100a8, S100a9*	CD11b, Ly6G
Macrophages	*Cd14*, *Cd68*, *Lyz2*, *Itgam*, *Adgre1*	CD11b, CD68, F4/80
DCs	*Itgax, Cd209a*, *Ccr7*	CD11c
NK cells	*Nkg7, Gzma*, *Klrb1c*	NK1.1
T cells	*Cd3d, Cd3e, Cd3g*, *Cd28*	CD3
B cells	*Cd19, Cd79a*, *Cd79b*	CD19, CD79b
Endothelial cells	*Cdh5, Pecam1, Fabp4*	-
VSMCs	*Myh11, Tagln, Acta2*	-
Fibroblasts	*Dcn, Col1a1, Col3a1*	-
Myofibroblasts	*Cthrc1*	-

3.8.7 Analysis of gene ontology, pathway responsive genes and scoring of biological processes

Gene Ontology (GO) analysis was performed using the R package *ClusterProfiler v.4.12.0.*[143, 144] Function *enrichGO()* was used to find enriched gene sets for each cluster or disease based on the database *org.Mm.eg.db v.3.19.1.*[145] Benjamini and Hochberg's method was applied to adjust the resulting p-values. *pvalueCutoff()* was set to 0.05, *qvalueCutoff()* was set to 0.2.

Progeny v1.26.0[146] was used to infer the activity of 14 pathways based on consensus gene signatures that were obtained from perturbation experiments.[146]

To further characterize the cell clusters, a score of inflammation and proliferation was calculated by averaging the expression of gene signatures related to these processes. 197 inflammation-related genes were derived from GSEA MM3890[147] and 312 genes associated with leukocyte proliferation were obtained from GSEA MM9599 (GO:0070663).

3.8.8 Cell-cell communication analysis

For the inference and analysis of cell–cell communication CellChat v2.1.2[148, 149] was used. CellChat infers cell-cell communication based on gene expression data and the ligand-receptor interaction database CellChatDB.mouse. In short, CellChat identified differentially over-expressed ligands and receptors for each cell group utilizing Wilcoxon rank sum test. Each interaction was assigned with a probability score that is modeled by the law of mass action based on the average expression values of a ligand by one cell group and that of a receptor by another cell group, as well as their cofactors. In the analysis presented in this work the effect of cell proportion in each cell group was considered for the probability calculation. Then significant interactions were identified with a permutation test.

3.8.9 Bioinformatic modeling of a flow cytometric gating strategy to identify and sort IFNICs

The macrophage populations present in the CITE-seq dataset were bioinformatically isolated. *FindAllMarkers()* was used to identify marker proteins for each subpopulation. Proteins that were suitable to distinguish IFNICs from one or more other subsets were used to bioinformatically model a gating strategy for flow cytometry. The gating was simulated by defining a threshold for the expression level and continuing the analysis only with cells that were above the threshold. After each subdivision step the gating efficiency was evaluated visually by a UMAP-plot. For better comparison to flow cytometric gating, gating of all immune cells present in aneurysmal tissue in the CITE-seq data was additional performed by displaying the log transformed expression in bi-axial gating plots and selecting the cells using the function *CellSelector()*.

3.8.10 scRNA-TCR-BCR-sequencing analysis

T cells were defined by expression of *Cd3e*, *Cd3d*, *Cd3g*, and *Cd28*. B cells were defined by the expression of *Cd19*, *Cd79a*, and *Cd79b*. T and B cells were isolated bioinformatically and merged with the preprocessed scRNA-TCR-BCR-seq data.

Preprocessing of the scRNA-TCR-BCR-seq data included quality control and adding the library of the hashtag antibodies. Only receptors with exactly one alpha/heavy chain and one beta/light chain were used for analysis. Sequences of single chains, more than two chains per receptor, and non-matching chains were excluded from the analysis. The hashtag information was merged with the 10X output file to enable the assignment of TCRs and BCRs to the different mice. The Immunarch package v 0.6.9[150] was used to analyze CDR3

length distribution, clone abundance, repertoire overlap, germline gene V-gene usage, clonal expansion, and diversity estimation. We defined a clone as a set of T or B cells expressing the same receptor that consists of the same V-, D-, and J-genes and encodes an identical CDR3 nucleotide sequence. Two-sample permutation-based Kolmogorov–Smirnov test was used to compare CDR3 length distributions with the function *ks_test*() from R package "twosamples". Bonferroni correction was used for multiple comparisons. To compare the correlation strength of the V-gene usage in the TCR alpha chain with the V-gene usage in the TCR beta chain, the individual correlation coefficients were compared with a two-tailed Mann–Whitney U test.

3.8.11 Database comparison (TCR and BCR)

The two databases vdjdb[151] (version from 30.03.2022) and McPAS[152] (version from 05.08.2021) were used for comparison with the AAA data. The databases contain TCR CDR3 sequences from different species for various diseases. Only murine CDR3 sequences were used for comparison and sequences with less than 4 amino acids and diseases with less than 5 CDR3 sequences were excluded. Categories and diseases that made no sense for our analysis were removed ("HomoSapiens", "GallusGallus", "Synthetic", "MusMusculus"). For vdjdb 5206 sequences and for McPAS 3530 sequences remained for analysis. After merging the two databases and filtering for unique CDR3 sequences, 4331 CDR3 sequences remained for comparison with the AAA data set. One-sided Fisher's exact test with Bonferroni or Benjamini-Hochberg correction was performed using R v4.0 software to examine the overrepresentation of TCR clones in our data set that are associated with diseases or antigens according to the two databases. Differences with $p < 0.05$ were considered significant.

3.9 Flow cytometry

Two different antibody panels were used to stain aortic cells (Table 4). The "differential leukocyte panel" was used to analyze the distribution of neutrophils, macrophages, NK cells, T cells and B cells in aneurysmal tissue. The CD40 panel was used to examine CD40 expression on neutrophils, macrophages and B cells.

For flow cytometric analysis, 100 µl of single-cell suspensions obtained from aortic tissue were transferred into a 96-well v-bottom plate. CountBright™ Absolute Counting Beads (cat#C36950, Thermo Fisher Scientific) were added to each sample stained with the "Differential leukocyte panel" to determine cell counts after processing. The cells were

centrifuged for 5 min at 500 x g and 4°C and stained with Fc receptor blocker (cat#101320, TruStain FcX™ anti-mouse CD16/32, BioLegend, 1:100) and viability stain (cat#423102, Zombie Aqua™ Fixable Viability Kit, BioLegend, 1:500) at RT for 10 min in the dark. After centrifugation (5 min, 500 x g, 4°C), supernatant was discarded and cells were stained for 20 min at RT in the dark with the "Differential leukocyte panel" or the "CD40 panel" (Table 4). Cells were centrifuged (5 min, 500 × g, 4°C) and resuspended in DPBS supplemented with 0.5% bovine serum albumin.

Table 4: Fluorochrome-labelled antibodies used for flow cytometric analysis. The table shows the antibodies with their fluorochrome, the clone, the dilution, the cat#, the manufacturer and in which panel the antibody was used.

Antibody-Conjugate	Clone	Dilution	Cat#	Manufacturer	Panel
CD45-V450	30-F11	1:200	103133	BioLegend	Both
CD11b-APC-Cy7	M1/70	1:200	101225	BioLegend	Both
Ly6C-PE	HK1.4	1:133.3	128007	BioLegend	Both
Ly6G-PerCP-Cy5	1A8	1:100	127615	BioLegend	Both
CD19-FITC	MB19-1	1:100	101505	BioLegend	Both
NK1.1-PE-Cy7	PK136	1:200	108713	BioLegend	Differential leukocyte panel
CD3-APC	145-2C11	1:200	100312	BioLegend	Differential leukocyte panel
CD40-APC	3/23	1:80	124611	BioLegend	CD40 panel

The samples were acquired with the BD FACSVerse™ Cell Analyzer (BD, Heidelberg, Germany), and data were analyzed using FlowJo software v10.5.3 (Becton Dickenson GmbH). Figure 8 shows the gating strategies to analyze immune cell numbers (A) and CD40 expression (B) on different immune cells in aortic tissue. Absolute cell numbers were calculated using the following formula according to the user guide of the CountBright™ Absolute Counting Beads:

$$Absolute\ Count\ \left(\frac{cells}{\mu l}\right) = \frac{(Cell\ Count\ x\ Counting\ beads\ volume)}{(Counting\ beads\ count\ x\ Cell\ volume)}\ x\ Counting\ beads\ concentration\ (\frac{beads}{\mu l})$$

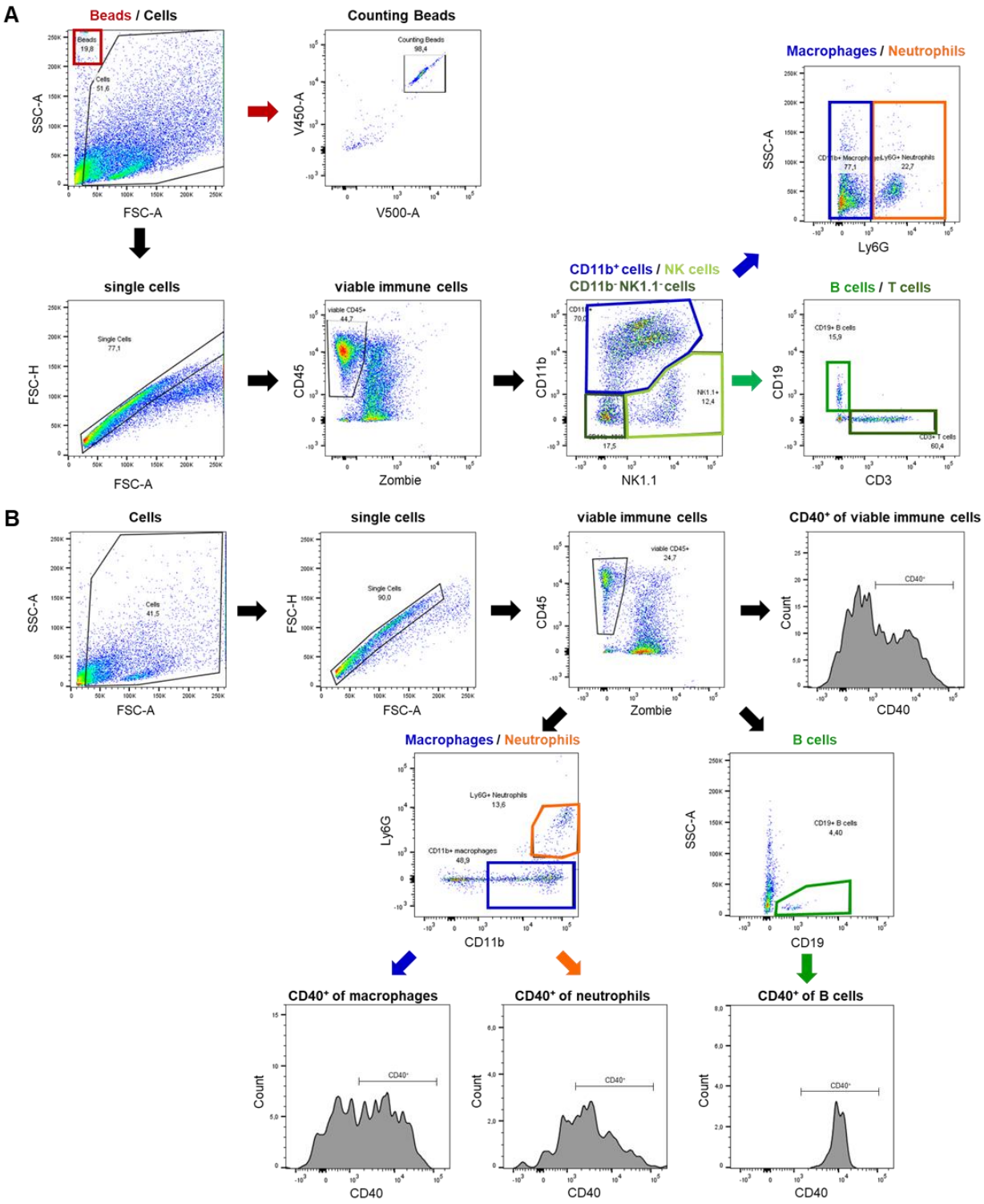

Figure 8: Flow cytometric gating strategies to measure the number of immune cells and their CD40 expression in aortic tissue. A: Representative gating strategy for the differential leukocyte panel. Counting beads were identified using forward- and sideward scatter-area (FSC-A, SSC-A) and their positivity for V450 and V500. Single cells were detected using forward scatter-height (FSC-H) and FSC-A. Viable leukocytes were determined by a positive signal for $CD45^+$ and a negative signal for the viability dye Zombie. Viable leukocytes where then distinguished in neutrophils ($CD11b^+Ly6G^+$), macrophages ($CD11b^+Ly6G^-$), NK cells ($NK1.1^+$), B cells ($CD19^+$) and T cells ($CD3^+$). **B:** Representative gating strategy for the CD40 panel. Single cells were again detected using FSC-H and FSC-A. Viable cells, neutrophils, macrophages and B cells were identified by the same protein expression patterns that were used in the differential leukocyte panel. Then, the CD40 expression of the different cell types was determined by measuring the mean fluorescence intensity (MFI).

3.9.1 IFNIC panel

To detect IFNIC macrophages in the aortic tissue, single-cell suspensions were stained with the IFNIC panel (Table 5) and measured by flow cytometry. First, cells were transferred to a FACS tube and CountBright™ Absolute Counting Beads (cat#C36950, Thermo Fisher Scientific) were added. Then the samples were centrifuged (500 x g, 5 min, 4°C) and the supernatant was discarded. The cell pellet was stained with Fc receptor blocker (cat#101320, TruStain FcX™ anti-mouse CD16/32, BioLegend, 1:100) and viability stain (cat#C36628, Viakrome808 fixable viability dye, Beckman Coulter, 1:40) at RT for 20 min in the dark. Cells were centrifuged (500 x g, 5 min, 4°C), supernatant was removed and cells were incubated with the IFNIC panel for 20 min at RT in the dark. After that, cells were centrifuged (5 min, 500 × g, 4°C) and resuspended in DPBS with 0.5% bovine serum albumin. Samples were acquired with the CytoFLEX LX flow cytometer equipped with basic optical filter setup (Beckman Coulter) and analyzed with the FlowJo software v10.5.3 (Table 5). Absolute cell numbers were calculated according to the user guide of the CountBright™ Absolute Counting Beads as mentioned before. The IFNIC panel was established by master student Noura Kharrat under my supervision.

Table 5: Antibodies used for the IFNIC panel. The table shows the antibodies with their fluorochrome, the clone, the dilution, the cat# and the manufacturer.

Antibody-Conjugate	Clone	Dilution	Cat#	Manufacturer
CD45-BUV496	30-F11	1:40	364-0451-80	Thermo Fisher Scientific eBioscience™
CD11b-BUV661	M1/70	1:200	376-0112-82	Thermo Fisher Scientific eBioscience™
CD3-BV510	17A2	1:200	100234	Biolegend
CD11c-BV510	N418	1:200	117337	Biolegend
CD19-BV510	6D5	1:100	115546	Biolegend
NK1.1-BV510	PK136	1:100	108738	Biolegend
Ly-6A/E-BV605	D7	1:200	108133	Biolegend
CD40-BV785	3/23	1:200	124645	Biolegend
CD36-Alexa488	HM36	1:100	102608	Biolegend
Ly6G-PerCP-Cy5	1A8	1:200	127616	Biolegend
Ly6C-PE	HK1.4	1:80	128007	Biolegend
IFNAR1-APC	MAR1-5A3	1:200	127314	Biolegend

3.9.2 Sorting of IFNIC macrophages

For sorting, the cells were stained with the IFNIC panel as described above, but instead of Viakrome808 Zombie NIR™ Fixable Viability Kit (cat#4231025, BioLegend) was used as viability dye. Sorting of the cells was performed with a FACS Symphony S6 (BD) by Dr. Stefanie Lichtenberg and Dennis Müller (Core Facility Flow Cytometry, University hospital Düsseldorf). Sorted cells were collected into Eppendorf tubes containing RLT lysis buffer (cat#1015762, Qiagen, Hilden, Germany).

3.10 RNA Isolation, reverse transcription, pre-amplification and qPCR

Quantitative polymerase chain reaction (qPCR) was used to quantify the expression of type-I IFN signature genes in different macrophage subsets isolated from experimental AAA tissue by cell sorting.

RNA isolation of sorted cells was performed with the RNeasy® Micro Kit (cat#74004, Qiagen, Hilden, Germany) according to manufacturer's instruction. As a final step, RNA was eluted with 14 µl RNAse free water. RNA concentration was determined with the DS-11 FX spectrophotometer (DeNovix, Wilmington, USA). All samples were diluted to the lowest RNA concentration, transcribed into cDNA and amplified with the SuperScript™ IV Single Cell/LowInput cDNA PreAmp Kit (cat#11752048, ThermoFisher Scientific) according to the manufacturer's protocol. This kit enables uniform and global preamplification of full-length cDNA that can be further used for qPCR. Reverse transcription and preamplification with 11 cycles were performed on a Fast Gene Ultra Cycler Gradient FG-TC01 thermocycler (Nippon Genetics Europe, Düren, Germany). qPCR was performed with the TaqMan™ Fast Advanced Master-Mix (cat#4444557, ThermoFisher Scientific) using a Quantstudio 7 Flex real-time-PCR-system (Thermo Fisher Scientific). Interferon regulatory factor 7 (*Irf7*, cat# Mm00516793_g1, Thermo Fisher Scientific), interferon-stimulated gene 15 (*Isg15*, cat# Mm01705338_s1, Thermo Fisher Scientific), Interferon-induced protein with tetratricopeptide repeats 3 (*Ifit3*, cat# Mm01704846_s1, Thermo Fisher Scientific), C-X-C- motif chemokine 10 (*Cxcl10*, cat# Mm00445235_m1, Thermo Fisher Scientific) and *Cd40* (cat# Mm00441891_m1, Thermo Fisher Scientific) were used as target genes. Glycerinaldehyd-3-phosphat-Dehydrogenase (*Gapdh*, cat#Mm99999915_g1; Thermo Fisher Scientific) served as house-keeping gene.

3.11 Embedding and sectioning of aortae

Harvested aneurysms were fixed in 4% paraformaldehyde (cat#J61984-AP, ThermoFisher Scientific) for 1 h at RT and dehydrated in 30% sucrose (cat#S1888, Merck) in DPBS at 4°C overnight. Afterwards, aneurysms were embedded in Tissue-Tek® O.C.T. compound (cat#4583, Sakura Finetek, Amsterdam, the Netherlands) and stored at -80°C until cryo sectioning. Each aneurysm was cut into 5 µm thin sections (cryotome CM 3050 S, Leica) according to a predefined scheme. To obtain a complete overview of the entire aneurysm, sections from 16 different levels of the aneurysm are collected on four different slides (A (levels 1-4), B (levels 5-8), C (levels 9-12) and D (levels 13-16)). In order to be able to perform different histological examinations of an aneurysm, 20 such slide combinations were prepared per aneurysm. For this purpose, consecutive sections from each level were applied to 20 different slide sets. The trimming size between each layer was adjusted to the size of the aneurysms. For small aneurysms (0 – 3 mm) 100 µm were trimmed, for medium-sized aneurysms (3 – 3.5 mm) 150 µm were trimmed and for large aneurysms (> 3.5 mm) 200 µm were trimmed between the 16 layers.

3.12 Immunofluorescence co-staining

For each aneurysm the largest tissue section and the two neighboring sections were selected for immunofluorescence co-staining to evaluate immune cell numbers and their CD40 expression in aneurysmal tissue. Cryo sections were thawed for 20 – 30 min at RT and subsequently baked at 60°C for 30 min. The tissue sections were re-hydrated for 5 min in DPBS and incubated in block and permeabilization solution containing 0.5% BSA (cat#8076.3, Carl Roth GmbH, Karlsruhe, Germany), 0.1% saponin (cat#S4521, Merck) and 0.2% fish gelatine (cat#G7765, Merck) for 1 h. Afterwards sections were stained with either Ly6G (cat#551459, BD Biosciences, end concentration 5 µg/ml in blocking solution), F4/80 (cat#ab6640, Abcam, end concentration 5 µg/ml in blocking solution), CD11c (cat#14-0114-82, Thermo Fisher Scientific, end concentration 5 µg/ml in blocking solution), CD19 (cat#152402, Biolegend, end concentration 5 µg/ml in blocking solution) or CD3e (cat#553058, BD Biosciences, end concentration 10 µg/ml in blocking solution) at 4°C overnight. On the next day, tissue sections were washed three times for 3 minutes with DPBS and incubated with the corresponding secondary antibody either Donkey anti-Rat IgG (H+L) Highly Cross-Adsorbed Secondary Antibody Alexa Fluor™ 594 (cat#A-21209, Thermo Fisher Scientific, 1:1000 in DPBS) or Goat Anti-Armenian hamster IgG H&L Alexa Fluor® 568 (cat#ab175716, Abcam, 1:100 in DPBS) for 1 h at RT. After washing thrice with DPBS,

sections were incubated with either CD40 (cat#ab13545, Abcam, end concentration 10 µg/ml in blocking solution) or CD40L (#cat PA5-78983, Thermo Fisher Scientific, end concentration 10 µg/ml in blocking solution) at 4°C overnight. Tissue sections were washed three times for 3 minutes with DPBS, incubated with Goat anti-Rabbit IgG (H+L) Highly Cross-Adsorbed Secondary Antibody Alexa Fluor™ 660 (cat#A-21074, Thermo Fisher Scientific, 1:1000 in DPBS) for 1 h at RT and washed again thrice with DPBS. The autofluorescence of the tissue was quenched using the Vector® TrueVIEW™ autofluorescence quenching kit (cat#SP-8400-15, Vector Laboratories, Newark, California, USA) according to the manufacturers' instruction. This was followed by a washing step with DPBS. Tissue sections were stained with DAPI (cat#62248, Thermo Fisher Scientific, 1:1000) for one minute and mounted using ProLong™ Diamond Antifade Mountant (cat#P36961, Thermo Fisher Scientific). Immunofluorescence stainings were carried out by bachelor student Kea Mara Tönnißen under my supervision.

3.13 RNAscope®

A RNA fluorescent in situ hybridization assays (RNA FISH) was used to detect IFNIC macrophages in human and murine aneurysmal tissue sections. Double "Z" oligo RNAscope® probes were hybridize to the target RNAs *Irf7* (Mm-Irf7-C3, cat#534541-C3, ACD™ Bio-Techne, Minneapolis, Minnesota, USA) and *Adgre1* (Mm-Adgre1_C1, cat#460651, ACD™ Bio-Techne) defining IFNIC macrophages. In this assay, the signal amplification technology for RNA FISH is combined with Tyramide Signal Amplification (TSA) technology for an enhanced detection of the fluorescent-labeled target RNAs in tissue sections. The amplified RNA signal by RNAscope® probes were visualized by TSA Vivid™ fluorophores depending on the RNAscope® probe channel.

In line to the company protocol for the RNAscope® Multiplex Fluorescence Reagent Kit v2 (cat#323100, ACD™ Bio-Techne), preamplifiers, amplifiers and dyes were used regarding each specific probe channel. In short, cryo sections were baked for 30 min at 60°C and then immersed in 4% paraformaldehyde for 15 minutes at 4°C. The sections were dehydrated sequentially for 5 minutes each in 50% ethanol, 70% ethanol and twice in 100% ethanol, followed by air drying. To block tissue peroxidases, RNAscope® hydrogen peroxidase was applied to each section and incubated for 10 min at RT. Sections were washed in distilled water. For antigen retrieval, slides were transferred into pre-warmed target retrieval solution and boiled for 5 min at 98 - 102°C. After boiling, slides were rinsed in distilled water at RT, followed by a washing step in 100% ethanol, and air dried. Next, 60 µl of RNAscope® Protease III were added to each section and slides were incubated in a humidity chamber at

40°C for 30 minutes. Afterwards, the slides were washed twice with distilled water. For probe hybridization, excess liquid was removed, and 50 µl of the desired probe was applied to each section. Slides were incubated at 40°C for 3 hours. After incubation, slides were washed twice for 2 minutes in wash buffer. To amplify the probes, 60 µl of Amplifier 1 were applied to each section and incubated at 40°C for 30 minutes in a humidity chamber. Then slides were washed twice for 2 minutes with wash buffer. This procedure was repeated for Amplifiers 2 and 3, with Amplifier 3 incubated for 15 minutes. The amplification was followed by horseradish peroxidase (HRP) treatment, that was dependent on the used probe channel. The sections were covered with the appropriate HRP of the channel and incubated for 15 minutes at 40°C. After washing, the selected fluorescent dye (e.g. TSA Vivid™ Dye 520, 580 or 650, 1:750 in TSA buffer) was applied on the slide and incubated for 30 minutes at 40°C. Afterwards slides were washed two times for 2 minutes in wash buffer. Four drops of HRP blocker were added and incubated for 15 minutes at 40°C, followed by washing with wash buffer.

In addition to the RNA scopes, an antibody-based immunofluorescence staining using the macrophage marker F4/80 (cat# ab6640, Abcam, end concentration 5 µg in DPBS) and the Alexa Fluor 488 linked donkey anti-Rat IgG (H+L) secondary antibody (cat#A-21208, Thermo fisher scientific, 1:1000 in DPBS) was performed as described before. After incubation of the secondary antibody and the following washing step, the autofluorescence of the tissue was quenched using the Vector® TrueVIEW™ autofluorescence quenching kit. After washing, tissue sections were covered with mounting medium ProLong™ Diamond Antifade Mountant with DAPI (cat#P36971, Thermo fisher scientific). RNA scope staining was performed by Dr. Susanne Pfeiler.

3.14 Image acquisition and analysis

The stained tissue sections were imaged using a HC PL APO 40x/0.95 objective on a Leica DM6 B microscope equipped with a DFC9000 fluorescence camera. Images were obtained using the LASX software (Leica).

3.15 Statistical analysis

Data are presented as mean ± standard deviation (SD). Statistical analysis and graphical illustrations of data obtained from ultrasound measurements, flow cytometry, immunofluorescence staining and qPCR were performed using GraphPad Prism 8 (Graphpad Prism Inc., La Jolla, USA). Normal distribution of the data was tested using the Kolmogorov-Smirnov test. Unpaired T-test with Welch's correction was used to test for

significant differences between two groups of normal distributed data. If data was not normally distributed the unpaired Mann-Whitney (two-tailed) test was used to compare two groups. One-way analysis of variance (ANOVA) with Tukey's multiple comparisons or Kruskal-Wallis-test with Dunn's multiple comparison was used to examine the influence of one categorical independent variable on a continuous dependent variable for normally or non-normally distributed data, respectively. Two-way ANOVA with Sidak's multiple comparisons was used to examine the influence of two different categorical independent variables on a continuous dependent variable. The Log-rank (Mantel-Cox) test was performed to compare the distributions of survival of two groups. Significant differences of AAA incidence between two groups were tested with the two-sided Fisher's exact test. The incidence of an AAA/TAA or no AAA/TAA was expressed and presented as percentage. $P<0.05$ was considered as statistically significant and further significance levels were stated as *$p \leq 0.05$, **$p \leq 0.01$, ***$p \leq 0.001$, ****$p \leq 0.0001$.

4 Results

4.1 Characterization of the immune response in AAA using scRNA- and CITE-seq

4.1.1 Identification of immune cells in CVDs using CITE-seq

Inflammation plays a crucial role in CVDs. Atherosclerosis and AAA are both chronic inflammatory diseases, while MI is characterized by an acute inflammatory response. The three diseases are linked, as atherosclerosis is the major underlying cause of MI and can be a risk factor for AAA. Moreover, all three diseases share risk factors and are based on similar pathologies. CITE-seq was used to compare the different CVDs and investigate whether similar inflammatory processes and cell types are essential for the three diseases.

The workflow of the CITE-seq experiment is described in Figure 9. Previously described mouse models were used to mimic atherosclerosis, AAA and MI. Shortly before organ harvesting, mice were injected i.v. with a CD45-FITC antibody to label circulating immune cells. Atherosclerotic aortae from aged *Apoe*$^{-/-}$ mice (n = 2), aneurysmal tissue harvested at day 3 (n = 1), 7 (n = 1) and 14 (n = 1) after elastase-perfusion, and hearts removed at day 1 (n = 1) and 5 (n = 1) after ischemia reperfusion were digested into single cells. For each condition two mice were pooled. Single-cell suspensions were stained with a viability dye, CD45-APC-Cy7 as well as an individual hashtag antibody that enable unique labeling of all cells of a particular sample. Additional, cells were stained with a cocktail of 119 antibodies for CITE-seq. Only immune cells present in the tissues (CD45-APC-Cy7^{+} cells) were collected and subjected to sequencing. Thus, this dataset enables a comprehensive and parallel analysis of atherosclerosis, AAA, and MI without batch effects.

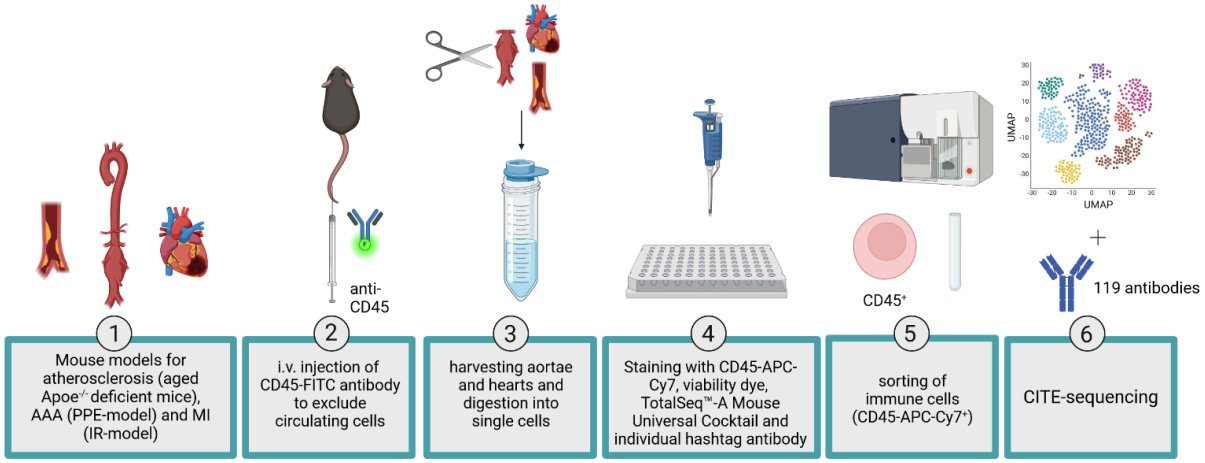

Figure 9: Experimental workflow of CITE-seq. Atherosclerotic aortae from aged *Apoe*$^{-/-}$ mice, AAA induced by elastase-perfusion and infarcted hearts induced by I/R surgery were used. Shortly before organ harvesting, mice were injected i.v. with an CD45-FITC antibody. Aortae and hearts were harvested and digested into single cells. Single-cell suspensions were stained with a viability dye, a CD45-APC-Cy7 antibody, a cocktail of 119 CITE-seq antibodies and an individual hashtag antibody. CD45-APC-Cy7^{+} immune cells were collected and subjected to CITE-seq.

After preprocessing and quality control of the CITE-seq data, 2,833 immune cells obtained from atherosclerotic aortae, 4,049 immune cells received from aneurysmal tissue and 2,400 immune cells obtained from infarcted cardiac tissue were used for analysis. CITE-seq data was used to identify different immune cell types present in atherosclerosis, AAA and MI based on marker genes and by expression of surface proteins. Neutrophils, macrophages, DCs, NK cells, T cells and B cells could be identified (Figure 10 A). Neutrophils were defined by mRNA expression of *S100a8* and *S100a9* (Figure 10 B) and by protein expression of Ly6G and CD11b (Figure 10 C). mRNA expression of *Cd14*, *Cd68*, *Lyz2*, *Adgre1* and *Itgam* was used to identify macrophages (Figure 10 B). On protein level, macrophages were confirmed by expression of CD11b, CD68, and F4/80 (Figure 10 C). DCs were defined based on mRNA expression of *Itgax* and *Cd209a* (Figure 10 B) and protein expression of CD11c (Figure 10 C). NK cells were identified by mRNA expression of *Nkg7, Gzma* and *Klrb1c* (Figure 10 B) and confirmed by protein expression of NK1.1 (Figure 10 C). mRNA expression of *Cd3d, Cd3e, Cd3g* and *Cd28* (Figure 10 B) as well as protein expression of CD3 (Figure 10 C) were used to define T cells. For identification of B cells *Cd19, Cd79a* and *Cd79b* were used as marker genes (Figure 10 B). Protein expression of CD19 and CD79b confirmed the annotation (Figure 10 C).

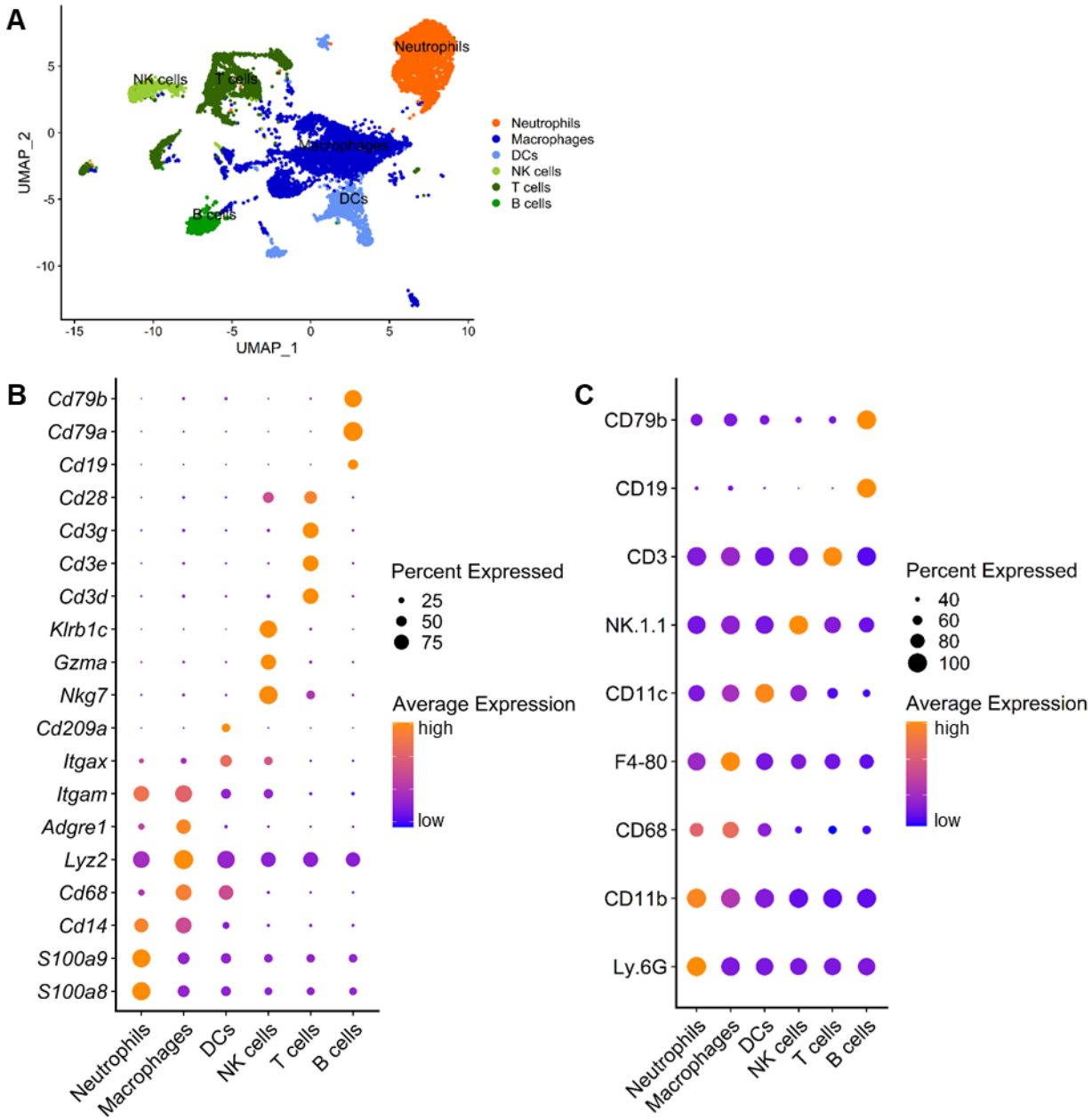

Figure 10: Identification of immune cell clusters in CVDs using mRNA and protein markers. A: UMAP-Plot displaying the main immune cell clusters present in atherosclerosis, AAA and MI. Neutrophils, macrophages, DCs NK cells, T cells and B cells were detected in aortic and cardiac tissue using CITE-seq. **B:** Dotplot diagram showing the normalized and log-transformed expression level of marker genes that were used to identify the different immune cell clusters. **C:** Dotplot diagram displaying the protein expression of surface markers used to identify different immune cell types. The color of the dot shows the expression level (orange = high expression, blue = low expression) and the size of the dot indicates the percentage of cells inside the cluster expressing the gene or protein.

4.1.2 Different cell types and pathways play a role in atherosclerosis, AAA, and MI

After identifying the immune cell types present in the three CVDs, the distribution of immune cells was compared between atherosclerosis, AAA and MI. The UMAP-plot displays cells associated with atherosclerosis in yellow, cells present in AAA in turquoise and cells detected in MI in purple (Figure 11 A). Overall, the pattern of the cell clusters appeared similar for all three disease models, but some differences could be observed. Different subsets of neutrophils were present in AAA and MI. Furthermore, two macrophage clusters appeared specific for MI and one T cell cluster was mainly present in atherosclerosis (Figure 11 A). The comparison of the proportion of immune cell types revealed that atherosclerosis was dominated by T cells that accounted for 47.8% of all immune cells, while AAA and MI were dominated by macrophages (32.4% and 48.3%) and neutrophils (27.5% and 34.8%; Figure 11 B). Atherosclerosis contained also more B cells than AAA and MI. The highest proportion of NK cells was detected in AAA (Figure 11 B). The comparison of the different time points of AAA showed an increase of T cells from 6.2% at day 3 to 28% at day 14 (Figure 11 C). In contrast, the proportion of neutrophils strongly decreased from 62.8% at day 3 to 7.4% at day 7 and 13% at day 14 of AAA formation. Macrophages, which represented the largest proportion of immune cells, accounted for 16.9% on day 3 of AAA formation, were most abundant on day 7 with 47.3%, and slightly decreased to 32.9% on day 14. Only small differences in the immune cell distribution were observed between day 1 and 5 after MI (Figure 11 C). The proportion of neutrophils decreased from 43% on day 1 to 28.6% on day 5, and instead the proportion of macrophages increased from 36.2% on day 1 to 57.3% on day 5.

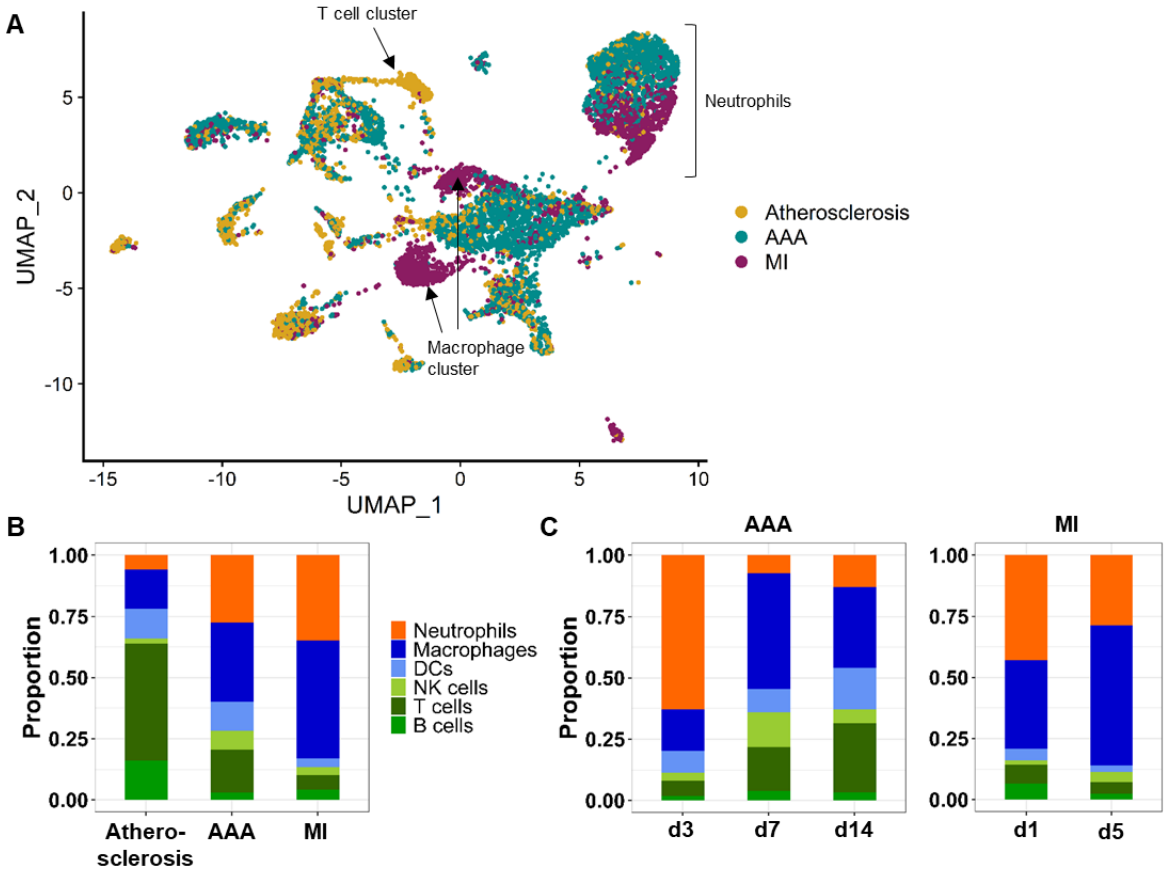

Figure 11: Differences in immune cell proportions in atherosclerosis, AAA and MI. A: UMAP-plot displaying the immune cells detected in atherosclerosis, AAA and MI. Each disease is shown in a different color. Immune cells obtained from atherosclerosis, AAA and MI are colored in yellow, turquoise and purple respectively. **B:** Proportion of neutrophils, macrophages, DCs, NK cells, T cells and B cells in atherosclerosis, AAA and MI. **C:** Percentage distribution of neutrophils, macrophages, DCs, NK cells, T cells and B cells at day 3, 7 and 14 after elastase-induced AAA formation (left panel) and at day 1 and 5 after reperfused MI (right panel).

GO analysis was performed to gain insights into the immunological processes involved in atherosclerosis, AAA and MI. Differentially-expressed genes (DEGs) were identified for each disease and used to find enriched gene sets that are associated with biological processes. In comparison to AAA and MI, atherosclerosis contained enriched gene sets associated with synapse translation, lymphocyte and T cell differentiation, antigen receptor-mediated signaling pathway, as well as positive regulation of cell activation (Figure 12). Genes involved in regulation and activation of the innate immune response were enriched in AAA. In addition, genes associated with pattern recognition receptor signaling pathway, cytokine-mediated signaling pathway and extrinsic apoptotic signaling pathway were enhanced in AAA. MI showed predominantly an enrichment of genes associated with immune cell migration, chemotaxis and regulation of the inflammatory response. Genes involved in response to molecule of bacterial origin and lipopolysaccharide were also enhanced (Figure 12).

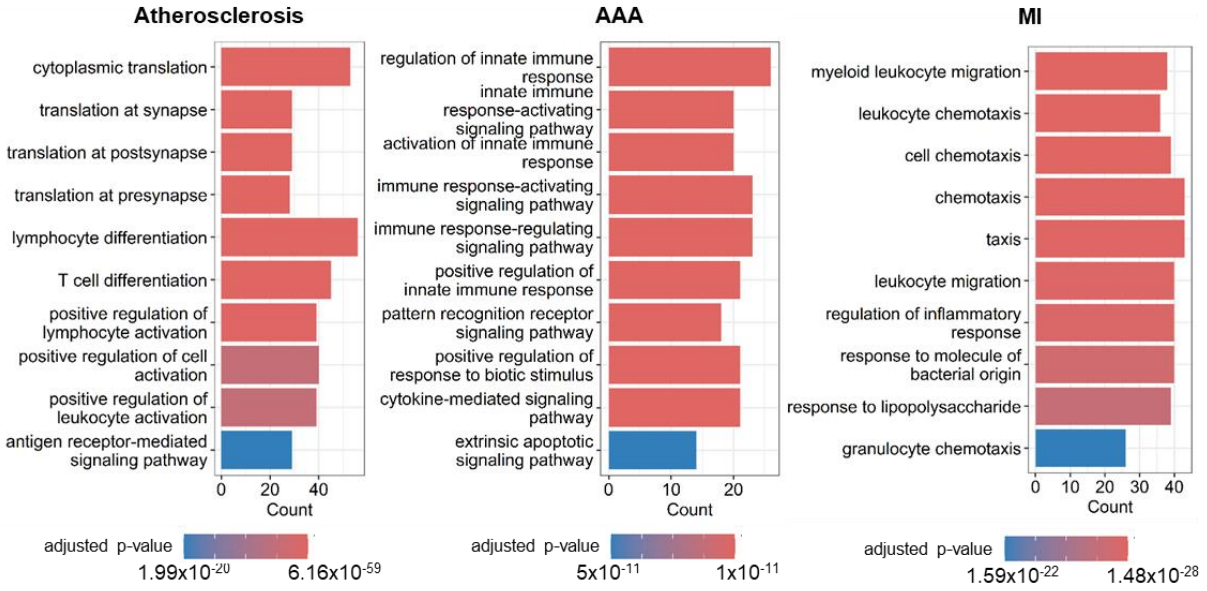

Figure 12: Upregulated biological processes in atherosclerosis, AAA and MI. Bar plots displaying the top ten enriched gene ontology (GO) terms for atherosclerosis, AAA and MI. The GO terms are shown on the y-axis and the gene count is displayed on the x-axis. The color code indicates the adjusted p-value.

4.1.3 Characterization of the immune response in AAA progression

Even though, CITE-seq revealed differences in immune cell distribution in all three investigated CVDs, this work mainly focuses on the role of different immune cell types and signaling pathways in the development and progression of AAA. To characterize the immune response at different stages of AAA, the general distribution of several immune cell types was investigated 3, 7, 14 and 28 days after elastase-induced AAA formation using flow cytometry and immunofluorescence stainings. Ultrasound imaging was performed to monitor the development of AAA. The absolute number of infiltrated leukocytes, neutrophils, macrophages, NK cells, B cells and T cells was assessed with flow cytometry. Immunofluorescence staining were additionally used to count and localize neutrophils, macrophages, DCs, T cells and B cells in the aneurysmal tissue. Furthermore, scRNA-sequencing was performed to investigate the immune response in different stages of elastase-induced AAA progression in more detail by characterization of subpopulations, analysis of signaling pathways and investigation of cell-cell communication patterns.

Ultrasound measurements showed a significant increase in aortic diameter of aortae perfused with elastase compared to control aortae perfused with saline 3, 7, 14 and 28 days after the surgery (Figure 13). Baseline measurements revealed an average diameter of 0.7 mm for healthy aortae. AAA was defined as an increase in aortic diameter of at least 1.5 fold. In saline-perfused aortae no AAA development was observed, although a slight increase in aortic diameter was measured compared to baseline. Elastase-perfused aortae already

showed a significant larger aortic diameter than saline-perfused aortae after 3 days. However, a 1.5-fold dilation of the aorta was first reached at day 7. The aortic diameter increased further from day 7 to day 28. In detail, elastase-perfusion led to an average aortic diameter of 0.99 mm (fold change: 1.41) on day 3, 1.17 mm (fold change 1.67) on day 7, 1.21 mm (fold change 1.73) on day 14 and 1.34 mm (fold change 1.91) on day 28.

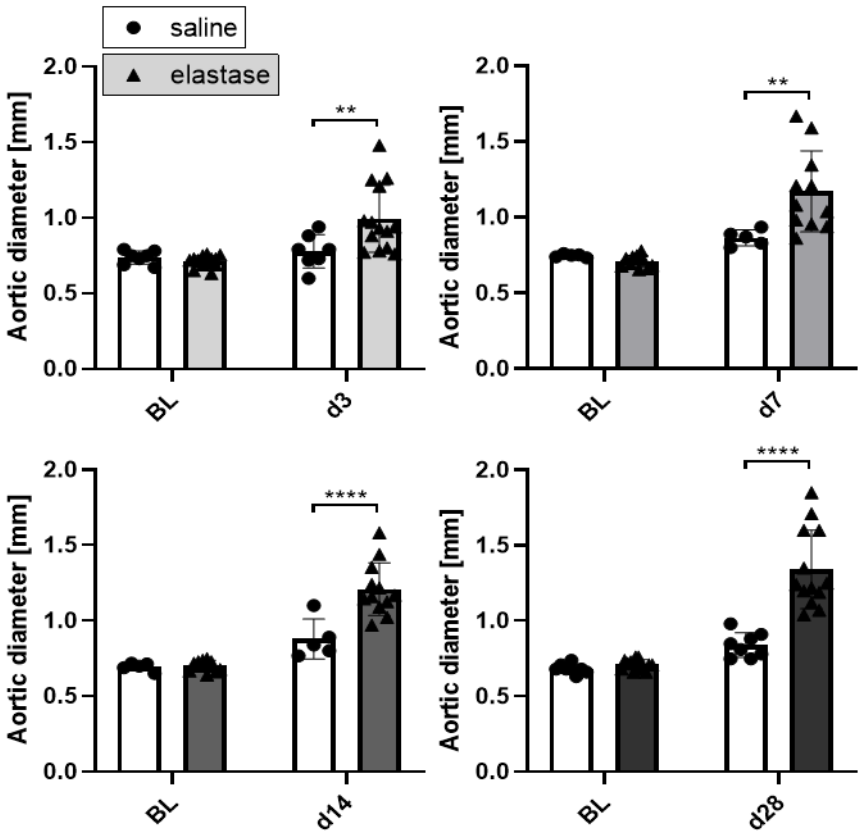

Figure 13: Analysis of abdominal aortic diameter using ultrasound measurement baseline (BL) and 3, 7, 14 and 28 days post saline or elastase perfusion of the aorta. AAA was defined as an increase in aortic diameter of at least 1.5-fold. Two-way ANOVA with Sidak's multiple comparison test. **p<0.01, ****p < 0.0001.

Flow cytometric analysis of aortic tissue revealed a significant increase of $CD45^+$ immune cells 3, 7, 14 and 28 days after elastase perfusion compared to saline perfusion (Figure 14 A). The highest immune cell infiltration in saline-perfused aortae was observed after 3 days and decreased over time, indicating that the surgery itself triggers an inflammatory reaction. The highest number of immune cells in aneurysmal tissue was detected 7 days after AAA induction and the absolute number of leukocytes was significantly higher on day 7 compared to day 28 (Figure 14 B). Neutrophils (Figure 14 D), macrophages (Figure 14 E), NK cells (Figure 14 F), T cells (Figure 14 G) and B cells (Figure 14 H) also reached the highest cell number in aneurysmal tissue 7 days after elastase perfusion. Overall, macrophages were the most abundant immune cell type in AAA (Figure 14 C). Three days after elastase perfusion

the infiltrated immune cells in aneurysmal tissue encompassed mainly macrophages and neutrophils, whereas NK, B and T cells were barely abundant. On day 7 and 14 a strong infiltration of all immune cell types was observed. The least inflammation was observed 28 days after elastase-induced AAA formation. The detected immune cells on day 28 were predominantly macrophages and lymphocytes, mainly T cells (Figure 14 C-H).

For each embedded and sectioned AAA, the tissue section with the largest dilation was identified and selected for immunofluorescence staining together with adjacent sections. In total, four consecutive tissue sections of each AAA, harvested 3, 7, 14 or 28 days after elastase-induced AAA formation, were stained for neutrophils, macrophages, DCs, T cells and B cells. The average number of cells counted in all four sections was calculated. Consistent with the flow cytometry results, the highest number of neutrophils (Figure 15 A), macrophages (Figure 15 B), DCs (Figure 15 C), T cells (Figure 15 D) and B cells (Figure 15 E) was found 7 days after elastase-induced AAA formation. The number of B cells was even significantly higher at day 7 compared to all other time points (Figure 15 E). From day 14 to day 28 the number of B cells also increased significantly. Overall macrophages and neutrophils were the most abundant immune cells (Figure 15 A+B). The representative images of immunofluorescence stainings showed that the immune cells mainly accumulate in the adventitia (Figure 15 A-E). Neutrophils were also found in the media (Figure 15 A). DCs (Figure 15 C) and B cells (Figure 15 E) seemed to form clusters in specific areas of the AAA, while the other cells were distributed over the whole aneurysm.

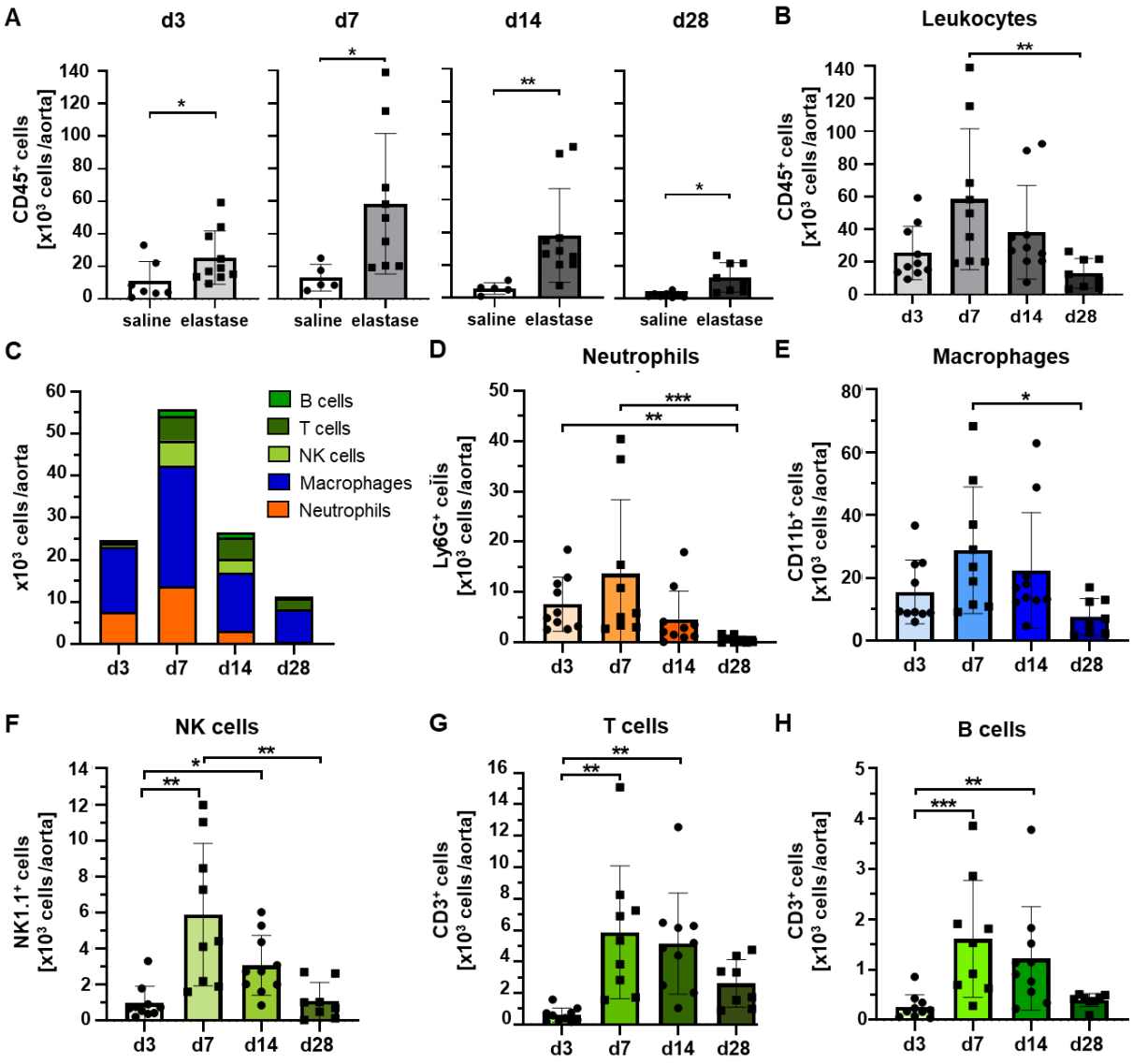

Figure 14: Flow cytometric analysis of the immune cell distribution in aortic tissue from mice 3, 7, 14 and 28 days after saline or elastase perfusion of the aorta. **A:** Absolute number of CD45$^+$ immune cells in the aortic tissue 3, 7, 14 and 28 days after elastase perfusion compared to saline perfusion. Unpaired T-test with Welch's correction or Mann Whitney test. **B:** Absolute number of CD45$^+$ immune cells at day 3, 7, 14 and 28 after elastase perfusion. Kruskal-Wallis-test with Dunn's multiple comparison. **C:** Stacked bar plot presenting the average number of neutrophils, macrophages, NK cells, T cells and B cells at day 3, 7, 14 and 28 after elastase-induced AAA formation. **D-H:** Absolute cell numbers of neutrophils **(D)**, macrophages **(E)**, NK cells **(F)**, T cells **(G)** and B cells **(H)** in aortic tissue at day 3, 7, 14 and 28. Statistical analyses were performed using one-way ANOVA with Tukey's multiple comparison or Kruskal-Wallis-test with Dunn's multiple comparison. Data are presented as Mean±SD. *p<0.05, **p<0.01, ***p < 0.001.

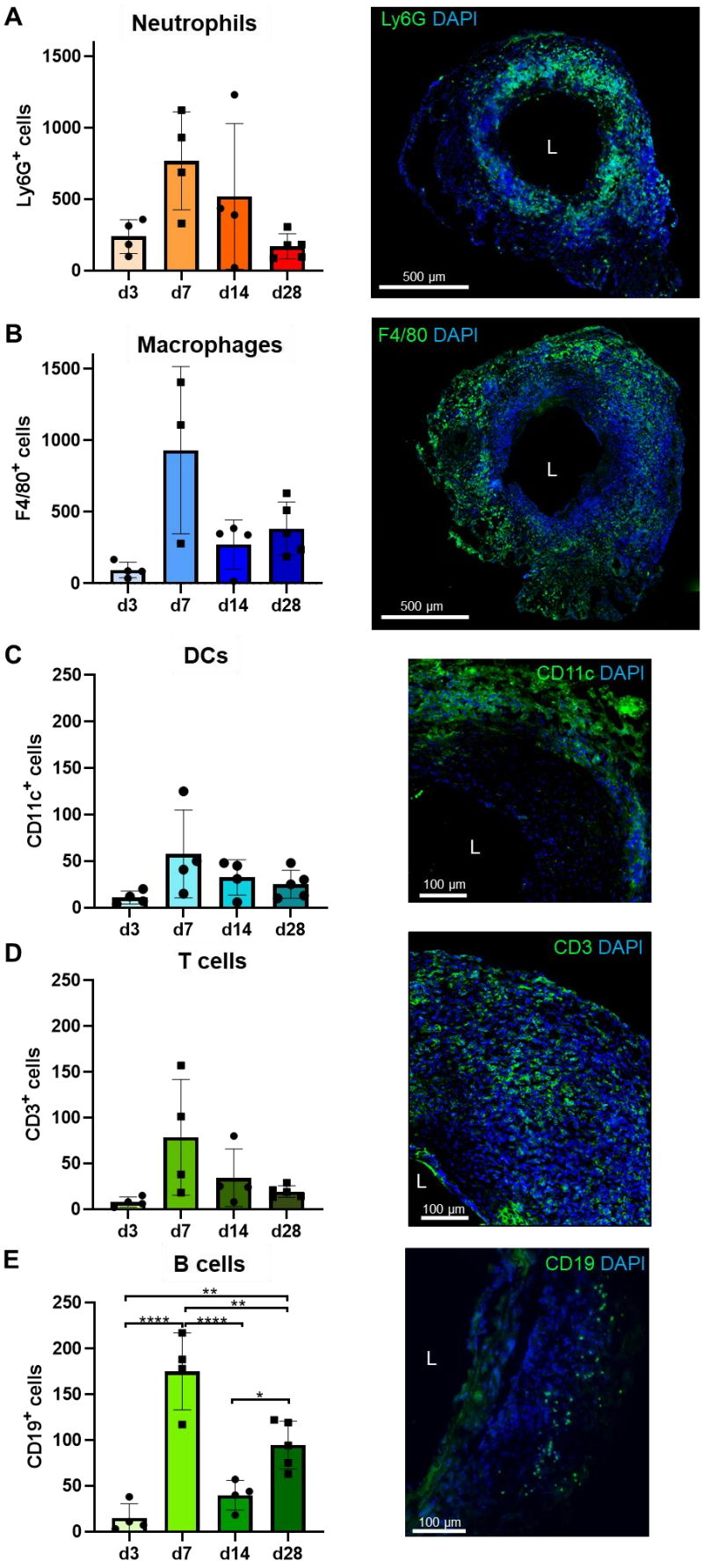

Figure 15: Immunofluorescence analysis reveals accumulation of immune cells in the adventitia. Average number of Ly6G$^+$ neutrophils **(A)**, F4/80$^+$ macrophages **(B)**, CD11c$^+$ DCs **(C)** and CD19$^+$ B cells **(D)** counted in four consecutive tissue sections per AAA 3, 7, 14 and 28 days after elastase-perfusion of the aorta and representative images of immunofluorescence stainings (day 7, right). Neutrophils **(A)**, macrophages **(B)**, DCs **(C)** and B cells **(D)** are displayed in green. Nuclei that were stained with DAPI are shown in blue. Scale bar 500 µm (overview) and 100 µm (zoom); L = Lumen. Data are presented as Mean±SD. Statistical analyses were performed using one-way ANOVA with Tukey's multiple comparison. **p<0.01, ****p < 0.0001.

scRNA-seq was performed to further analyze immune cell content in AAA progression (Figure 16). Infrarenal aneurysms were harvested at day 3 (n = 5), day 7 (n = 5), day 14 (n = 2) and day 28 (n = 4) after elastase perfusion. Saline-perfused aortae harvested at day 3 (n = 3) and day 28 (n = 3), as well as non-perfused aortae (n = 2; three aortae were pooled into one sample) were used as controls. The experimental workflow started with the induction of AAA or a sham surgery by perfusing the infrarenal aorta of male C57BL/6J mice with elastase or saline. Shortly before organ harvesting, mice were injected i.v. with a CD45-FITC antibody to label circulating immune cells. The infrarenal parts of the aortae were isolated, digested into single-cell suspensions and stained with viability dye, CD45-APC-Cy7 as well as an individual hashtag antibody. Equal amounts of immune cells ($CD45^+$) and non-immune cells ($CD45^-$) were collected and subjected to scRNA-seq and TCR-BCR-sequencing.

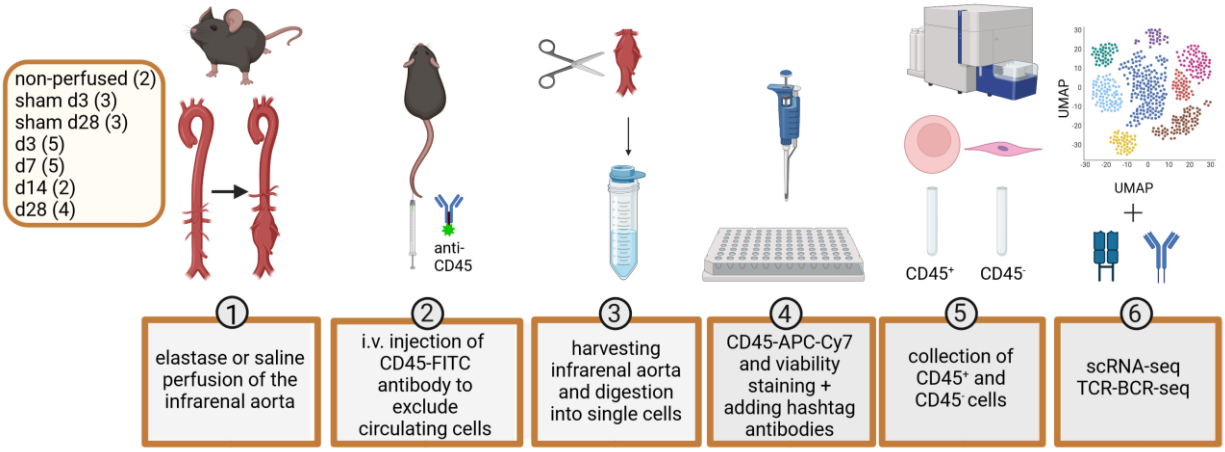

Figure 16: Experimental workflow of scRNA-seq and TCR-BCR-seq. Aortae were harvested 3, 7, 14 and 28 days after elastase-perfusion and 3 and 28 days after saline perfusion. Non-perfused aortae were used as controls. Shortly before organ harvesting, mice were injected i.v. with an CD45-FITC antibody. Infrarenal parts of the aortae were harvested and digested into single cells. Single-cell suspensions were stained with viability dye, CD45-APC-Cy7 antibody and an individual hashtag antibody. $CD45^+$ immune cells and $CD45^-$ non-immune cells were collected and subjected to scRNA-seq and TCR-BCR-seq.

Immune cells as well as non-immune cells present in aneurysmal tissue were analyzed by scRNA-seq. After quality control and pre-processing 19,479 cells were used for analysis. VSMCs, endothelial cells, myofibroblasts, fibroblasts, neutrophils, macrophages, DCs, T cells, NK cells and B cells could be detected in aneurysmal tissue (Figure 17 A). First, immune cells were identified by expression of *Ptprc* (encoding for CD45) and non-immune cells by absence of *Ptprc* expression (Figure 17 B). *Ptprc* negative cells were further identified as VSMCs by expression of *Myh11, Acta2* and *Tagln* (Figure 17 C), endothelial cells by expression of *Pecam1, Fabp4* and *Cdh5* (Figure 17 D), myofibroblasts by expression of *Cthrc1* (Figure 17 E) and fibroblasts by expression of *Dcn, Col1a1* and *Col3a1* (Figure 17 F).

Within the immune cell fraction, neutrophils, macrophages, DCs, B cells, T cells and NK cells were found. Neutrophils were defined by mRNA expression of *S100a8* and *S100a9* (Figure 17 G). mRNA expression of *Cd14*, *Cd68*, *Lyz2*, *Itgam* and *Adgre1* was used to identify macrophages (Figure 17 H). DCs were defined based on mRNA expression of *Cd209a* and *Itgax* (Figure 17 I). mRNA expression of *Cd3d, Cd3e, Cd3g* and *Cd28* was used to define T cells (Figure 17 J). NK cells were identified based on mRNA expression of *Gzma*, *Nkg7* and *Klrb1c* (Figure 17 K) and *Cd19, Cd79a* and *Cd79b* were used for the identification of B cells (Figure 17 L).

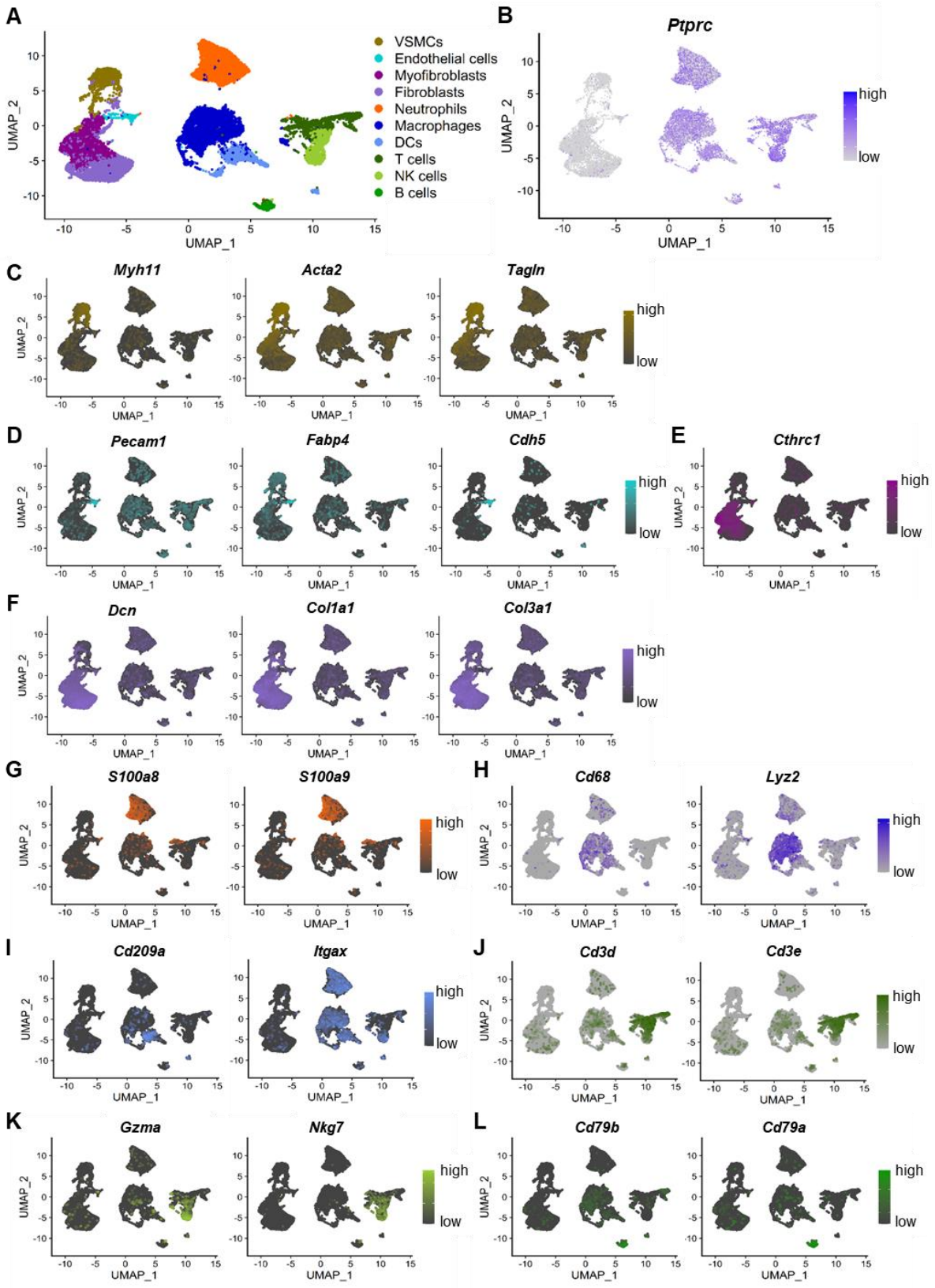

Figure 17: Identification of immune and non-immune cell clusters in AAA using scRNA-seq. A: UMAP-Plot displaying the main cell clusters detected in aneurysmal tissue after elastase perfusion. VSMCs, endothelial cells, myofibroblasts, fibroblasts, neutrophils, macrophages, DCs, T cells, NK cells and B cells were detected in aortic tissue. **B-L:** Feature plots showing the normalized and log-transformed expression level of representative mRNAs used as marker for immune cells **(B)**, VSMCs **(C)**, endothelial cells **(D)**, myofibroblasts **(E)**, fibroblasts **(F)**, neutrophils **(G)**, macrophages **(H)**, DCs **(I)**, T cells **(J)**, NK cells **(K)** and B cells **(L)**.

The main focus of this thesis lays on the inflammatory immune response involved in AAA pathology, thus immune cells were further characterized. To visualize the extent of immune cell infiltration in aortic tissue at different time points, the percentage of viable, infiltrating immune cells from the single cell gate obtained from the cell sorting was calculated for each sample used for scRNA-seq (supplementary figure 1, supplementary table 2). The average percentage of viable infiltrating immune cells from the single cell gate was calculated for each time point and is displayed in the size of the pie charts (Figure 18 A). The proportion represented by each cluster was calculated, since the number of cells contained in the scRNA-seq data set used for analysis did not accurately reflect the numbers of immune cells present in aortic tissue at the different stages of AAA. The highest ratio of living infiltrating immune cells to single cells was observed at day 14, followed by day 7 and day 3. The proportion of different immune cell types showed that neutrophils were most abundant at day 3, while macrophages were the predominant cell type at day 7 and 14. At day 28, T cells were the most abundant cells and the proportion of B cells increased in comparison to the earlier time points, although the overall number of immune cells present in aortic tissue was strongly reduced (Figure 18 A). Due to inflammation caused by the surgery, some immune cells were detected 3 days after saline perfusion but their number strongly decreased until day 28. The distribution pattern of the different immune cell types in the controls was similar to the immune cell distribution of the corresponding AAA samples, but in much lower numbers. Healthy aortae of non-treated mice contained only a few immune cells (0.03% of single cells, supplementary table 2).

GO analysis was performed to gain insights into the immunological processes involved in different stages of AAA development. This analysis revealed an enrichment of genes involved in chemotaxis and migration of leukocytes, neutrophils and granulocytes at day 3 after AAA induction (Figure 18 B). At day 7 genes associated with response to virus, interferon beta (IFNβ) and cytokine mediated signaling pathways were enriched. Genes involved in B cell-mediated immunity, complement activation and positive regulation of fibroblast apoptosis were enhanced on day 14 in comparison to the other time points. GO analysis showed an enrichment of genes associated with positive regulation of cell-cell adhesion and T cell-mediated immunity 28 days after elastase-induced AAA formation. In control mice, genes involved in structure organization were enriched (Figure 18 B).

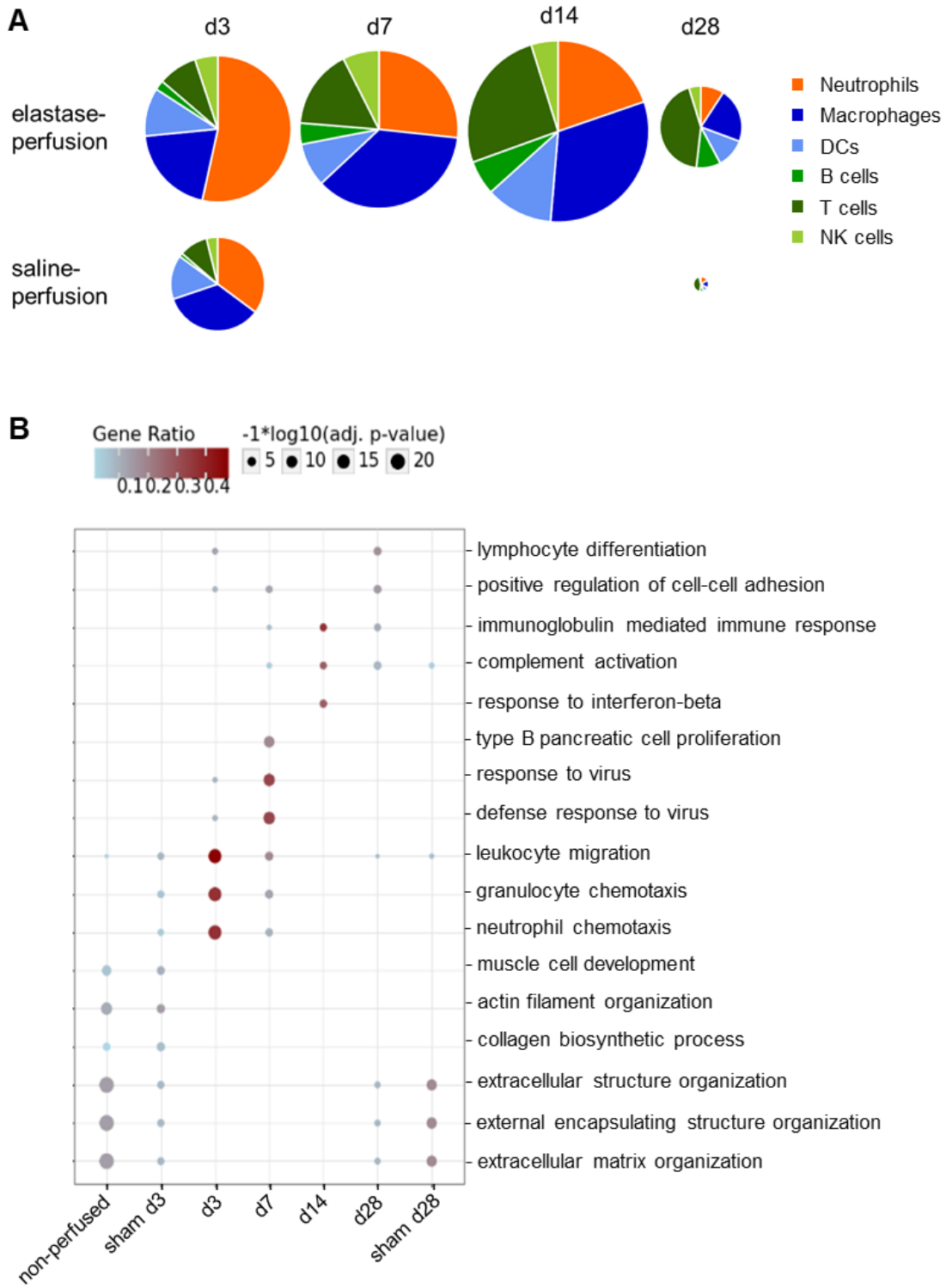

Figure 18: Distribution of immune cells and upregulated biological processes at different time points post elastase-induced AAA formation analyzed with scRNA-seq. A: Percentage distribution of neutrophils, macrophages, DCs, B cells, T cells and NK cells during AAA progression and in sham controls. The size of the pie charts represents the average ratio of viable immune cells to single cells based on the data from cell sorting. **B:** Dotplot displaying the top three enriched GO terms for non-perfused aortae, saline-perfused aortae at day 3 and 28, as well as elastase-induced AAA at day 3, 7, 14 and 28. The color code indicates the gene ratio equals the number of differentially expressed genes against the number of genes associated with a GO term. The size of the dot represents the log-normalized adjusted p-value.

scRNA-seq was used to identify and characterize subpopulations of the different immune cell types in AAA. To improve clustering resolution, 3,956 neutrophils, 5,351 macrophages/DCs, and 3,385 lymphocytes, including T, B, and NK cells, were selected, separately reclustered and analyzed. Reclustering of the cells resulted in 8 distinct neutrophil subsets (Figure 19 A), 4 DC subpopulations (Figure 20 A), 12 different macrophage subsets (Figure 20 A) and 10 lymphocyte clusters (Figure 21 A). To identify the different subpopulations, DEGs were identified for each cluster (supplementary table 3-5). For further characterization analysis of GO and signaling pathway activities were performed to gain insights into the functional roles of the different immune cell subsets. In addition, inflammation and proliferation scores were calculated for each cluster by averaging the expression of 197 inflammation-related genes and 312 proliferation-related genes. Moreover, the distribution of the different immune cell subsets over AAA progression was studied. The main findings of these analyses are summarized in the following paragraph. A detailed characterization of each neutrophil subset, each DC and macrophage subtype, as well as each lymphocyte population can be found in chapter 4.1.4, 4.1.5 and 4.1.6.

Of the 8 neutrophil subsets found, one was excluded from analysis as it accounted only for 0.16% of all immune cells included in this analysis. The remaining 7 clusters were identified as two pro-inflammatory neutrophil subtypes, interferon-inducible cells (IFNIC) neutrophils, young neutrophils, *Mmp9*$^+$ neutrophils, *Cd74*$^+$ neutrophils and remodeling neutrophils (Figure 19). Pro-inflammatory and IFNIC neutrophils represented the largest neutrophil subsets at all time points of AAA formation (Figure 19 B). They were associated with chemotaxis, migration and type-I IFN signaling (Figure 19 D). In addition, pro-inflammatory pathways such as Tnfα, TGFβ and JAK-STAT-signaling were upregulated in these cells (Figure 19 E) and they received a high inflammation score (Figure 19 F). Non-inflammatory neutrophil subsets, such as remodeling neutrophils and *Mmp9*$^+$ neutrophils, accounted for only a small proportion (Figure 19 B).

Within the DCs classical DCs, *Cd103*$^+$ DCs, activated DCs and pDCs were found in elastase-induced AAA (Figure 20 and Figure 21). According to GO all DC subsets were involved in antigen processing and presentation via MHC II (Figure 20 D). Activated DCs, which showed a high CD40 expression, were additionally involved in regulation of leukocyte cell-cell adhesion, leukocyte proliferation and lymphocyte activation (Figure 20 C and D). They represented the smallest, but most inflammatory DC subset (Figure 20 B and F). Classical DCs accounted for the largest proportion of DCs and showed no striking changes in their proportion during AAA progression (Figure 20 B). *Cd103*$^+$ DCs were anti-inflammatory and

increased with AAA progression. pDCs were most abundant at day 7 and 14 and barely present in controls (Figure 21 B).

Two of the 12 detected macrophage subsets, were excluded from analysis due to low cell number and ribosomal RNA contamination. The remaining 10 clusters were identified as IFNIC macrophages, *Pf4*$^{+}$ macrophages, *Cd72*$^{+}$ macrophages, *Lgals3*$^{+}$ macrophages, *Chil3*$^{+}$ macrophages, pro-inflammatory macrophages, T cell-like macrophages, proliferative macrophages, proliferative T cell-like macrophages and remodeling macrophages (Figure 20). *Pf4*$^{+}$ macrophages exhibited a gene signature associated with resident macrophages and constituted the largest macrophage subset in healthy aorta and sham-operated controls (Figure 20 B and C). In contrast, they represented only a small part of macrophages in AAA. Pro-inflammatory macrophages, IFNIC macrophages, and *Lgals3*$^{+}$ macrophages expressed inflammation-related genes and were involved in chemotaxis, type-I IFN signaling and leukocyte migration (Figure 20 C and D). Their proportion highly increased in AAA compared to controls (Figure 20 B). *Lgals3*$^{+}$ macrophages were not present in healthy aorta and were most abundant at day 3 and 7 after elastase-induced AAA. IFNIC macrophages accounted for the largest macrophage subset at day 7 and 14 of AAA formation. Their proportion strongly decreased at day 28 and they were not so frequent in controls. IFNIC macrophages were characterized by a type-I IFN gene signature and a strong activation of the JAK-STAT pathway (Figure 20 D and E). Genes involved in Trail, Hypoxia, NFκB and TNFα signaling were also upregulated (Figure 20 D). Moreover, IFNIC macrophages reached the second highest inflammation score of all macrophage subsets (Figure 20 F). *Cd72*$^{+}$ macrophages, *Chil3*$^{+}$ macrophages and remodeling macrophages were less inflammatory and more associated with structural changes such as wound healing, cell junction disassembly and ECM remodeling (Figure 20 D and F). Two macrophage clusters were found to express T cell associated genes and were therefore termed T cell-like macrophages (Figure 20 C). Both clusters comprised a high number of cells and were detected in three independent scRNA-seq experiments. One of this T cell-like macrophage clusters additionally expressed proliferating genes (Figure 20 C). However, proliferating macrophages accounted for only a small proportion of all macrophages (Figure 20 B).

Within the lymphocytes, NK cells, NKT cells, ILC type 2 and 3, B cells and 4 distinct subtypes of T cells, including *Cd4*$^{+}$ T cells, *Cd8*$^{+}$ T cells, pro-inflammatory T cells and Tregs, were identified (Figure 21). Another cluster that accounted only for 0.14% of all immune cells, was excluded from further analysis. NK and NKT cells together constituted the majority of lymphocytes at all time points of AAA formation (Figure 21 B). They reached their highest

proportion at day 3 and decreased with AAA progression. In contrast, ILCs, B cells and *Cd4*$^+$ T cells increased with AAA progression and peaked at day 28. *Cd4*$^+$ T helper cells, which represented the largest T cell subset in AAA, were associated with T cell activation and differentiation as well as leukocyte cell-cell adhesion (Figure 21 B-D). Cd8$^+$ T cells were mainly involved in lymphocyte differentiation and expressed genes associated with a memory phenotype (Figure 21 C and D). Tregs represented only a small subset in AAA and were more abundant in controls (Figure 21 B). ILC3s were more frequent than ILC2s in AAA.

4.1.4 Detailed characterization of neutrophil subpopulations in AAA by scRNA-seq

Reclustering of 3,956 neutrophils resulted in 8 distinct subpopulations (Figure 19 A). DEGs for each cluster can be found in supplementary table 3. Cluster 7 contained only 21 cells and accounted for 0.16% of all immune cells included in this analysis and was therefore excluded from further analysis. All other clusters were further characterized.

Neutrophils belonging to cluster 0 and 4 showed high expression of pro-inflammatory chemokines and cytokines such as *Cxcl2, Tnf, Ccl3, Il1a, Nlrp3* and *Il1rn*, and are further referred to as pro-inflammatory neutrophils (Figure 19 C). Pro-inflammatory neutrophils 1 (Cluster 0) was one of the two predominant subsets of all neutrophils at all investigated time points (Figure 19 B). Pro-inflammatory neutrophils 2 (Cluster 4) represented only a small proportion of neutrophils in AAA (Figure 19 B). GO analysis showed that cluster 0 was involved in neutrophil migration and chemotaxis and cluster 4 was associated with reactive oxygen species metabolic processes (Figure 19 D). Examination of the activities of various metabolic pathways using *PROGENy*[146] revealed that the pro-inflammatory pathways Tnfα and NFκB were higher upregulated in cluster 4 than in cluster 0. Genes involved in the proliferation-promoting MAPK pathway were most strongly upregulated in cluster 4 (Figure 19 E). To further differentiate cluster 0 from cluster 4, scores for inflammation and proliferation were calculated by averaging the expression of 197 inflammation-related genes and 312 proliferation-related genes. The inflammation score was similar in both clusters, whereas cluster 4 exhibited a slightly higher proliferation score than cluster 0 (Figure 19 F).

Cluster 1 represented the second major neutrophil population and consisted of previously described interferon-inducible cells (IFNIC)[153, 154] (Figure 19 A and B). They showed a high expression of many interferon-stimulated genes (ISGs) and directly interferon regulatory factor 3 (IRF3)-dependent genes (Figure 19 C). IFNIC neutrophils were highly responsive to IFNβ and the JAK-STAT pathway, that is activated by IFNs[155], was highly upregulated in these cells (Figure 19 D and E). Genes involved in the inflammatory pathways NFκB and

TNFα were also upregulated in IFNIC neutrophils compared to the other neutrophil clusters. Furthermore, IFNIC neutrophils received the highest inflammation score (Figure 19 F).

Young, immature neutrophils are described by an expression of *Mmp8, Retnlg, Ifitm6, Slpi* and *Wfdc17*[154, 156], representing cluster 2, the third largest neutrophil population in AAA (Figure 19 A-C). According to GO analysis young neutrophils were involved in defense response to bacterium and antimicrobial response as well as cell chemotaxis (Figure 19 D).

Cluster 3 contained *Mmp9* expressing neutrophils and was associated with cellular response to oxidative stress (Figure 19 C and D). *Mmp9*$^+$ neutrophils accounted for only a small proportion of neutrophils in AAA, except for day 3 post AAA formation, where they represented the second largest population with 25% (Figure 19 B). However, they reached the lowest inflammation score of all neutrophil clusters (Figure 19 F).

Cluster 5 represented a small subpopulation that highly expressed *Cd74* and other genes associated with antigen processing and presentation of exogenous peptide antigen via MHC class II, and was termed *Cd74*$^+$ neutrophils (Figure 19 A-D). A similar subset of neutrophils, termed HLA-DR$^+$CD74$^+$, was previously described as terminally mature neutrophil subset.[157] No striking differences were found in up- or downregulation of signaling pathways or in the inflammation and proliferation score compared to the other neutrophil clusters (Figure 19 E and F).

Neutrophils of cluster 6 expressed *Mgp, Col3a1, Col1a2, Col1a1* that were involved in collagen fibril and extracellular matrix organization and *Sparc* and *Dcn* that were associated with regulation of vasculature development (Figure 19 C and D). This population was barely abundant during AAA progression and reached the highest proportion in the sham control at day 28 (Figure 19 B). Analysis of pathway responsive genes showed an upregulation of genes involved in TGFβ in these remodeling neutrophils (Figure 19 E). The majority of remodeling neutrophils received a low inflammation score (Figure 19 F).

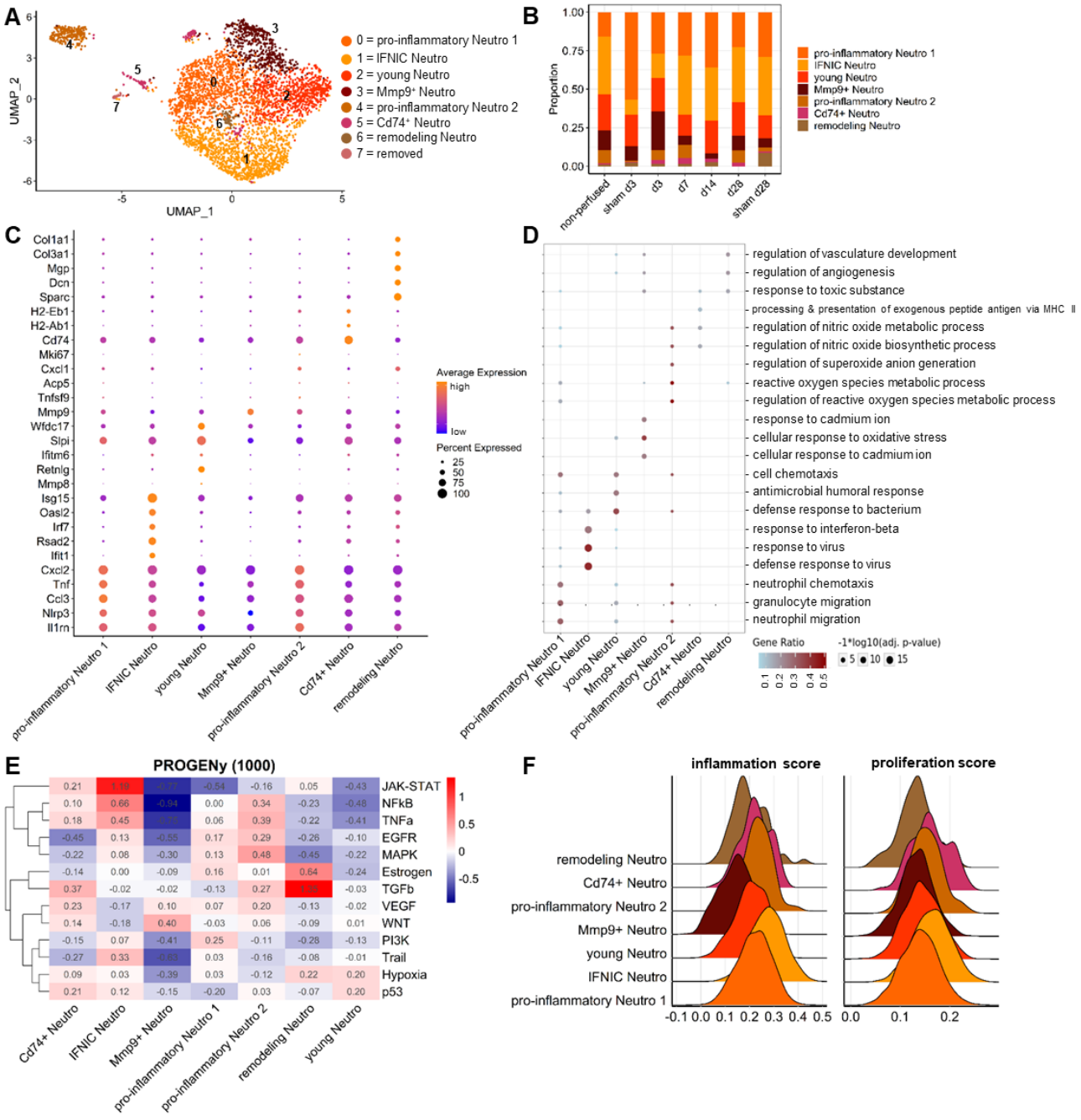

Figure 19: Characterization of neutrophil subtypes in AAA. A: UMAP-Plot showing eight different neutrophil clusters. Cluster 7 was removed from further analysis. The other clusters were identified as pro-inflammatory neutrophils 1, IFNIC neutrophils, young neutrophils, *Mmp9*$^{+}$ neutrophils, pro-inflammatory neutrophils 2, *Cd74*$^{+}$ neutrophils and remodeling neutrophils. **B:** Percentage distribution of the identified neutrophil subsets over progression of AAA and in the controls. **C:** Dotplot displaying the normalized and log-transformed expression level of marker genes for each cluster. The color of the dot shows the expression level (orange = high expression, blue = low expression) and the size of the dot indicates the percentage of cells inside the cluster expressing the gene. **D:** Dotplot presenting the top three enriched GO terms for each neutrophil cluster. The color code indicates the gene ratio equals the number of DEGs against the number of genes associated with a GO term. The size of the dot represents the log-transformed adjusted p-value**. E:** Heatmap showing the activity of different pathways in the neutrophil subpopulations based on the expression of pathway responsive genes. **F:** Inflammation score (left panel) and proliferation score (right panel) are presented in a ridgeline plot as average expression of 197 inflammation-related genes and 312 proliferation-related genes for all neutrophils clusters.

4.1.5 Detailed characterization of DC and macrophage subpopulations in AAA by scRNA-seq

Reclustering of 5,351 cells yielded 3 DC and 12 macrophage subpopulations (Figure 20 A). DEGs for each DC and macrophage cluster can be found in supplementary table 4. Cluster 7 yielded only a few DEGs including long non-coding RNA (lncRNAs) *Gm42418* and *Gm26917* (Figure 20 C) that are associated with ribosomal RNA contamination.[158] Cluster 14 encompassed only 31 cells, representing 0.24% of all immune cells. Based on that cluster 7 and 14 were removed from further analysis.

The first DC cluster (cluster 1) represented the largest DC cluster in AAA and was characterized by expression of *Klrd1*, *Ifitm1* and many MHC II associated genes such as *Cd74, H2-Ab1, H2-Aa* (Figure 20 B and C). GO analysis likewise revealed expression of genes that are involved in antigen processing and presentation via MHC II as well as peptide antigen assembly (Figure 20 D). Thus, cluster 1 was further referred to as classical DCs.

The second DC subpopulation (cluster 9) expressed DC-associated genes *Flt3, Irf8*, *Clec9a, Wdfy4* and *Itgae* (Figure 20 C). Based on the expression of *Itgae,* encoding for CD103, this population was termed *Cd103*$^+$ DCs, that are also known as classical Flt3-dependent DCs.[42] *Cd103*$^+$ DCs increased with AAA progression and were most abundant at day 28 (Figure 20 B). GO analysis revealed expression of genes that are involved in peptide antigen assembly, antigen processing and presentation via MHC II (Figure 20 D). The analysis of pathway responsive genes using PROGENy showed a slight upregulation of genes involved in WNT signaling and downregulation of genes associated with Hypoxia, Trail, NFκB and TNFα signaling in *Cd103*$^+$ DCs (Figure 20 E).

The third and smallest DC population (cluster 11) was identified as activated DCs. They expressed among others *Fscn1, Ccr7, Il4i1* and *Cd40*. Activated DCs were involved in regulation of leukocyte cell-cell adhesion, leukocyte proliferation and lymphocyte activation (Figure 20 D). In addition, TGFβ and PI3K signaling pathways were upregulated (Figure 20 E). Activated DCs received a higher inflammation score compared to the other two DC subtypes (Figure 20 F).

Within the macrophage subpopulations we found interferon-inducible cells, termed IFNIC macrophages, (cluster 0) that were first described in an experimental model of myocardial infarction[159] and were also identified in atherosclerosis[160] and AAA[161]. Similar to the previously described IFNIC neutrophils, IFNIC macrophages were characterized by

expression of ISGs and directly IRF3-dependent genes (Figure 20 C). GO analysis revealed that IFNIC macrophages were also responsive to IFNβ and involved in virus response (Figure 20 D). In IFNIC macrophages the JAK-STAT pathway was most strongly upregulated, but also genes involved in Trail, Hypoxia, NFκB and TNFα signaling were upregulated compared to the other clusters (Figure 20 E). IFNIC macrophages reached the second highest inflammation score of all macrophage subsets (Figure 20 F). Interestingly, the number of IFNIC macrophages changed to a greater extent during the course of AAA than most of the other populations (Figure 20 B). In the early phase of AAA (day 3-14), they occurred much more frequently than in the late stage and the controls. At day 7 and 14 IFNIC macrophages accounted for the largest macrophage subset with 30.5% and 27.1%.

Cluster 2 showed high expression of *Pf4* (Figure 20 C) and was therefore termed *Pf4*$^{+}$ macrophages. *Pf4*, encoding CXCL4, was already shown to be expressed on macrophages, is chemotactic for neutrophils, monocytes and fibroblasts, promotes monocyte survival and induces differentiation of monocytes into macrophages.[162, 163] *Pf4*$^{+}$ macrophages expressed genes associated with resident-like macrophages (e.g. *F13a1, Gas6, Mrc1, Ccl8,* and *Cbr2).*[56, 57] The percentage distribution showed that this resident-like *Pf4*$^{+}$ macrophages constitute the largest macrophage subset in healthy aorta and the sham controls (Figure 20 B). During AAA formation, these cells represented only a small fraction of macrophages. *Pf4*$^{+}$ macrophages were associated with chemokine-mediated signaling (Figure 20 D).

Cluster 3 consisted of *Cd72*$^{+}$ macrophages that were associated with leukocyte migration (Figure 20 C and D). CD72^{hi} macrophages were previously described as bone-marrow derived, pro-inflammatory macrophage subset that may serve as a therapeutic target for CVDs.[164] In this dataset, *Cd72*$^{+}$ macrophages obtained a moderate inflammation score (Figure 20 F). *Cd72*$^{+}$ macrophages were detected at all time points of AAA and reached the highest proportion at day 14.

Cluster 4 highly expressed *Lgals3*, encoding Galectin-3/Mac-2 (Figure 20 C), which regulates chemotaxis and inflammation, including macrophage activation and migration.[165, 166] GO analysis confirmed that *Lgals3*$^{+}$ macrophages were involved in leukocyte migration and chemotaxis (Figure 20 D). *Lgals3*$^{+}$ macrophages were not present in healthy aorta and were most abundant at day 3 and 7 after elastase-induced AAA (Figure 20 B).

Cluster 5, further referred to as *Chil3*$^{+}$ macrophages, showed relatively higher expression of chitinase-like protein 3 (*Chil3)* also known as Ym1 (Figure 20 C). Ym1 was shown to be mainly expressed on macrophages and neutrophils and is upregulated in the acute stage of

inflammatory injury.[167] This is also reflected in this dataset as the highest proportion of *Chil3*$^{+}$ macrophages was detected at day 3 after elastase or saline perfusion of the aorta (Figure 20 B).

Pro-inflammatory mediators such as *Cxcl2, Ccl3, Il1b, Tnf, Tlr2* and *Nlrp3* were highly expressed in cluster 6 (Figure 20 C). These pro-inflammatory macrophages were most abundant at day 3 of AAA and were associated with migration and chemotaxis of immune cells (Figure 20 B and D). They showed the strongest upregulation of the inflammatory pathways NFκb and TNFα and also reached the highest inflammation score compared to the other macrophage clusters (Figure 20 E and F).

Cluster 10 and 12 consisted of proliferative macrophages that expressed many genes involved in cell division and proliferation e.g. *Stmn1, Ccna2, Top2a, Birc5, Hmgb2, Smc2, Tubb5, Cks1b, Mki67* and *Cdca8* (Figure 20 C and D). In both proliferative macrophage clusters genes associated with MAPK signaling were highly upregulated and genes associated with cell cycle arrest and apoptosis (p53 and Trail) were downregulated (Figure 20 E). In addition, genes involved in estrogen and EGFR signaling, both activating the MAPK pathway, were upregulated.

Two of the macrophage clusters (8 and 12) expressed the T cell associated genes *Cd3d, Cd3e, Cd3g, Cd4, Cd8a, Cd8b1* (Figure 20 A, B and C). Cluster 12 seemed to be a proliferative form of cluster 8. Thus, cluster 8 was termed T cell-like macrophages and cluster 12 proliferative T cell-like macrophages. Based on the proportion these T cell-like macrophages were most frequent on day 28 post AAA (Figure 20 B).

Cluster 13 represented the smallest macrophage subset and was identified as remodeling macrophages based on expression of genes associated with collagen fibril organization and ECM organization such as *Col1a1, Col1a2, Col3a1, Dcn, Bgn, Sparc* and *Mgp* (Figure 20 A, B, C and D). Genes involved in TGFβ signaling that promotes synthesis of ECM molecules especially of collagen type 1 were highly upregulated in remodeling macrophages (Figure 20 E).

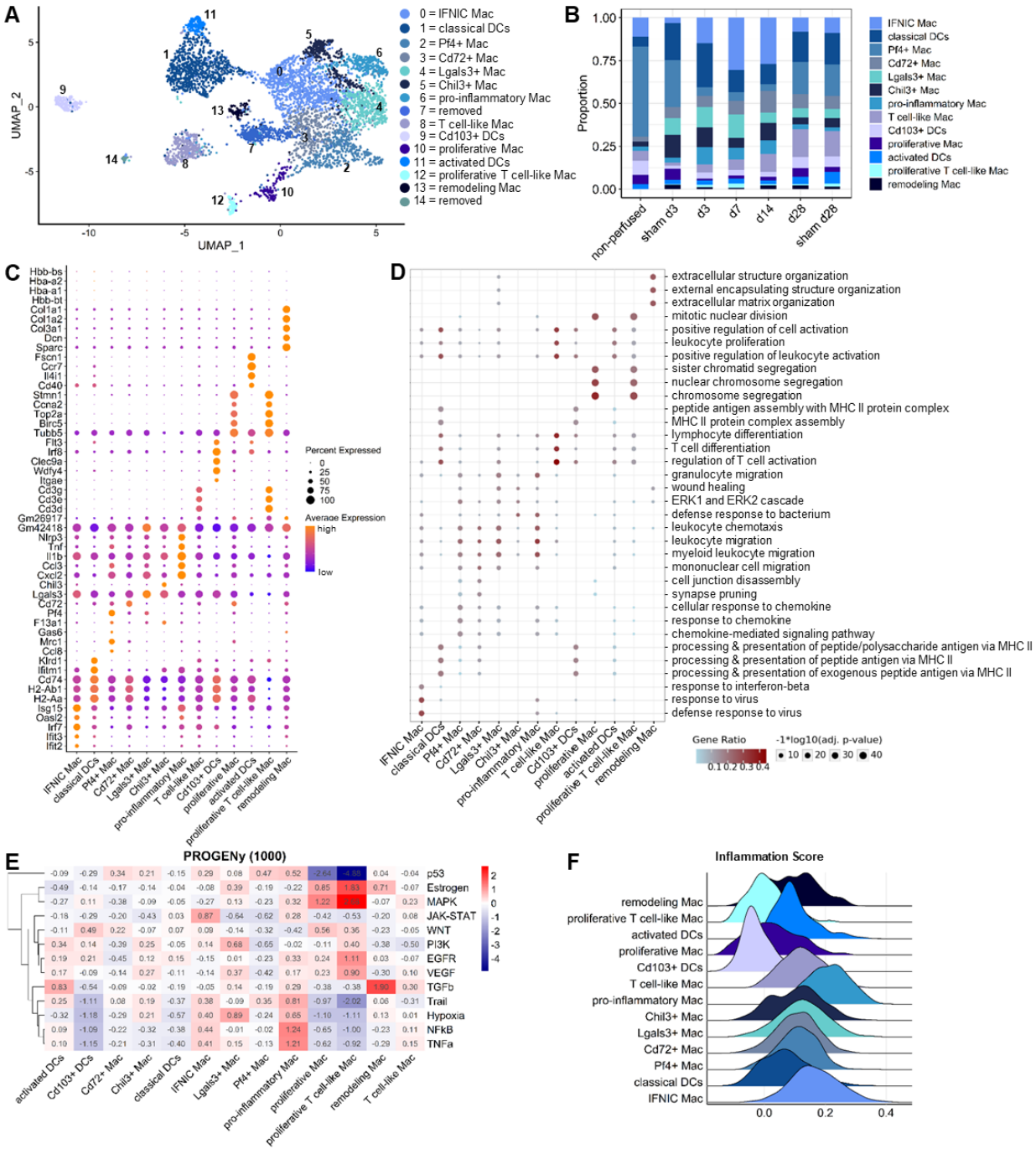

Figure 20: Characterization of DC and macrophages subtypes in AAA. A: UMAP-plot displaying 3 distinct DC and 12 different macrophage cluster. IFNIC macrophages, classical DCs, *Pf4*$^{+}$ macrophages, *Cd72*$^{+}$ macrophages, *Lgals3*$^{+}$ macrophages, *Chil3*$^{+}$ macrophages, pro-inflammatory macrophages, T cell-like macrophages, *Cd103*$^{+}$ DCs, proliferative macrophages, activated DCs, proliferative T cell-like macrophages and remodeling macrophages were identified in AAA. Cluster 7 and 14 were removed from further analysis. **B:** Percentage distribution of the identified DC and macrophages clusters during progression of AAA and in the controls. **C:** Dotplot showing the normalized and log-transformed expression level of marker genes for each cluster. The color of the dot shows the expression level (orange = high expression, blue = low expression) and the size of the dot indicates the percentage of cells inside the cluster expressing the gene. **D:** The top 3 enriched GO terms for each DC and macrophage cluster are presented in a dotplot. The color code indicates the gene ratio equals the number of DEGs against the number of genes associated with a GO term. The size of the dot represents the log-transformed adjusted p-value. **E:** Heatmap showing the activity of different pathways in the different subpopulations of DCs and macrophages based on expression of pathway responsive genes. **F:** The inflammation score is presented in a ridgeline plot as average expression of 197 inflammation-related genes for all subsets.

4.1.6 Detailed characterization of lymphocyte subpopulations in AAA by scRNA-seq

Reclustering of 3,385 lymphocytes resulted in 11 distinct subpopulations (Figure 21 A). DEGs for each lymphocyte cluster can be found in supplementary table 5.

Cluster 4 and 10 contained B cells that were identified by expression of *Cd79a* and *Cd79b*. Cluster 10 accounted only for 0.14% of all immune cells and was therefore excluded from further analysis. Cluster 4 showed high expression of *Ighm* and low expression of *Ighd* and was identified as B2 cells (Figure 21 A and C). B2 cells were associated with antigen presentation via MHC II and represented a small fraction of lymphocytes in AAA most frequently on day 28 (Figure 21 B and D).

NKT cells (cluster 0) expressed the T cell markers C*d8a, Cd8b1, Cd3e*, *Cd3d* and the NK cell markers *Klrc1*, *Nkg7* and *Gramd3* (Figure 21 A and C). NKT cells were associated with thymic T cell selection as well as NK cell mediated immunity and cytotoxicity (Figure 21 D). Cluster 1 was identified as NK cells based on the expression of *Irf8, Nkg7, Klre1, Klrk1, Klrb1c* and *Gzma* (Figure 21 C). Genes involved in cell killing were enriched in this cluster (Figure 21 D). NKT and NK cells together were the predominant lymphocyte cluster at all time points and accounted for 26.7-51.8% of all lymphocytes present in AAA (Figure 21 B).

Cluster 2 contained *Cd4*$^{+}$ T cells that were associated with T cell activation and differentiation as well as leukocyte cell-cell adhesion (Figure 21 A, C and D). The proportion of *Cd4*$^{+}$ T cells increased with progression of AAA until day 14, where they represented the second largest lymphocyte cluster (Figure 21 B).

Based on mRNA expression of *Ltb, Il7r* (encoding CD127), *Junb, Ikzf3* and *Cd40lg* cluster 3 was identified as innate lymphoid cells (ILC) type 3[168] (Figure 21 A and C). Cluster 9 showed high expression of *Gata3, Il7r, Rora, Areg,* and *Klrg1* and thus, was identified as ILC2 cells[168-171] (Figure 21 A and C). ILC2 cells were associated with regulation of leukocyte differentiation (Figure 21 D). Both ILC cluster were most abundant at day 28 after sham- or PPE-surgery (Figure 21 B).

Cluster 5 expressed several pro-inflammatory genes such as *Il1b, Cxcl2, Clec4e, Ccrl2 and Il1r2* and were termed pro-inflammatory T cells (Figure 21 A and C). According to GO analysis genes involved in chemotaxis were enriched in this cluster (Figure 21 D). Furthermore, pro-inflammatory T cells received the highest inflammation score (Figure 21 E).

Cluster 6 represented a small lymphocyte subset and contained *Cd8*$^{+}$ T cells that were mainly involved in lymphocyte differentiation (Figure 21 A, B and D). *Cd8*$^{+}$ T cells further expressed *S1pr1*, *Ccr7*, *Tcf7* and *Klf2* (Figure 21 C), indicating a memory phenotype.[172]

Cluster 7 was identified as Tregs based on the expression of *Tnfrsf18, Ctla4, Il2ra, Ikzf2* and *Foxp3*[172] and represented only a small proportion of the lymphocytes detected in AAA (Figure 21 A, B and C).

Cluster 8 expressed the DC marker genes *Itgax* and *Cd209a* as well as *Cd8* (Figure 21 C) which indicates that these cells might be pDCs. This cluster further expressed *Ptprc, Bst2* and *Siglech* (Figure 21 C) that are known to be expressed on pDCs. GO analysis additionally revealed that pDCs were associated with antigen processing and presentation via MHC II (Figure 21 D). pDCs were mostly present at day 7 and 14 of AAA progression and barely abundant in controls (Figure 21 B).

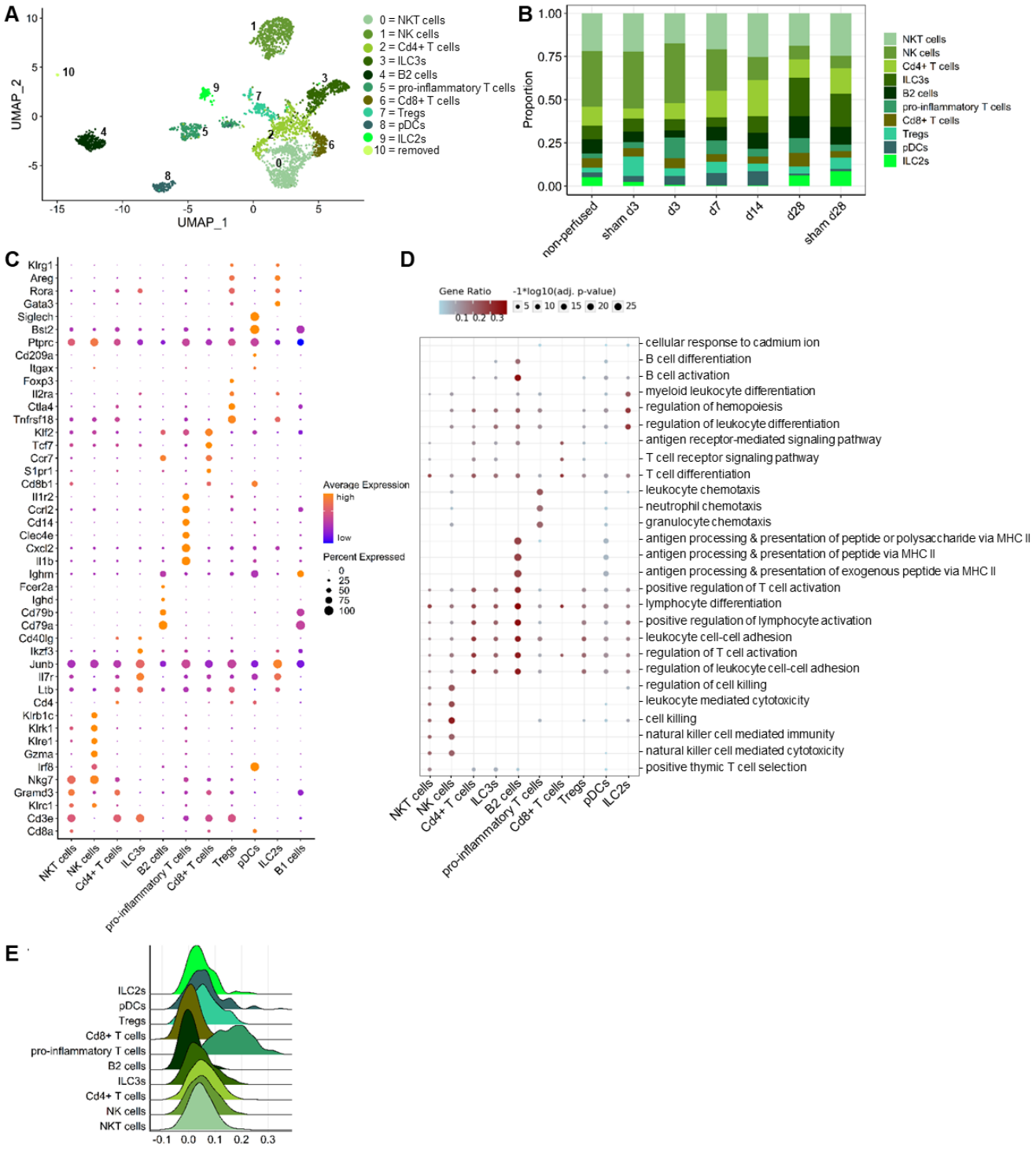

Figure 21: Characterization of lymphocyte subsets in AAA. A: UMAP-Plot displaying 11 different lymphocyte populations detected in AAA. NKT cells, NK cells, *Cd4*⁺ T cells, ILC3s, B2 cells, pro-inflammatory T cells, *Cd8*⁺ T cells, Tregs, pDCs and ILCs were identified. Cluster 10 was removed from further analysis. **B:** Percentage distribution of the identified lymphocyte subsets over progression of AAA and in the sham and non-perfused controls. **C:** Dotplot showing the normalized and log-transformed expression level of marker genes for each cluster. The color of the dot shows the expression level (orange = high expression, blue = low expression) and the size of the dot indicates the percentage of cells inside the cluster expressing the gene. **D:** The top 3 enriched GO terms for each lymphocyte cluster are presented in a dotplot. The color code indicates the gene ratio equals the number of DEGs against the number of genes associated with a GO term. The size of the dot represents the log-transformed adjusted p-value. **E:** The inflammation score is presented in a ridgeline plot as average expression of 197 inflammation-related genes for all lymphocyte subsets.

4.1.7 Cell-cell communication analysis in AAA progression

CellChat[148, 149] was used to infer and analyze the cell–cell communication at different stages of elastase-induced AAA. Since immune cells not only communicate with each other, but also exchange signals with structural cells, the communication between all immune cells as well as endothelial cells, VSMCs, fibroblast and myofibroblasts detected with scRNA-seq was analyzed. The highest number of interactions was predicted for day 7 and 28 (Figure 22 A). Greater differences between the time points were observed in the interaction strength, which reflects the calculated communication probability. The effect of cell proportions that are reflected in the size of the dots in the circle plots was considered for calculation of the communication probability (Figure 22 B). The strongest interaction was received at day 7 of AAA progression and the weakest interaction at day 28 (Figure 22 A). At day 3, cell-cell communication was dominated by myofibroblasts and neutrophils, especially young and pro-inflammatory neutrophils (Figure 22 B and C). Neutrophils showed a strong autocrine signaling as well as outgoing interaction with macrophages. They received the strongest signaling from myofibroblasts, fibroblasts and macrophages. Myofibroblasts showed high outgoing interaction with macrophages and neutrophils, while also signaling autocrine (Figure 22 C). At day 7, myofibroblasts and neutrophils were still strongly involved in cell-cell communication, but the interaction strength of macrophages was much higher than at day 3 (Figure 22 C). In particular, IFNIC macrophages showed a large increase in signaling strength and were the main receiver of communication signals at day 7. In addition, IFNICs, myofibroblasts and fibroblasts had the strongest outgoing interaction strength at day 7. Myofibroblasts and fibroblasts were also the main signal senders 14 days post elastase-induced AAA. Macrophages, especially IFNICs, and VSMCs were the dominant receivers of communication signals. Furthermore, macrophages showed a strong autocrine signaling (Figure 22 B and C). The interaction strength of neutrophils was reduced in comparison to day 3 and 7. At day 28, fibroblasts drove the cell-cell communication by sending strong signals to macrophages, in particular to *Pf4*$^{+}$ and T cell-like macrophages. Fibroblasts also interacted with all other cell types. In contrast to the earlier time points, NK cells and T cells were more strongly involved in cell-cell communication at day 28, whereas the interaction strength of IFNICs was highly reduced at this later time point (Figure 22 C). Overall, the most prominent immune cell infiltration as well as the strongest intercellular communication was obtained on day 7, indicating a critical time point in AAA development. Among the immune cells, IFNIC macrophages were most involved in cell-cell signaling, especially at day 7, and appear to play an important role.

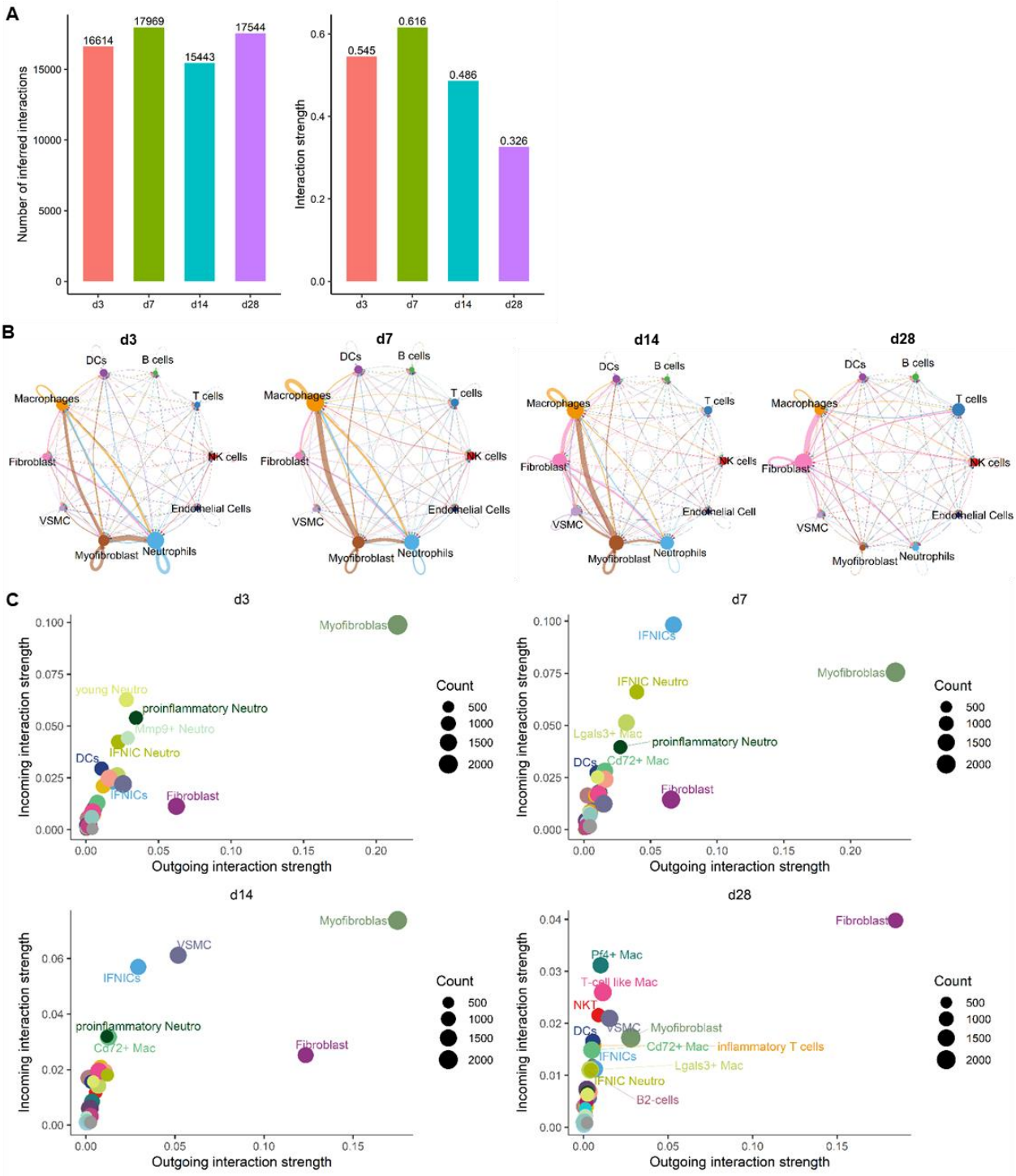

Figure 22: CellChat inference of cell-cell communication reveals strongest interaction at day 7 with IFNIC macrophages and myofibroblasts as main drivers of communication. A: Number of inferred interactions and interaction strength at day 3, 7, 14 and 28 after elastase-induced AAA of all cells. **B:** The interaction strength between the main immune cells, including neutrophils, DCs, macrophages, NK cells, T cells and B cells, and structural cells, including endothelial cells, VSMCs, fibroblasts and myofibroblasts, 3, 7, 14 and 28 days after elastase-induced AAA formation is displayed in circle plots. Circle sizes are proportional to the number of cells in each cell group. Line colors are consistent with the sources as sender. The thickness of the lines indicates the signal strength. **C:** Comparison of major sources and targets of communication signals in 2D space at different stages of elastase-induced AAA. For each subpopulation the count is represented by the circle size, the outgoing interaction strength is shown on the x-axis and the incoming interaction strength is displayed on the y-axis.

4.1.8 CITE-seq can be used to validate subpopulations identified by scRNA-seq

Identification of immune cell subpopulations can be challenging and there is no commonly used nomenclature yet. Information on protein expression obtained from CITE-seq can be helpful in verifying and confirming subpopulations identified by scRNA-seq. Thus, the cluster labels from the scRNA-seq data were transferred to the CITE-seq data to further analyze the subpopulations. Except for *Cd74*$^{+}$ neutrophils, remodeling neutrophils and remodeling macrophages, which represented the smallest clusters in AAA, all subpopulations identified in the scRNA-seq data could be also detected in the CITE-seq data (Figure 23 A). Overall, the label transfer showed high accuracy with an average prediction score of 0.81. The prediction score is a value between 0 and 1 indicating the accuracy of predicted cell annotation based on label transfer (Figure 23 B). Cell annotation was most accurate for DCs and lymphocytes with average prediction scores of 0.93 and 0.90, respectively. Lower accuracy was shown for macrophages with 0.75 and neutrophils with the lowest prediction score of 0.69 for label transfer (Figure 23 B).

CITE-seq data was utilized to examine the expression of proteins corresponding to the mRNAs used to identify clusters by scRNA-seq. CITE-seq data confirmed that *Cd103*$^{+}$ DCs identified by mRNA expression of *Itgae* additionally express CD103 at protein level (Figure 23 C). CD40, which is known to be upregulated on activated DCs[173], was also more strongly expressed at protein level on activated DCs compared to classical and *Cd103*$^{+}$ DCs (Figure 23 C). Next, the two macrophage clusters T cell-like macrophages and proliferative T cell-like macrophages, which expressed macrophage markers as well as T cell markers on mRNA level, were investigated with CITE-seq. For T cell-like macrophages, CITE-seq data revealed strong expression of the macrophage marker CD11b, and low expression of the T cell associated proteins CD3, CD4 and CD8a (Figure 23 D), while proliferative T cell-like macrophages expressed less CD11b, and showed stronger expression of CD3, CD4 and CD8a compared to all other macrophage subsets. The annotation of *Cd4*$^{+}$ and *Cd8*$^{+}$ T cells could be validated with CITE-seq, as *Cd4*$^{+}$ T cells strongly expressed CD4 at protein level and *Cd8*$^{+}$ T cells strongly expressed CD8a at protein level (Figure 23 E). In addition, protein expression of the pDC markers CD8b, B220 and Siglec H was detected in the cluster identified as pDCs by scRNA-seq (Figure 23 E and F). Lastly, strong CD127 expression in ILC2s and ILC3s confirmed that both clusters were properly identified as ILCs (Figure 23 G).

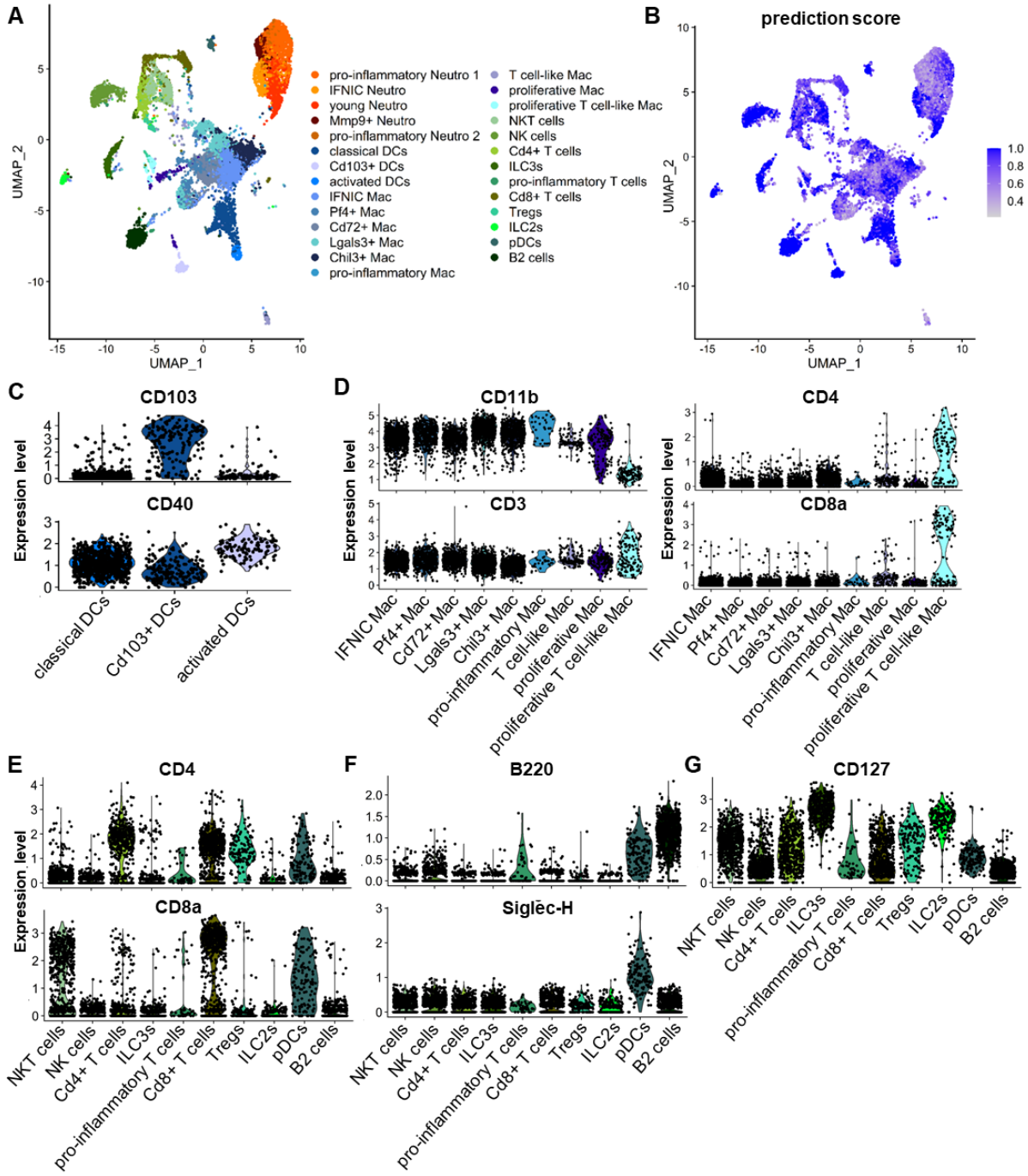

Figure 23: Validation of subpopulations identified by scRNA-seq using protein expression measured with CITE-seq. A: UMAP-plot showing all subpopulations that could be detected in the CITE-seq data. Each dot represents a single cell. Each subpopulation is displayed in a different color. **B:** The prediction score that indicates the accuracy of the label transfer from scRNA-seq data to CITE-seq data is presented for each single cell in a feature plot. The color code represents the prediction score. **C:** CD103 and CD40 protein expression in classical DCs, *Cd103*$^+$ DCs and activated DCs. **D:** Protein expression of CD11b, CD3, CD4 and CD8a across the macrophage subpopulations IFNIC Mac, *Pf4*$^+$ Mac, *Cd72*$^+$ Mac, *Lgals3*$^+$ Mac, *Chil3*$^+$ Mac, pro-inflammatory Mac, T cell-like Mac, proliferative Mac and proliferative T cell-like Mac. **E:** CD4 and CD8a protein expression on the lymphocyte subsets NKT cells, NK cells, *Cd4*$^+$ T cells, ILC3s, pro-inflammatory T cells, *Cd8*$^+$ T cells, Tregs, ILC2s, pDCs and B2 cells. **F:** Expression level of the pDC marker proteins B220 and Siglec-H on lymphocyte subsets. **G:** Protein expression of the ILC marker CD127 across lymphocyte subsets.

4.1.9 CITE-seq is a powerful method for examining mRNA-protein-correlation

Based on the previously described results, protein expression appears to correspond to mRNA expression. However, this is not always the case and correlation between mRNA and protein abundances in mammals is known to be weak.[174, 175] To examine the degree of mRNA-protein-correlation in the CITE-seq dataset, the spearman correlation for all 119 detected proteins with their corresponding mRNA expression was calculated separately for each cell cluster (Figure 24). Red color indicates a positive correlation, blue color shows a negative correlation and grey color represents a Spearman's rho of 0, which indicates no correlation. Overall, the heatmap displayed a mixed pattern. Some of the proteins, e.g. Ly6G and Ly6C, showed no correlation with their corresponding mRNA expression for almost all cell clusters (Figure 24). Ly6C was highly expressed on protein level, but no expression could be detected on mRNA level (Figure 25 A), resulting in an overall Spearman's rho of -0.005 (Figure 25 B). For other proteins, e.g. CD11c, CD73, CD49d and Ly6A/E, a positive correlation with their mRNA expression was obtained for the majority of clusters (Figure 24). Ly6A/E showed corresponding mRNA and protein expression across the different cell types (Figure 25 C), as reflected in a moderate positive correlation ($r = 0.57$, Figure 25 D). The majority of the proteins obtained a strong positive correlation between protein and mRNA expression for specific cell types, but no correlation for other cell populations (Figure 24). The protein expression of the macrophage marker F4/80 for example positively correlated with the mRNA expression in one neutrophil and one DC subset and in 7 of 9 macrophage subsets. In all other cell types, no correlation was observed (Figure 24). Few proteins like B220 and CD185 showed even a negative correlation between mRNA and protein expression (Figure 24).

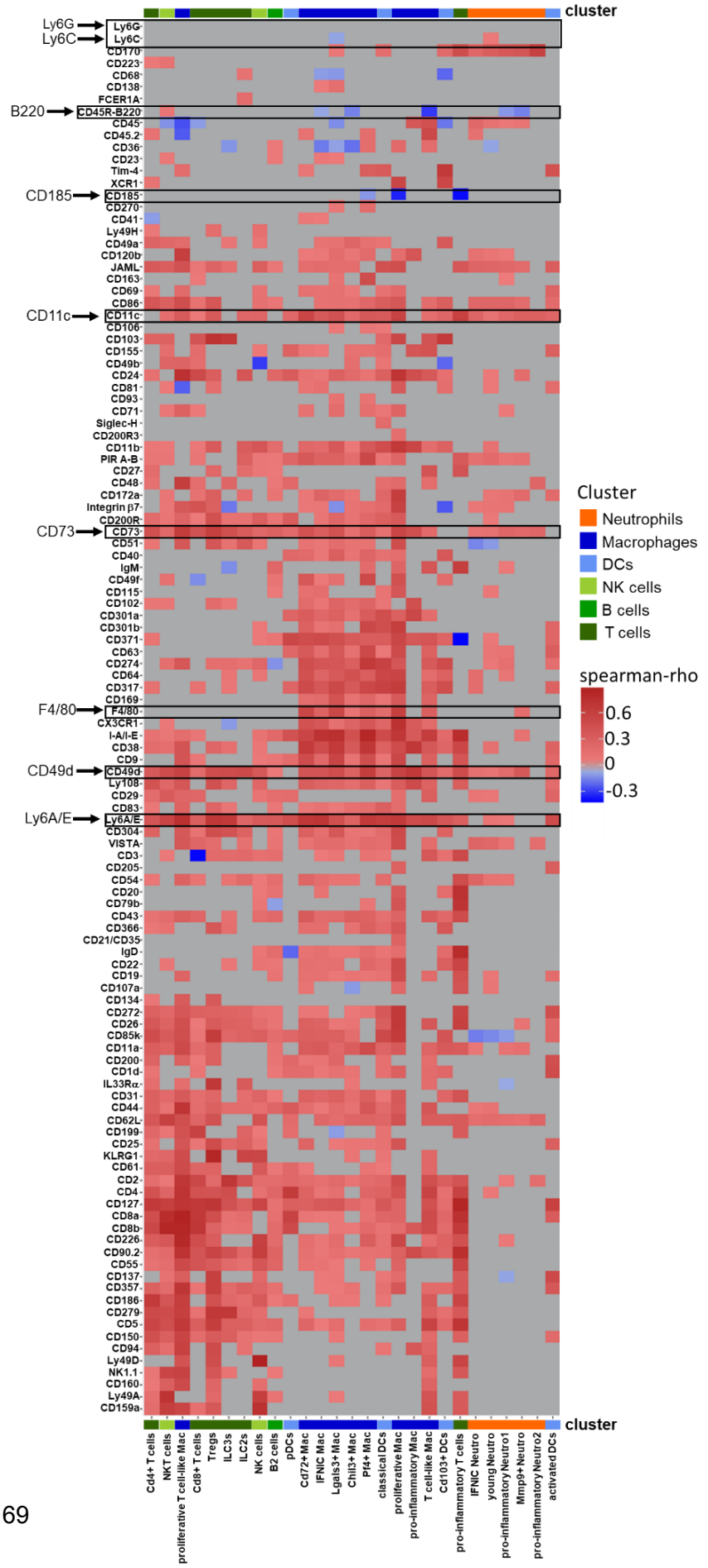

Figure 24: Spearman correlation between mRNA and protein expression of 119 proteins across cell clusters detected by CITE-seq. Protein names are shown on the left side of the heatmap and cluster names are shown at the bottom. Color bars on top and bottom of the heatmap indicate the immune cell type of the cluster (neutrophils, macrophages, DCs, NK cells, B cells, T cells). The color gradient of the heatmap represents the obtained spearman-rho. Red indicates a positive correlation, blue shows a negative correlation grey represents no correlation (r = 0). Black arrows and boxes highlight examples of proteins with no correlation to corresponding RNA expression (Ly6G, Ly6C), strong positive correlation (CD11c, CD73, CD49d, Ly6A/E), positive correlation for specific cell types (F4/80) and negative correlation (B220, CD185).

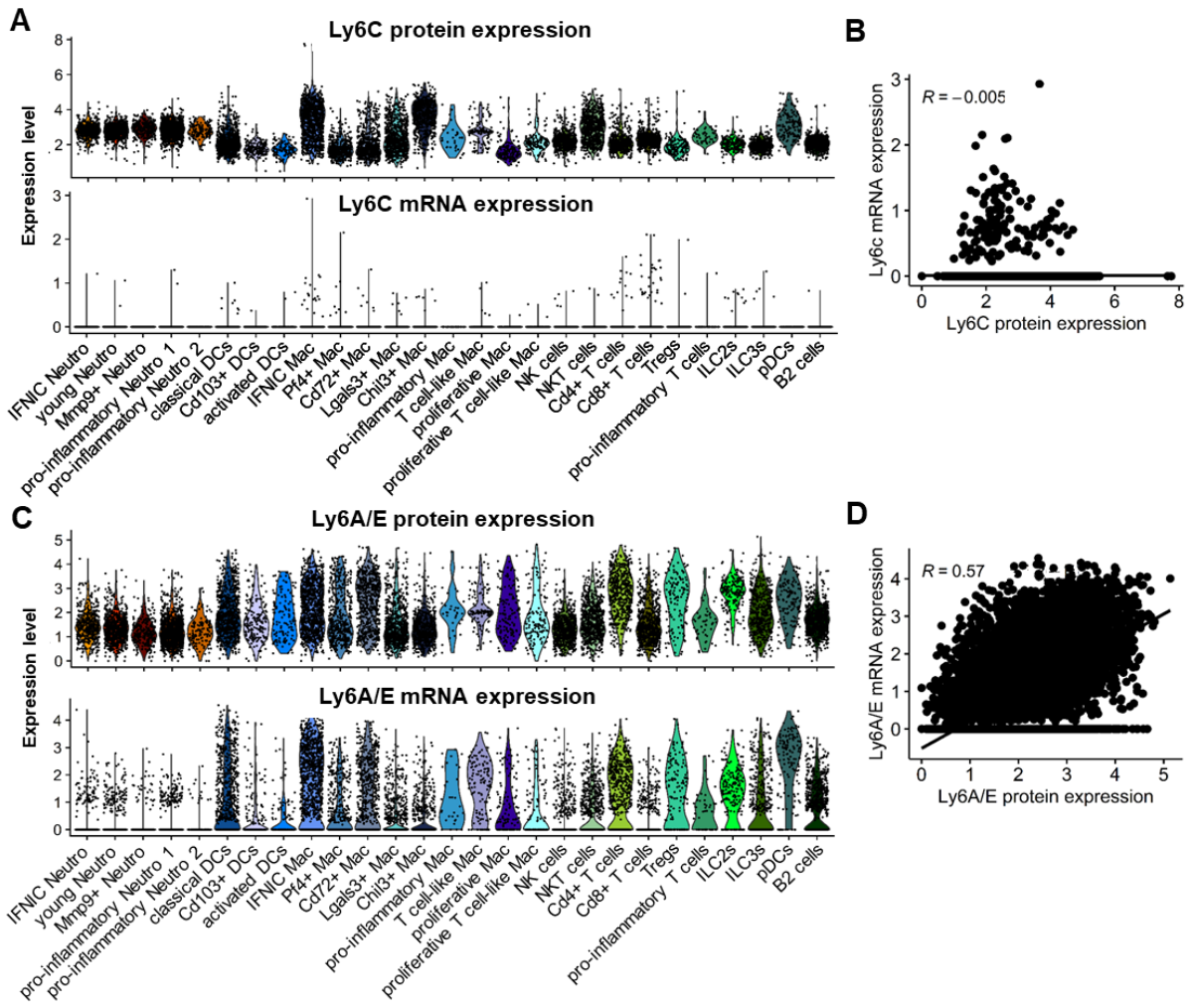

Figure 25: Representative comparison of protein and mRNA expression across all clusters and resulting overall spearman correlation for Ly6C and Ly6A/E in all cell types. A: Normalized and log-transformed expression level of Ly6C protein and mRNA across all clusters displayed in a violin plot. **B:** Overall spearman correlation of Ly6C protein and mRNA expression for all cell types. R = -0.005. **C:** Normalized and log-transformed expression level of Ly6A/E protein and mRNA across all clusters shown in a violin plot. **B:** Overall spearman correlation of Ly6A/E protein and mRNA expression for all cell types. R = 0.57.

4.2 The role of CD40 and CD40L signaling in AAA

Inflammatory processes are a hallmark of AAA pathology and are regulated by the interaction of co-stimulatory molecules like CD40 and CD40L. Previous works already showed that CD40-CD40L signaling plays a crucial role in AAA development and progression. CD40L-deficiency and pharmacological blocking of downstream CD40 signaling via TRAF6 protects against AAA formation and rupture.[84, 130] One aim of this work was to further investigate the role of CD40-CD40L signaling in AAA and to identify the cell types involved in the underlying pathophysiology.

4.2.1 CD40-deficiency protects from aortic aneurysm formation and rupture

First, the effect of global CD40-deficiency on AngII-induced aortic aneurysm formation and rupture was examined using CD40-deficient *Apoe*$^{-/-}$*Cd40*$^{fl/fl}$*CreER*^{T2} mice and their *Apoe*$^{-/-}$*Cd40*$^{fl/fl}$*CreER*^{wt} littermates as control. In contrast to the elastase-perfusion model used in this work so far, mice in the AngII-model develop not only aneurysms in the abdominal section of the aorta but also thoracic aortic aneurysms (TAA). In addition, the rupture of aortic aneurysms can be studied in the AngII-model. The Kaplan-Meier curve showed improved survival of CD40-deficient mice, suggesting fewer ruptures of AAA or TAA in *Apoe*$^{-/-}$*Cd40*$^{fl/fl}$*CreER*^{T2} mice compared to their *Apoe*$^{-/-}$*Cd40*$^{fl/fl}$*CreER*^{wt} littermates (Figure 26 C). Nevertheless, the difference in survival did not reach the significance level ($p = 0.15$). Next, the incidence of aortic aneurysms was examined. AAAs and TAAs that reached a 1.5-fold expansion in aortic diameter or that ruptured were classified as aortic aneurysms. The incidence of AAA or TAA formation was significantly reduced in CD40-deficient mice (Figure 26 D). In addition, this was reflected in macroscopic images (Figure 26 A) and ultrasound measurements that revealed a significantly decreased abdominal aortic diameter in CD40-deficient mice on day 28 after AngII-pump implantation (Figure 26 B and E).

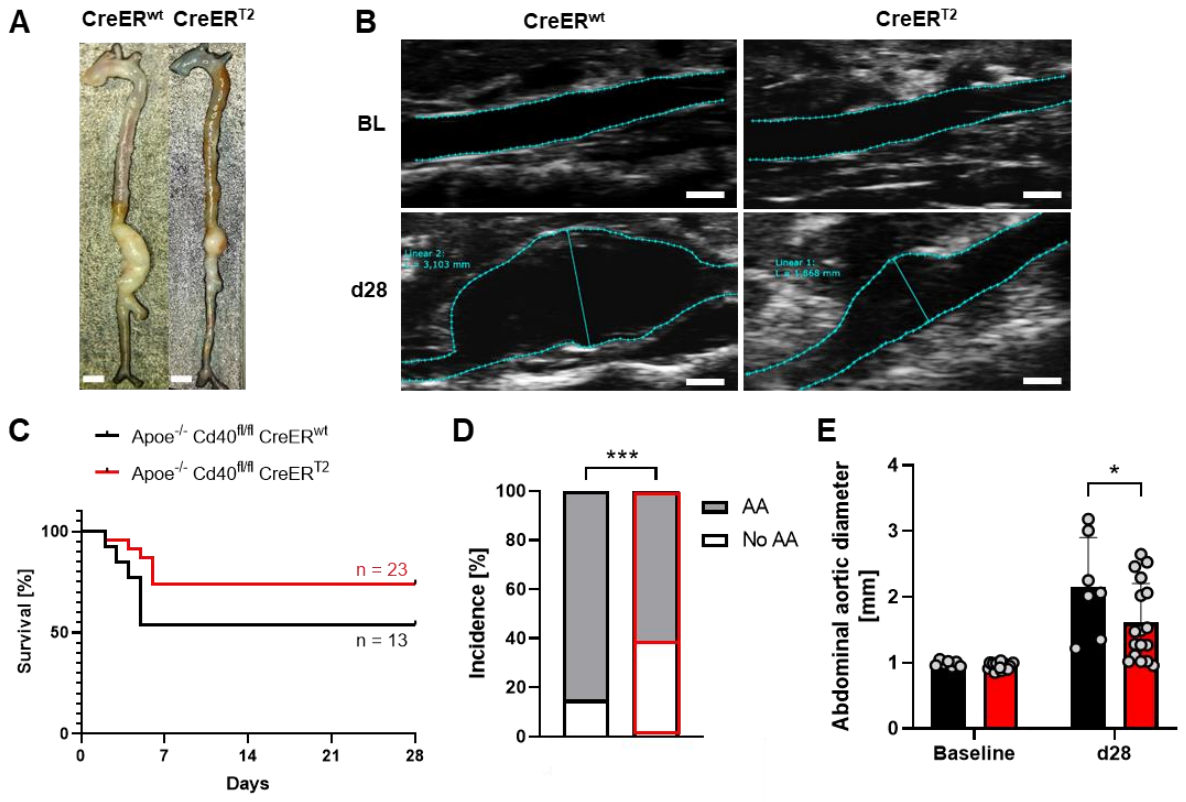

Figure 26: Global CD40-deficiency protects against aortic aneurysm (AA) formation induced via AngII infusion. A: Representative macroscopic images of aortae harvested from *Apoe*$^{-/-}$*Cd40*$^{fl/fl}$*CreER*^{T2} and *Apoe*$^{-/-}$*Cd40*$^{fl/fl}$*CreER*^{wt} mice 28 days after AngII-induced AAA formation. Scale bar = 2 mm. **B:** Representative ultrasound images of the abdominal aorta baseline (BL) and 28 days after AngII pump implantation of *Apoe*$^{-/-}$*Cd40*$^{fl/fl}$*CreER*^{T2} and *Apoe*$^{-/-}$*Cd40*$^{fl/fl}$*CreER*^{wt} mice. Scale bar = 1 mm. **C:** Kaplan-Meier survival curve of CD40-deficient *Apoe*$^{-/-}$*Cd40*$^{fl/fl}$*CreER*^{T2} mice (n = 23) and their *Apoe*$^{-/-}$*Cd40*$^{fl/fl}$*CreER*^{wt} littermates (n = 13) after AngII-pump implantation. Log-rank (Mantel-Cox) test. p = 0.15. **D:** Incidence of AAA or TAA, in *Apoe*$^{-/-}$*Cd40*$^{fl/fl}$*CreER*^{T2} mice (n = 23) and their *Apoe*$^{-/-}$*Cd40*$^{fl/fl}$*CreER*^{wt} littermates (n = 13) after AngII-pump implantation. Mice that died due to AAA or TAA rupture were included in this analysis. Two-sided Fisher exact test. p = 0.0002. **E:** Ultrasound measurements of abdominal aortic diameter baseline and at day 28 after AngII-pump implantation of *Apoe*$^{-/-}$*Cd40*$^{fl/fl}$*CreER*^{T2} mice (n = 17) and their *Apoe*$^{-/-}$*Cd40*$^{fl/fl}$*CreER*^{wt} littermates (n = 7). Data are presented as mean ± SD. Two-way ANOVA with Sidak's multiple comparison post-test. *p<0.05, ***p<0.001.

4.2.2 Expression patterns of CD40 and CD40L in elastase-induced AAA

To examine CD40 and CD40L expression and identify CD40- and CD40L-expressing cell types in AAA, scRNA-seq, CITE-seq, flow cytometry and immunofluorescence stainings were used. First CD40 mRNA expression was examined in human AAA tissue using the published scRNA-seq dataset GSE166676.[176] Re-analysis of this dataset containing human AAA tissue and control tissue showed expression of *CD40* on all identified cell types, including T cells, epithelial cells, neutrophils, B cells, NK cells, macrophages, fibroblasts/SMCs and endothelial cells in human AAA tissue (Figure 27 A). B cells exhibited the strongest *CD40* expression in human AAA. In control tissue, *CD40* was barely expressed. Next, mRNA expression of CD40 was studied in the scRNA-seq dataset presented in this work containing experimental elastase-induced AAA in mice. In murine AAA *Cd40* was likewise stronger expressed in AAA

compared to control tissue, but instead of B cells, macrophages and DCs were the predominant *Cd40*-expressing cells (Figure 27 B). Comparison of *Cd40* expression on macrophages and DCs at the different time points revealed the highest number of *Cd40* expressing macrophages and DCs at day 7 after elastase-induced AAA formation (Figure 27 C). However, this is probably due to the fact that there is a higher number of macrophages and DCs in aneurysmal tissue at day 7 compared to the other time points. *Cd40* was expressed on almost all macrophage and DC subsets with IFNIC macrophages, classical DCs and activated DCs exhibiting the strongest *Cd40* expression (Figure 27 D). Protein expression of CD40 in murine AAA was examined using the CITE-seq dataset. On protein level, CD40 was strongest expressed on B cells, followed by DCs and macrophages (Figure 27 E). CD40 protein was expressed on all macrophage and DC subsets and on B2 cells (Figure 27 F). Activated DCs exhibited the strongest CD40 protein expression.

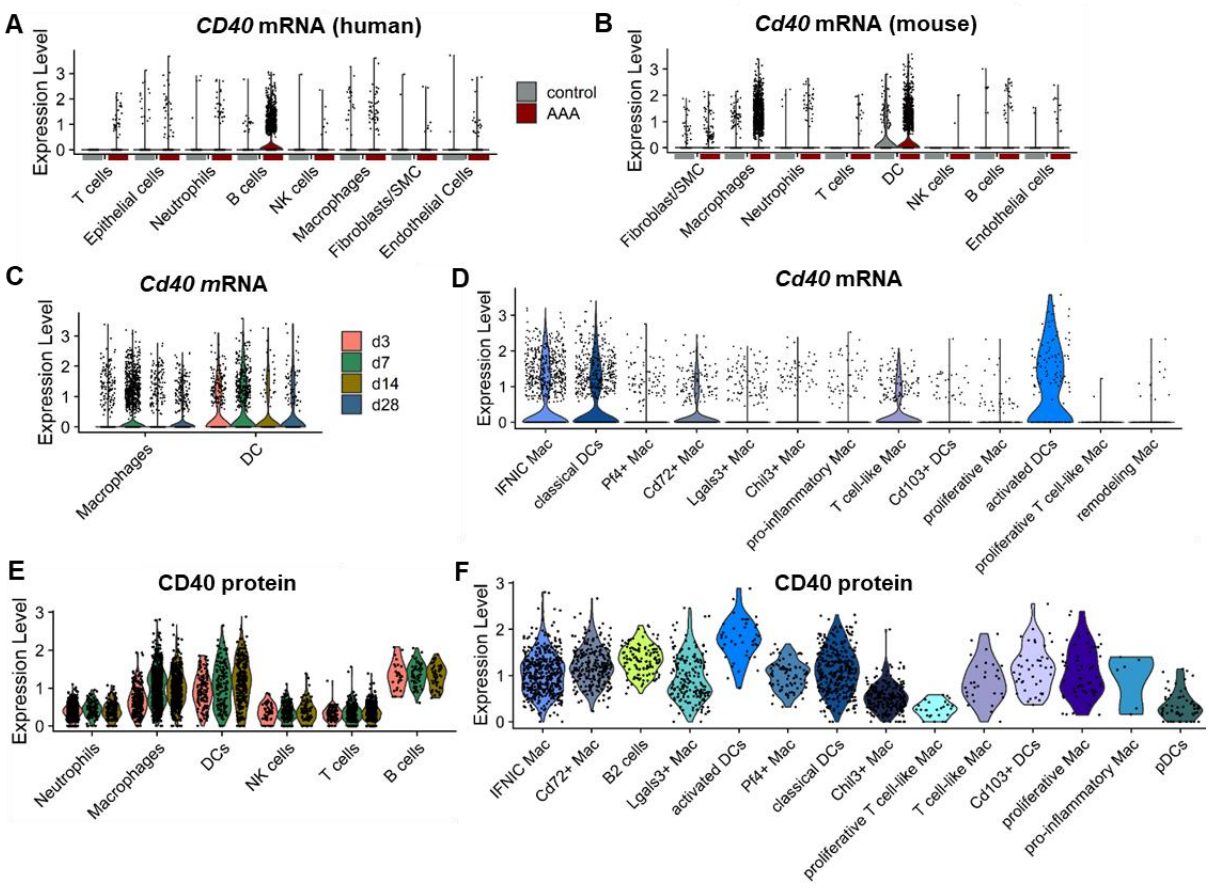

Figure 27: CD40 expression patterns in AAA obtained from scRNA-seq and CITE-seq. A: *CD40* mRNA expression on T cells, epithelial cells, neutrophils, B cells, NK cells, macrophages, fibroblasts/SMC and endothelial cells in human AAA tissue (red) and control tissue (grey). Re-analysis of the scRNA-seq dataset GSE166676. **B:** *Cd40* mRNA expression on fibroblast/SMC, macrophages, neutrophils, T cells, DCs, NK cells, B cells and endothelial cells in elastase-induced AAA (red) compared to saline and non-perfused controls (grey) obtained from scRNA-seq. **C**: Expression level of *Cd40* mRNA in macrophages and DCs at day 3, 7, 14 and 28 in the scRNA-seq dataset. **D:** *Cd40* mRNA expression level on macrophage and DC subpopulations in the scRNA-seq dataset. E: CD40 protein expression level obtained from CITE-seq on macrophages, neutrophils, T cells, DCs, B cells and NK cells at day 3, 7 and 14. **F:** CD40 protein expression on macrophage, DC and B cell subsets present in the CITE-seq dataset.

Flow cytometry was used to examine differences in the expression of CD40 on neutrophils, macrophages and B cells between saline- and elastase-perfused aorta, as well as between day 3, 7, 14 and 28 post surgery using mean fluorescence intensity (MFI) (Figure 28). Samples with less than 10 neutrophils, macrophages or B cells were excluded from analysis. For neutrophils no significant differences in the expression level of CD40 were observed (Figure 28 A). The samples showed a high variation especially at day 3 and 28, which is probably due to low cell numbers (Figure 28 B). While the CD40 expression on macrophages seemed to decrease in saline-perfused aortae from day 3 to day 28, it tended to increase in elastase-perfused aortae. On day 28, CD40 expression on macrophages was even significantly increased in elastase-perfused aortae compared to saline-perfused aortae. In B cells CD40 expression was higher in elastase-perfused aortae compared to saline-perfused aortae at all time points (Figure 28 C). However, the differences were not significant.

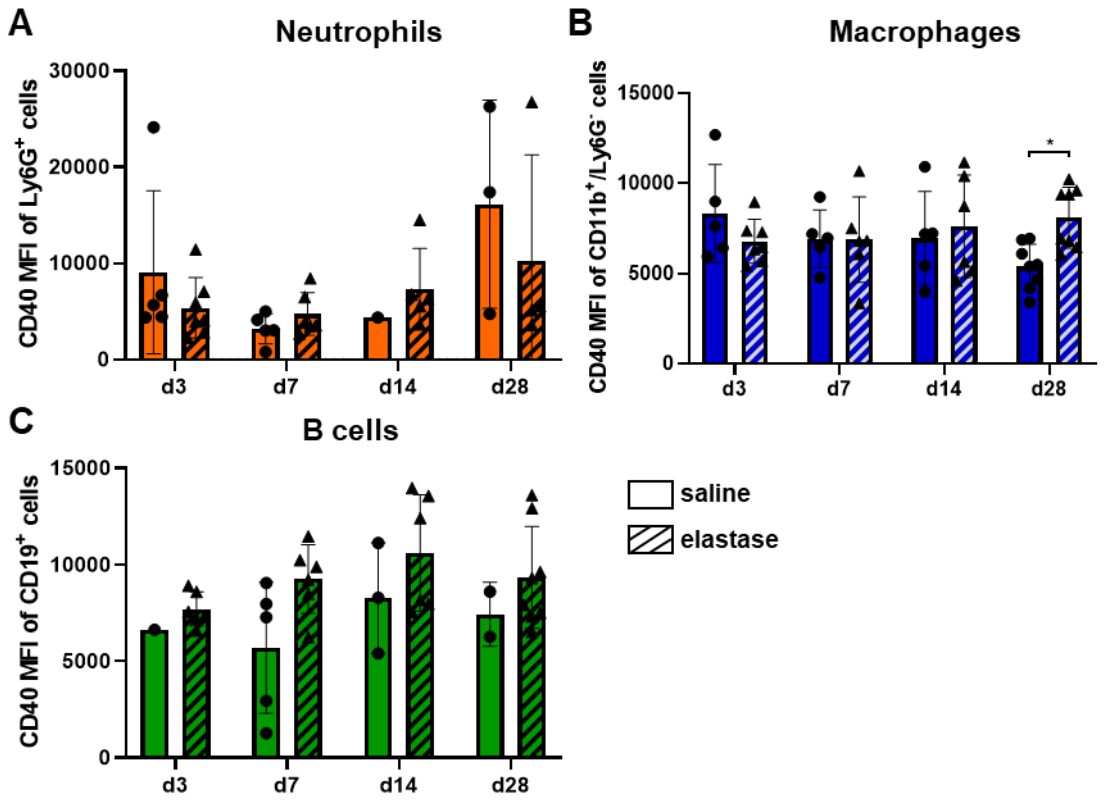

Figure 28: CD40 expression on immune cells at different stages of AAA formation measured with flow cytometry. Mean fluorescence intensity (MFI) of CD40 measured on Ly6G$^+$ neutrophils **(A)**, CD11b$^+$Ly6G$^-$ macrophages **(B)** and CD19$^+$ B cells **(C)** at day 3, 7, 14 and 28 after elastase or saline perfusion of the aorta. Data are presented as mean ± SD. Statistical analysis was performed using two-way ANOVA with Sidak's multiple comparison post-test. *p<0.05.

These flow cytometric analyses of CD40 expression on immune cells was corroborated by histological analyses. Immunofluorescence co-staining of neutrophils, macrophages, DCs and B cells with CD40 showed that approximately 60% to 80% of the immune cells expressed CD40 (Figure 29 A-D). Neutrophils and macrophages displayed the strongest CD40 expression 7 days after elastase-induced AAA formation (Figure 29 A and B). The proportion of CD40-expressing cells was significantly higher on day 7 compared to day 28. For DCs and B cells no significant differences in the proportion of CD40-expressing cells between the different time points were observed (Figure 29 C and D).

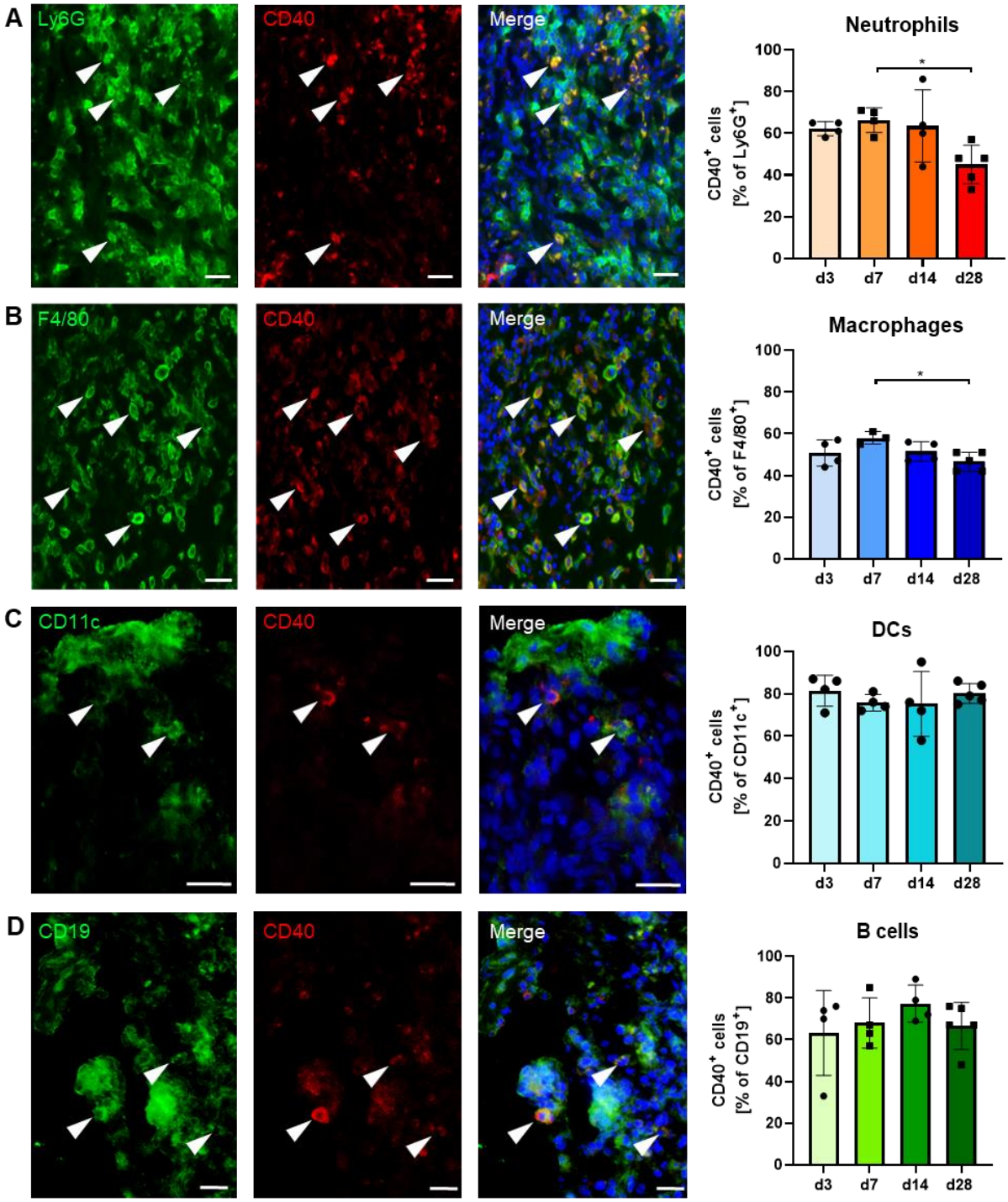

Figure 29: Proportion and localization of CD40-expressing immune cells in aneurysmal tissue. Percentage of CD40-expressing neutrophils **(A)**, macrophages **(B)**, DCs **(C)** and B cells **(D)** detected with immunofluorescence staining 3, 7, 14 and 28 days after elastase perfusion. Representative images of different immune cells (green), CD40 expression (red) and merged images, as well as quantification of the proportion of CD40-expressing cells. Nuclei were stained with DAPI (blue). White arrows indicate double positive cells. Scale bar = 20 µm. Statistical analysis was performed using one-way ANOVA with Tukey's multiple comparison post-test or Kruskal-Wallis test with Dunn's multiple comparison post-test. *p<0.05

CD40L mRNA expression in human and murine AAA was examined using the published scRNA-seq dataset GSE166676[176] and the scRNA-seq dataset presented in this work, which contains experimental elastase-induced AAA in mice. Protein expression of CD40 was investigated with immunofluorescence staining. In human AAA, *CD40L* was mainly expressed on T cells and on few NK cells (Figure 30 A). In murine elastase-induced AAA *Cd40lg* was likewise predominantly expressed on T cells, but also detected on some macrophages, DCs and NK cells (Figure 30 B). Very low *Cd40lg* expression was only occasionally detected in the controls of both datasets (Figure 30 A and B). The highest number of *Cd40lg*-expressing T cells was observed 28 days after elastase-induced AAA formation (Figure 30 C). *Cd40lg* was predominantly expressed on $Cd4^+$ T cells and ILC3s (Figure 30 D). Few pro-inflammatory T cells, $Cd8^+$ T cells and Tregs also expressed *Cd40lg*, while no expression was detected on ILC2s. Immunofluorescence co-staining of CD3 with CD40L revealed that on average 80% of the T cells expressed CD40L 3, 7 and 14 days after elastase-induced AAA formation (Figure 30 E). On day 28, the proportion of CD40L-expressing T cells increased and 96.8% of all T cells expressed CD40L.

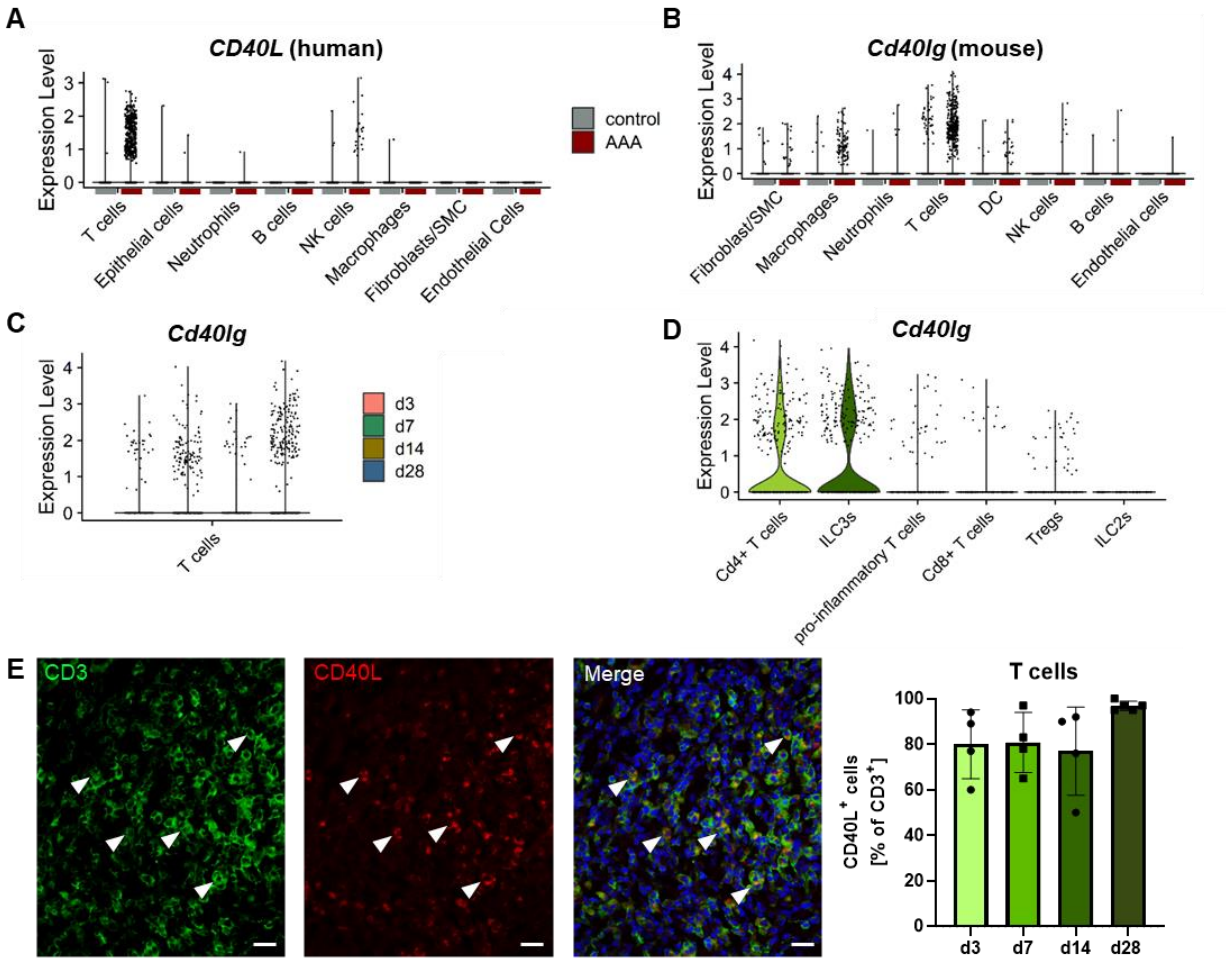

Figure 30: CD40L expression patterns in human and murine AAA. A: *CD40L* mRNA expression on T cells, epithelial cells, neutrophils, B cells, NK cells, macrophages, fibroblasts/SMC and endothelial cells in human AAA tissue (grey) and control tissue (red). Re-analysis of the scRNA-seq dataset GSE166676**. B: m**RNA expression level of *Cd40lg* on fibroblast/SMC, macrophages, neutrophils, T cells, DCs, NK cells, B cells and endothelial cells in elastase-induced AAA (grey) compared to saline and non-perfused controls (red). **C**: Expression level of *Cd40lg* on T cells at day 3, 7, 14 and 28. **D:** *Cd40lg* expression level on T cell subsets present in aneurysmal tissue obtained by scRNA-seq. **E:** Percentage of CD40L-expressing $CD3^+$ T cells detected with immunofluorescence staining 3, 7, 14 and 28 days after elastase perfusion (bar plot). Representative images of immunofluorescence co-staining of $CD3^+$ T cells (green) and CD40L (red). Nuclei were stained with DAPI (blue). White arrows indicate double positive cells. Scale bar = 20 µm. Data presented as mean ± SD.

4.2.3 IFNIC macrophages are the main receiver of CD40 signaling in AAA

CellChat can be used to investigate specific signaling pathways by identifying signaling roles of cell groups, computing the contribution of each ligand-receptor pair, visualizing the gene expression of ligands and receptors as well as visualizing cell-cell communication mediated by a single ligand-receptor pair. Since this chapter focus on the role of the co-stimulatory molecules CD40 and CD40L, which were shown to be most expressed at day 7 after elastase-induced AAA, CellChat was utilized to predict CD40 signaling at day 7 of AAA development. This prediction identified *Cd4*$^+$ T cells as strongest sender of CD40 signaling, followed by ILC3 cells, proliferative T cell-like macrophages and Tregs (Figure 31 A). The

dominant receiver of the CD40 signal were IFNIC macrophages and *Lgals3*$^{+}$ macrophages. Myofibroblasts, DCs, as well as most of the neutrophil and macrophage subpopulations were also predicted to receive CD40 signaling. All macrophage and DC subsets and the pro-inflammatory T cells functioned as influencers of CD40 signaling. The CD40 signaling pathway in the CellChat database includes not only signaling via CD40L and CD40, it also contains the interaction of CD40L with *Itgam*+*Itgb2* (encoding for CD11b and CD18, which is also known as Mac-1), and *Itga5*+*Itgb1* (encoding for CD49e and CD29, also known as VLA-5).[177] Looking at the contribution of each ligand-receptor pair involved in CD40 signaling, the CD40L-CD40 interaction was predicted to have the weakest impact in AAA at day 7 (Figure 31 B). However, considering the expression pattern of CD40L and its different receptors, the CD40 expression was restricted to all three DC subsets, IFNIC macrophages, *Cd72*$^{+}$- and T cell-like macrophages, while the other two receptors were expressed on almost all cell types (Figure 31 C). Accordingly, CD40L-CD40 interaction seemed to be most specific in AAA at day 7 and was predicted to occur predominantly between *Cd4*$^{+}$ T cells and IFNIC macrophages or classical DCs (Figure 31 D). IFNIC macrophages also interacted with CD40L expressing *Cd4*$^{+}$ T cells or ILC3s via Mac-1, but not via VLA-5. CD40L-Mac-1 interaction was observed in almost all cell types (Figure 31 D). CD40L-VLA5 signaling was strongest between *Cd4*$^{+}$ T cells and myofibroblast, as well as *Lgals3*$^{+}$ macrophages (Figure 31 D).

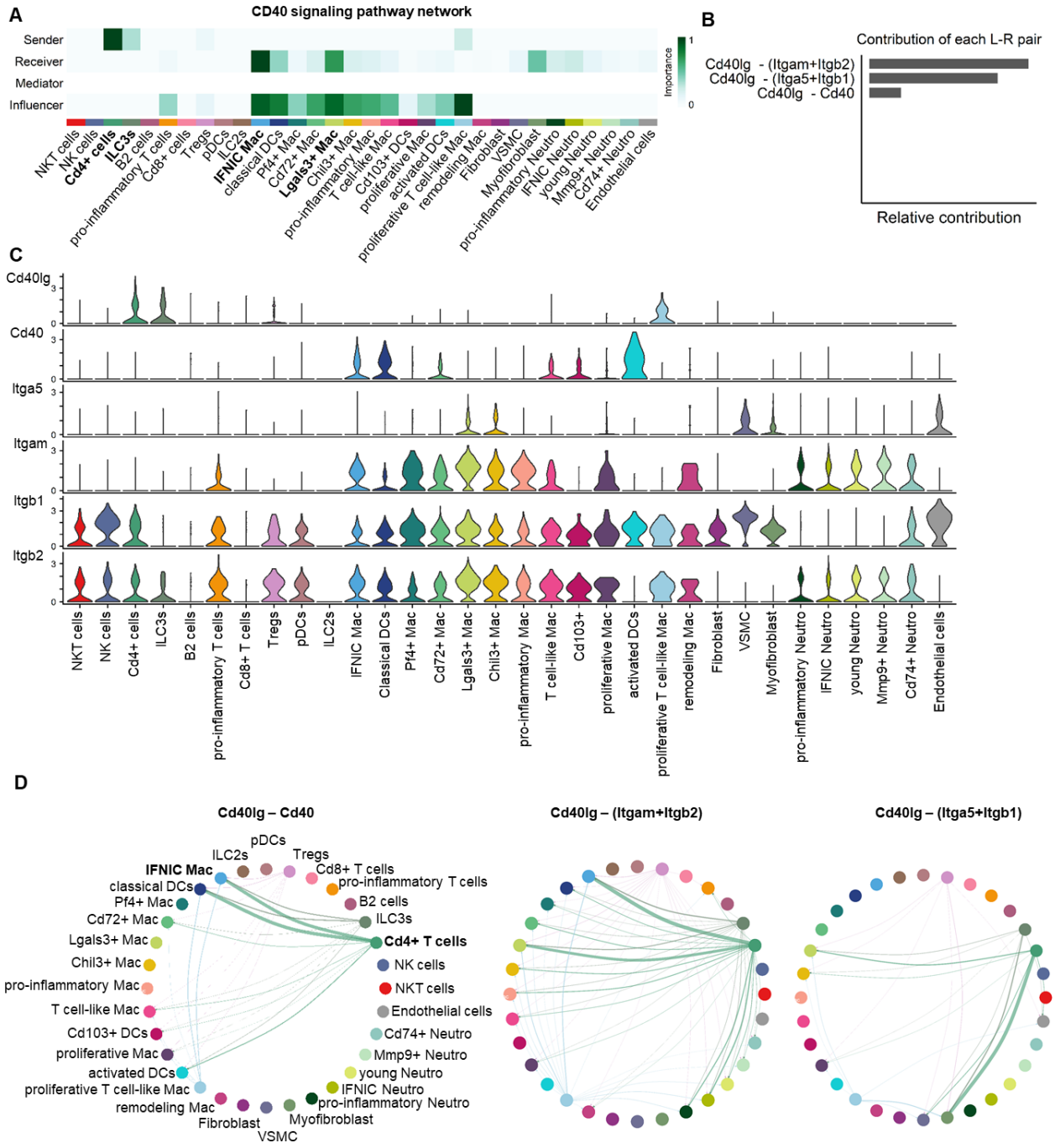

Figure 31: CD40 signaling at day 7 post elastase-induced AAA. A: Heatmap showing the CD40 signaling pathway network at day 7 indicating dominant senders and receivers of CD40 signaling, as well as mediators and influencers. The color code represents the importance of the cell type. **B:** The relative contribution of the three ligand-receptor pairs *Cd40lg*-(*Itgam+Itgb2*), *Cd40lg*-(*Itga5+Itgb1*) and *Cd40lg-Cd40* to CD40 signaling 7 days after AAA formation is presented in a bar plot. **C:** Violin plots showing the expression level of *Cd40lg, Cd40, Itga5, Itgam, Itbg1* and *Itgb2* across all cell types. **D:** Circle plots displaying the cell-cell communication via *Cd40lg-Cd40* (left panel), *Cd40lg*-(*Itgam+Itgb2*) (middle panel) and *Cd40lg*-(*Itga5+Itgb1*) (right panel). Line colors are consistent with the sources as sender. The thickness of the lines indicates the signal strength.

4.3 Detection and isolation of IFNIC macrophages in CVDs

The previous results showed that IFNIC macrophages represented a crucial immune cell population at day 7 and 14 after elastase-induced AAA, when immune cell infiltration and inflammation are most prominent. Their highly inflammatory properties and extensive communication with other cells, especially as primary recipients of CD40 signaling, highlight their potential as crucial mediators of AAA-related inflammation and immune responses. Thus, investigating IFNIC macrophages could provide valuable insights into the mechanism driving AAA and identify potential therapeutic targets. To enable further investigation of IFNIC macrophages this part of the thesis aimed to establish a method to identify and isolate these cells from aneurysmal tissue.

IFNIC macrophages were detected in AAA, atherosclerosis and MI using CITE-seq (Figure 32 A). Of the three CVDs, IFNICs were most frequently in AAA and least abundant in atherosclerosis. In AAA, they reached the highest proportion on day 7 with 19.7% of all immune cells. On day 14 they accounted for 12.7% of all immune cells and on day 3 only for 1.5% (Figure 32 B). In atherosclerosis, IFNIC macrophages represented only 0.2% and 1.1% of all immune cells. In MI, the proportion of IFNIC macrophages increased from 2.6% on day 1 to 7.3% of all immune cells on day 5 (Figure 32 B). In addition, IFNIC macrophages were identified and localized in aneurysmal tissue using RNA scope staining in combination with a usual antibody staining (Figure 32 C). At the RNA level, RNA scopes for *Irf7*, which was previously defined as one of the best markers for IFNIC macrophages by scRNA-seq, and the macrophage marker *Adgre1* were used. To confirm the detection of the cells on protein expression level, anti-F4/80 antibody was used. The co-localization of the IFNIC marker *Irf7* with the macrophage marker *Adgre1* and F4/80 antibody defined the detection of IFNIC macrophages in aneurysmal tissue (Figure 32 C).

To further investigate IFNIC macrophages, a flow cytometry panel was designed to identify IFNIC macrophages in aneurysmal tissue and collect them for further investigations. As some of the planned experiments for further downstream applications require viable cells, intracellular stainings that include fixation of the cells were not suitable for the panel. Accordingly, it was not feasible to use the corresponding proteins for the identified IFNIC marker genes, as most of the proteins are intracellular and correlation between gene and protein expression is poor.[175, 178] Thus, the CITE-seq data was used to identify surface proteins that were expressed on IFNIC macrophages and can be used to distinguish IFNIC macrophages from the other macrophage subsets.

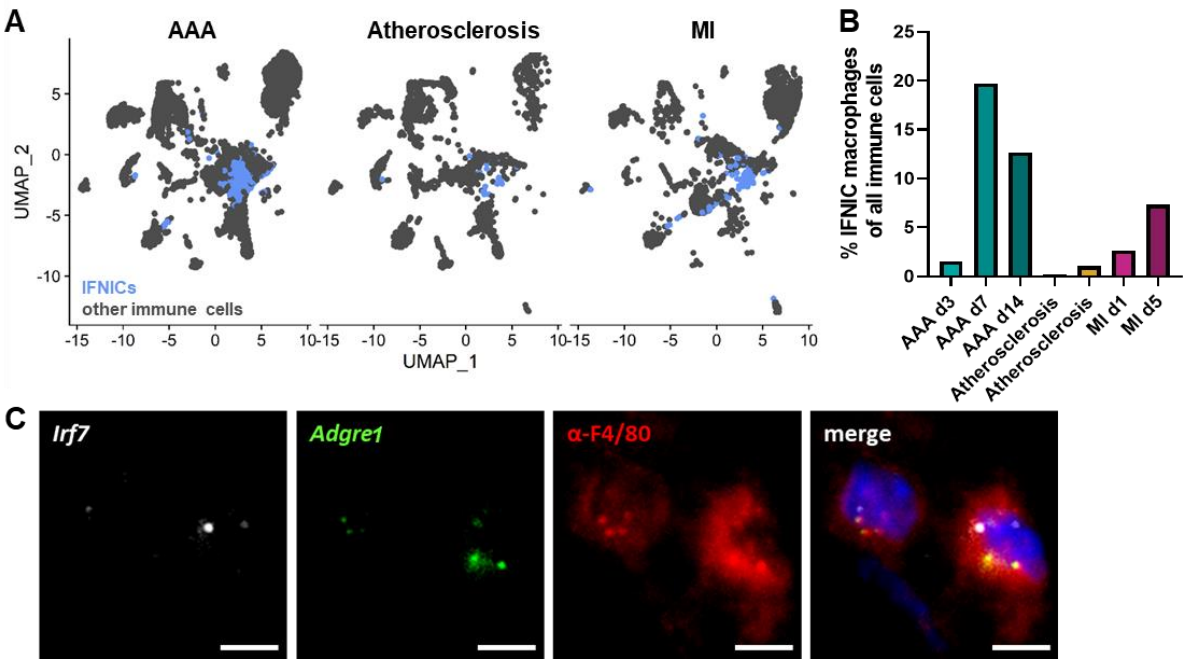

Figure 32: Detection of IFNIC macrophages in experimental AAA, atherosclerosis and MI A: UMAP-plot of immune cell clusters in AAA, atherosclerosis and MI observed with CITE-seq. IFNIC macrophages are highlighted in blue, while all other cells are displayed in grey. **B:** Bar plot presenting the proportion of IFNIC macrophages of all immune cells in AAA at day 3, 7 and 14, atherosclerosis and MI at day 1 and 5. **C:** Representative images of the identification of IFNIC macrophages in AAA tissue based on *Irf7* (white) and *Adgre1* (green) RNA expression (RNA scope staining) in combination with antibody staining for macrophages with F4/80 antibody (red). Scale bar 5 µm.

First, all macrophage subpopulations present in aneurysmal tissue were bioinformatically isolated and differentially-expressed proteins for each macrophage subset were identified using the *Seurat* function *FindAllMarkers()* (supplementary table 6). Overall, the expression profile of the 119 antibodies detected with CITE-seq was rather similar for the different macrophage subsets resulting in only few marker proteins for the different clusters. For IFNIC macrophages only two differentially-expressed proteins (CD36 and Ly6C) were found (Figure 33 A, supplementary table 6). Both marker proteins were not exclusively expressed on IFNIC macrophages as CD36 and Ly6C were even higher expressed on *Chil3*$^{+}$ macrophages. Proliferative T cell-like macrophages, proliferative macrophages and pro-inflammatory macrophages could be clearly identified and distinguished from the other subsets by exclusively expressed proteins (Figure 33 A). All other macrophage subsets were difficult to distinguish based on the obtained marker proteins.

As no specific marker proteins for IFNIC macrophages could be found using CITE-seq, a combination of CD11b, Ly6C, CD36 and Ly6A/E was used to distinguish IFNIC macrophages (colored in pink) from the other macrophage subclusters (Figure 33 B). For each of the proteins a threshold for the expression level was defined and only cells above this threshold were used for further analysis. First, only macrophages that showed a CD11b expression

higher than 2.5 were selected leading to the elimination of proliferative T-cell like macrophages (Figure 33 B). Next, cells that highly expressed Ly6C (expression level > 2.5) were bioinformatically isolated, resulting in the exclusion of almost all *Pf4*$^{+}$ macrophages and proliferative macrophages. Further subdivision of cells with an expression level of CD36 >1.5 eliminated the remaining proliferative macrophages. Last, all cells with a protein expression level of Ly6A/E higher than 2 were bioinformatically isolated. Unfortunately, almost half of the IFNIC macrophage population was lost during this rigorous gating step. However, this step was necessary to get rid of the majority of *Lgals3*$^{+}$ and *Chil3*$^{+}$ macrophages. In the end, mostly IFNIC macrophages were left, but it was not possible to isolate IFNICs solely, as *Cd72*$^{+}$ macrophages could not be clearly distinguished from IFNICs with the available protein markers in the CITE-seq dataset (Figure 33 C). In the end, this bioinformatically sequential subdivision of the cells led to a computed isolation and enrichment of IFNIC macrophages that were defined as CD11b^{+}, Ly6C^{high}, CD36^{+} and Ly6A/E^{+} .

For easier transfer to flow cytometry, “bi-axial” gating plots and the function *CellSelector()* were used to model the gating strategy similar to flow cytometry gating (Figure 33 D). For this gating model, all immune cells present in aneurysmal tissue were isolated from the CITE-seq data. First, protein expression level of CD45 and CD11b on all immune cells were displayed in an “bi-axial” gating plot. All immune cells expressed CD45, but only neutrophils, macrophages and DCs expressed CD11b. CD11b^{+} cells were selected and the expression of Ly6G and Ly6C on these cells was examined. In this step, neutrophils could be distinguished from macrophages and DCs by their Ly6G expression. After excluding Ly6G^{+} neutrophils, Ly6C^{high} cells were selected for further gating as the majority of IFNIC macrophages was identified as Ly6C^{high}. Finally, IFNIC macrophages were selected as Ly6A/E^{+} and CD36^{+} cells (Figure 33 D).

As the CITE-seq dataset is limited to the 119 used antibodies, it is likely that other surface proteins not included in the CITE-seq dataset would represent better markers for IFNICs. Thus, interferon-alpha/beta receptor subunit 1 (IFNAR1), that activates the JAK-STAT signaling pathway upon binding of type-I IFNs[159, 179], was included in the final flow cytometry panel. Finally, IFNIC macrophages were characterized as CD11b^{+}, Ly6C^{high}, CD36^{+}, Ly6A/E^{+}, IFNAR^{+}. To investigate the CD40 expression on IFNIC macrophages, CD40 was also included in the panel. The panel was complemented with a viability dye, the leukocyte marker CD45, with a dump channel containing CD3, CD19, CD11c and NK1.1 to exclude T cells, B cells, DCs and NK cells, respectively, and with Ly6G to exclude neutrophils (Table 5 in method section).

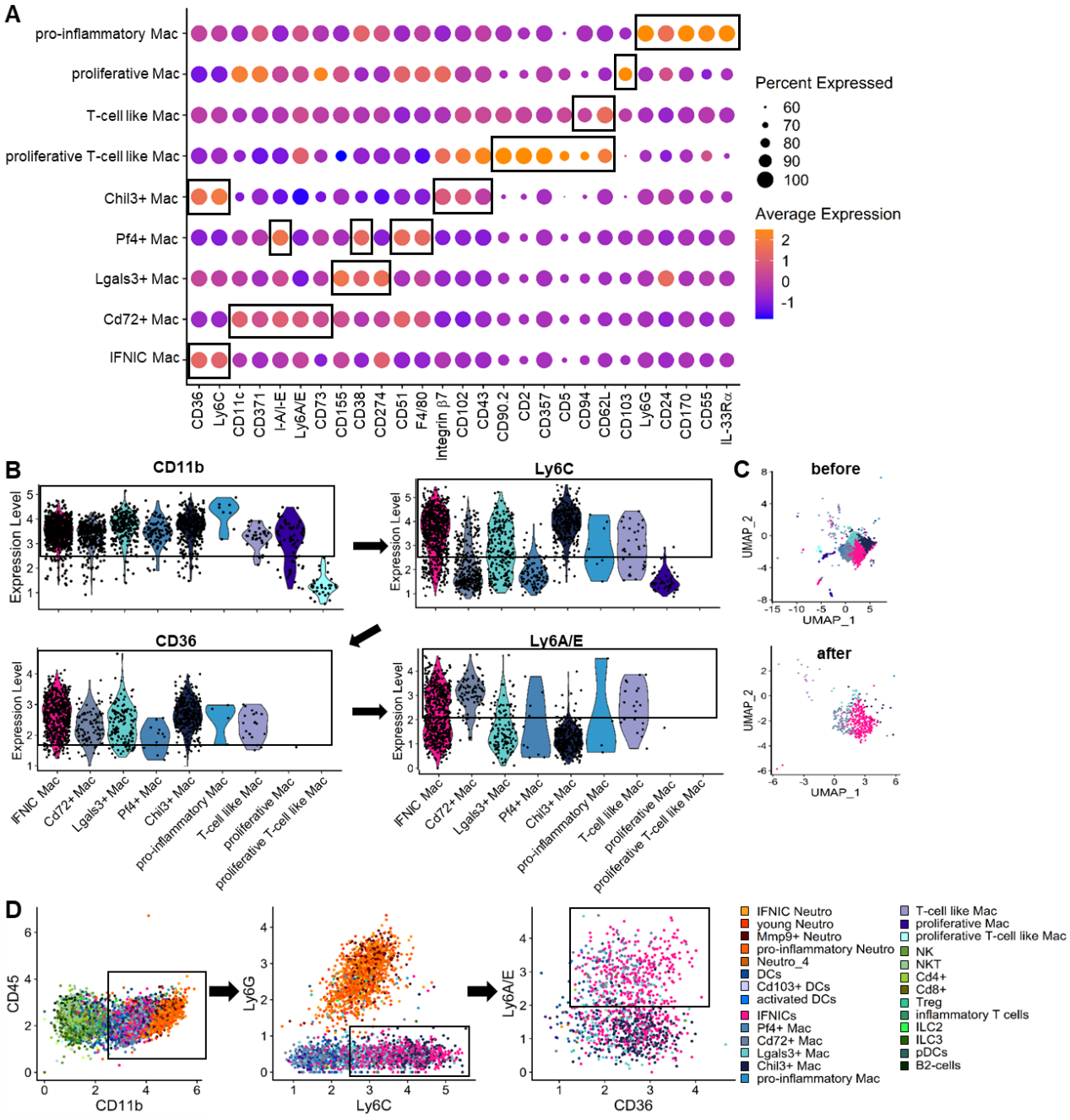

Figure 33: Marker proteins of macrophage subsets and gating strategy to identify IFNIC macrophages based on CITE-seq data. Macrophages present in aneurysmal tissue were bioinformatically isolated from the CITE-seq dataset. *FindAllMarkers()* was used to identify differentially-expressed proteins for each cluster. Selected proteins were used to model a flow cytometric gating strategy to identify IFNIC macrophages. **A:** The top markers for each macrophage subtype are presented in a dotplot. The size of the dot represents the percentage of cells belonging to one cluster that expressed the protein. The color code indicates the average expression level of the protein in the cluster. Black boxes indicate the identified marker genes per cluster. **B-D:** Bioinformatically modeled gating strategy using CD11b, Ly6C, CD36 and Ly6A/E to bioinformatically enrich IFNIC macrophages. IFNIC macrophages are colored pink. **B:** Expression level of CD11b, Ly6C, CD36 and Ly6A/E on macrophages is show in violin plots. Black boxes indicate the selected cells for subsequent gating. Cells with CD11b and Ly6C expression >2.5, CD36 expression > 1.5 and Ly6A/E expression > 2 were selected, leading to exclusion of most other macrophage subsets but also of some IFNIC macrophages. **C:** Dimplots before and after gating demonstrating the bioinformatically enrichment of IFNIC macrophages. **D:** Bi-axial gating plots of protein expression and *CellSelector()* function were used to model the gating strategy similar to flow cytometry gating. All immune cells present in aneurysmal tissue were used and each cell type is displayed in a different color. First, $CD45^{+}CD11b^{+}$ cells were selected, then $Ly6G^{-}Ly6C^{high}$ cells were gated and finally IFNIC macrophages were identified as $Ly6A/E^{+}CD36^{+}$ cells.

The resulting flow cytometry panel was used to identify and collect IFNIC macrophages from murine tissue. Since IFNIC macrophages are also present in MI and a larger number of mice with reperfused MI were more easily accessible than mice with AAA, mice hearts were harvested 5 days after inducing experimental MI, digested into single-cells, stained with the IFNIC panel and subjected to cell sorting. The collected cells were further analyzed using qPCR. $CD11b^{+}Ly6C^{low}$ cells (Sort 1) were collected as negative control (Figure 34 A). $CD11b^{+}Ly6C^{high}Ly6A/E^{+}IFNAR1^{+}$ cells (Sort 2) and $CD11b^{+}Ly6C^{high}Ly6A/E^{+}IFNAR1^{-}$ cells (Sort 3) were collected as assumed IFNICs. RNA was isolated from the 3 samples collected, pre-amplified and analyzed with qPCR for the expression of the IFNIC-marker genes *Irf7*, *Isg15*, *Ifit3*, *Cxcl10,* and *Cd40*. The $CD11b^{+}Ly6C^{high}Ly6A/E^{+}IFNAR1^{+}$ cells of sort 2 and the $CD11b^{+}Ly6C^{high}Ly6A/E^{+}IFNAR1^{-}$ cells of sort 3 showed a higher expression of *Irf7*, *Isg15*, *Ifit3* and *Cxcl10* compared to the $CD11b^{+}Ly6C^{low}$ cells of sort 1 (Figure 34 B). While the expression of *Isg15* and *Ifit3* was similar in sort 2 and sort 3, *Irf7* and *Cxcl10* were slightly higher expressed in sort 3 compared to sort 2. *Cd40* expression was highest in sort 3, followed by sort 1 and lowest in sort 2.

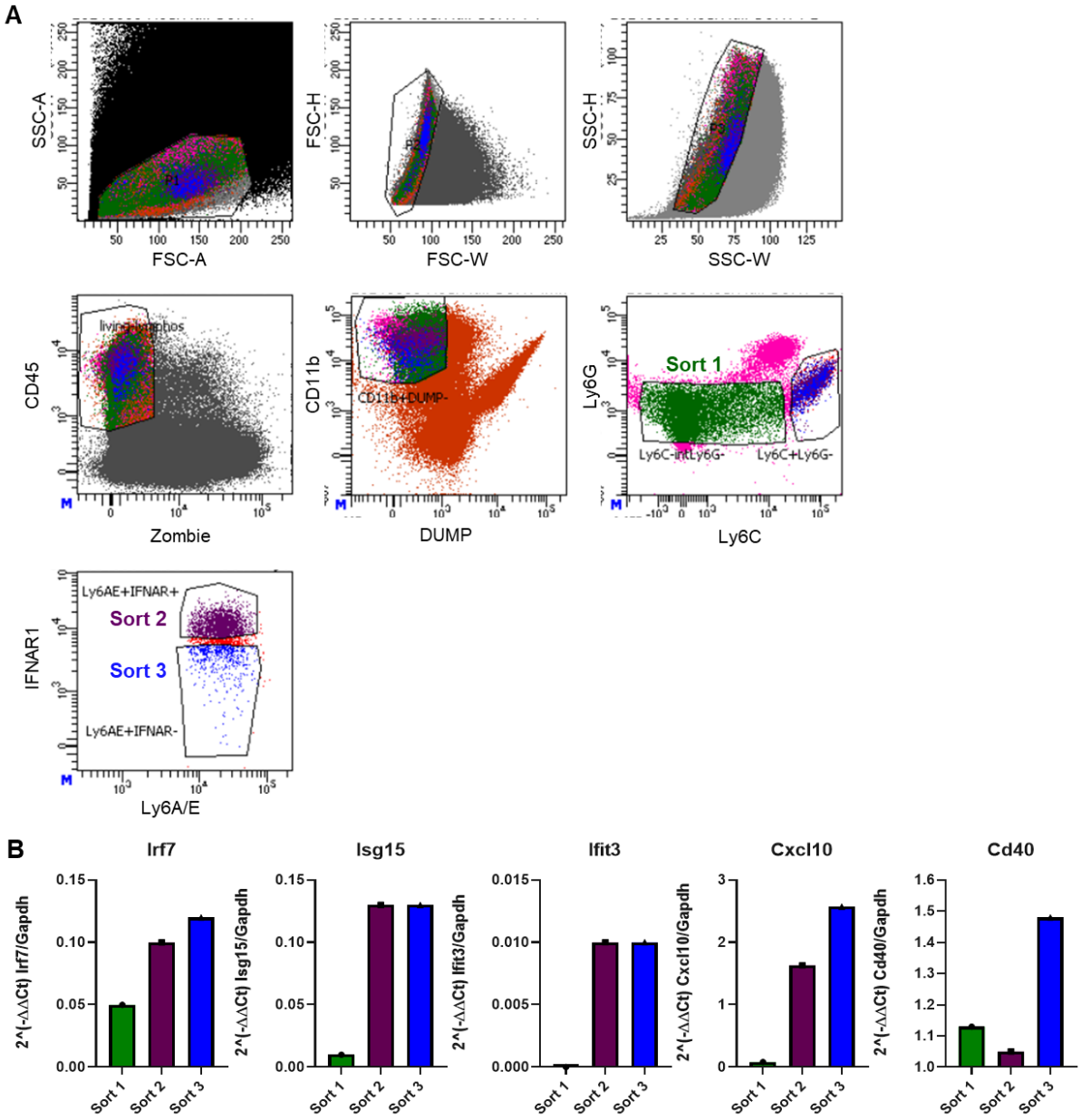

Figure 34: Cell sorting of IFNIC macrophages from infarcted hearts and analysis with qPCR. A: Gating strategy for sorting and collecting of CD11b^{+}Ly6C^{low} cells (Sort 1, green), CD11b^{+}Ly6C^{high}Ly6A/E^{+}IFNAR1^{+} cells (Sort 2, purple) and CD11b^{+}Ly6C^{high}Ly6A/E^{+}IFNAR1^{-} cells (Sort 3, blue). **B:** Expression of *Irf7*, *Isg15*, *Ifit3*, *Cxcl10* and *Cd40* normalized to *Gapdh* expression in the three different sorts obtained by qPCR.

Next, the IFNIC panel was used to quantify the number of IFNIC macrophages present in elastase-induced AAA compared to saline-perfused aortae 7 days after the surgery. The gating strategy to detect IFNIC macrophages is displayed in Figure 35 A and B for a representative experiment. First single-cells were identified using forward scatter-height versus forward scatter-area. Then viable immune cells were determined with CD45 and the viability marker Viakrome808. From the viable immune cells only CD11b^{+} myeloid cells were selected. DCs, NK cells, B cells and T cells were excluded using the markers CD11c, NK1.1, CD19 and CD3. The CD11b^{+} myeloid cells were distinguished in macrophages and

neutrophils with Ly6G. Within the CD11b^{+}Ly6G^{-} macrophages IFNIC macrophages were identified as Ly6C^{high}, IFNAR1^{+} and Ly6A/E^{+}. The gating strategies of saline-perfused control aorta (Figure 35 A) and elastase-perfused aorta (Figure 35 B) showed already a difference in overall number of cells and also in abundance of IFNIC macrophages. In the saline-perfused aorta no IFNIC macrophages were detected, while IFNIC macrophages could be detected in elastase-perfused aorta. The quantification of absolute cell number of IFNIC macrophages in the whole aortic tissue using counting beads revealed significant more IFNIC macrophages in elastase-induced AAA compared to saline-perfused controls (Figure 35 C). On average 937 IFNIC macrophages were detected in AAA, while only 13 IFNIC macrophages could be found in controls.

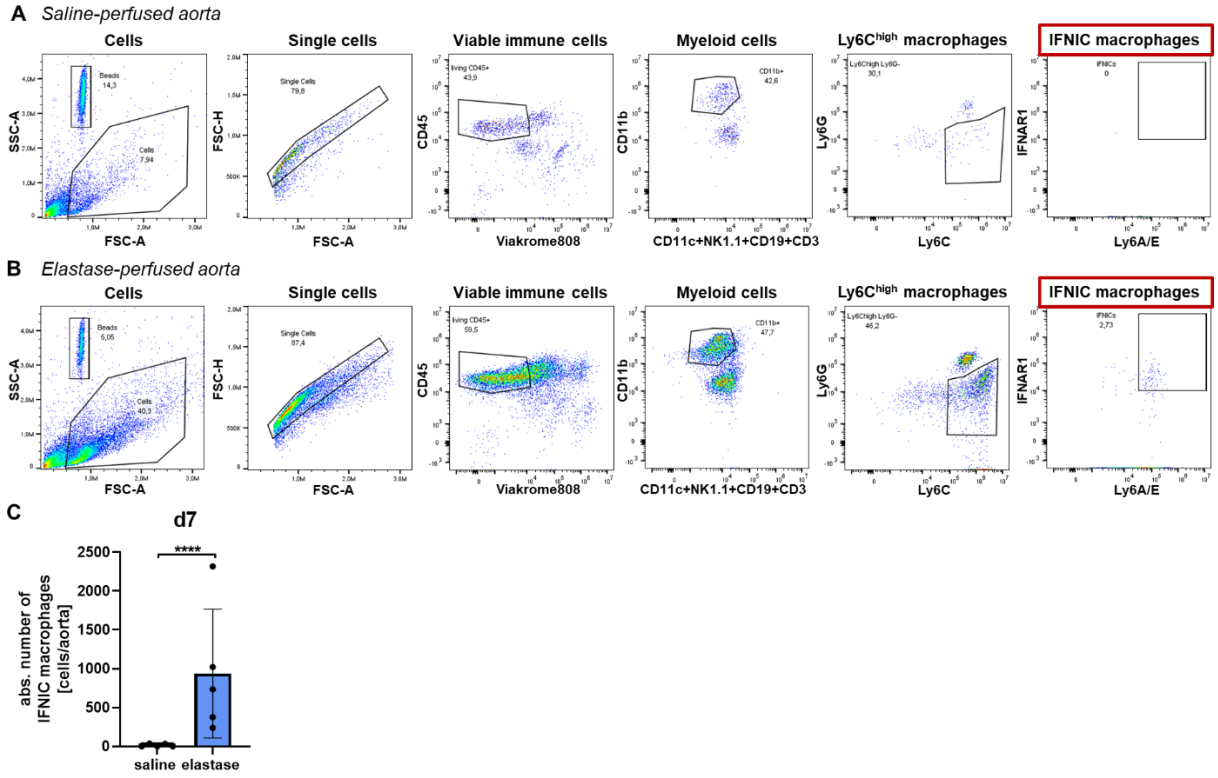

Figure 35: Flow-cytometric quantification of IFNIC macrophage count in elastase-induced AAA and saline-perfused control aortae 7 days after surgery. Gating strategy for IFNIC macrophages in saline-perfused aorta **(A)** and elastase-induced AAA **(B)** 7 days after surgery. Cells and counting beads were identified using sideward- and forward scatter-area (SSC-A, FSC-A). Single cells were detected using forward scatter-height (FSC-H) and FSC-A. Viable immune cells were determined as CD45^{+} and negative for the viability dye Viakrome808. Next, CD11b^{+} and CD11c^{-}, CD19^{-}, CD3^{-} and NK1.1^{-} were selected. From these cells only Ly6G^{-} and Ly6C^{high} cells were selected. Finally, IFNICs were identified as IFNAR1^{+} and Ly6A/E^{+} Ly6C^{high} macrophages. **C:** Absolute number of IFNIC macrophages in aortic tissue 7 days after saline- (n=5) or elastase- (n=5) perfusion. Unpaired T-test with Welch's correction. ****p<0.0001

4.4 Investigation of T and B cell clonality in elastase-induced experimental murine abdominal aortic aneurysm

The adaptive immune system is also known to play an important role in AAA formation. T and B cells infiltrate the aneurysmal tissue in high numbers and characteristics of an autoimmune response are described in AAA. To investigate a potential antigen-specific immune response, we examined T and B cell clonality in elastase-induced AAA using scRNA-TCR-BCR-seq. The following results were published as scientific paper in Frontiers in Cardiovascular Medicine in 2023.[102]

4.4.1 scRNA sequencing workflow

The experimental workflow started with the induction of AAA by perfusing the infrarenal aorta of male C57BL/6J mice with elastase or NaCl (Figure 36 A). AAA formation was monitored and analyzed via ultrasound imaging prior to surgery, at d7, d14 and d28. Infrarenal aortae were harvested on day 3, 7, 14 and 28 after PPE surgery and on day 3 and 28 after sham surgery and images were taken for macroscopic analysis. Additionally, infrarenal aortae from 6 non-treated C57BL/6J mice of which three were pooled into one sample were harvested for sequencing. In total 24 samples were subjected to scRNA sequencing and immunoreceptor analysis. All mice that underwent PPE surgery developed an AAA confirmed by ultrasound or macroscopic analysis of the infrarenal aorta (Figure 16 B and supplementary figure 2). Aortae were harvested and digested into single cell suspensions. Single cells were stained and sorted and then subjected to scRNA sequencing as well as scRNA-TCR-BCR-seq.

Consistent preprocessing of immune receptor scRNA-seq data is crucial for comparable data. We suggest using only those immune receptor data, with all fragments intact and both chains (α/β for TCR or heavy/light for BCR) present. Receptors with only one, or more than two chains, that can appear in the data frame due to sequencing errors, were excluded. After that, the information of the hashtag antibodies was added to the data to assign an immune receptor specifically to one cell of a specific mouse. Subsequently, the receptors were assigned to the corresponding cell in our scRNA-seq dataset. The majority of the immune receptor analysis such as clonality, repertoire overlap, V-gene usage and diversity was performed with the R package *immunarch.*[150] In addition, comparison of the AAA data with public databases to identify disease-associated receptors was performed (Figure 36 C).

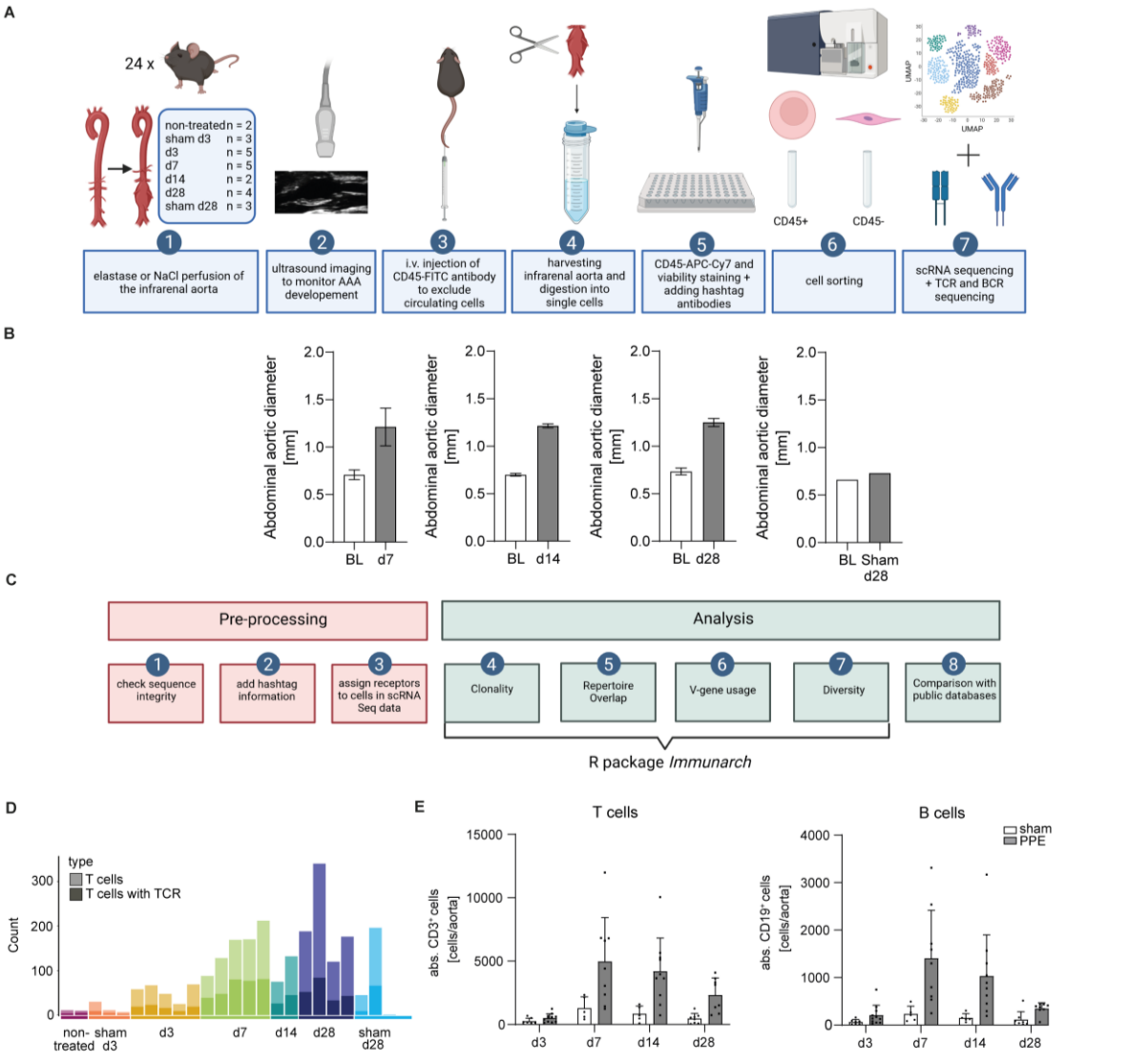

Figure 36: Experimental and bioinformatic workflow as well as quality control of the data. A: Experimental workflow. AAA was induced in mice via perfusion of the infrarenal aorta with elastase. NaCl perfusion of the aorta served as sham-operated control. AAA development was monitored by ultrasound imaging. Prior to organ harvesting mice were intravenously injected with a fluorophore labeled CD45 antibody. Harvested infrarenal aortae were digested into single cells and stained with antibodies and hashtags. Cells were sorted for living leukocytes and living non-leukocytes. scRNA-seq as well as scRNA-TCR-BCR-seq was performed. **B:** Abdominal aortic diameter was analyzed using ultrasound images of baseline (BL), d7 (n=5), d14 (n=2) and d28 (n=2) post PPE surgery and BL and d28 (n=1) post sham surgery. **C:** Bioinformatic workflow including preprocessing and data analysis. Three preprocessing steps were performed as quality control for the data. Only fully intact sequences are retained for analysis. The information for the hashtag antibodies was added to the scRNA-TCR-BCR-seq data. The receptors were assigned to the corresponding cells in the scRNA-seq data set. The main data analysis including clonality, repertoire overlap, V-gene usage and diversity was performed with the immunarch R package. In addition, the data was compared with public databases. **D:** T cell amounts (light bar color) and T cell amount exhibiting an intact TCR (dark bar color) in aortic tissue on different AAA disease stages received from scRNA-seq data. The amount of T cells increases with AAA progression. **E:** Flow cytometric analysis of T and B cell numbers in aortic tissue 3 (n=7), 7 (n=5), 14 (n=5) and 28 (n=8) days after sham operation and 3 (n=11), 7 (n=9), 14 (n=10) and 28 (n=8) days after PPE-induced AAA formation.

4.4.2 Analysis of scRNA-TCR-BCR-seq data

To assure adequate data quality, we processed the TCR and BCR sequencing data and evaluated basic statistics. The raw data contained 3370 TCR sequences (1484 TCR alpha chains (TRA), 1886 TCR beta chains (TRB)) and 1745 BCR sequences (570 immunoglobulin heavy chains (IgH), 1131 immunoglobulin kappa (IgK) light chains, 44 immunoglobulin lambda (IgL) light chains). We observed a high number of immune receptors with only one sequenced chain and some receptors with more than two chains, which were excluded from subsequent analysis (supplementary figure 3). Only T cells with both productive TRA and TRB chains and B cells with both productive heavy and light chains were used for analysis. After that step 2296 TCR chains (1148 pairs of TRA and TRB chains) and 980 BCR chains (490 pairs of heavy and light chains) remained. We next filtered for receptors that could be associated with a hash-tagged cell and retained 2012 TCR chains and 770 BCR chains. Assignment of the immune receptors to the corresponding cells in our scRNA-seq data revealed that only 47% of BCRs were expressed in B cells (defined by mRNA expression of *Cd19, Cd79a, Cd79b*) while, the majority of TCRs (79%) was expressed in T cells (defined by mRNA expression of *Cd3e, Cd3d, Cd3g, Cd28*), whereas the remaining immune receptors were found on other cell types (supplementary figure 4). TCRs and BCRs not expressed in the respective lineage were excluded to avoid analysis of false positive receptors due to sequencing artifacts. The final analysis included 1592 TCR chains (796 pairs of TCRs) and 358 BCR chains (179 pairs of BCRs).

We next compared the number of immune receptors with that of T and B cells which were present in our scRNA-seq dataset and displayed the distribution across the time points and samples (Figure 36 D, supplementary figure 5, supplementary table 7). Overall, there were less B cells (325) than T cells (2376) in AAA tissue and 3 out of 24 samples did not contain B cells (non-treated, d3, sham d28) (supplementary figure 5, supplementary table 7). The total number of T and B cells increased with AAA progression until day 7 (Figure 36 D and supplementary figure 5). We corroborated our findings by flow cytometry revealing a peak of lymphocytes at day 7 in AAA. Of note, only few cells were detected in sham operated mice (Figure 36 E). A fully productive TCR could be assigned to 33.5% of the present T cells (2376 T cells, 796 TCRs) (Figure 36 D). Thus, a large proportion of TCR sequences present in AAA were missing due to inefficient sequencing. In our data 55.1% of B cells had a matching BCR (325 B cells, 179 BCR). In 4 out of 24 samples no BCRs could be detected, these were sham-operated or early time points (non-treated, sham d3, d3, sham d28) (supplementary figure 5 B, supplementary table 7).

4.4.3 Estimating clonal expansion by spectratyping

Spectratyping identifies the pattern of the CDR3 length distribution.[180] Comparing the shape of the CDR3 length distribution between control and disease can indicate presence of clonal expansion in a repertoire. Deviations from the normal pattern might be due to the high frequency of a specific CDR3 sequence and are therefore associated with clonal expansion.[100] We compared the CDR3 length distribution of TCRs in AAA across all time points, and controls using the two-sample permutation-based Kolmogorov-Smirnov test (Figure 37 A). The resulting p-value of 0.92 suggests that the CDR3 length followed the same distribution in AAA and controls. To compare the CDR3 length distribution between the different disease stages, we performed pairwise two-sample permutation-based Kolmogorov-Smirnov tests and used Bonferroni correction for multiple comparisons. We did not observe significant differences between the CDR3 length distribution at the different time points (Figure 37 B).

Receptor clonality can also be investigated by determining the number of unique clones and the clone abundance. A clone was defined as set of cells expressing the same receptor that consists of the same V-, (D-) and J-genes, and encode an identical CDR3 nucleotide sequence. The majority of TCRs in AAA, sham-operated, and non-treated aortae were unique (Figure 37 C, supplementary table 8). Only one sample of the sham-operated and non-treated aortae and 11 AAA samples contained T cell clones (Figure 37 C, supplementary table 8). However, the clones were infrequent in AAA samples (occurring 2 to 5 times), whereas in the one sham-operated sample, 1 of the 4 T cell clones present encompassed 25 cells (Figure 37 D, supplementary table 8). The frequencies of the T cell clones, their V-, D- and J genes of alpha and beta chain, as well as their CDR3 nucleotide and amino acid sequences are shown in supplementary table 9. The extent of receptor clonality can be indicated with an evenness profile of the repertoire.[181] The alpha values represent different diversity indices with different weights on expanded clones. Higher alpha values give more weight to expanded clones, while alpha = 0 weights every clone equally regardless of its frequency. Therefore, high receptor clonality is indicated as a highly uneven curve and no receptor clonality is associated with a completely even curve (Figure 37 E). In our study, the sham operated d28 sample, in which one clone was identified 25 times (Figure 37 D), exhibited also the highest clonality, whereas all other sham operated or non-treated samples showed no clonality (Figure 37 E). Additionally, 11 AAA samples from different time points showed a lower extent of receptor clonality.

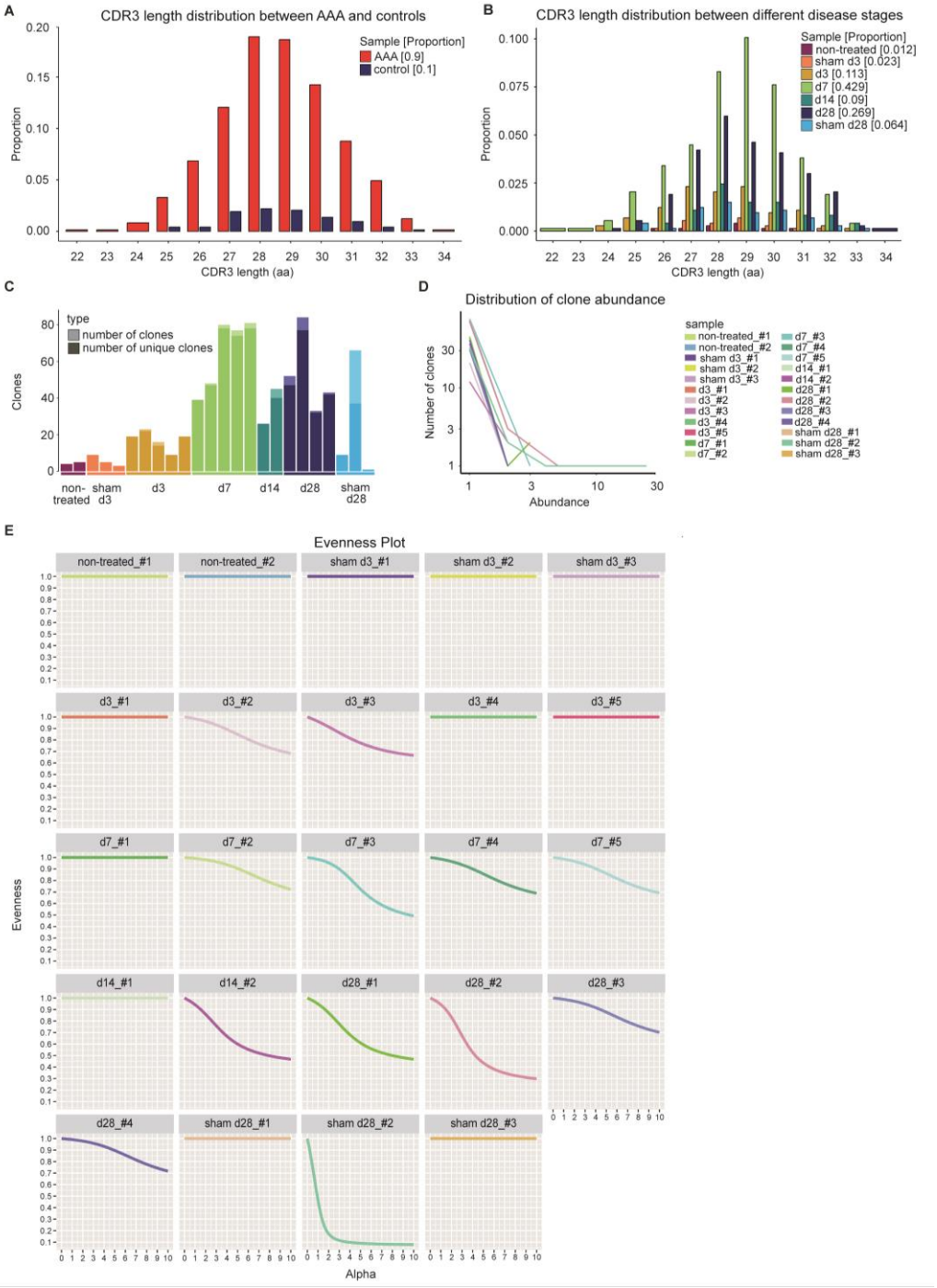

Figure 37: CDR3 length distribution and clone abundance indicates expanded T cell clones in elastase-induced aneurysm in mice. A: No changes in CDR3 length distribution of TCRs (paired chains) between AAA including all different disease stages (red) and control samples including sham operated and non-treated mice (blue). The proportion is plotted against the amino acid (aa) CDR3 length. **B:** No alterations in CDR3 length distribution of TCRs (paired chains) between samples of different disease stages (d3, d7, d14, d28) and sham operated as well as non-treated samples (different colors). The proportion is plotted against the amino acid (aa) CDR3 length. **C:** Amount of all TCR clones per sample (light bar color) including the amount of unique clones (dark bar color). The majority of TCR clones were found to be unique. Multiple copies of one clone appear only in one of the sham_d28 samples and in 11 of the AAA samples. **D:** Line Plot indicating the number and abundance of clones per sample. In the sham_d28 sample exhibiting clones with multiple copies, one clone is present 25 times. Whereas, in AAA samples one clone only appears 2 to 5 times **E**: Evenness Plots indicating the extent of clonal expansion for every sample One sham operated sample 28 days after perfusion exhibits the highest clonality. The other control samples show no receptor clonality. Eleven AAA samples show some clonal expansion. Abbreviations: CDR = complementarity determining regions.

4.4.4 Investigating the TCR repertoire similarity

Repertoire overlap analysis is commonly used to identify “public” TCRs that are shared between individuals.[182] The R package *immunarch* provides several methods to measure receptor similarities between individuals. Using the function “public” specified the exact number of shared immune receptors between different repertoires, thereby revealing that in 7 instances a TCR sequence was shared by 2 AAA samples (Figure 38 B). Additionally, repertoire similarity can be investigated by identifying TCRs of different individuals containing the same V-region genes. Fragments of V-region genes are classified into families according to their nucleotide sequence similarity (at least ~70%). Specific V-gene usage patterns have been associated with different diseases and were shown to change in response to therapeutic approaches.[183, 184] In our data the V-gene usage of the beta chain (TRBV) correlated stronger than the V-gene usage of the alpha chain (TRAV) of the TCR (Two-tailed Mann-Whitney test, $p = <0.0001$, Figure 38 C and D). A deeper analysis of the distribution and frequency of used TRBV genes revealed a high usage of TRBV3, TRBV19, and TRBV12-2+TRBV13-2 in AAA samples at day 7, 14 and 28 (Figure 38 E). TRBV12-2+TRBV13-2 is a term for a common alternate splicing between the first exon of TRBV12-2 and the second exon of TRBV13-2. TRBV19 was present in 5 and TRBV3 in 2 of the expanded clones. Further Vbeta genes that were used by 2-3 of the expanded TCRs are TRBV10, TRBV13-1, TRBV13-5, TRBV2, TRBV20 and TRBV29 (supplementary table 9).

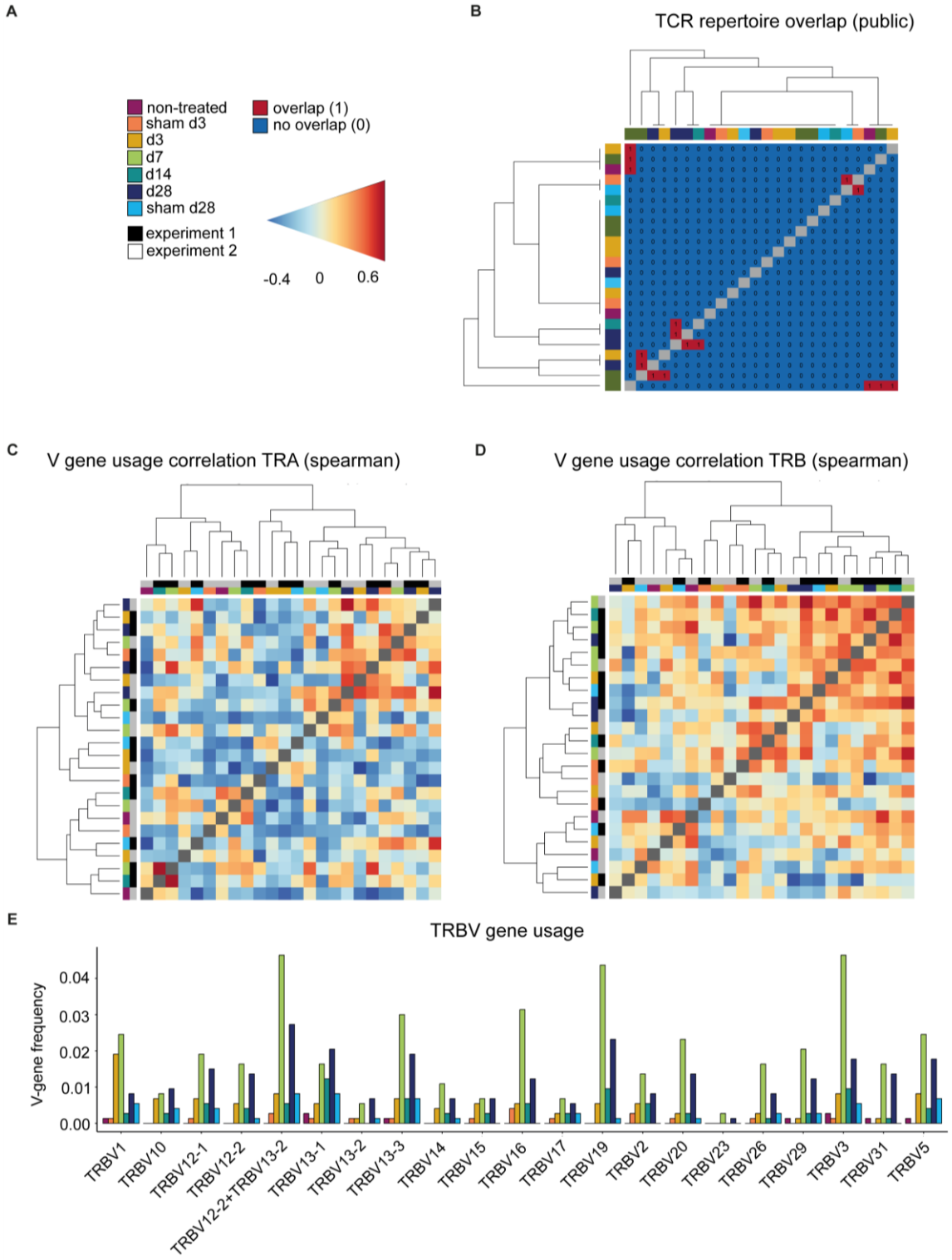

Figure 38: Comparing the different TCR repertoires reveals shared TCR sequences, a high correlation of the V-gene usage and several frequently used TRBV genes in AAA. A: Legend and color code. **B:** Analysis of the TCR repertoire overlap shows that in 7 instances two AAA samples contain one equal TCR. The color code in the heatmap indicates the different samples. **C+D:** The V-gene usage of the TCR alpha chain **(C)** and of the TCR beta chain **(D)** is correlated and hierarchical clustered between the different samples using spearman correlations. Color gradient indicates the level of correlation (blue = negative correlation, red = positive correlation). The color code on the axes indicates the different samples. **E:** Distribution and frequency of TRBV genes occurring in all samples. Frequently used TRBV genes in AAA samples are TRBV3, TRBV19, and TRBV12-2+TRBV13-2 at day 7, 14 and 28. Abbreviations: TRA = TCR alpha chain; TRAV = TCR alpha chain v gene; TRB = TCR beta chain; TRBV = TCR beta chain v gene.

4.4.5 Dataset comparison with public TCR and BCR databases

We compared the presence of CDR3 sequences in our dataset with the two public TCR databases VDJdb[151] and McPAS-TCR[152] to investigate if TCR clones in our dataset are associated with other diseases or antigens.[185] VDJdb is a curated database of TCR sequences with known antigen specificities containing TCR information of 3 different species (*Homo Sapiens*, *Macaca Mulatta* and *Mus Musculus*) and various diseases.[151] McPAS-TCR is a database of TCR sequences found in T cells that were associated with various pathological conditions in humans and in mice.[152] TCRs with less than 4 amino acids and diseases with less than 5 TCRs were excluded. Accordingly, for VDJdb 5206 TCRs found in Influenza (3156 TCRs), Lymphocytic choriomeningitis virus (LCMV) (151 TCRs), Murine cytomegalovirus (MCMV) (1463 TCRs), Plasmodium Berghei (245 TCRs), Respiratory syncytial virus (RSV) (125 TCRs) and Vesicular stomatitis virus (VSV) (66 TCRs) and for McPAS-TCR, 3530 TCRs which were assigned to 21 different diseases/pathogens were used for analysis (supplementary table 10). After merging the two databases and filtering for unique CDR3 sequences, we obtained 4331 CDR3 sequences for comparison with the AAA data set. One-sided Fisher's exact test was used to examine the overrepresentation of TCR clones in our data set that are associated with diseases or antigens according to the two databases (Figure 39 A). Our dataset shared 55 CDR3 sequences with the public databases which were assigned to MCMV, LCMV, Influenza, Plasmodium Berghei, VSV, Diabetes type 1 and Tumor. The obtained p-values were adjusted for multiple testing using Bonferroni correction. Bonferroni correction resulted in no significant p-values indicating there were no TCR clones overrepresented in our data set that are associated with diseases or antigens according to the two databases (Figure 39 B and supplementary table 11).

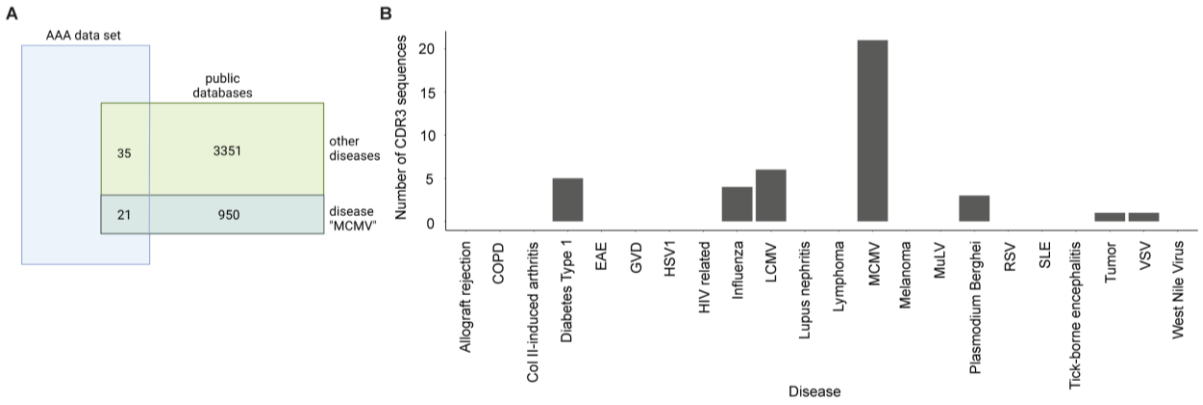

Figure 39: Overlap of AAA-associated CDR3 sequences with public databases. A: Venn diagram indicating the overlap of our TCR data with the public TCR databases (VDJdb and McPAS-TCR) representative for the disease MCMV. Our data shares 21 CDR3 sequences with the public databases that are associated with MCMV and 35 CDR3 sequences that are associated with other diseases. One-sided Fisher's exact test with Bonferroni correction for multiple comparison was used to examine the overrepresentation of TCR clones in our data set that are associated with diseases or antigens. **B:** Barplot displaying the amount of sequences per disease in our data. Abbreviation: Abbreviation: COPD = chronic obstructive pulmonary disease, Col II = collagen II, EAE = experimental autoimmune encephalomyelitis, GVD = Graft vs host disease, HSV1 = Herpes simplex virus 1, HIV = human immunodeficiency virus, LCMV = Lymphocytic choriomeningitis virus, MCMV = Murine cytomegalovirus, MuLV = murine leukemia virus, RSV = Respiratory Syncytial Virus, SLE = systemic lupus erythematosus, VSV = Vesicular stomatitis virus.

4.4.6 No clonal expansion or repertoire overlap of BCRs in elastase-induced aneurysm in mice

The CDR3 length distribution of the BCRs showed no differences between AAA and control at the disease stages (Figure 40 B, pairwise two-sample permutation-based Kolmogorov-Smirnov test resulted in no significant differences). 98% of BCR clones were unique (176 of 179 clones were unique). As mentioned before, BCRs were present in only 20 of 24 samples in our dataset. The samples that lacked BCRs were control samples or early disease stages that are known to contain few B cells overall (non-treated, sham d3, sham d28, d3). BCRs that appear more than once were found in two of these 20 samples. One day 28 sample contained one BCR that was present thrice, one day 7 sample had one BCR that appeared twice (Figure 40 C). The evenness profile likewise indicated a higher clonality for these two AAA samples in comparison to all other samples that showed no clonality (Figure 40 D and supplementary figure 6). Next, we investigated the isotype distribution of the BCR heavy chains. The most frequent isotype was IGHM, followed by IGHD (Figure 40 E). The similarity measurement of the BCR repertoire present in the different samples showed that two AAA samples (d7 and d28) share 1 BCR (Figure 40 F). Otherwise, there was no similarity between the different samples. The correlation of V-gene usage between the different samples was likewise low (Figure 40 G). The strongest, yet still weak correlation was found between one non-treated control and one d3 sample (r = 0.701). Overall, these data revealed no evidence for clonality among B cells in AAA.

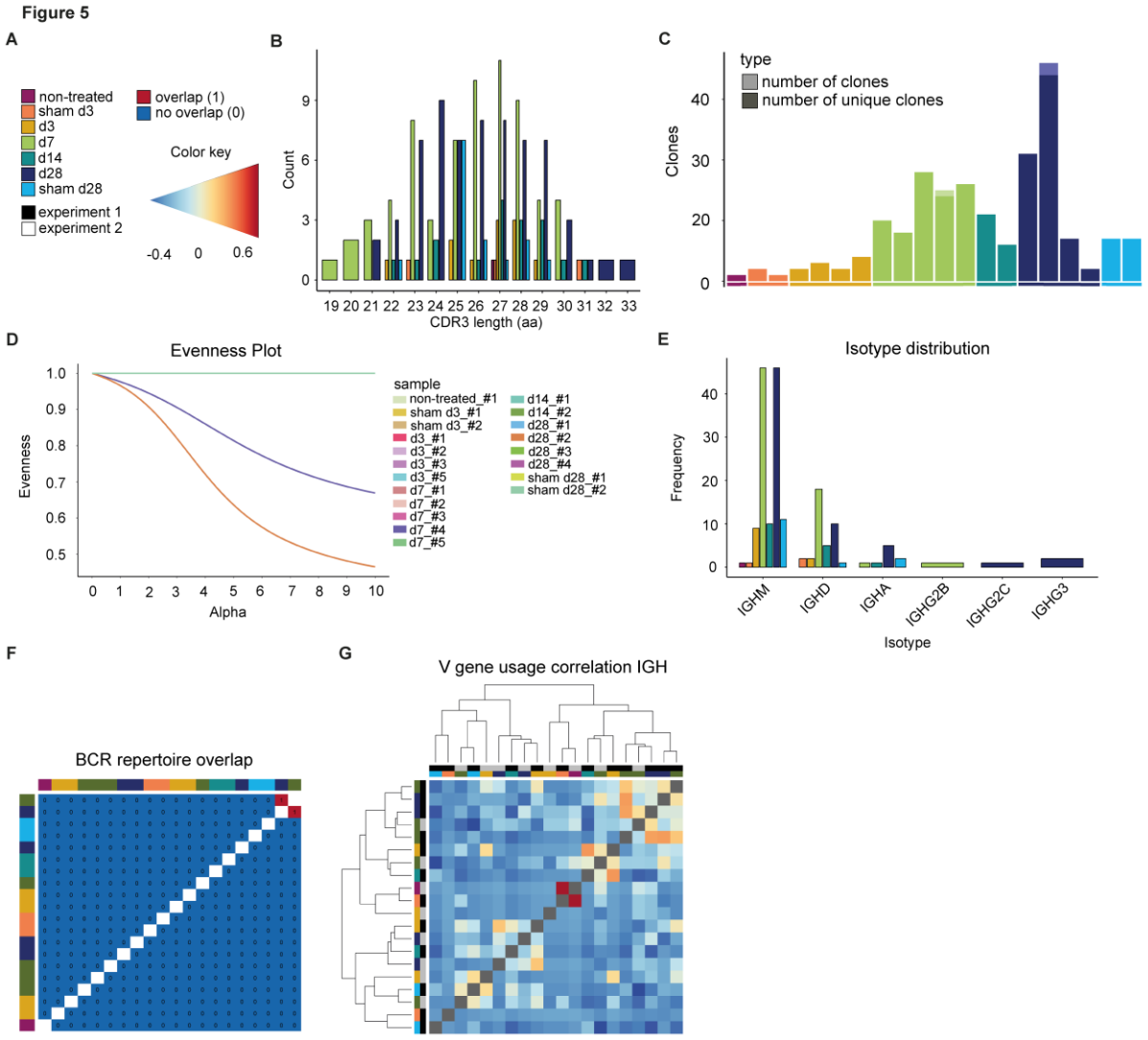

Figure 40: Elastase-induced AAA shows no BCR clonality. A: Legend and color code. **B:** Histogram indicating the CDR3 length distribution of the BCRs (paired chains). The proportion is plotted against the amino acid (aa) CDR3 length. The color indicates whether the TCRs belong to an aorta isolated at d3, d7, d14 or d28 after PPE or sham surgery or to a non-treated aorta. **C:** Barplot displaying the number of all BCR clones (pale color) and only unique clones (vibrant color) per mice. Almost all BCR clones are unique. **D:** Evenness Plot indicating the extent of clonal expansion for every sample. **E:** Barplot indicating the isotype distribution of the BCR heavy chain (IGH) in the different conditions. Most frequent isotypes for all conditions are IGM and IGD. **F:** BCR repertoire overlap displayed in a heatmap. Color bars on the top and left side of the heatmap indicate the time point. **G:** Heatmap presenting the spearman correlation and hierarchical clustering of the BCR heavy chain (IGH) V-gene usage of the different samples. Color gradient indicates the level of correlation (blue = weak correlation, red = strong correlation). Color bars on the top and left side of the heatmap indicate the experiment and the time point.

5 Discussion

This study aimed to investigate different aspects of the immune reaction involved in AAA pathology. First, the immune cell types present at different stages of elastase-induced AAA formation and their interaction were characterized in detail. The aim of this comprehensive study was to identify key players and signaling pathways in AAA to enable better treatment of AAA patients. Next, the role of CD40-CD40L signaling in AAA, which is a promising target for therapies, was investigated. Based on the results, IFNIC macrophages were identified as potential key player in AAA and CD40 signaling, and were thus further studied. In a further approach to better characterize and identify the pathogenesis of AAA, this study investigated whether autoimmune processes play a role in AAA progression. For this purpose, scRNA-TCR-BCR-seq was used to investigate T and B cell clonality in AAA.

5.1 Characterization of the immune response in AAA

In this work, flow cytometry, immunofluorescence staining, scRNA-seq and CITE-seq was used for a detailed characterization of immune cell types that are involved in elastase-induced AAA progression. In addition, the immune response involved in AAA was compared with inflammatory processes occurring in related CVDs such as atherosclerosis and MI.

Inflammation is a common denominator of atherosclerosis, AAA and MI, and all three disease share common risk factors. Moreover, all three diseases are linked, as atherosclerosis is the underlying cause of MI and can be a risk factor for AAA.[4, 6] Based on the many similarities between AAA and atherosclerosis, it has long been thought that AAA is dependent on atherosclerosis. Recent evidence suggests that both diseases are independent of each other but share risk profiles and pathological processes.[6] In this work, CITE-seq was used for a comprehensive comparison of the immune response in atherosclerosis, AAA and MI. While most cell types were present in all three diseases, their proportions differed. In general, atherosclerosis was dominated by T cells, while in AAA and MI macrophages and neutrophils were the predominant immune cells. MI is in the first days characterized by acute inflammation involving infiltration of cells of the innate immune system, including neutrophils and macrophages.[11, 12] Atherosclerosis is characterized by chronic inflammation, mainly characterized by infiltration of lymphocytes and macrophages.[4, 5] Although AAA is described as chronic inflammatory disease[17], it contained mostly acute inflammatory cells according to CITE-seq. This discrepancy may be explained by the early time points after elastase-induced AAA formation that were studied, reflecting acute rather

than chronic inflammation. However, 14 days after elastase-perfusion a strong increase in T cells and a strong decrease in neutrophils were observed, which may indicate the shift from acute to chronic inflammation. In detail, different neutrophil subsets appeared to play a crucial role in AAA compared to MI, two macrophage clusters seemed to be specific for MI and one T cell cluster for atherosclerosis. In addition, GO analysis revealed enrichment of different genes and pathways. Atherosclerosis was linked to adaptive immune response, AAA to innate immune activation and cytokine signaling, and MI to chemotaxis and leukocyte migration. Despite similarities, some immune cells and pathways appear to be disease-specific or to play a larger role in one of the diseases, supporting the concept that AAA is independent of atherosclerosis. To make a conclusive comparison between AAA and atherosclerosis, it will also be necessary to examine cell interactions at later time points in AAA development in the future.

Next, the immune response at different time points after elastase-induced AAA formation was studied in more detail. In addition, appropriate controls using sham-operated mice 3 and 28 days after the surgery were included. These controls are important to determine that the changes observed are due to AAA formation and not to the previous surgery for AAA induction in the animal model when analyzing immunoregulatory processes. Neutrophils, macrophages, DCs, NK, T and B cells, were detected at day 3, 7, 14 and 28 after elastase-perfusion, but differed in their proportion in these stages of AAA progression. Although the surgery itself triggered inflammation, the number of infiltrated immune cells was significantly less in saline-perfused aortae compared to elastase-perfused aortae. Therefore, the inflammation triggered by the surgery seems to have no high impact on the results and is negligible. Non-perfused aortae contained only few immune cells. The strongest immune cell infiltration into the aneurysmal tissue was observed 7 days after elastase-perfusion. Immunofluorescence staining showed that the majority of immune cells was located in the adventitia. Overall, macrophages were the most abundant immune cells, which is consistent with other studies.[45, 46, 186, 187] As expected, neutrophils, that are the first responders to tissue damage[28], were most frequent at the earliest time point day 3, followed by day 7 and were barely abundant at later stages. T and B cells, which are part of the adaptive immune response and require activation by APCs[27], were barely observed on day 3. Their absolute number peaked on day 7, and in percentage terms they accounted for the majority of immune cells on day 28. Overall, T cells were much more frequent than B cells. In human AAA, T and B cells are described as predominant infiltrating immune cells.[71-73] Human AAA tissue used for studies usually comes from patients who have undergone surgery, implying an advanced stage of the AAA. Therefore, day 28 after elastase-induced AAA formation is

most comparable to human AAA samples. However, this emphasizes the importance of mouse models that allow studies at early stages of AAA formation, which is necessary for a better understanding of AAA pathology and can help to identify potential therapeutic strategies. The comparison of the different time points of AAA development revealed not only differences in the proportion of immune cells, but also in immunological processes and cell-cell communication. The strongest cell-cell communication was observed at day 7, where IFNIC macrophages and myofibroblasts were the main driver of communication. In general, inflammatory cell subsets and myofibroblasts were the strongest sender and receivers of communication signals at all studied time points.

The cellular heterogeneity of AAA was investigated in other studies using different experimental models to induce AAA such as AngII model, $CaCl_2$ model or the external peri-adventitial PPE application (ePPE).[186-191] Two of these studies provide a detailed characterization of immune cell types present in ePPE-induced AAA formation at day 7 and 14.[186, 187] Yang et al. studied the $CaCl_2$ model at day 4, but focused only on macrophages, SMCs and fibroblasts.[188] The three studies investigating the AngII model at day 28, provide no detailed characterization of immune cell subtypes.[189-191] This study is the first that performed scRNA-seq of AAAs induced by the PPE model and that compared multiple time points of AAA formation, providing valuable insights into disease progression. Moreover, this work presents the first CITE-seq data of AAA, enabling simultaneous measurement of RNA and protein expression. None of the mouse models completely mimics the complex pathology of human AAA, but each model provides insights on specific aspects.[192] Therefore, systematic scRNA-seq studies in different animal models are needed to better understand the complex pathology and diversity of factors contributing to AAA. The PPE model is considered the best model to resemble human AAA, as it features fusiform AAA growth in the infrarenal part of the aorta, altered hemodynamics, fibrosis, humoral immune response, imbalanced proteolysis and angiogenesis.[192] However, thrombus formation and rupture, that are important characteristics of human AAA, cannot be studied with the PPE model.

In this thesis, 30 different immune cell subsets were identified by scRNA-seq in AAA. Seven distinct neutrophils subsets, including two clusters of pro-inflammatory neutrophils, IFNIC neutrophils, young neutrophils, *Mmp9*$^+$ neutrophils, *Cd74*$^+$ neutrophils and remodeling neutrophils, were identified. Since scRNA-seq of neutrophils can be challenging due to their low RNA content[193], neutrophils were confirmed by protein expression of Ly6G by CITE-seq. Yuan et al. is the only other study that characterized neutrophil subsets. They identified one proliferative subset, two pro-inflammatory subtypes and two late-stage neutrophil clusters.[187]

The majority of neutrophils detected in this thesis showed inflammatory characteristics and was associated with chemotaxis, migration and type-I IFN signaling. Non-inflammatory neutrophil subsets, such as remodeling neutrophils and *Mmp9*$^{+}$ neutrophils, accounted for only a small proportion. In addition, neutrophils were strong senders of communication signals to other cells in the first 7 days of AAA formation. This emphasizes the important role of neutrophils as a driver of inflammation and AAA development, which has also been shown in other studies where neutrophil depletion or reduced neutrophil recruitment led to attenuated AAA formation.[34-36]

So far, the role of DCs in AAA is not well known, but depletion of DCs limited AAA growth in mice.[41] Yuan et al. identified 5 different DC subsets in ePPE-induced AAA including monocyte-derived DCs, conventional DCs type 1 and type 2, pDCs and migratory DCs.[187] In this thesis, classical DCs, CD103^{+} DCs, activated DCs and pDCs were identified in elastase-induced AAA. Since pDCs also express T cell markers, they were initially mistaken for lymphocytes in the analysis and later identified as pDCs upon more precise characterization. Therefore, they were analyzed together with lymphocytes. Classical DCs represented the largest DC population and showed no striking changes in their proportion during AAA progression. CD103^{+} DCs, that were described as atheroprotective[42], were anti-inflammatory and increased with AAA progression. Activated DCs were the smallest, but most inflammatory DC subset. pDCs were most abundant at day 7 and 14 and barely present in controls, suggesting a critical role in AAA formation. Specific depletion of pDCs was shown to result in reduced AAA formation.[38] According to the CellChat analysis DCs played a minor role in cell-cell-communication in AAA. Overall, DCs contribute to inflammation by activating the adaptive immune response, and depletion of DCs appears to be effective in reducing inflammation and thus AAA formation. However, the specific roles of different DC subsets, needs to be further investigated.

In total, 10 different macrophage subsets were identified in AAA, including resident macrophages and monocyte-derived macrophages. The resident-like *Pf4*$^{+}$ macrophages were the largest macrophage subset in healthy aorta and sham controls, but represented only a small part of macrophages in AAA. This was likewise observed by Zhao et al. in the ePPE mouse model.[186] The majority of monocyte-derived macrophages exhibited an inflammatory gene signature. Only the three subsets *Cd72*$^{+}$ macrophages, *Chil3*$^{+}$ macrophages and remodeling macrophages were less inflammatory and more associated with structural changes such as wound healing, cell junction disassembly and ECM remodeling. This is consistent with other studies that described inflammatory and reparative

macrophages in the ePPE model.[186, 187] It is described that pro-inflammatory macrophages dominate against anti-inflammatory macrophages in AAA and that modulating this ratio by increasing anti-inflammatory macrophage polarization inhibits AAA formation.[53, 54] In this thesis, the proportion of the inflammatory macrophage subsets, such as pro-inflammatory macrophages, IFNIC macrophages, *Lgals3*$^{+}$ macrophages and T cell-like macrophages, was highly increased in AAA compared to healthy aorta. IFNIC macrophages represented the largest macrophage subset at day 7 and 14. IFNIC macrophages were also described in the ePPE model and were recently reported to play a detrimental role in AAA.[186, 187, 194] Galectin-3 (*Lgals3*) can promote AAA progression by activation of inflammatory macrophages that contribute to apoptosis of VSMCs.[165] In addition, proliferative macrophages were identified in elastase-induced AAA. Proliferative macrophages were also found in ePPE- and CaCl2-induced AAA, but represented only a minor macrophage subtype in both models.[186, 188] In atherosclerosis a recent study revealed that the majority of macrophages is derived from local proliferation and suggest that targeting macrophage proliferation may represent a new therapeutic option.[195] In elastase perfusion-induced AAA, proliferating cells accounted for only a very small proportion of all macrophages and the impact of these proliferating cells needs to be further investigated. Lastly, two macrophage clusters expressing T cell associated genes were found in AAA by scRNA-seq. To date, nothing similar has been described in the literature, which can be due to three possible explanations. First, this could be explained by the fact that other datasets contain a significantly smaller number of cells and therefore these populations were not detected. Second, these cells might be specific for elastase perfusion-induced AAA, and to date there is no other scRNA-seq dataset available for this model. Third, these cells may have been excluded as contaminants in other analyses. Since duplicates were removed during preprocessing and these cells did not have a high mitochondrial RNA or a higher RNA count than the other clusters, it can be excluded that these cells are duplicates. Furthermore, both clusters comprised a high number of cells and were detected in three independent scRNA-seq experiments, making a contamination unlikely. The tissue dissociation could have led to artificial changes in cell transcription patterns[196], but some of these cells even expressed T cell markers on protein level measured by CITE-seq. It is feasible that these two cluster contain macrophages that have phagocytosed apoptotic T cells. Liebold et al could show that the cellular identity of the ingested apoptotic cell contributes to macrophage gene expression and function.[197] Altogether, the data presented in this study emphasizes the large heterogeneity of macrophage subsets and functions and their important role in AAA formation. Furthermore, it shows that the classical division into M1 and M2 macrophages is oversimplified and does not

reflect macrophage heterogeneity *in vivo*. However, the specific role of different subsets is still unclear and should be further investigated.

Within the lymphocytes, NK cells, NKT cells, ILC type 2 and 3, B cells and 4 distinct subtypes of T cells were identified by scRNA-seq. B2 cells were much more frequent than B1 cells, that were excluded from further analysis, as they accounted for less than 0.5% of all immune cells. Notably, this corroborates previous reports of B2 dominating the B cell pool in mouse AAA.[75] The proportion of NK cells and NKT cells was highest at day 3 and decreased with AAA progression, while the frequency of ILCs, T cells and B cells increased with AAA progression and peaked at day 28, which is in line with previous studies.[187] Different types of lymphocytes play diverse roles in AAA progression. $CD4^+$ T helper cells, which represented the largest T cell subset in AAA, secrete cytokines to recruit and activate other immune cells, thus amplifying the immune response.[81] Tregs, that are important for maintaining homeostasis and limiting excessive inflammation, accounted for a larger proportion in controls than in AAA.[87] Several studies have found a protective role of Tregs in AAA, suggesting the elevation of Tregs as a potential treatment option.[88, 198, 199] $CD8^+$ cytotoxic T cells and NKT cells are involved in ECM degradation.[90, 187] The role of ILCs in AAA is not well known. ILCs were most abundant at day 28 of AAA formation, with ILC3s being more prevalent than ILC2s. Yuan et al. also identified NKT cells, $CD4^+$ T cells, $CD8^+$ T cells and Tregs in ePPE-induced AAA.[187] However, they did not detect ILCs. In return, they found gamma-delta T cells and *Ifit*-expressing T cells, which were not detected in this study. These differences might be due to the different mouse models used to induce AAA formation or differences in the bioinformatics workflow. Since there is no uniform nomenclature for subpopulations identified with scRNA-seq, it could also be that subsets are similar but were termed differently.

scRNA-seq is widely used to decipher cellular heterogeneity and cell type functions in complex tissues. It enables a wide range of analyses, such as DEGs, GO enrichment, signaling pathways, lineage tracing, cell-cell communication and cell cycle.[131] However, all analyses are based on mRNA expression of the single cells, and mRNA-protein correlation is known to be poor, as the relation between transcription and translation is non-linear and complex.[174, 175] Usually pearson correlation coefficients for mammalian tissues are about 0.6.[178] Tian et al. compared mRNA and protein expression of 425 genes in murine bone marrow-derived cells and received a pearson correlation coefficient of 0.59.[200] Thus, information obtained from scRNA-seq are limited and should be combined with proteomics data. CITE-seq enables to study protein expression and mRNA expression simultaneously,

and advances scRNA-seq by layering an extra dimension on top of the data.[133] First, this study utilized CITE-seq to confirm cluster identification by scRNA-seq and to further characterize identified cell types at protein level. This is especially useful to characterize rare, previously unexplored subpopulations at the protein level, which enables further investigation of these cells with antibody-based methods. In addition, CITE-seq was used to examine the extent of mRNA-protein correlation. Therefore, a Spearman correlation was calculated for each cell type for all 119 proteins detected in the CITE-seq data with their corresponding mRNA expression. Most proteins showed a strong positive correlation with their corresponding mRNA in specific cell types, and no correlation in other cell populations. Proteins that are known to be expressed on macrophages for example, showed a good correlation with mRNA expression in macrophages, but not in other cell types. Some proteins showed a positive correlation to mRNA expression in almost all cell types, while other proteins showed no correlation with their corresponding mRNA expression, regardless of the cell type. For few proteins even a negative correlation between mRNA and protein expression was obtained. Buccitelli et al. and other groups have shown that mRNA-protein correlation can be influenced by various post-transcriptional and post-translational parameters.[175, 178] The individual half-life of proteins, that can range from a few seconds to several days, is the major post-translational factor influencing mRNA-protein correlation. Other factors are RNA half-life, RNA secondary structure, transcription and translation rates that are influenced by translational modulators like regulatory proteins and small RNAs (sRNAs), the ribosomal density and ribosome occupancy.[175, 178] One study found that while varying mRNA levels showed a strong correlation with corresponding protein levels ($r = 0.89$), genes with steady mRNA expression exhibited fluctuating protein levels throughout the cell cycle ($r = 0.2$).[174] In addition, technical issues also influence the correlation. Both RNA and protein measurements suffer from noise and biases that can affect accuracy.[178] The 10x Genomics' scRNA-seq technology for example has a higher sensitivity for shorter genes and genes with a higher GC content.[201] In CITE-seq, ADT levels per cell were found to be higher than mRNA levels of the same genes and less prone to drop-out events.[133] In general, mRNA levels should not be interpreted as final output of gene expression. Thus, it is recommended to use a combination of transcriptomic and proteomic data as it provides information that cannot be obtained from either type of data alone.

In summary, this works provides a detailed and comprehensive analysis of immune cell subtypes and inflammatory processes involved in AAA pathology. As scRNA-seq techniques generate a large amount of data, this part of the thesis became considerable long and complex. To prevent the work from becoming even more extensive, an attempt was made to

focus on the most essential aspects. However, this means that some aspects are only dealt with superficially and in-depth analyses are lacking in some places. Some of these more detailed analyses were carried out already but were not included in this thesis or are planned for future studies.

5.2 The role of CD40 signaling in AAA

The co-stimulatory molecules CD40 and CD40L are expressed on a wide range of cell types including immune cells and non-immune cells and regulate the immune response.[110, 111] CD40-CD40L signaling was previously shown to play a critical role in AAA formation and progression. Kusters et al. observed reduced AAA incidence and less rupture 28 days after AngII-induced AAA formation in CD40L-deficient mice.[84] Blocking of downstream CD40 signaling via TRAF6 using a small molecule inhibitor also protects against AngII-induced AAA formation and rupture as well as elastase-induced AAA as shown by our group.[130] However, the involved cell types and the underlying mechanism of the protective effect of blocking CD40 signaling remain unclear. The aim of this study was to further investigate the role of CD40 signaling in AAA and to identify the cell types involved.

Consistent with previous studies, in this work, significantly lower AAA incidence and significantly reduced abdominal aortic diameter was observed in CD40-deficient mice compared to control mice 28 days after AngII-pump implantation. In addition, CD40-deficient mice showed an improved survival rate as there were less AAA ruptures. CD40 expression was examined at day 3, 7, 14 and 28 after elastase-induced AAA formation on RNA level using scRNA-seq and on protein level using CITE-seq, flow cytometry and immunofluorescence staining. At mRNA level, CD40 was barely expressed in controls and highly expressed in murine and human AAA tissue. In human AAA, B cells were identified as predominant CD40 expressing cells, while in mice the majority of CD40 expressing cells were macrophages and DCs. This might be due to the early time points of AAA formation that were used in the mouse scRNA-seq data. However, on protein level measured with CITE-seq B cells showed the strongest CD40 expression, followed by DCs and macrophages. B cells are known to highly express CD40 as it is required for isotype switching and promotes survival, proliferation, Ig production and cytokine secretion of B cells.[110] The highest number of CD40 expressing macrophages and DCs was observed at day 7 after elastase-induced AAA formation. CD40 mRNA expression was observed in the majority of activated DCs and in some classical DCs. Only few $CD103^+$ DCs showed CD40 mRNA expression. On protein level, CD40 expression was observed on all detected DCs, with activated DCs exhibiting the strongest CD40 expression. CD40 signaling leads to full

maturation of DCs and expression of CD40 is therefore used as activation marker for DCs.[173] On mRNA level, IFNIC macrophages were the most CD40-positive macrophages. They also highly expressed CD40 on protein level, but most other macrophage subsets expressed CD40 at a similar extent. The discrepancy between CD40 mRNA and protein expression is probably due to the fact that CD40 is quite stable with a half-life of approximately 13 hours and does not need to be regenerated frequently, so that no further mRNA transcripts are required for translation into protein.[202] In addition to CITE-seq, flow cytometry and immunofluorescence staining were used to study CD40 protein expression on neutrophils, DCs, macrophages and B cells. CD40 expression was observed on all studied cell types. B cells and macrophages showed a trend to higher CD40 expression in aneurysmal tissue compared to controls. Between the different time points after elastase perfusion of the aorta only minor differences in CD40 expression were observed, indicating that CD40 plays a role at all stages of AAA formation and progression and is involved in both acute and chronic inflammation. In particular, CD40 signaling is a central pathway in activation of DCs and IFNIC macrophages.

CD40L expression was examined using scRNA-seq and immunofluorescence staining. CD40L expression was found in human and murine AAA tissue, while almost no expression of CD40L was detected in controls. As expected, and in accordance with literature, CD40L was mainly expressed on T cells. RNA expression of CD40L was also observed on some NK cells and macrophages, which is described under inflammatory conditions.[110, 111] The highest number of CD40L-expressing T cells was found 28 days after elastase-perfusion, which is probably due to the overall increase of T cells on day 28. Within the different lymphocyte subsets *Cd4*$^+$ T cells and ILC3s exhibited the strongest expression of CD40L. CD40L expression was shown to be involved in activation of *Cd4*$^+$ T cells, secretion of immunomodulatory cytokines and apoptosis.[203, 204] CD40L expression on ILCs was already described and CD40L-expressing ILC3s were found to promote B cell survival, proliferation and differentiation.[205, 206] ILC2 cells, that were described to have a protective role in AAA[61], was the only cluster were CD40L expression was completely absent.

scRNA-seq data was additionally used to identify key senders and receivers of CD40 signaling using CellChat. Cell-cell communication analysis predicted IFNIC macrophages as main receivers and *Cd4*$^+$ T cells as dominant senders of CD40 signaling. The analysis included not only signaling of CD40L via its receptor CD40, but also via its other two receptors Mac-1 and VLA-5. Mac-1 is known to be expressed on monocytes, macrophages, neutrophils and NK cells, and is required for the adhesion of immune cells to endothelial

cells.[177] CD40L that is expressed on activated endothelial cells binds to Mac-1 on rolling immune cells to enable their firm adhesion. VLA-5 is reported to be expressed on endothelial cells, fibroblasts, monocytes and macrophages.[177] Binding of CD40L to VLA-5 was shown to induce ERK-signaling and IL-8 expression in monocytes, and mediates cytokine production and adhesion of CD40L expressing T cells with fibroblasts.[207, 208] Both receptors do not interfere with binding of CD40L to CD40. Competitive binding assays showed that Mac-1 binding did not compete with CD40.[209] VLA-5 binds to another region of CD40L than CD40, allowing both receptors to bind to CD40L simultaneously.[210] Of these 3 receptors, CD40 was predicted to contribute the least to overall CD40L signaling in AAA. This finding was based on the fact that the receptors Mac-1 and VLA-5 were expressed across many different cell types, while CD40 expression was restricted to the three DC subsets, IFNIC macrophages, *Cd72*$^{+}$- and T cell-like macrophages. Thus, CD40L-CD40 signaling displays a more specific pathway than CD40L signaling via Mac-1 and VLA-5, and affects only some specific cell types, making it a suitable target for therapeutic approaches. IFNIC macrophages were predicted to also interact with CD40L via Mac-1, but not via VLA-5. It should be noted, that this analysis calculates a probability score based on gene expression of ligands and receptors, and the law of mass action, which is a simplified model and does not reflect the real complexity of cell-cell communication.[148, 149] In addition, the effect of cell proportion in each cell group was considered for the probability calculation. Although these results are only a prediction and should be confirmed with further experiments, these data provide a solid basis and orientation for further research.

5.3 The role of IFNIC macrophages in AAA

In this study, IFNIC macrophages were identified as potential key player in AAA formation and progression, as they were highly inflammatory and accounted for the largest macrophage subset at day 7 and 14 after elastase-induced AAA formation. In detail, they compromised 30.5% and 27.1% of the macrophages, respectively, and were barely present in control conditions. IFNIC macrophages were first described as monocyte-derived macrophages with a type-I IFN gene signature by King et al. in a mouse model of MI in 2017.[159] The IFNIC macrophages found in AAA in this study exhibited the same type-I IFN gene signature by showing a high expression of ISGs and directly IRF3-dependent genes, including *Ifit1*, *Ifit2, Ifit3*, *Irf7*, *Isg15*, *Cxcl10*, *Rsad2*, *Usp18* and *Oasl2*. Furthermore, GO and PROGENy analysis revealed that IFNIC macrophages were responsive to IFNβ, and the JAK-STAT-signaling pathway was highly upregulated in these cells. The JAK-STAT signaling pathway is activated by binding of interferons and promotes the expression of ISGs.[179, 211] Le

et al. detected IFNIC macrophages in AngII-induced AAA in mice and also showed that JAK-STAT-signaling is highly upregulated in these cells.[194] Inhibition of this pathway with the inhibitor Ruxolitinib decreased mRNA expression of ISGs, suggesting a critical role of JAK-STAT signaling pathway in the differentiation of IFNICs.[194]

Type-I IFN signaling is classically known in context of viral infections and studying IFNs in non-viral immunity is relatively novel. Type-I IFNs regulate the innate immune response by mediating cytokine production and inflammatory pathways as well as facilitating NK cell function and antigen presentation.[179] In addition, type-I IFNs can stimulate the adaptive immune response by triggering high-affinity antigen-immune cell responses and the development of an immunological memory.[179] Macrophages produce IFNs under various inflammatory conditions, ranging from viral and bacterial infections to exposures with endogenous ligands.[211] Thus, macrophages have a broad range of nucleic acid sensors, including retinoic acid inducible gene I (RIG-I), melanoma differentiation-associated protein 5 (MDA5), toll-like receptors (TLRs) and cyclic GMP-AMP synthase (cGas). cGAS detects double-stranded DNA (dsDNA) and induces IFN production via stimulator of interferon genes (STING) (Figure 41).[211] It was shown that the pathway of DNA damage and cytosolic DNA sensing is upregulated in IFNICs and cytosolic DNA accumulation was found in macrophages in AAA tissues.[194] In the non-viral context of AAA pathology, it is assumed that macrophages phagocyte dsDNAs released from apoptotic VSMCs, which bind to cGAS, leading to type-I IFN production via STING. These type-I IFNs then bind to IFNAR and activate the JAK-STAT signaling pathway, which induces the expression of ISGs and changes macrophages into the IFNIC phenotype (Figure 41).[159, 194]

In this study, IFNIC macrophages were found to additionally express CD40 and were identified as major receiver of CD40-CD40L signaling sent by *Cd4*$^{+}$ T cells. CD40-CD40L-signaling is known to play an important role in AAA. Inhibition of CD40-TRAF6 signaling resulted in reduced AAA formation after elastase-perfusion, which was accompanied by a reduction in CD40 expressing macrophages and downregulation of *Ifit2* at day 7.[130] CD40 was shown to enhance the STING-mediated type-I IFN response by increasing STING protein levels and reducing ubiquitination of STING.[212] Binding of CD40 to STING was mediated by TRAF2/3 and TRAF6 binding domains (Figure 41). In addition, IFNβ and STING levels were significantly reduced in CD40-deficient mice after N67 infection.[212] However, the relation between CD40 signaling and type-I IFN response, as well as the role of CD40 signaling in IFNIC macrophages needs to be further investigated.

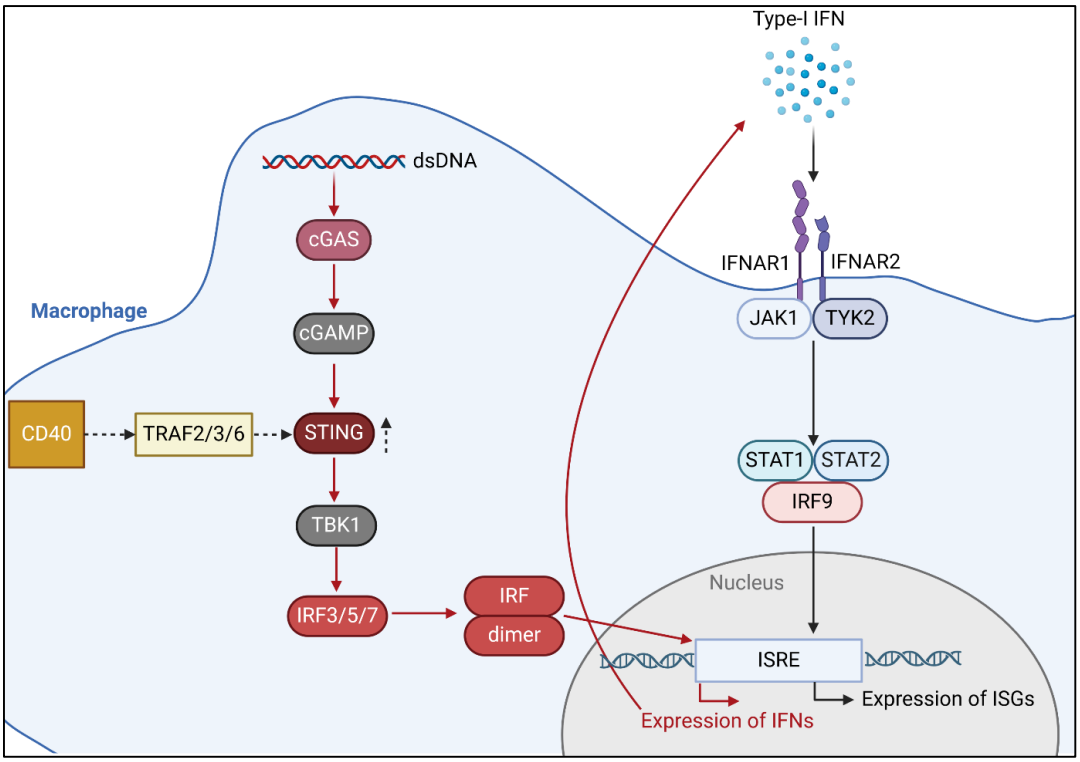

Figure 41: Type-I IFN signaling in macrophages. Engulfed dsDNA from apoptotic cells is bound by the cytosolic DNA sensor cGAS that activates STING via cGAMP. STING can be enhanced by binding of CD40 via TRAF2, 3 or 6 and activates TBK1. TBK1 leads to activation and dimerization of IRF3, IRF5, and IRF7. The IRF dimer translocates into the nucleus and induces the expression of IFNs via IFN-stimulated response elements (ISRE). Secreted IFNs bind to the surface receptor complex IFNAR1/IFNAR2 that recruits JAK1 and TYK2. This leads to the phosphorylation and activation of STAT1 and STAT2 that recruit IRF9. This complex translocates to the nucleus and binds ISREs that promote the expression of ISGs resulting in a type-I IFN signature of the macrophage Abbreviations: dsDNA = double-stranded DNA; cGAS = cyclic GMP-AMP synthase; cGAMP = Cyclic guanosine monophosphate–adenosine monophosphate, CD40 = cluster of differentiation 40; TRAF = tumor necrosis factor receptor-associated factors; STING = stimulator of interferon genes; TBK1 = TANK-binding kinase 1; IRF = interferon regulatory factor; ISRE = IFN-stimulated response elements, IFNs = interferons; IFNAR1/3 = interferon-alpha/beta receptor subunit 1/2; JAK1 = janus kinase 1; TYK2 = tyrosine kinase 2, STAT = signal transducer and activator of transcription proteins, ISGs = interferon-stimulated genes. Figure created with Biorender based on figures from Siebeler et al.[211]

IFNIC macrophages were also found in atherosclerosis and MI in the CITE-seq dataset used in this study, which is consistent with other studies.[57, 159, 160] However, IFNICs were much more frequently represented in AAA than in atherosclerosis and MI. Type-I IFN signaling was shown to promote atherosclerosis and to increases macrophage accumulation in the plaques.[213] Moreover, IFNIC macrophages were found to be highly enriched in progressive atherosclerotic plaques in mice.[160] In context of MI and AAA, IFNIC macrophages were shown to play a detrimental role. IRF3- or IFNAR- deficient mice or mice treated with an IFNAR neutralizing antibody showed an improved cardiac function and survival after MI compared to controls.[159] This was accompanied by decreased inflammatory cell infiltration and decreased expression of inflammatory cytokines and chemokines. In AAA, myeloid cell-specific ablation of *Sting1* lead to reduced aortic diameter and less rupture in AngII-induced AAA formation and prevented completely from elastase-induced AAA formation.[194] In

addition, *Apoe*$^{-/-}$ mice that received bone marrow transplantation from mice globally deficient in *Ifnar1* or *Sting1* four weeks prior to AngII infusion had improved survival, lower AAA incidence, and reduced aortic diameter compared to mice that received bone marrow from WT mice.

The type-I IFN phenotype is not restricted to macrophages and can occur in several cell types.[214] In this study, also IFNIC neutrophils were identified that showed similar characteristics to IFNIC macrophages. They exhibited a similar gene signature, were responsive to IFNβ and the JAK-STAT pathway was highly upregulated. Furthermore, IFNIC neutrophils received the highest inflammation score of all neutrophil clusters and the inflammatory pathways NFκB and TNFα were upregulated. Other studies detected fibroblasts, VSMCs and also neutrophils with a type-I IFN gene signature.[153, 154, 214, 215] One study identified IRF3 as key driver of the transition of VSMCs to an inflammatory phenotype in AAA.[215] Similar to the induction of IFNIC macrophages, the inflammatory VSMC phenotype was induced by double-stranded DNA-STING-IRF3 signaling. In *Sting*$^{-/-}$ mice, the aortic stress-induced transition of VSMCs into this inflammatory phenotype was prevented.[215] Ninh et al. referred to all cells expressing ISGs collectively as IFNICs and found that colonies of IFNICs are located around the infarct border zone after MI.[214] Furthermore, these IFNIC colonies were located in close proximity to the sites of ventricular rupture, and mice lacking IFNICs were protected from rupture. There is evidence that the type-I IFN response may increase susceptibility to rupture through its inhibitory effect on fibroblast activation and function.[214] This assumption can be applied to AAAs and would explain why studies in which type-I IFN signaling was blocked observed smaller, more stable AAAs and less ruptures.

Accordingly, IFNIC macrophages play a critical role in CVDs and display a potential therapeutic target. To date, IFNIC macrophages are mainly characterized on RNA level by scRNA-seq and information about protein expression is lacking, hampering further investigations of these cells using antibody-based methods. In this study, CITE-seq was used to explore protein expression of IFNIC macrophages and identified them as CD11b^{+}, Ly6C^{high}, CD36^{+}, Ly6A/E^{+}. Based on this information a flow cytometry panel that additional included IFNAR1 was established to detect and isolate IFNIC macrophages. The flow-cytometric quantification of IFNIC macrophage count in aortic tissue showed significant more IFNIC macrophages in elastase-induced AAA compared to saline-perfused controls 7 days after surgery. With an average number of 13 only very few IFNIC macrophages were detected in controls. In contrast, an average of 937 IFNIC macrophages were found in AAA.

However, the number of IFNIC macrophages detected per AAA was high variable, which might stem from differences in AAA size. Furthermore, it should be considered, that the identification of markers for IFNIC macrophages was limited to the 119 antibodies detectable in our CITE-seq data, and that the identified markers were not exclusively expressed on IFNICs. As a result, a large proportion of IFNIC macrophages were lost during the gating strategy. Thus, the actual number of IFNIC macrophages in AAA is probably much higher than the number of IFNIC macrophages detected by the panel. Furthermore, the final gate did not contain a pure IFNIC population, as the used marker combination was not able to fully distinguish IFNIC macrophages from all other macrophage subsets. To identify better markers, IFNIC macrophages will be isolated with the flow cytometry panel and subjected to mass spectrometry or proteomics in the future. Nevertheless, the panel is suitable to detect and isolate IFNIC macrophages from aortic tissue and enables further investigations of these cells. In future studies, IFNIC macrophages could be co-cultured with fibroblasts and T cells to investigate their interaction. Furthermore, the effect of CD40 activation and inhibition on IFNIC macrophages could be studied.

5.4 T and B cell clonality in AAA

The following part of the discussion was published in a scientific paper in Frontiers in Cardiovascular Medicine in 2023.[102]

We assessed TCR and BCR clonality in elastase-induced AAA in mice at different disease stages using scRNA-TCR-BCR sequencing. Our results show no differences in CDR3 length distribution of TCRs and BCRs between the different disease stages, indicating no strong clonal expansion of immune cell receptors in elastase-induced AAA. The clone abundance analysis likewise revealed no clonal expansion of BCRs in AAA. We found expanded T cell clones in 68% of AAA samples and no clonality in control samples except for one. Comparison of the immune receptor repertoires showed a low similarity between the individual samples. Spearman correlation to compare the V-gene usage between the different AAA samples and controls revealed that the V-gene usage of the TCR beta chain correlates stronger than the V-gene usage of the TCR alpha chain. The most frequently used V-genes in the TCR beta chain in AAA are TRBV3, TRBV19 and TRBV12-2+TRBV13-2. Comparison of TCR clones identified by us revealed no overrepresentation of TCR clones associated with diseases or antigens annotated in two public databases. The main Ig isotype in our BCR dataset is IgM followed by IgD. While this may prompt speculation of enrichment of B1 cells that predominantly express IgM, the overall scRNA-Seq data set suggests that B2

cells are approximately 20-fold more frequent than B1 cells. Notably, this corroborates previous reports of B2 dominating the B cell pool in mouse AAA.[75]

Antigen recognition by immune cell receptors activates naive lymphocytes prompting them to proliferate. This process is termed clonal expansion and enables a targeted, adaptive immune response. Yet, the term of clonal expansion still remains strongly debated as there is no clear and consensus definition. Lu et al. investigated T cell clonality in aneurysmal lesions of AAA patients and defined clonal expansion as presence of multiple identical copies of TCR transcripts.[107] They reasoned that the size of the T cell repertoire makes it unlikely that multiple identical copies of a TCR transcript would be found by chance in an independent sample of T cells.[107] According to this definition we found clonal expansion in 11 of 16 AAA samples and in 1 of 8 control samples.

Public TCRs are shared across different individuals due to VDJ recombination biases and might target common antigens.[182] The repertoire similarity of the AAA samples was low. In 7 instances a TCR sequence and only one BCR sequence was shared by two individual AAA samples. Next to clonal expansion and public TCRs there is also T cell convergence. Convergent T cells are cells expressing TCRs with the identical CDR3 amino acid sequences and variable genes, but different CDR3 nucleotide sequences.[216] Convergent T cells arise due to codon degeneracy and can be observed in almost every individual. Pan and Li showed that convergent T cells are different from public TCRs and seem to be antigen-specific. According to their results TCR convergence might be a better indicator of antigen specificity than clonal expansion. Since convergent T cells constitute only a small proportion of the total population of T cells, studies of TCR convergence require a large number of sequenced T cells.[216] We did not find convergent T cells in our dataset, probably due to the small number of T cells, but expect that investigating T cell convergence in larger datasets may be a feasible and worthwhile approach to address this important component of an antigen-specific T cell response.

Studies with patients demonstrated the presence of clonally expanded TCRs in AAA or TAA, supporting the paradigm of AAA as a disease driven by an antigen-specific T cell response.[79, 106-108] In particular, clonal expansion of TCR beta[79, 107] and alpha[106] chains was demonstrated in AAA lesions of patients while others reported clonal expansion of γ/δ T cells in AAA.[79] Furthermore, TCRs were investigated in different types of TAA (patients with Marfan syndrome, familial TAA and sporadic aneurysm) and the results indicate a similar clonal nature of the TCRs present in TAA.[108] He et al. found a preferential usage of the V-genes Vb22 and Vb25 in lesions from patients with TAA.[108] Lu et al. reported multiple

appearances (at least twice) of TRBV3 in 60% of AAA patients.[107] Atherosclerotic vascular disease, which is also a risk factor for AAA development while it also shares some common (immuno-)pathophysiological pathways[6], is likewise associated with T cell expansion and clonality. In particular, TCRs containing Vβ6 are expanded in atherosclerotic lesions of mice.[217] Moreover, a decreased diversity of the TCR β chain repertoire was shown in human atherosclerotic plaques due to expansion of a few T cell subclones.[218]

The main limitation of this study is the relatively small number of lymphocytes resulting in potential undersampling. The limited number of T and B cells resulted from the naturally scarce source (i.e. minimal aneurysm size in mice), from additional sorting procedures (sorting of all leukocytes and not specifically T and B cells), and not fully efficient sequencing. Indeed, we had to exclude many TCR and BCR sequences from the data due to inefficient sequencing. The undersampling leads to the issue that the TCR and BCR copies in our data do not represent the real absolute number of copies present in AAA, and even the ratio of the various clones to each other does not reflect the real ratio.[219] Accordingly, this data should be interpreted cautiously and presents restricted value for biological interpretation. Further experiments are needed to verify the evidence of T cell clonality in elastase-induced AAA. Until now, mouse models are gold-standard for studying mechanisms of human pathophysiology. Yet, there are considerable differences between species regarding genetics, physiology, and immunology which have to be considered. Although the PPE model is the mouse model most closely resembling human AAA, it does not fully mimic the complexity of AAA development in humans.[192, 220] Human AAA feature a complex and long-lasting disease development that is only partially resembled in experimental rodent models that aim to recapitulate disease patterns in a few weeks. Thus, effects observed in mice have to extrapolated with cautions to human aneurysmal and atherosclerotic disease.

To overcome the problem of undersampling, we suggest sorting at least 5000 to 10000 B and T cells instead of including all leukocytes. We detected by flow cytometry on average 120 to 430 B cells and 400 to 1600 T cells per mg AAA tissue depending on the stage of AAA development, while lymphocyte numbers are lower in control conditions (e.g., native or sham-operated mice; on average 120-300 B cells, 400-500 T cells/mg aortic tissue). Thus, pooling of aneurysms from several mice is necessary to obtain a sufficient number of lymphocytes. In this case, we recommend the use of Hashtag antibodies before pooling to enable the assignment of the lymphocytes to the corresponding mouse and to monitor clonality for each individual. Next, the choice of experimental model should be carefully considered, as each model has limitations and mimics specific features of human AAA.[192] Li

et al. induced AAA in mice with elastase and $CaPO_4$, performed scRNA sequencing combined with TCR sequencing of 41341 $CD4^+$ T cells isolated from AAA and found a clonal expansion of regulatory T cells.[109] This suggests that the number of analyzed cells is an important factor for investigating TCR clonality and a high number of cells facilitates the identification of clonal expansion. Higher cell counts increase the likelihood of detecting rare TCR and BCR clones and allow additional investigation of T cell convergence. We would like to recommend prioritized sequencing of the TCR and BCR libraries and to include DNA-barcoded antibodies against B cells (CD19) and T cells (CD3), which allows for superior identification of subpopulations in comparison to identification by mRNA expression of feature genes. In addition to analyzing the aneurysmatic tissue itself future studies may also include sequencing of secondary lymphoid organs (e.g., draining lymph nodes) to identify changes in clonality, migration and activity of lymphocytes. scRNA-TCR-BCR-seq has the advantage of a high-throughput, multi-parametric analysis of target cells. Drop-sequencing approaches, like the commercially available 10x Genomics solution used here, allow to interrogate the transcriptome, TCR and BCR of thousands of cells simultaneously. However, there is a high dropout in detecting lowly expressed genes, which bears limitations: 1) this technology is particularly advantageous in describing a diverse cell population, while other approaches might be superior in studying transcriptional changes in related subpopulations, 2) full length transcripts of TCRs and BCRs for both chains might not be detectable in all cells (we here identified full length TCRs and BCRs in 33.5% and 55.1% of all cells). To uncover detailed transcriptional changes in T cell subpopulations, this approach could be complemented by sorting these cells and performing bulk transcriptomics, which delivers a deeper insight. Additionally, beta repertoire sequencing can be used to approximate T cell clonality on a global level and confirm observations made by scRNA-TCR-seq. However, this method does not provide information about the transcriptome of an individual cell or the corresponding paired TCR alpha chain, thus not reflecting the true complex clonality. In summary, scRNA-TCR-BCR-seq is an excellent tool for investigating TCR and BCR clonality if the above-mentioned points are taken into account during planning of experiments and data analysis.

6 Conclusion and future perspectives

AAA is a life-threatening multifactorial disease that is characterized by chronic inflammation. To date, the complexity of AAA pathology is not fully understood and pharmacological treatment options are lacking, but modulating the inflammation in AAA is a promising approach for therapies. This thesis aimed to investigate various aspects of the immune response involved in AAA pathology, including deciphering immune cell heterogeneity and dynamics, investigating the role of CD40 signaling, and examining the clonality of T and B cells. This study provides the first detailed characterization of immune cells in elastase-induced AAA using scRNA-seq and CITE-seq. In total, 30 different immune cell subtypes that are involved in AAA formation and progression were characterized. Their specific roles and functions require further study and could help to identify new therapeutic targets, as limiting inflammation by depletion or blocking of different immune cell types is a promising therapeutic strategy. The highest level of immune cell infiltration as well as the strongest intercellular communication was observed 7 days after elastase-perfusion, indicating day 7 as critical time point in experimental AAA development. However, the possibilities for early treatment of patients are limited, as early detection of AAA formation is difficult due to the commonly asymptomatic course of the disease. To successfully inhibit AAA growth in patients, not only effective drugs but also better methods for detection, such as clinical biomarkers, are needed. Thus, future studies should additionally focus on identifying suitable biomarkers, such as signatures of inflammatory proteins in plasma.

CD40 signaling was shown to play a critical role in all stages of AAA formation, as no striking differences in CD40 expression were observed between the time points. Blocking of CD40 signaling is a promising therapeutic approach, but the mechanism is still lacking. In this study, IFNIC macrophages and $CD4^+$ T cells were identified as key players in CD40 signaling 7 days after AAA formation. Although these results obtained from scRNA-seq analysis should be interpreted with caution and need to be validated with further experiments, future studies of the effects of CD40 inhibition on these cell types could be promising and may lead to a better understanding of the protective effect of CD40 inhibition.

Type-I IFN signaling plays a crucial role in CVDs and inhibition of this pathway is a promising therapeutic strategy. Since type-I IFN signaling in a non-viral context and the discovery of IFNIC macrophages is very novel, not much is known about their exact interactions and functions in CVDs. In this work, IFNIC macrophages were identified as key player in AAA and a flow cytometry panel was established to detect and isolate IFNIC macrophages enabling further investigations of these cells. Especially, the interplay of type-I IFN and CD40

signaling, both complex pathways that regulate inflammation, needs to be further investigated and offers great potential for finding new approaches for therapies.

Furthermore, evidence of clonal expansion of T cells, but not of B cells, was found in experimental elastase-induced AAA, supporting the notion that specific antigen-driven T cells play a role in AAA formation. Due to the small number of cells further experiments are needed to verify the evidence of T cell clonality. Since other studies found TCR clonality in AAA lesions of patients and considering the paradigm of an autoimmune response in aneurysmal disease, further examination of TCR- and BCR-clonality is important. The findings of this study imply that a precise characterization of TCR and BCR distribution requires a more extensive number of lymphocytes to prevent undersampling and to allow for detection of rare clones and convergent T cells. This study provides an in-depth analysis of TCR and BCR sequencing data, emphasizes the potential drawbacks and constraints of these experiments, and offers recommendations for future investigations in this area.

Overall, this thesis highlights the critical role of inflammation in the development of AAA and offers several options for new therapeutic approaches in further studies. In particular, type I-IFN and CD40 signaling in AAA will be further investigated, while interventions that target the adaptive immune response appear also promising.

7 References

1. World Health Organization. Cardiovascular Diseases [Available from: https://www.who.int/health-topics/cardiovascular-diseases#tab=tab_1.
2. World Heart Report 2023: Confronting the World's Number One Killer. Geneva, Switzerland. World Heart Federation. 2023.
3. Lindstrom M, DeCleene N, Dorsey H, et al. *Global Burden of Cardiovascular Diseases and Risks Collaboration, 1990-2021*. J Am Coll Cardiol. 2022;80(25):2372-425.http://dx.doi.org/10.1016/j.jacc.2022.11.001
4. Libby P, Buring JE, Badimon L, Hansson GK, Deanfield J, Bittencourt MS, Tokgozoglu L, Lewis EF. *Atherosclerosis*. Nat Rev Dis Primers. 2019;5(1):56.http://dx.doi.org/10.1038/s41572-019-0106-z
5. Wolf D, Ley K. *Immunity and Inflammation in Atherosclerosis*. Circ Res. 2019;124(2):315-27.http://dx.doi.org/10.1161/CIRCRESAHA.118.313591
6. Toghill BJ, Saratzis A, Bown MJ. *Abdominal aortic aneurysm-an independent disease to atherosclerosis?* Cardiovasc Pathol. 2017;27:71-5.http://dx.doi.org/10.1016/j.carpath.2017.01.008
7. Bentzon JF, Otsuka F, Virmani R, Falk E. *Mechanisms of plaque formation and rupture*. Circ Res. 2014;114(12):1852-66.http://dx.doi.org/10.1161/CIRCRESAHA.114.302721
8. Charla E, Mercer J, Maffia P, Nicklin SA. *Extracellular vesicle signalling in atherosclerosis*. Cell Signal. 2020;75:109751.http://dx.doi.org/10.1016/j.cellsig.2020.109751
9. Mendis S, Thygesen K, Kuulasmaa K, Giampaoli S, Mahonen M, Ngu Blackett K, Lisheng L, Writing group on behalf of the participating experts of the WHOcfroWHOdomi. *World Health Organization definition of myocardial infarction: 2008-09 revision*. Int J Epidemiol. 2011;40(1):139-46.http://dx.doi.org/10.1093/ije/dyq165
10. Reed GW, Rossi JE, Cannon CP. *Acute myocardial infarction*. Lancet. 2017;389(10065):197-210.http://dx.doi.org/10.1016/S0140-6736(16)30677-8
11. Ong SB, Hernandez-Resendiz S, Crespo-Avilan GE, Mukhametshina RT, Kwek XY, Cabrera-Fuentes HA, Hausenloy DJ. *Inflammation following acute myocardial infarction: Multiple players, dynamic roles, and novel therapeutic opportunities*. Pharmacol Ther. 2018;186:73-87.http://dx.doi.org/10.1016/j.pharmthera.2018.01.001
12. Prabhu SD, Frangogiannis NG. *The Biological Basis for Cardiac Repair After Myocardial Infarction: From Inflammation to Fibrosis*. Circ Res. 2016;119(1):91-112.http://dx.doi.org/10.1161/CIRCRESAHA.116.303577
13. Matter MA, Paneni F, Libby P, et al. *Inflammation in acute myocardial infarction: the good, the bad and the ugly*. Eur Heart J. 2024;45(2):89-103.http://dx.doi.org/10.1093/eurheartj/ehad486
14. Thygesen K, Alpert JS, Jaffe AS, Chaitman BR, Bax JJ, Morrow DA, White HD, Executive Group on behalf of the Joint European Society of Cardiology /American College of Cardiology /American Heart Association /World Heart Federation Task Force for the Universal Definition of Myocardial I. *Fourth Universal Definition of Myocardial Infarction (2018)*. Circulation. 2018;138(20):e618-e51.http://dx.doi.org/10.1161/CIR.0000000000000617
15. Sakalihasan N, Michel J-B, Katsargyris A, Kuivaniemi H, Defraigne J-O, Nchimi A, Powell JT, Yoshimura K, Hultgren R. *Abdominal aortic aneurysms*. Nature Reviews Disease Primers. 2018;4(1):34.http://dx.doi.org/10.1038/s41572-018-0030-7
16. Authors/Task Force M, Czerny M, Grabenwoger M, et al. *EACTS/STS Guidelines for Diagnosing and Treating Acute and Chronic Syndromes of the Aortic Organ*. Ann Thorac Surg. 2024.http://dx.doi.org/10.1016/j.athoracsur.2024.01.021
17. Kuivaniemi H, Platsoucas CD, Tilson MD, 3rd. *Aortic aneurysms: an immune disease with a strong genetic component*. Circulation. 2008;117(2):242-52.http://dx.doi.org/10.1161/circulationaha.107.690982
18. Song P, He Y, Adeloye D, Zhu Y, Ye X, Yi Q, Rahimi K, Rudan I, Global Health Epidemiology Research G. *The Global and Regional Prevalence of Abdominal Aortic Aneurysms: A Systematic Review and Modeling Analysis*. Ann Surg. 2023;277(6):912-9.http://dx.doi.org/10.1097/SLA.0000000000005716
19. Tsao CW, Aday AW, Almarzooq ZI, et al. *Heart Disease and Stroke Statistics-2023 Update: A Report From the American Heart Association*. Circulation. 2023;147(8):e93-e621.http://dx.doi.org/10.1161/CIR.0000000000001123

20. Force USPST, Owens DK, Davidson KW, et al. *Screening for Abdominal Aortic Aneurysm: US Preventive Services Task Force Recommendation Statement*. JAMA. 2019;322(22):2211-8.http://dx.doi.org/10.1001/jama.2019.18928
21. Golledge J, Thanigaimani S, Powell JT, Tsao PS. *Pathogenesis and management of abdominal aortic aneurysm*. Eur Heart J. 2023.http://dx.doi.org/10.1093/eurheartj/ehad386
22. Gasser TC, Ogden RW, Holzapfel GA. *Hyperelastic modelling of arterial layers with distributed collagen fibre orientations*. J R Soc Interface. 2006;3(6):15-35.http://dx.doi.org/10.1098/rsif.2005.0073
23. Lu H, Du W, Ren L, Hamblin MH, Becker RC, Chen YE, Fan Y. *Vascular Smooth Muscle Cells in Aortic Aneurysm: From Genetics to Mechanisms*. J Am Heart Assoc. 2021;10(24):e023601.http://dx.doi.org/10.1161/JAHA.121.023601
24. Cho MJ, Lee MR, Park JG. *Aortic aneurysms: current pathogenesis and therapeutic targets*. Exp Mol Med. 2023;55(12):2519-30.http://dx.doi.org/10.1038/s12276-023-01130-w
25. Yuan Z, Lu Y, Wei J, Wu J, Yang J, Cai Z. *Abdominal Aortic Aneurysm: Roles of Inflammatory Cells*. Front Immunol. 2020;11:609161.http://dx.doi.org/10.3389/fimmu.2020.609161
26. Lowis C, Ramara Winaya A, Kumari P, Rivera CF, Vlahos J, Hermantara R, Pratama MY, Ramkhelawon B. *Mechanosignals in abdominal aortic aneurysms*. Front Cardiovasc Med. 2022;9:1021934.http://dx.doi.org/10.3389/fcvm.2022.1021934
27. Marshall JS, Warrington R, Watson W, Kim HL. *An introduction to immunology and immunopathology*. Allergy Asthma Clin Immunol. 2018;14(Suppl 2):49.http://dx.doi.org/10.1186/s13223-018-0278-1
28. Liew PX, Kubes P. *The Neutrophil's Role During Health and Disease*. Physiol Rev. 2019;99(2):1223-48.http://dx.doi.org/10.1152/physrev.00012.2018
29. Pfeiler S, Stark K, Massberg S, Engelmann B. *Propagation of thrombosis by neutrophils and extracellular nucleosome networks*. Haematologica. 2017;102(2):206-13.http://dx.doi.org/10.3324/haematol.2016.142471
30. Rosales C. *Neutrophil: A Cell with Many Roles in Inflammation or Several Cell Types?* Front Physiol. 2018;9:113.http://dx.doi.org/10.3389/fphys.2018.00113
31. Silvestre-Roig C, Fridlender ZG, Glogauer M, Scapini P. *Neutrophil Diversity in Health and Disease*. Trends Immunol. 2019;40(7):565-83.http://dx.doi.org/10.1016/j.it.2019.04.012
32. Houard X, Touat Z, Ollivier V, Louedec L, Philippe M, Sebbag U, Meilhac O, Rossignol P, Michel JB. *Mediators of neutrophil recruitment in human abdominal aortic aneurysms*. Cardiovasc Res. 2009;82(3):532-41.http://dx.doi.org/10.1093/cvr/cvp048
33. Shah AD, Denaxas S, Nicholas O, Hingorani AD, Hemingway H. *Neutrophil Counts and Initial Presentation of 12 Cardiovascular Diseases: A CALIBER Cohort Study*. J Am Coll Cardiol. 2017;69(9):1160-9.http://dx.doi.org/10.1016/j.jacc.2016.12.022
34. Eliason JL, Hannawa KK, Ailawadi G, et al. *Neutrophil depletion inhibits experimental abdominal aortic aneurysm formation*. Circulation. 2005;112(2):232-40.http://dx.doi.org/10.1161/CIRCULATIONAHA.104.517391
35. Pagano MB, Bartoli MA, Ennis TL, Mao D, Simmons PM, Thompson RW, Pham CT. *Critical role of dipeptidyl peptidase I in neutrophil recruitment during the development of experimental abdominal aortic aneurysms*. Proc Natl Acad Sci U S A. 2007;104(8):2855-60.http://dx.doi.org/10.1073/pnas.0606091104
36. He L, Fu Y, Deng J, et al. *Deficiency of FAM3D (Family With Sequence Similarity 3, Member D), A Novel Chemokine, Attenuates Neutrophil Recruitment and Ameliorates Abdominal Aortic Aneurysm Development*. Arterioscler Thromb Vasc Biol. 2018;38(7):1616-31.http://dx.doi.org/10.1161/ATVBAHA.118.311289
37. Delbosc S, Alsac JM, Journe C, et al. *Porphyromonas gingivalis participates in pathogenesis of human abdominal aortic aneurysm by neutrophil activation. Proof of concept in rats*. PLoS One. 2011;6(4):e18679.http://dx.doi.org/10.1371/journal.pone.0018679
38. Yan H, Zhou HF, Akk A, Hu Y, Springer LE, Ennis TL, Pham CTN. *Neutrophil Proteases Promote Experimental Abdominal Aortic Aneurysm via Extracellular Trap Release and Plasmacytoid Dendritic Cell Activation*. Arterioscler Thromb Vasc Biol. 2016;36(8):1660-9.http://dx.doi.org/10.1161/ATVBAHA.116.307786
39. Meher AK, Spinosa M, Davis JP, Pope N, Laubach VE, Su G, Serbulea V, Leitinger N, Ailawadi G, Upchurch GR, Jr. *Novel Role of IL (Interleukin)-1beta in Neutrophil Extracellular Trap Formation and Abdominal Aortic Aneurysms*. Arterioscler Thromb Vasc Biol. 2018;38(4):843-53.http://dx.doi.org/10.1161/ATVBAHA.117.309897

40. Liu K. Dendritic Cells. In: Ralph AB, Philip DS, editors. Encyclopedia of Cell Biology. Waltham: Academic Press; 2016. p. 741-9.
41. Krishna SM, Moran CS, Jose RJ, Lazzaroni S, Huynh P, Golledge J. *Depletion of CD11c+ dendritic cells in apolipoprotein E-deficient mice limits angiotensin II-induced abdominal aortic aneurysm formation and growth*. Clin Sci (Lond). 2019;133(21):2203-15.http://dx.doi.org/10.1042/CS20190924
42. Choi JH, Cheong C, Dandamudi DB, et al. *Flt3 signaling-dependent dendritic cells protect against atherosclerosis*. Immunity. 2011;35(5):819-31.http://dx.doi.org/10.1016/j.immuni.2011.09.014
43. Serbina NV, Salazar-Mather TP, Biron CA, Kuziel WA, Pamer EG. *TNF/iNOS-producing dendritic cells mediate innate immune defense against bacterial infection*. Immunity. 2003;19(1):59-70.http://dx.doi.org/10.1016/s1074-7613(03)00171-7
44. Lendeckel U, Venz S, Wolke C. *Macrophages: shapes and functions*. ChemTexts. 2022;8(2):12.http://dx.doi.org/10.1007/s40828-022-00163-4
45. Raffort J, Lareyre F, Clement M, Hassen-Khodja R, Chinetti G, Mallat Z. *Monocytes and macrophages in abdominal aortic aneurysm*. Nat Rev Cardiol. 2017;14(8):457-71.http://dx.doi.org/10.1038/nrcardio.2017.52
46. Rateri DL, Howatt DA, Moorleghen JJ, Charnigo R, Cassis LA, Daugherty A. *Prolonged infusion of angiotensin II in apoE(-/-) mice promotes macrophage recruitment with continued expansion of abdominal aortic aneurysm*. Am J Pathol. 2011;179(3):1542-8.http://dx.doi.org/10.1016/j.ajpath.2011.05.049
47. Davis FM, Rateri DL, Daugherty A. *Abdominal aortic aneurysm: novel mechanisms and therapies*. Curr Opin Cardiol. 2015;30(6):566-73.http://dx.doi.org/10.1097/HCO.0000000000000216
48. Mellak S, Ait-Oufella H, Esposito B, Loyer X, Poirier M, Tedder TF, Tedgui A, Mallat Z, Potteaux S. *Angiotensin II mobilizes spleen monocytes to promote the development of abdominal aortic aneurysm in Apoe-/- mice*. Arterioscler Thromb Vasc Biol. 2015;35(2):378-88.http://dx.doi.org/10.1161/ATVBAHA.114.304389
49. Hans CP, Koenig SN, Huang N, Cheng J, Beceiro S, Guggilam A, Kuivaniemi H, Partida-Sanchez S, Garg V. *Inhibition of Notch1 signaling reduces abdominal aortic aneurysm in mice by attenuating macrophage-mediated inflammation*. Arterioscler Thromb Vasc Biol. 2012;32(12):3012-23.http://dx.doi.org/10.1161/ATVBAHA.112.254219
50. Michineau S, Franck G, Wagner-Ballon O, Dai J, Allaire E, Gervais M. *Chemokine (C-X-C motif) receptor 4 blockade by AMD3100 inhibits experimental abdominal aortic aneurysm expansion through anti-inflammatory effects*. Arterioscler Thromb Vasc Biol. 2014;34(8):1747-55.http://dx.doi.org/10.1161/ATVBAHA.114.303913
51. Moehle CW, Bhamidipati CM, Alexander MR, Mehta GS, Irvine JN, Salmon M, Upchurch GR, Jr., Kron IL, Owens GK, Ailawadi G. *Bone marrow-derived MCP1 required for experimental aortic aneurysm formation and smooth muscle phenotypic modulation*. J Thorac Cardiovasc Surg. 2011;142(6):1567-74.http://dx.doi.org/10.1016/j.jtcvs.2011.07.053
52. Iida Y, Xu B, Xuan H, et al. *Peptide inhibitor of CXCL4-CCL5 heterodimer formation, MKEY, inhibits experimental aortic aneurysm initiation and progression*. Arterioscler Thromb Vasc Biol. 2013;33(4):718-26.http://dx.doi.org/10.1161/ATVBAHA.112.300329
53. Dale MA, Xiong W, Carson JS, Suh MK, Karpisek AD, Meisinger TM, Casale GP, Baxter BT. *Elastin-Derived Peptides Promote Abdominal Aortic Aneurysm Formation by Modulating M1/M2 Macrophage Polarization*. J Immunol. 2016;196(11):4536-43.http://dx.doi.org/10.4049/jimmunol.1502454
54. Pope NH, Salmon M, Davis JP, Chatterjee A, Su G, Conte MS, Ailawadi G, Upchurch GR, Jr. *D-series resolvins inhibit murine abdominal aortic aneurysm formation and increase M2 macrophage polarization*. FASEB J. 2016;30(12):4192-201.http://dx.doi.org/10.1096/fj.201600144RR
55. Yu L, Zhang Y, Liu C, Wu X, Wang S, Sui W, Zhang Y, Zhang C, Zhang M. *Heterogeneity of macrophages in atherosclerosis revealed by single-cell RNA sequencing*. FASEB J. 2023;37(3):e22810.http://dx.doi.org/10.1096/fj.202201932RR
56. Cochain C, Vafadarnejad E, Arampatzi P, Pelisek J, Winkels H, Ley K, Wolf D, Saliba AE, Zernecke A. *Single-Cell RNA-Seq Reveals the Transcriptional Landscape and Heterogeneity of Aortic Macrophages in Murine Atherosclerosis*. Circ Res. 2018;122(12):1661-74.http://dx.doi.org/10.1161/CIRCRESAHA.117.312509
57. Zernecke A, Winkels H, Cochain C, et al. *Meta-Analysis of Leukocyte Diversity in Atherosclerotic Mouse Aortas*. Circ Res. 2020;127(3):402-26.http://dx.doi.org/10.1161/CIRCRESAHA.120.316903

58. Vivier E, Artis D, Colonna M, et al. *Innate Lymphoid Cells: 10 Years On*. Cell. 2018;174(5):1054-66.http://dx.doi.org/10.1016/j.cell.2018.07.017
59. Walker JA, Barlow JL, McKenzie AN. *Innate lymphoid cells--how did we miss them?* Nat Rev Immunol. 2013;13(2):75-87.http://dx.doi.org/10.1038/nri3349
60. Roberts LB, Lord GM, Howard JK. *Heartbreakers or Healers? Innate Lymphoid Cells in Cardiovascular Disease and Obesity*. Front Immunol. 2022;13:903678.http://dx.doi.org/10.3389/fimmu.2022.903678
61. Zhang Y, Liu T, Deng Z, et al. *Group 2 Innate Lymphoid Cells Protect Mice from Abdominal Aortic Aneurysm Formation via IL5 and Eosinophils*. Adv Sci (Weinh). 2023;10(7):e2206958.http://dx.doi.org/10.1002/advs.202206958
62. Mace EM. *Human natural killer cells: Form, function, and development*. J Allergy Clin Immunol. 2023;151(2):371-85.http://dx.doi.org/10.1016/j.jaci.2022.09.022
63. Chan WL, Pejnovic N, Hamilton H, Liew TV, Popadic D, Poggi A, Khan SM. *Atherosclerotic abdominal aortic aneurysm and the interaction between autologous human plaque-derived vascular smooth muscle cells, type 1 NKT, and helper T cells*. Circ Res. 2005;96(6):675-83.http://dx.doi.org/10.1161/01.RES.0000160543.84254.f1
64. Patel A, Jagadesham VP, Porter KE, Scott DJ, Carding SR. *Characterisation of fractalkine/CX3CL1 and fractalkine receptor (CX3CR1) expression in abdominal aortic aneurysm disease*. Eur J Vasc Endovasc Surg. 2008;36(1):20-7.http://dx.doi.org/10.1016/j.ejvs.2008.01.014
65. Forester ND, Cruickshank SM, Scott DJ, Carding SR. *Increased natural killer cell activity in patients with an abdominal aortic aneurysm*. Br J Surg. 2006;93(1):46-54.http://dx.doi.org/10.1002/bjs.5215
66. Hinterseher I, Schworer CM, Lillvis JH, Stahl E, Erdman R, Gatalica Z, Tromp G, Kuivaniemi H. *Immunohistochemical analysis of the natural killer cell cytotoxicity pathway in human abdominal aortic aneurysms*. Int J Mol Sci. 2015;16(5):11196-212.http://dx.doi.org/10.3390/ijms160511196
67. Miao T, Wang T, Feng T, et al. *Activated invariant natural killer T cells infiltrate aortic tissue as key participants in abdominal aortic aneurysm pathology*. Immunology. 2021;164(4):792-802.http://dx.doi.org/10.1111/imm.13401
68. van Puijvelde GHM, Foks AC, van Bochove RE, et al. *CD1d deficiency inhibits the development of abdominal aortic aneurysms in LDL receptor deficient mice*. PLoS One. 2018;13(1):e0190962.http://dx.doi.org/10.1371/journal.pone.0190962
69. Saito A, Ishimori N, Tokuhara S, Homma T, Nishikawa M, Iwabuchi K, Tsutsui H. *Activation of Invariant Natural Killer T Cells by alpha-Galactosylceramide Attenuates the Development of Angiotensin II-Mediated Abdominal Aortic Aneurysm in Obese ob/ob Mice*. Front Cardiovasc Med. 2021;8:659418.http://dx.doi.org/10.3389/fcvm.2021.659418
70. Pisetsky DS. *Pathogenesis of autoimmune disease*. Nat Rev Nephrol. 2023;19(8):509-24.http://dx.doi.org/10.1038/s41581-023-00720-1
71. Lu S, White JV, Nwaneshiudu I, Nwaneshiudu A, Monos DS, Solomides CC, Oleszak EL, Platsoucas CD. *Human abdominal aortic aneurysm (AAA): Evidence for an autoimmune antigen-driven disease*. Autoimmun Rev. 2022;21(10):103164.http://dx.doi.org/10.1016/j.autrev.2022.103164
72. Koch AE, Haines GK, Rizzo RJ, Radosevich JA, Pope RM, Robinson PG, Pearce WH. *Human abdominal aortic aneurysms. Immunophenotypic analysis suggesting an immune-mediated response*. Am J Pathol. 1990;137(5):1199-213
73. Forester ND, Cruickshank SM, Scott DJ, Carding SR. *Functional characterization of T cells in abdominal aortic aneurysms*. Immunology. 2005;115(2):262-70.http://dx.doi.org/10.1111/j.1365-2567.2005.02157.x
74. Furusho A, Aoki H, Ohno-Urabe S, et al. *Involvement of B Cells, Immunoglobulins, and Syk in the Pathogenesis of Abdominal Aortic Aneurysm*. J Am Heart Assoc. 2018;7(6).http://dx.doi.org/10.1161/JAHA.117.007750
75. Meher AK, Johnston WF, Lu G, et al. *B2 cells suppress experimental abdominal aortic aneurysms*. Am J Pathol. 2014;184(11):3130-41.http://dx.doi.org/10.1016/j.ajpath.2014.07.006
76. Saraff K, Babamusta F, Cassis LA, Daugherty A. *Aortic dissection precedes formation of aneurysms and atherosclerosis in angiotensin II-infused, apolipoprotein E-deficient mice*. Arterioscler Thromb Vasc Biol. 2003;23(9):1621-6.http://dx.doi.org/10.1161/01.ATV.0000085631.76095.64
77. Tian K, Xia C, Liu H, et al. *Temporal and Quantitative Analysis of Aortic Immunopathologies in Elastase-Induced Mouse Abdominal Aortic Aneurysms*. J Immunol Res. 2021;2021:6297332.http://dx.doi.org/10.1155/2021/6297332

78. Griepke S, Grupe E, Lindholt JS, et al. *Selective inhibition of soluble tumor necrosis factor signaling reduces abdominal aortic aneurysm progression*. Front Cardiovasc Med. 2022;9:942342.http://dx.doi.org/10.3389/fcvm.2022.942342
79. Platsoucas CD, Lu S, Nwaneshiudu I, et al. *Abdominal aortic aneurysm is a specific antigen-driven T cell disease*. Ann N Y Acad Sci. 2006;1085:224-35.http://dx.doi.org/10.1196/annals.1383.019
80. Piacentini L, Werba JP, Bono E, Saccu C, Tremoli E, Spirito R, Colombo GI. *Genome-Wide Expression Profiling Unveils Autoimmune Response Signatures in the Perivascular Adipose Tissue of Abdominal Aortic Aneurysm*. Arterioscler Thromb Vasc Biol. 2019;39(2):237-49.http://dx.doi.org/10.1161/ATVBAHA.118.311803
81. Sun L, Su Y, Jiao A, Wang X, Zhang B. *T cells in health and disease*. Signal Transduct Target Ther. 2023;8(1):235.http://dx.doi.org/10.1038/s41392-023-01471-y
82. Xiong W, Zhao Y, Prall A, Greiner TC, Baxter BT. *Key roles of CD4+ T cells and IFN-gamma in the development of abdominal aortic aneurysms in a murine model*. J Immunol. 2004;172(4):2607-12.http://dx.doi.org/10.4049/jimmunol.172.4.2607
83. Dale MA, Ruhlman MK, Baxter BT. *Inflammatory cell phenotypes in AAAs: their role and potential as targets for therapy*. Arterioscler Thromb Vasc Biol. 2015;35(8):1746-55.http://dx.doi.org/10.1161/atvbaha.115.305269
84. Kusters PJH, Seijkens TTP, Beckers L, et al. *CD40L Deficiency Protects Against Aneurysm Formation*. Arterioscler Thromb Vasc Biol. 2018;38(5):1076-85.http://dx.doi.org/10.1161/atvbaha.117.310640
85. Schonbeck U, Sukhova GK, Gerdes N, Libby P. *T(H)2 predominant immune responses prevail in human abdominal aortic aneurysm*. Am J Pathol. 2002;161(2):499-506.http://dx.doi.org/10.1016/S0002-9440(10)64206-X
86. Sharma AK, Lu G, Jester A, et al. *Experimental abdominal aortic aneurysm formation is mediated by IL-17 and attenuated by mesenchymal stem cell treatment*. Circulation. 2012;126(11 Suppl 1):S38-45.http://dx.doi.org/10.1161/CIRCULATIONAHA.111.083451
87. Vignali DA, Collison LW, Workman CJ. *How regulatory T cells work*. Nat Rev Immunol. 2008;8(7):523-32.http://dx.doi.org/10.1038/nri2343
88. Zhou Y, Wu W, Lindholt JS, Sukhova GK, Libby P, Yu X, Shi GP. *Regulatory T cells in human and angiotensin II-induced mouse abdominal aortic aneurysms*. Cardiovasc Res. 2015;107(1):98-107.http://dx.doi.org/10.1093/cvr/cvv119
89. Suh MK, Batra R, Carson JS, Xiong W, Dale MA, Meisinger T, Killen C, Mitchell J, Baxter BT. *Ex vivo expansion of regulatory T cells from abdominal aortic aneurysm patients inhibits aneurysm in humanized murine model*. J Vasc Surg. 2020;72(3):1087-96 e1.http://dx.doi.org/10.1016/j.jvs.2019.08.285
90. Zhou HF, Yan H, Cannon JL, Springer LE, Green JM, Pham CT. *CD43-mediated IFN-gamma production by CD8+ T cells promotes abdominal aortic aneurysm in mice*. J Immunol. 2013;190(10):5078-85.http://dx.doi.org/10.4049/jimmunol.1203228
91. Hoffman W, Lakkis FG, Chalasani G. *B Cells, Antibodies, and More*. Clin J Am Soc Nephrol. 2016;11(1):137-54.http://dx.doi.org/10.2215/CJN.09430915
92. Zhang L, Wang Y. *B lymphocytes in abdominal aortic aneurysms*. Atherosclerosis. 2015;242(1):311-7.http://dx.doi.org/10.1016/j.atherosclerosis.2015.07.036
93. Schaheen B, Downs EA, Serbulea V, et al. *B-Cell Depletion Promotes Aortic Infiltration of Immunosuppressive Cells and Is Protective of Experimental Aortic Aneurysm*. Arterioscler Thromb Vasc Biol. 2016;36(11):2191-202.http://dx.doi.org/10.1161/ATVBAHA.116.307559
94. Liu X, Wu J. *History, applications, and challenges of immune repertoire research*. Cell Biol Toxicol. 2018;34(6):441-57.http://dx.doi.org/10.1007/s10565-018-9426-0
95. Rosati E, Dowds CM, Liaskou E, Henriksen EKK, Karlsen TH, Franke A. *Overview of methodologies for T-cell receptor repertoire analysis*. BMC Biotechnol. 2017;17(1):61.http://dx.doi.org/10.1186/s12896-017-0379-9
96. Zarnitsyna VI, Evavold BD, Schoettle LN, Blattman JN, Antia R. *Estimating the diversity, completeness, and cross-reactivity of the T cell repertoire*. Front Immunol. 2013;4:485.http://dx.doi.org/10.3389/fimmu.2013.00485
97. Greiff V, Menzel U, Miho E, et al. *Systems Analysis Reveals High Genetic and Antigen-Driven Predetermination of Antibody Repertoires throughout B Cell Development*. Cell Rep. 2017;19(7):1467-78.http://dx.doi.org/10.1016/j.celrep.2017.04.054

98. Elhanati Y, Sethna Z, Marcou Q, Callan CG, Jr., Mora T, Walczak AM. *Inferring processes underlying B-cell repertoire diversity*. Philos Trans R Soc Lond B Biol Sci. 2015;370(1676).http://dx.doi.org/10.1098/rstb.2014.0243
99. Davis FM, Tsoi LC, Ma F, Wasikowski R, Moore BB, Kunkel SL, Gudjonsson JE, Gallagher KA. *Single-cell Transcriptomics Reveals Dynamic Role of Smooth Muscle Cells and Enrichment of Immune Cell Subsets in Human Abdominal Aortic Aneurysms*. Ann Surg. 2022;276(3):511-21.http://dx.doi.org/10.1097/sla.0000000000005551
100. Miqueu P, Guillet M, Degauque N, Dore JC, Soulillou JP, Brouard S. *Statistical analysis of CDR3 length distributions for the assessment of T and B cell repertoire biases*. Mol Immunol. 2007;44(6):1057-64.http://dx.doi.org/10.1016/j.molimm.2006.06.026
101. Minervina A, Pogorelyy M, Mamedov I. *T-cell receptor and B-cell receptor repertoire profiling in adaptive immunity*. Transpl Int. 2019;32(11):1111-23.http://dx.doi.org/10.1111/tri.13475
102. Elster C, Ommer-Blasius M, Lang A, et al. *Application and challenges of TCR and BCR sequencing to investigate T- and B-cell clonality in elastase-induced experimental murine abdominal aortic aneurysm*. Front Cardiovasc Med. 2023;10:1221620.http://dx.doi.org/10.3389/fcvm.2023.1221620
103. Fujii K, Kanekura T. *Next-Generation Sequencing Technologies for Early-Stage Cutaneous T-Cell Lymphoma*. Front Med (Lausanne). 2019;6:181.http://dx.doi.org/10.3389/fmed.2019.00181
104. Zhou HF, Yan H, Bertram P, Hu Y, Springer LE, Thompson RW, Curci JA, Hourcade DE, Pham CT. *Fibrinogen-specific antibody induces abdominal aortic aneurysm in mice through complement lectin pathway activation*. Proc Natl Acad Sci U S A. 2013;110(46):E4335-44.http://dx.doi.org/10.1073/pnas.1315512110
105. Chew DK, Knoetgen J, Xia S, Tilson MD. *The role of a putative microfibrillar protein (80 kDa) in abdominal aortic aneurysm disease*. J Surg Res. 2003;114(1):25-9.http://dx.doi.org/10.1016/s0022-4804(03)00208-7
106. Lu S, White JV, Judy RI, et al. *Clonally expanded alpha-chain T-cell receptor (TCR) transcripts are present in aneurysmal lesions of patients with Abdominal Aortic Aneurysm (AAA)*. PLoS One. 2019;14(7):e0218990.http://dx.doi.org/10.1371/journal.pone.0218990
107. Lu S, White JV, Lin WL, et al. *Aneurysmal lesions of patients with abdominal aortic aneurysm contain clonally expanded T cells*. J Immunol. 2014;192(10):4897-912.http://dx.doi.org/10.4049/jimmunol.1301009
108. He R, Guo DC, Sun W, et al. *Characterization of the inflammatory cells in ascending thoracic aortic aneurysms in patients with Marfan syndrome, familial thoracic aortic aneurysms, and sporadic aneurysms*. J Thorac Cardiovasc Surg. 2008;136(4):922-9, 9 e1.http://dx.doi.org/10.1016/j.jtcvs.2007.12.063
109. Li J, Xia N, Li D, et al. *Aorta Regulatory T Cells with a Tissue-Specific Phenotype and Function Promote Tissue Repair through Tff1 in Abdominal Aortic Aneurysms*. Adv Sci (Weinh). 2022;9(9):e2104338.http://dx.doi.org/10.1002/advs.202104338
110. Elgueta R, Benson MJ, de Vries VC, Wasiuk A, Guo Y, Noelle RJ. *Molecular mechanism and function of CD40/CD40L engagement in the immune system*. Immunol Rev. 2009;229(1):152-72.http://dx.doi.org/10.1111/j.1600-065X.2009.00782.x
111. van Kooten C, Banchereau J. *CD40-CD40 ligand*. J Leukoc Biol. 2000;67(1):2-17.http://dx.doi.org/10.1002/jlb.67.1.2
112. Paulie S, Ehlin-Henriksson B, Mellstedt H, Koho H, Ben-Aissa H, Perlmann P. *A p50 surface antigen restricted to human urinary bladder carcinomas and B lymphocytes*. Cancer Immunol Immunother. 1985;20(1):23-8.http://dx.doi.org/10.1007/BF00199769
113. Bishop GA, Moore, C.R., Xie, P., Stunz, L.L., Kraus, Z.J. TRAF Proteins in CD40 Signaling , bookTitle= TNF Receptor Associated Factors (TRAFs). New York, NY: Springer New York; 2007. 131--51 p.
114. Hanissian SH, Geha RS. *Jak3 is associated with CD40 and is critical for CD40 induction of gene expression in B cells*. Immunity. 1997;6(4):379-87.http://dx.doi.org/10.1016/s1074-7613(00)80281-2
115. van Essen D, Kikutani H, Gray D. *CD40 ligand-transduced co-stimulation of T cells in the development of helper function*. Nature. 1995;378(6557):620-3.http://dx.doi.org/10.1038/378620a0
116. Arpin C, Dechanet J, Van Kooten C, Merville P, Grouard G, Briere F, Banchereau J, Liu YJ. *Generation of memory B cells and plasma cells in vitro*. Science. 1995;268(5211):720-2.http://dx.doi.org/10.1126/science.7537388

117. Strohm L, Ubbens H, Munzel T, Daiber A, Daub S. *Role of CD40(L)-TRAF signaling in inflammation and resolution-a double-edged sword*. Front Pharmacol. 2022;13:995061. http://dx.doi.org/10.3389/fphar.2022.995061
118. Yan JC, Zhu J, Gao L, Wu ZG, Kong XT, Zong RQ, Zhan LZ. *The effect of elevated serum soluble CD40 ligand on the prognostic value in patients with acute coronary syndromes*. Clin Chim Acta. 2004;343(1-2):155-9.http://dx.doi.org/10.1016/j.cccn.2004.01.012
119. Schonbeck U, Varo N, Libby P, Buring J, Ridker PM. *Soluble CD40L and cardiovascular risk in women*. Circulation. 2001;104(19):2266-8.http://dx.doi.org/10.1161/hc4401.099447
120. Li J, Wang Y, Lin J, Wang D, Wang A, Zhao X, Liu L, Wang C, Wang Y, Investigators C. *Soluble CD40L Is a Useful Marker to Predict Future Strokes in Patients With Minor Stroke and Transient Ischemic Attack*. Stroke. 2015;46(7):1990-2.http://dx.doi.org/10.1161/STROKEAHA.115.008685
121. Tascanov MB, Tanriverdi Z, Gungoren F, Besli F, Erkus ME, Gonel A, Koyuncu I, Demirbag R. *Association between the No-Reflow Phenomenon and Soluble CD40 Ligand Level in Patients with Acute ST-Segment Elevation Myocardial Infarction*. Medicina (Kaunas). 2019;55(7). http://dx.doi.org/10.3390/medicina55070376
122. Daub S, Lutgens E, Munzel T, Daiber A. *CD40/CD40L and Related Signaling Pathways in Cardiovascular Health and Disease-The Pros and Cons for Cardioprotection*. Int J Mol Sci. 2020;21(22).http://dx.doi.org/10.3390/ijms21228533
123. Mach F, Schonbeck U, Sukhova GK, Atkinson E, Libby P. *Reduction of atherosclerosis in mice by inhibition of CD40 signalling*. Nature. 1998;394(6689):200-3.http://dx.doi.org/10.1038/28204
124. Kawai T, Andrews D, Colvin RB, Sachs DH, Cosimi AB. *Thromboembolic complications after treatment with monoclonal antibody against CD40 ligand*. Nat Med. 2000;6(2):114.http://dx.doi.org/10.1038/72162
125. Boumpas DT, Furie R, Manzi S, Illei GG, Wallace DJ, Balow JE, Vaishnaw A, Group BGLNT. *A short course of BG9588 (anti-CD40 ligand antibody) improves serologic activity and decreases hematuria in patients with proliferative lupus glomerulonephritis*. Arthritis Rheum. 2003;48(3):719-27.http://dx.doi.org/10.1002/art.10856
126. Lutgens E, Lievens D, Beckers L, et al. *Deficient CD40-TRAF6 signaling in leukocytes prevents atherosclerosis by skewing the immune response toward an antiinflammatory profile*. J Exp Med. 2010;207(2):391-404.http://dx.doi.org/10.1084/jem.20091293
127. Seijkens TTP, van Tiel CM, Kusters PJH, et al. *Targeting CD40-Induced TRAF6 Signaling in Macrophages Reduces Atherosclerosis*. J Am Coll Cardiol. 2018;71(5):527-42.http://dx.doi.org/10.1016/j.jacc.2017.11.055
128. Witkowski S. The role of co-stimulatory molecules CD40/CD40L during the immune response after acute myocardial infarction [Dissertation]: Heinrich-Heine University Düsseldorf; 2023.
129. Bosch L, de Haan J, Seijkens T, van Tiel C, Brans M, Pasterkamp G, Lutgens E, de Jager S. *Small molecule-mediated inhibition of CD40-TRAF6 reduces adverse cardiac remodelling in pressure overload induced heart failure*. Int J Cardiol. 2019;279:141-4.http://dx.doi.org/10.1016/j.ijcard.2018.12.076
130. Ommer-Bläsius M, Vajen T, Elster C, et al. *Inhibition of CD40-TRAF6 signaling protects against aneurysm development and progression*. bioRxiv. 2023:2023.03.24.534110.http://dx.doi.org/10.1101/2023.03.24.534110
131. Jovic D, Liang X, Zeng H, Lin L, Xu F, Luo Y. *Single-cell RNA sequencing technologies and applications: A brief overview*. Clin Transl Med. 2022;12(3):e694.http://dx.doi.org/10.1002/ctm2.694
132. Tang F, Barbacioru C, Wang Y, et al. *mRNA-Seq whole-transcriptome analysis of a single cell*. Nat Methods. 2009;6(5):377-82.http://dx.doi.org/10.1038/nmeth.1315
133. Stoeckius M, Hafemeister C, Stephenson W, Houck-Loomis B, Chattopadhyay PK, Swerdlow H, Satija R, Smibert P. *Simultaneous epitope and transcriptome measurement in single cells*. Nat Methods. 2017;14(9):865-8.http://dx.doi.org/10.1038/nmeth.4380
134. Mazzotti L, Gaimari A, Bravaccini S, et al. *T-Cell Receptor Repertoire Sequencing and Its Applications: Focus on Infectious Diseases and Cancer*. Int J Mol Sci. 2022;23(15).http://dx.doi.org/10.3390/ijms23158590
135. Lacy M, Burger C, Shami A, et al. *Cell-specific and divergent roles of the CD40L-CD40 axis in atherosclerotic vascular disease*. Nat Commun. 2021;12(1):3754.http://dx.doi.org/10.1038/s41467-021-23909-z

136. Percie du Sert N, Hurst V, Ahluwalia A, et al. *The ARRIVE guidelines 2.0: Updated guidelines for reporting animal research*. PLoS Biol. 2020;18(7):e3000410.http://dx.doi.org/10.1371/journal.pbio.3000410
137. Pyo R, Lee JK, Shipley JM, Curci JA, Mao D, Ziporin SJ, Ennis TL, Shapiro SD, Senior RM, Thompson RW. *Targeted gene disruption of matrix metalloproteinase-9 (gelatinase B) suppresses development of experimental abdominal aortic aneurysms*. J Clin Invest. 2000;105(11):1641-9.http://dx.doi.org/10.1172/JCI8931
138. Daugherty A, Manning MW, Cassis LA. *Angiotensin II promotes atherosclerotic lesions and aneurysms in apolipoprotein E-deficient mice*. J Clin Invest. 2000;105(11):1605-12.http://dx.doi.org/10.1172/JCI7818
139. Wischmann P, Kuhn V, Suvorava T, et al. *Anaemia is associated with severe RBC dysfunction and a reduced circulating NO pool: vascular and cardiac eNOS are crucial for the adaptation to anaemia*. Basic Res Cardiol. 2020;115(4):43.http://dx.doi.org/10.1007/s00395-020-0799-x
140. Hu D, Yin C, Mohanta SK, Weber C, Habenicht AJ. *Preparation of Single Cell Suspensions from Mouse Aorta*. Bio Protoc. 2016;6(11).http://dx.doi.org/10.21769/bioprotoc.1832
141. Hao Y, Hao S, Andersen-Nissen E, et al. *Integrated analysis of multimodal single-cell data*. Cell. 2021;184(13):3573-87 e29.http://dx.doi.org/10.1016/j.cell.2021.04.048
142. McGinnis CS, Murrow LM, Gartner ZJ. *DoubletFinder: Doublet Detection in Single-Cell RNA Sequencing Data Using Artificial Nearest Neighbors*. Cell Syst. 2019;8(4):329-37 e4.http://dx.doi.org/10.1016/j.cels.2019.03.003
143. Wu T, Hu E, Xu S, et al. *clusterProfiler 4.0: A universal enrichment tool for interpreting omics data*. Innovation (Camb). 2021;2(3):100141.http://dx.doi.org/10.1016/j.xinn.2021.100141
144. Yu G, Wang LG, Han Y, He QY. *clusterProfiler: an R package for comparing biological themes among gene clusters*. OMICS. 2012;16(5):284-7.http://dx.doi.org/10.1089/omi.2011.0118
145. Carlson M. org.Mm.eg.db: Genome wide annotation for Mouse. R package version 3.8.2. 2019 [Available from: https://bioconductor.org/packages/release/data/annotation/html/org.Mm.eg.db.html.
146. Schubert M, Klinger B, Klunemann M, Sieber A, Uhlitz F, Sauer S, Garnett MJ, Bluthgen N, Saez-Rodriguez J. *Perturbation-response genes reveal signaling footprints in cancer gene expression*. Nat Commun. 2018;9(1):20.http://dx.doi.org/10.1038/s41467-017-02391-6
147. Howe DG, Blake JA, Bradford YM, et al. *Model organism data evolving in support of translational medicine*. Lab Anim (NY). 2018;47(10):277-89.http://dx.doi.org/10.1038/s41684-018-0150-4
148. Jin S, Guerrero-Juarez CF, Zhang L, Chang I, Ramos R, Kuan CH, Myung P, Plikus MV, Nie Q. *Inference and analysis of cell-cell communication using CellChat*. Nat Commun. 2021;12(1):1088.http://dx.doi.org/10.1038/s41467-021-21246-9
149. Jin S, Plikus MV, Nie Q. *CellChat for systematic analysis of cell-cell communication from single-cell and spatially resolved transcriptomics*. bioRxiv. 2023:2023.11.05.565674. http://dx.doi.org/10.1101/2023.11.05.565674
150. Team I. immunarch: An R Package for Painless Bioinformatics Analysis of T-Cell and B-Cell Immune Repertoires. 2019.
151. Goncharov M, Bagaev D, Shcherbinin D, et al. *VDJdb in the pandemic era: a compendium of T cell receptors specific for SARS-CoV-2*. Nat Methods. 2022;19(9):1017-9.http://dx.doi.org/10.1038/s41592-022-01578-0
152. Tickotsky N, Sagiv T, Prilusky J, Shifrut E, Friedman N. *McPAS-TCR: a manually curated catalogue of pathology-associated T cell receptor sequences*. Bioinformatics. 2017;33(18):2924-9.http://dx.doi.org/10.1093/bioinformatics/btx286
153. Xie X, Shi Q, Wu P, et al. *Single-cell transcriptome profiling reveals neutrophil heterogeneity in homeostasis and infection*. Nat Immunol. 2020;21(9):1119-33.http://dx.doi.org/10.1038/s41590-020-0736-z
154. Deerhake ME, Reyes EY, Xu-Vanpala S, Shinohara ML. *Single-Cell Transcriptional Heterogeneity of Neutrophils During Acute Pulmonary Cryptococcus neoformans Infection*. Front Immunol. 2021;12:670574.http://dx.doi.org/10.3389/fimmu.2021.670574
155. Schoggins JW. *Interferon-Stimulated Genes: What Do They All Do?* Annu Rev Virol. 2019;6(1):567-84.http://dx.doi.org/10.1146/annurev-virology-092818-015756
156. Nederlof R, Reidel S, Spychala A, Godecke S, Heinen A, Lautwein T, Petzsch P, Kohrer K, Godecke A. *Insulin-Like Growth Factor 1 Attenuates the Pro-Inflammatory Phenotype of Neutrophils in Myocardial Infarction*. Front Immunol. 2022;13:908023.http://dx.doi.org/10.3389/fimmu.2022.908023

157. Wu Y, Ma J, Yang X, et al. *Neutrophil profiling illuminates anti-tumor antigen-presenting potency*. Cell. 2024;187(6):1422-39 e24.http://dx.doi.org/10.1016/j.cell.2024.02.005
158. Liu Y, Cook C, Sedgewick AJ, et al. *Single-Cell Profiling Reveals Divergent, Globally Patterned Immune Responses in Murine Skin Inflammation*. iScience. 2020;23(10):101582.http://dx.doi.org/10.1016/j.isci.2020.101582
159. King KR, Aguirre AD, Ye YX, et al. *IRF3 and type I interferons fuel a fatal response to myocardial infarction*. Nat Med. 2017;23(12):1481-7.http://dx.doi.org/10.1038/nm.4428
160. Lin JD, Nishi H, Poles J, et al. *Single-cell analysis of fate-mapped macrophages reveals heterogeneity, including stem-like properties, during atherosclerosis progression and regression*. JCI Insight. 2019;4(4).http://dx.doi.org/10.1172/jci.insight.124574
161. Le S, Wu J, Liu H, et al. *Single-cell RNA sequencing identifies IFNICs as a cellular target for mitigating the progression of abdominal aortic aneurysm and rupture risk*. Cardiovasc Res. 2024.http://dx.doi.org/10.1093/cvr/cvae117
162. Scheuerer B, Ernst M, Durrbaum-Landmann I, Fleischer J, Grage-Griebenow E, Brandt E, Flad HD, Petersen F. *The CXC-chemokine platelet factor 4 promotes monocyte survival and induces monocyte differentiation into macrophages*. Blood. 2000;95(4):1158-66
163. Yeo L, Adlard N, Biehl M, Juarez M, Smallie T, Snow M, Buckley CD, Raza K, Filer A, Scheel-Toellner D. *Expression of chemokines CXCL4 and CXCL7 by synovial macrophages defines an early stage of rheumatoid arthritis*. Ann Rheum Dis. 2016;75(4):763-71.http://dx.doi.org/10.1136/annrheumdis-2014-206921
164. Ni SH, Xu JD, Sun SN, et al. *Single-cell transcriptomic analyses of cardiac immune cells reveal that Rel-driven CD72-positive macrophages induce cardiomyocyte injury*. Cardiovasc Res. 2022;118(5):1303-20.http://dx.doi.org/10.1093/cvr/cvab193
165. Lu HY, Shih CM, Huang CY, Wu ATH, Cheng TM, Mi FL, Shih CC. *Galectin-3 Modulates Macrophage Activation and Contributes Smooth Muscle Cells Apoptosis in Abdominal Aortic Aneurysm Pathogenesis*. Int J Mol Sci. 2020;21(21).http://dx.doi.org/10.3390/ijms21218257
166. Di Gregoli K, Somerville M, Bianco R, Thomas AC, Frankow A, Newby AC, George SJ, Jackson CL, Johnson JL. *Galectin-3 Identifies a Subset of Macrophages With a Potential Beneficial Role in Atherosclerosis*. Arterioscler Thromb Vasc Biol. 2020;40(6):1491-509. http://dx.doi.org/10.1161/ATVBAHA.120.314252
167. Kang Q, Li L, Pang Y, Zhu W, Meng L. *An update on Ym1 and its immunoregulatory role in diseases*. Front Immunol. 2022;13:891220.http://dx.doi.org/10.3389/fimmu.2022.891220
168. Bjorklund AK, Forkel M, Picelli S, Konya V, Theorell J, Friberg D, Sandberg R, Mjosberg J. *The heterogeneity of human CD127(+) innate lymphoid cells revealed by single-cell RNA sequencing*. Nat Immunol. 2016;17(4):451-60.http://dx.doi.org/10.1038/ni.3368
169. Mazzurana L, Czarnewski P, Jonsson V, et al. *Tissue-specific transcriptional imprinting and heterogeneity in human innate lymphoid cells revealed by full-length single-cell RNA-sequencing*. Cell Res. 2021;31(5):554-68.http://dx.doi.org/10.1038/s41422-020-00445-x
170. Ferreira ACF, Szeto ACH, Heycock MWD, et al. *RORalpha is a critical checkpoint for T cell and ILC2 commitment in the embryonic thymus*. Nat Immunol. 2021;22(2):166-78.http://dx.doi.org/10.1038/s41590-020-00833-w
171. Yao HC, Zhu Y, Lu HY, Ju HM, Xu SQ, Qiao Y, Wei SJ. *Type 2 innate lymphoid cell-derived amphiregulin regulates type II alveolar epithelial cell transdifferentiation in a mouse model of bronchopulmonary dysplasia*. Int Immunopharmacol. 2023;122:110672.http://dx.doi.org/10.1016/j.intimp.2023.110672
172. Zhai L, Hu W, Li J, et al. *Unravelling CD4(+) T cell diversity and tissue adaptation of Tregs in abdominal aortic aneurysms through single-cell sequencing*. Immunology. 2024;172(4):600-13.http://dx.doi.org/10.1111/imm.13796
173. Ma DY, Clark EA. *The role of CD40 and CD154/CD40L in dendritic cells*. Semin Immunol. 2009;21(5):265-72.http://dx.doi.org/10.1016/j.smim.2009.05.010
174. Greenbaum D, Colangelo C, Williams K, Gerstein M. *Comparing protein abundance and mRNA expression levels on a genomic scale*. Genome Biol. 2003;4(9):117.http://dx.doi.org/10.1186/gb-2003-4-9-117
175. Maier T, Guell M, Serrano L. *Correlation of mRNA and protein in complex biological samples*. FEBS Lett. 2009;583(24):3966-73.http://dx.doi.org/10.1016/j.febslet.2009.10.036

176. Davis FM, Tsoi LC, Melvin WJ, et al. *Inhibition of macrophage histone demethylase JMJD3 protects against abdominal aortic aneurysms*. J Exp Med. 2021;218(6).http://dx.doi.org/10.1084/jem.20201839
177. Michel NA, Zirlik A, Wolf D. *CD40L and Its Receptors in Atherothrombosis-An Update*. Front Cardiovasc Med. 2017;4:40.http://dx.doi.org/10.3389/fcvm.2017.00040
178. Buccitelli C, Selbach M. *mRNAs, proteins and the emerging principles of gene expression control*. Nat Rev Genet. 2020;21(10):630-44.http://dx.doi.org/10.1038/s41576-020-0258-4
179. Ji L, Li T, Chen H, Yang Y, Lu E, Liu J, Qiao W, Chen H. *The crucial regulatory role of type I interferon in inflammatory diseases*. Cell Biosci. 2023;13(1):230.http://dx.doi.org/10.1186/s13578-023-01188-z
180. Currier JR, Robinson MA. *Spectratype/immunoscope analysis of the expressed TCR repertoire*. Curr Protoc Immunol. 2001;Chapter 10:10 28 1-10 28 4.http://dx.doi.org/10.1002/0471142735.im1028s38
181. Greiff V, Bhat P, Cook SC, Menzel U, Kang W, Reddy ST. *A bioinformatic framework for immune repertoire diversity profiling enables detection of immunological status*. Genome Med. 2015;7(1):49.http://dx.doi.org/10.1186/s13073-015-0169-8
182. Li H, Ye C, Ji G, Han J. *Determinants of public T cell responses*. Cell Res. 2012;22(1):33-42.http://dx.doi.org/10.1038/cr.2012.1
183. Simark-Mattsson C, Bergenholtz G, Jontell M, Tarkowski A, Dahlgren UI. *T cell receptor V-gene usage in oral lichen planus; increased frequency of T cell receptors expressing V alpha 2 and V beta 3*. Clin Exp Immunol. 1994;98(3):503-7.http://dx.doi.org/10.1111/j.1365-2249.1994.tb05519.x
184. Glusman G, Rowen L, Lee I, Boysen C, Roach JC, Smit AF, Wang K, Koop BF, Hood L. *Comparative genomics of the human and mouse T cell receptor loci*. Immunity. 2001;15(3):337-49.http://dx.doi.org/10.1016/s1074-7613(01)00200-x
185. Amoriello R, Chernigovskaya M, Greiff V, et al. *TCR repertoire diversity in Multiple Sclerosis: High-dimensional bioinformatics analysis of sequences from brain, cerebrospinal fluid and peripheral blood*. EBioMedicine. 2021;68:103429.http://dx.doi.org/10.1016/j.ebiom.2021.103429
186. Zhao G, Lu H, Chang Z, Zhao Y, Zhu T, Chang L, Guo Y, Garcia-Barrio MT, Chen YE, Zhang J. *Single-cell RNA sequencing reveals the cellular heterogeneity of aneurysmal infrarenal abdominal aorta*. Cardiovasc Res. 2021;117(5):1402-16.http://dx.doi.org/10.1093/cvr/cvaa214
187. Yuan Z, Shu L, Fu J, et al. *Single-Cell RNA Sequencing Deconstructs the Distribution of Immune Cells Within Abdominal Aortic Aneurysms in Mice*. Arterioscler Thromb Vasc Biol. 2024;44(9):1986-2003.http://dx.doi.org/10.1161/ATVBAHA.124.321129
188. Yang H, Zhou T, Stranz A, DeRoo E, Liu B. *Single-Cell RNA Sequencing Reveals Heterogeneity of Vascular Cells in Early Stage Murine Abdominal Aortic Aneurysm-Brief Report*. Arterioscler Thromb Vasc Biol. 2021;41(3):1158-66.http://dx.doi.org/10.1161/ATVBAHA.120.315607
189. Qian W, Hadi T, Silvestro M, et al. *Microskeletal stiffness promotes aortic aneurysm by sustaining pathological vascular smooth muscle cell mechanosensation via Piezo1*. Nat Commun. 2022;13(1):512.http://dx.doi.org/10.1038/s41467-021-27874-5
190. Hadi T, Boytard L, Silvestro M, et al. *Macrophage-derived netrin-1 promotes abdominal aortic aneurysm formation by activating MMP3 in vascular smooth muscle cells*. Nat Commun. 2018;9(1):5022.http://dx.doi.org/10.1038/s41467-018-07495-1
191. Boytard L, Hadi T, Silvestro M, et al. *Lung-derived HMGB1 is detrimental for vascular remodeling of metabolically imbalanced arterial macrophages*. Nat Commun. 2020;11(1):4311.http://dx.doi.org/10.1038/s41467-020-18088-2
192. Busch A, Bleichert S, Ibrahim N, Wortmann M, Eckstein HH, Brostjan C, Wagenhauser MU, Goergen CJ, Maegdefessel L. *Translating mouse models of abdominal aortic aneurysm to the translational needs of vascular surgery*. JVS Vasc Sci. 2021;2:219-34.http://dx.doi.org/10.1016/j.jvssci.2021.01.002
193. Grieshaber-Bouyer R, Radtke FA, Cunin P, et al. *The neutrotime transcriptional signature defines a single continuum of neutrophils across biological compartments*. Nat Commun. 2021;12(1):2856.http://dx.doi.org/10.1038/s41467-021-22973-9
194. Le S, Wu J, Liu H, et al. *Single-cell RNA sequencing identifies interferon-inducible monocytes/macrophages as a cellular target for mitigating the progression of abdominal aortic aneurysm and rupture risk*. Cardiovasc Res. 2024;120(11):1351-64.http://dx.doi.org/10.1093/cvr/cvae117
195. Robbins CS, Hilgendorf I, Weber GF, et al. *Local proliferation dominates lesional macrophage accumulation in atherosclerosis*. Nat Med. 2013;19(9):1166-72.http://dx.doi.org/10.1038/nm.3258

196. van den Brink SC, Sage F, Vertesy A, Spanjaard B, Peterson-Maduro J, Baron CS, Robin C, van Oudenaarden A. *Single-cell sequencing reveals dissociation-induced gene expression in tissue subpopulations*. Nat Methods. 2017;14(10):935-6.http://dx.doi.org/10.1038/nmeth.4437
197. Liebold I, Al Jawazneh A, Casar C, et al. *Apoptotic cell identity induces distinct functional responses to IL-4 in efferocytic macrophages*. Science. 2024;384(6691):eabo7027. http://dx.doi.org/10.1126/science.abo7027
198. Yodoi K, Yamashita T, Sasaki N, et al. *Foxp3+ regulatory T cells play a protective role in angiotensin II-induced aortic aneurysm formation in mice*. Hypertension. 2015;65(4):889-95.http://dx.doi.org/10.1161/HYPERTENSIONAHA.114.04934
199. Meng X, Yang J, Zhang K, An G, Kong J, Jiang F, Zhang Y, Zhang C. *Regulatory T cells prevent angiotensin II-induced abdominal aortic aneurysm in apolipoprotein E knockout mice*. Hypertension. 2014;64(4):875-82.http://dx.doi.org/10.1161/HYPERTENSIONAHA.114.03950
200. Tian Q, Stepaniants SB, Mao M, et al. *Integrated genomic and proteomic analyses of gene expression in Mammalian cells*. Mol Cell Proteomics. 2004;3(10):960-9.http://dx.doi.org/10.1074/mcp.M400055-MCP200
201. Xie Y, Chen H, Chellamuthu VR, Lajam ABM, Albani S, Low AHL, Petretto E, Behmoaras J. *Comparative Analysis of Single-Cell RNA Sequencing Methods with and without Sample Multiplexing*. Int J Mol Sci. 2024;25(7).http://dx.doi.org/10.3390/ijms25073828
202. Tucker TA, Schwiebert LM. *CD40 ligation decreases its protein half-life at the cell surface*. Eur J Immunol. 2008;38(3):864-9.http://dx.doi.org/10.1002/eji.200737828
203. Blair PJ, Riley JL, Harlan DM, et al. *CD40 ligand (CD154) triggers a short-term CD4(+) T cell activation response that results in secretion of immunomodulatory cytokines and apoptosis*. J Exp Med. 2000;191(4):651-60.http://dx.doi.org/10.1084/jem.191.4.651
204. van Os BW, Vos WG, Bosmans LA, van Tiel CM, Toom MD, Beckers L, Admiraal M, Hoeksema MA, de Winther MP, Lutgens E. *CD40L modulates CD4(+) T-cell activation through receptor for activated C kinase 1*. Eur J Immunol. 2023;53(12):e2350520.http://dx.doi.org/10.1002/eji.202350520
205. Magri G, Miyajima M, Bascones S, et al. *Innate lymphoid cells integrate stromal and immunological signals to enhance antibody production by splenic marginal zone B cells*. Nat Immunol. 2014;15(4):354-64.http://dx.doi.org/10.1038/ni.2830
206. Komlosi ZI, Kovacs N, van de Veen W, et al. *Human CD40 ligand-expressing type 3 innate lymphoid cells induce IL-10-producing immature transitional regulatory B cells*. J Allergy Clin Immunol. 2018;142(1):178-94 e11.http://dx.doi.org/10.1016/j.jaci.2017.07.046
207. Leveille C, Bouillon M, Guo W, et al. *CD40 ligand binds to alpha5beta1 integrin and triggers cell signaling*. J Biol Chem. 2007;282(8):5143-51.http://dx.doi.org/10.1074/jbc.M608342200
208. Loubaki L, Semlali A, Boisvert M, Jacques E, Plante S, Aoudjit F, Mourad W, Chakir J. *Crosstalk between T cells and bronchial fibroblasts obtained from asthmatic subjects involves CD40L/alpha 5 beta 1 interaction*. Mol Immunol. 2010;47(11-12):2112-8.http://dx.doi.org/10.1016/j.molimm.2010.03.011
209. Wolf D, Hohmann JD, Wiedemann A, et al. *Binding of CD40L to Mac-1's I-domain involves the EQLKKSKTL motif and mediates leukocyte recruitment and atherosclerosis--but does not affect immunity and thrombosis in mice*. Circ Res. 2011;109(11):1269-79.http://dx.doi.org/10.1161/CIRCRESAHA.111.247684
210. El Fakhry Y, Alturaihi H, Yacoub D, et al. *Functional interaction of CD154 protein with alpha5beta1 integrin is totally independent from its binding to alphaIIbbeta3 integrin and CD40 molecules*. J Biol Chem. 2012;287(22):18055-66.http://dx.doi.org/10.1074/jbc.M111.333989
211. Siebeler R, de Winther MPJ, Hoeksema MA. *The regulatory landscape of macrophage interferon signaling in inflammation*. J Allergy Clin Immunol. 2023;152(2):326-37.http://dx.doi.org/10.1016/j.jaci.2023.04.022
212. Yao X, Wu J, Lin M, Sun W, He X, Gowda C, Bolland S, Long CA, Wang R, Su XZ. *Increased CD40 Expression Enhances Early STING-Mediated Type I Interferon Response and Host Survival in a Rodent Malaria Model*. PLoS Pathog. 2016;12(10):e1005930.http://dx.doi.org/10.1371/journal.ppat.1005930
213. Goossens P, Gijbels MJ, Zernecke A, et al. *Myeloid type I interferon signaling promotes atherosclerosis by stimulating macrophage recruitment to lesions*. Cell Metab. 2010;12(2):142-53.http://dx.doi.org/10.1016/j.cmet.2010.06.008
214. Ninh VK, Calcagno DM, Yu JD, et al. *Spatially clustered type I interferon responses at injury borderzones*. Nature. 2024;633(8028):174-81.http://dx.doi.org/10.1038/s41586-024-07806-1

215. Chakraborty A, Li Y, Zhang C, et al. *Epigenetic Induction of Smooth Muscle Cell Phenotypic Alterations in Aortic Aneurysms and Dissections*. Circulation. 2023;148(12):959-77.http://dx.doi.org/10.1161/CIRCULATIONAHA.123.063332
216. Pan M, Li B. *T cell receptor convergence is an indicator of antigen-specific T cell response in cancer immunotherapies*. Elife. 2022;11.http://dx.doi.org/10.7554/eLife.81952
217. Paulsson G, Zhou X, Törnquist E, Hansson GK. *Oligoclonal T cell expansions in atherosclerotic lesions of apolipoprotein E-deficient mice*. Arterioscler Thromb Vasc Biol. 2000;20(1):10-7.http://dx.doi.org/10.1161/01.atv.20.1.10
218. Lin Z, Qian S, Gong Y, Ren J, Zhao L, Wang D, Wang X, Zhang Y, Wang Z, Zhang Q. *Deep sequencing of the T cell receptor beta repertoire reveals signature patterns and clonal drift in atherosclerotic plaques and patients*. Oncotarget. 2017;8(59):99312-22.http://dx.doi.org/10.18632/oncotarget.19892
219. Greiff V, Menzel U, Haessler U, Cook SC, Friedensohn S, Khan TA, Pogson M, Hellmann I, Reddy ST. *Quantitative assessment of the robustness of next-generation sequencing of antibody variable gene repertoires from immunized mice*. BMC Immunol. 2014;15:40.http://dx.doi.org/10.1186/s12865-014-0040-5
220. Golledge J, Krishna SM, Wang Y. *Mouse models for abdominal aortic aneurysm*. Br J Pharmacol. 2022;179(5):792-810.http://dx.doi.org/10.1111/bph.15260

8 Supplement

Supplementary table 6: List of antibodies used for CITE-seq (TotalSeq™-A Mouse Universal Cocktail, V1.0). In total 128 antibodies are listed, of which 119 are antibodies against cell surface antigens of immune cells and 9 isotype controls. The DNA_ID, the antibody description (name), the clone, the sequence and the ensemble ID are shown.

DNA_ID	Description	Clone	Sequence	Ensemble ID
A0001	anti-mouse CD4	RM4-5	AACAAGACCCTTGAG	ENSMUSG00000023274
A0002	anti-mouse CD8a	53-6.7	TACCCGTAATAGCGT	ENSMUSG00000053977
A0003	anti-mouse CD366 (Tim-3)	RMT3-23	ATTGGCACTCAGATG	ENSMUSG00000020399
A0004	anti-mouse CD279 (PD-1)	RMP1-30	GAAAGTCAAAGCACT	ENSMUSG00000026285
A0013	anti-mouse Ly-6C	HK1.4	AAGTCGTGAGGCATG	ENSMUSG00000022584
A0014	anti-mouse/human CD11b	M1/70	TGAAGGCTCATTTGT	ENSMUSG00000030786
A0015	anti-mouse Ly-6G	1A8	ACATTGACGCAACTA	ENSMUSG00000022582
A0070	anti-human/mouse CD49f	GoH3	TTCCGAGGATGATCT	ENSMUSG00000027111
A0073	anti-mouse/human CD44	IM7	TGGCTTCAGGTCCTA	ENSMUSG00000005087
A0074	anti-mouse CD54	YN1/1.7.4	ATAACCGACACAGTG	ENSMUSG00000037405
A0075	anti-mouse CD90.2	30-H12	CCGATCAGCCGTTTA	ENSMUSG00000032011
A0077	anti-mouse CD73	TY/11.8	ACACTTAACGTCTGG	ENSMUSG00000032420
A0078	anti-mouse CD49d	R1-2	CGCTTGGACGCTTAA	ENSMUSG00000027009
A0079	anti-mouse CD200 (OX2)	OX-90	TCAATTCCGGTAGTC	ENSMUSG00000022661
A0090	Mouse IgG1, κ isotype Ctrl	MOPC-21	GCCGGACGACATTAA	
A0091	Mouse IgG2a, κ isotype Ctrl	MOPC-173	CTCCTACCTAAACTG	
A0092	Mouse IgG2b, κ isotype Ctrl	MPC-11	ATATGTATCACGCGA	
A0093	anti-mouse CD19	6D5	ATCAGCCATGTCAGT	ENSMUSG00000030724
A0095	Rat IgG2b, κ Isotype Ctrl	RTK4530	GATTCTTGACGACCT	
A0096	anti-mouse CD45	30-F11	TGGCTATGGAGCAGA	ENSMUSG00000026395
A0097	anti-mouse CD25	PC61	ACCATGAGACACAGT	ENSMUSG00000026770
A0103	anti-mouse/human CD45R/B220	RA3-6B2	CCTACACCTCATAAT	ENSMUSG00000026395
A0104	anti-mouse CD102	3C4 (MIC2/4)	GATATTCAGTGCGAC	ENSMUSG00000001029
A0105	anti-mouse CD115 (CSF-1R)	AFS98	TTCCGTTGTTGTGAG	ENSMUSG00000024621
A0106	anti-mouse CD11c	N418	GTTATGGACGCTTGC	ENSMUSG00000030789
A0107	anti-mouse CD21/CD35 (CR2/CR1)	7 E9	GGATAATTTCGATCC	ENSMUSG00000026616
A0108	anti-mouse CD23	B3B4	TCTCTTGGAAGATGA	ENSMUSG00000005540
A0110	anti-mouse CD43	S11	TTGGAGGGTTGTGCT	ENSMUSG00000051457
A0111	anti-mouse CD5	53-7.3	CAGCTCAGTGTGTTG	ENSMUSG00000024669
A0112	anti-mouse CD62L	MEL-14	TGGGCCTAAGTCATC	ENSMUSG00000026581
A0113	anti-mouse CD93 (AA4.1, early B lineage)	AA4.1	GGTATTTCCTGTGGT	ENSMUSG00000027435
A0114	anti-mouse F4/80	BM8	TTAACTTCAGCCCGT	ENSMUSG00000004730
A0115	anti-mouse FcεRIα	MAR-1	AGTCACCTCGAAGCT	ENSMUSG00000005339
A0117	anti-mouse I-A/I-E	M5/114.15.2	GGTCACCAGTATGAT	ENSMUSG00000073421

DNA_ID	Description	Clone	Sequence	Ensemble ID
A0118	anti-mouse NK-1.1	PK136	GTAACATTACTCGTC	ENSMUSG00000030325
A0119	anti-mouse Siglec H	551	CCGCACCTACATTAG	ENSMUSG00000051504
A0120	anti-mouse TCR β chain	H57-597	TCCTATGGGACTCAG	
A0121	anti-mouse TCR γ/δ	GL3	AACCCAAATAGCTGA	
A0122	anti-mouse TER-119/Erythroid Cells	TER-119	GCGCGTTTGTGCTAT	
A0130	anti-mouse Ly-6A/E (Sca-1)	D7	TTCCTTTCCTACGCA	ENSMUSG00000075602
A0157	anti-mouse CD45.2	104	CACCGTCATTCAACC	ENSMUSG00000026395
A0182	anti-mouse CD3	17A2	GTATGTCCGCTCGAT	ENSMUSG00000002033
A0190	anti-mouse CD274 (B7-H1, PD-L1)	MIH6	TCGATTCCACCAACT	ENSMUSG00000016496
A0191	anti-mouse/rat/human CD27	LG.3A10	CAAGGTATGTCACTG	ENSMUSG00000030336
A0192	anti-mouse CD20	SA275A11	TCCACTCCCTGTATA	ENSMUSG00000024673
A0193	anti-mouse CD357 (GITR)	DTA-1	GGCACTCTGTAACAT	ENSMUSG00000041954
A0194	anti-mouse CD137	17B5	TCCCTGTATAGATGA	ENSMUSG00000028965
A0195	anti-mouse CD134 (OX-40)	OX-86	CTCACCTACCTATGG	ENSMUSG00000029075
A0197	anti-mouse CD69	H1.2F3	TTGTATTCCGCCATT	ENSMUSG00000030156
A0198	anti-mouse CD127 (IL-7Rα)	A7R34	GTGTGAGGCACTCTT	ENSMUSG00000003882
A0200	anti-mouse CD86	GL-1	CTGGATTTGTGTATC	ENSMUSG00000022901
A0201	anti-mouse CD103	2 E7	TTCATTAGCCCGCTG	ENSMUSG00000005947
A0202	anti-mouse CD64 (FcγRI)	X54-5/7.1	AGCAATTAACGGGAG	ENSMUSG00000015947
A0203	anti-mouse CD150 (SLAM)	TC15-12F12.2	CAACGCCTAGAAACC	ENSMUSG00000015316
A0212	anti-mouse CD24	M1/69	TATATCTTTGCCGCA	ENSMUSG00000047139
A0214	anti-human/mouse integrin β7	FIB504	TCCTTGGATGTACCG	ENSMUSG00000001281
A0226	anti-mouse CD106	429 (MVCAM.A)	CGTTCCTACCTACCT	ENSMUSG00000027962
A0230	anti-mouse CD8b (Ly-3)	YTS156.7.7	TTCCCTCTATGGAGC	ENSMUSG00000053044
A0236	Rat IgG1, κ isotype Ctrl	RTK2071	ATCAGATGCCCTCAT	
A0237	Rat IgG1, λ Isotype Ctrl	G0114F7	GGGAGCGATTCAACT	
A0238	Rat IgG2a, κ Isotype Ctrl	RTK2758	AAGTCAGGTTCGTTT	
A0240	Rat IgG2c, κ Isotype Ctrl	RTK4174	TCCAGGCTAGTCATT	
A0241	Armenian Hamster IgG Isotype Ctrl	HTK888	CCTGTCATTAAGACT	
A0250	anti-mouse/human KLRG1 (MAFA)	2F1/KLRG1	GTAGTAGGCTAGACC	ENSMUSG00000030114
A0378	anti-mouse CD223 (LAG-3)	C9B7W	ATTCCGTCCCTAAGG	ENSMUSG00000030124
A0417	anti-mouse CD163	S15049I	GAGCAAGATTAAGAC	ENSMUSG00000008845
A0421	anti-mouse CD49b	HMα2	CGCGTTAGTAGAGTC	ENSMUSG00000015533
A0422	anti-mouse CD172a (SIRPα)	P84	GATTCCCTTGTAGCA	ENSMUSG00000037902
A0429	anti-mouse CD48	HM48-1	AGAACCGCCGTAGTT	ENSMUSG00000015355
A0431	anti-mouse CD170 (Siglec-F)	S17007L	TCAATCTCCGTCGCT	ENSMUSG00000039013
A0440	anti-mouse CD169/Siglec-1	3D6.112	ATTGACGACAGTCAT	ENSMUSG00000027322
A0441	anti-mouse CD71	RI7217	ACCGACCAGTAGACA	ENSMUSG00000022797

DNA_ID	Description	Clone	Sequence	Ensemble ID
A0443	anti-mouse CD41	MWReg30	ACTTGGATGGACACT	ENSMUSG00000034664
A0450	anti-mouse IgM	RMM-1	AGCTACGCATTCAAT	ENSMUSG00000076617
A0551	anti-mouse CD301a	LOM-8.7	TGTATTTACTCACCG	ENSMUSG00000000318
A0552	anti-mouse CD304	3 E12	CCAGCTCATTCAACG	ENSMUSG00000025810
A0555	anti-mouse CD36	HM36	TTTGCCGCTACGACA	ENSMUSG00000002944
A0557	anti-mouse CD38	90	CGTATCCGTCTCCTA	ENSMUSG00000029084
A0558	anti-mouse CD55 (DAF)	RIKO-3	ATTGTTGTCAGACCA	ENSMUSG00000026399
A0559	anti-mouse CD63	NVG-2	ATCCGACACGTATTA	ENSMUSG00000025351
A0560	anti-mouse CD68	FA-11	CTTTCTTTCACGGGA	ENSMUSG00000018774
A0561	anti-mouse CD79b (Igβ)	HM79-12	TAACTCAGTGCGAGT	ENSMUSG00000040592
A0562	anti-mouse CD83	Michel-19	TCTCAGGCTTCCTAG	ENSMUSG00000015396
A0563	anti-mouse CX3CR1	SA011F11	CACTCTCAGTCCTAT	ENSMUSG00000052336
A0566	anti-mouse CD301b	URA-1	CTTGCCTTGCGATTT	ENSMUSG00000040950
A0567	anti-mouse Tim-4	RMT4-54	TGCTGGAGGGTATTC	ENSMUSG00000055546
A0568	anti-mouse/rat XCR1	ZET	TCCATTACCCACGTT	ENSMUSG00000060509
A0570	anti-mouse/rat CD29	HMβ1-1	ACGCATTCCTTGTGT	ENSMUSG00000025809
A0571	anti-mouse IgD	11-26c.2a	TCATATCCGTTGTCC	ENSMUSG00000104213
A0595	anti-mouse CD11a	M17/4	AGAGTCTCCCTTTAG	ENSMUSG00000030830
A0807	anti-mouse CD200R (OX2R)	OX-110	ATTCTTTCCCTCTGT	ENSMUSG00000022667
A0809	anti-mouse CD200R3	Ba13	ATCAACTTGGAGCAG	ENSMUSG00000036172
A0810	anti-mouse CD138 (Syndecan-1)	281-2	GCGTTTGTATGTACT	ENSMUSG00000020592
A0811	anti-mouse CD317 (BST2, PDCA-1)	927	TGTGGTAGCCCTTGT	ENSMUSG00000046718
A0813	anti-mouse CD9	MZ3	TAGCAGTCACTCCTA	ENSMUSG00000030342
A0825	anti-mouse CD371 (CLEC12A)	5D3/CLEC12A	GCGAGAAATCTGCAT	ENSMUSG00000053063
A0827	anti-mouse CD22	OX-97	AGGTCCTCTCTGGAT	ENSMUSG00000030577
A0837	anti-mouse IL-33Rα (IL1RL1, ST2)	DIH9	GCGATGGAGCATGTT	ENSMUSG00000026069
A0839	anti-mouse Ly49H	3D10	CCAGTAGGCTTATTA	ENSMUSG00000089727
A0841	anti-mouse Ly49D	4 E5	TATATCCCTCAACGC	ENSMUSG00000079852
A0842	anti-mouse Ly-49A	YE1/48.10.6	AATTCCGTCAGATGA	ENSMUSG00000079853
A0846	anti-mouse CD185 (CXCR5)	L138D7	ACGTAGTCACCTAGT	ENSMUSG00000047880
A0850	anti-mouse CD49a	HMα1	CCATTCATTTGTGGC	ENSMUSG00000042284
A0851	anti-mouse CD1d (CD1.1, Ly-38)	1B1	CAACTTGGCCGAATC	ENSMUSG00000028076
A0852	anti-mouse CD226 (DNAM-1)	10 E5	ACGCAGTATTTCCGA	ENSMUSG00000034028
A0854	anti-mouse CD199 (CCR9)	CW-1.2	CCCTCTGGTATGGTT	ENSMUSG00000029530
A0877	anti-mouse JAML	4 E10	GTTATGGTTCGTGTT	ENSMUSG00000048534
A0881	anti-mouse CD272 (BTLA)	6A6	TGACCCTATTGAGAA	ENSMUSG00000052013
A0882	anti-mouse PIR-A/B	6C1	TGTAGAGTCAGACCT	ENSMUSG00000081665
A0883	anti-mouse CD26 (DPP-4)	H194-112	ATGGCCTGTCATAAT	ENSMUSG00000035000
A0885	anti-mouse CD270 (HVEM)	HMHV-1B18	GATCCGTGTTGCCTA	ENSMUSG00000042333

DNA_ID	Description	Clone	Sequence	Ensemble ID
A0892	anti-mouse CD2	RM2-5	TTGCCGTGTGTTTAA	ENSMUSG00000027863
A0893	anti-mouse CD120b (TNF R Type II/p75)	TR75-89	GAAGCTGTATCCGAA	ENSMUSG00000028599
A0903	anti-mouse CD40	3/23	ATTTGTATGCTGGAG	ENSMUSG00000017652
A0904	anti-mouse CD31	390	GCTGTAGTATCATGT	ENSMUSG00000020717
A0905	anti-mouse CD107a (LAMP-1)	1D4B	AAATCTGTGCCGTAC	ENSMUSG00000031447
A0910	anti-mouse/rat CD61	2C9.G2 (HMβ3-1)	TTCTTTACCCGCCTG	ENSMUSG00000020689
A0915	anti-mouse VISTA (PD-1H)	MIH63	ACATTTCCCTTGCCT	ENSMUSG00000020101
A0926	anti-mouse CD186 (CXCR6)	SA051D1	TGTCAGGTTGTATTC	ENSMUSG00000048521
A0927	anti-mouse CD159a (NKG2AB6)	16A11	GTGTTTGTGTTCCTG	ENSMUSG00000030167
A0930	anti-mouse Ly108	330-AJ	CGATTCTTTGCGAGT	ENSMUSG00000015314
A1006	anti-mouse CD160	7H1	GCGTATGTCAGTACC	ENSMUSG00000038304
A1007	anti-mouse CD85k (gp49 Receptor)	H1.1	ATGTCAACTCTGGGA	ENSMUSG00000112148
A1008	anti-mouse CD51	RMV-7	GGAGTCAGGGTATTA	ENSMUSG00000027087
A1009	anti-mouse CD94	18d3	CACAGTTGTCCGTGT	ENSMUSG00000030165
A1010	anti-mouse CD205 (DEC-205)	NLDC-145	CATATTGGCCGTAGT	ENSMUSG00000026980
A1011	anti-mouse CD155 (PVR)	TX56	TAGCTTGGGATTAAG	ENSMUSG00000040511
A1064	anti-mouse/rat CD81	Eat-2	TTGTCACCAACTTCC	ENSMUSG00000037706

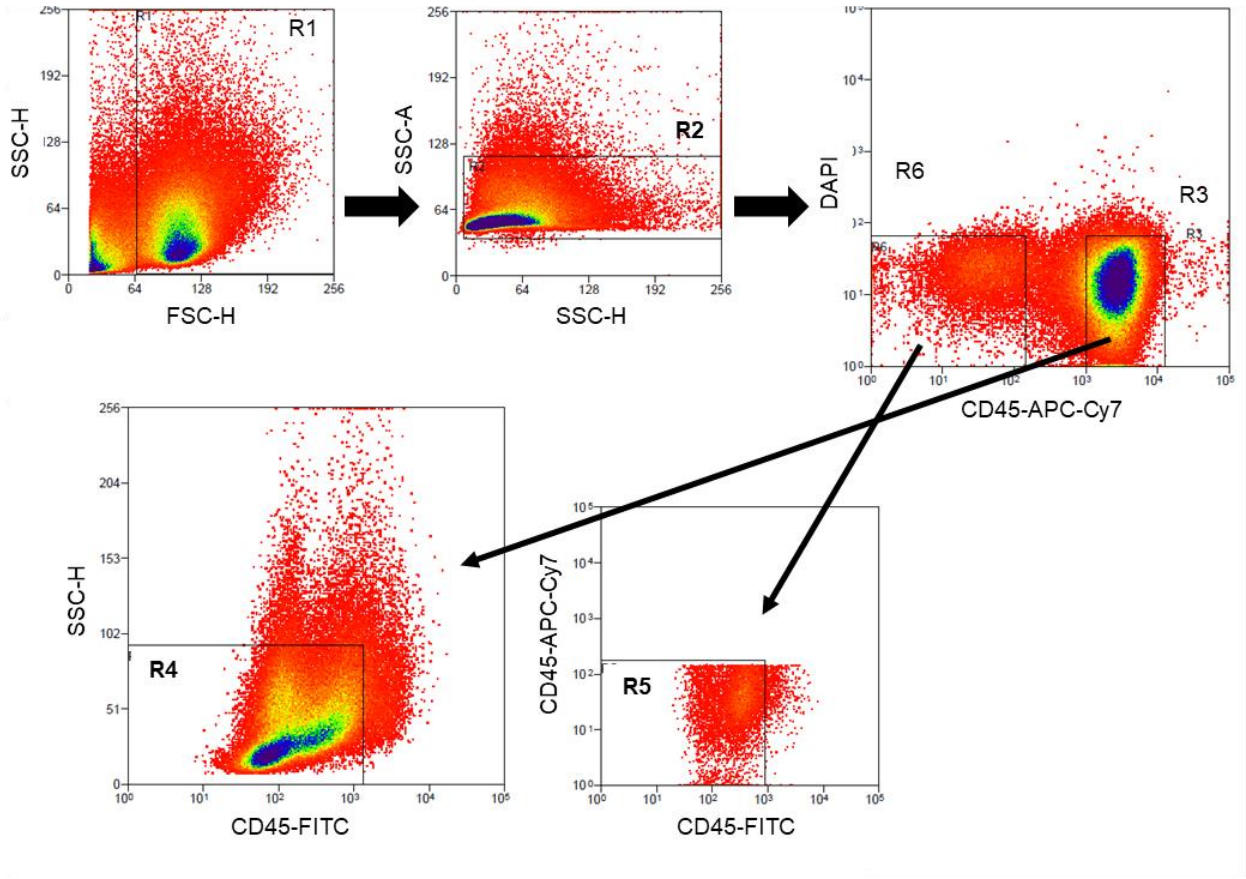

Supplementary Figure 1: Gating strategy for fluorescence activated cell sorting of single-cell suspension from infrarenal aortas. R1 = cells, R2 = single cells, R3 = all viable leukocytes, R4 = only viable leukocytes in the aortic tissue (circulating leukocytes are $FITC^+$), R5 = $CD45^-$ cells (for both CD45 antibodies), R6 = CD45 $APC\text{-}Cy7^-$ cells.

Supplementary table 2: The calculated ratio of viable CD45⁺ cells of single cells obtained from cell sorting for all aortae that were subjected to scRNA-seq. The table contains the time point, the number of single cells, the number of viable CD45⁺ cells and the calculated ratio of viable CD45⁺ cells of single cells for each mouse.

Mouse	Time point	Number of single cells (R2)	Number of viable CD45⁺ (R4)	Ratio R4/R2
#1	sham d28	6029	738	0.12
#2	sham d28	7205	2228	0.31
#3	d28	29285	12810	0.44
#4	d28	17960	4499	0.25
#5	d14	86524	60515	0.70
#6	d14	145203	106105	0.73
#7	d7	123142	89958	0.73
#8	d7	144286	109749	0.76
#9	d3	107520	82293	0.77
#10	d3	163035	125994	0.77
#11	sham d3	19265	10818	0.56
#12	sham d3	48294	31645	0.66
#13	sham d28	96	2	0.02
#14	non-perfused	4142	140	0.03
#15	d28	6460	2174	0.34
#16	d28	6792	2265	0.33
#17	d7	132522	75637	0.57
#18	d7	98928	54137	0.55
#19	d7	125281	71384	0.57
#20	d3	10423	5291	0.51
#21	d3	2681	1342	0.50
#22	d3	48041	22383	0.47
#23	sham d3	1893	79.6	0.04
#24	non-perfused	5286	149	0.03

Supplementary table 3-6 can be found on Sciebo under the following link:

https://uni-duesseldorf.sciebo.de/s/fFZ0ngujwdhGsVl Password: PhD-Thesis_Elster

Supplementary table 3: marker genes for neutrophils (online)

Supplementary table 4: marker genes for DC and macrophages (online)

Supplementary table 5: marker genes for lymphocytes (online)

Supplementary table 6: marker proteins for macrophages CITE-seq (online)

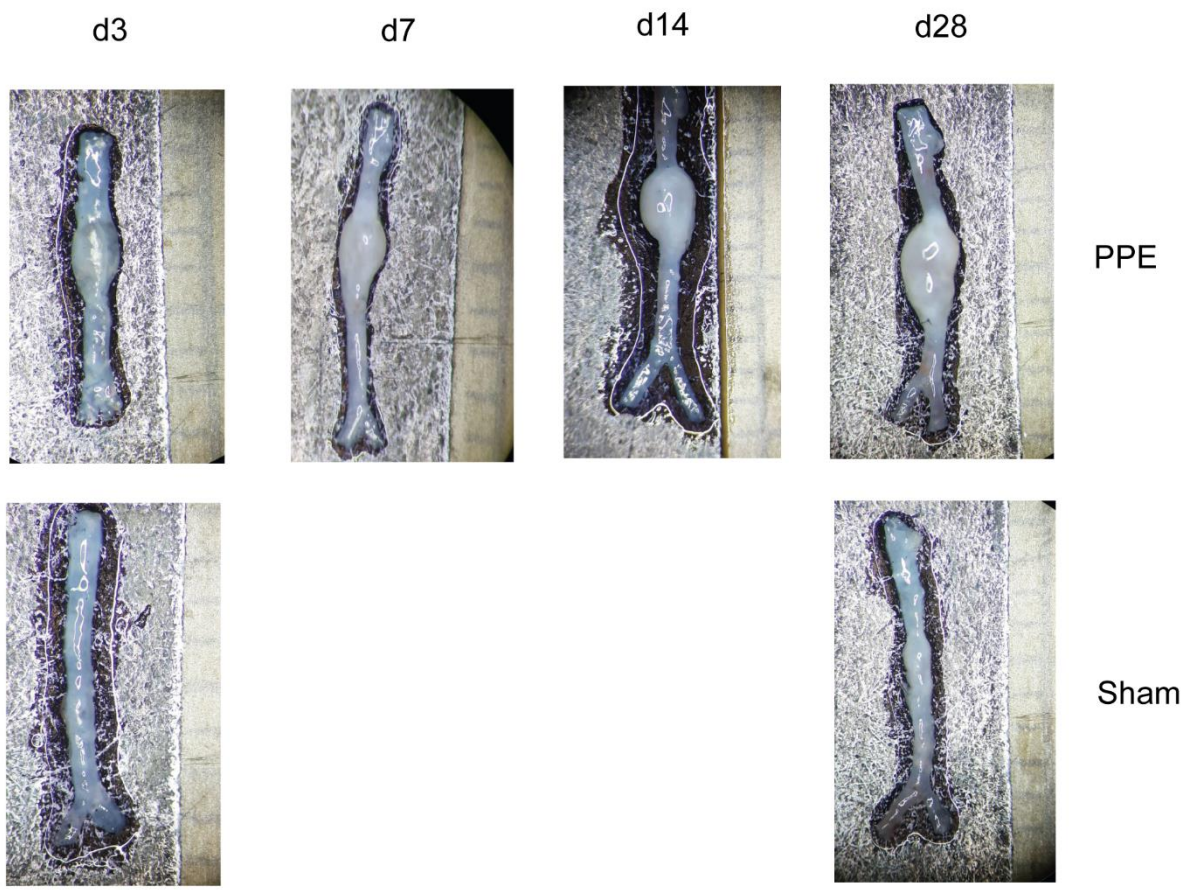

Supplementary figure 2: Representative macroscopic pictures of AAA progression over time. Representative macroscopic pictures of infrarenal aortae 3, 7, 14 and 28 post PPE surgery and 3 and 28 post sham surgery. Scale ruler: one unit represents 1 mm.

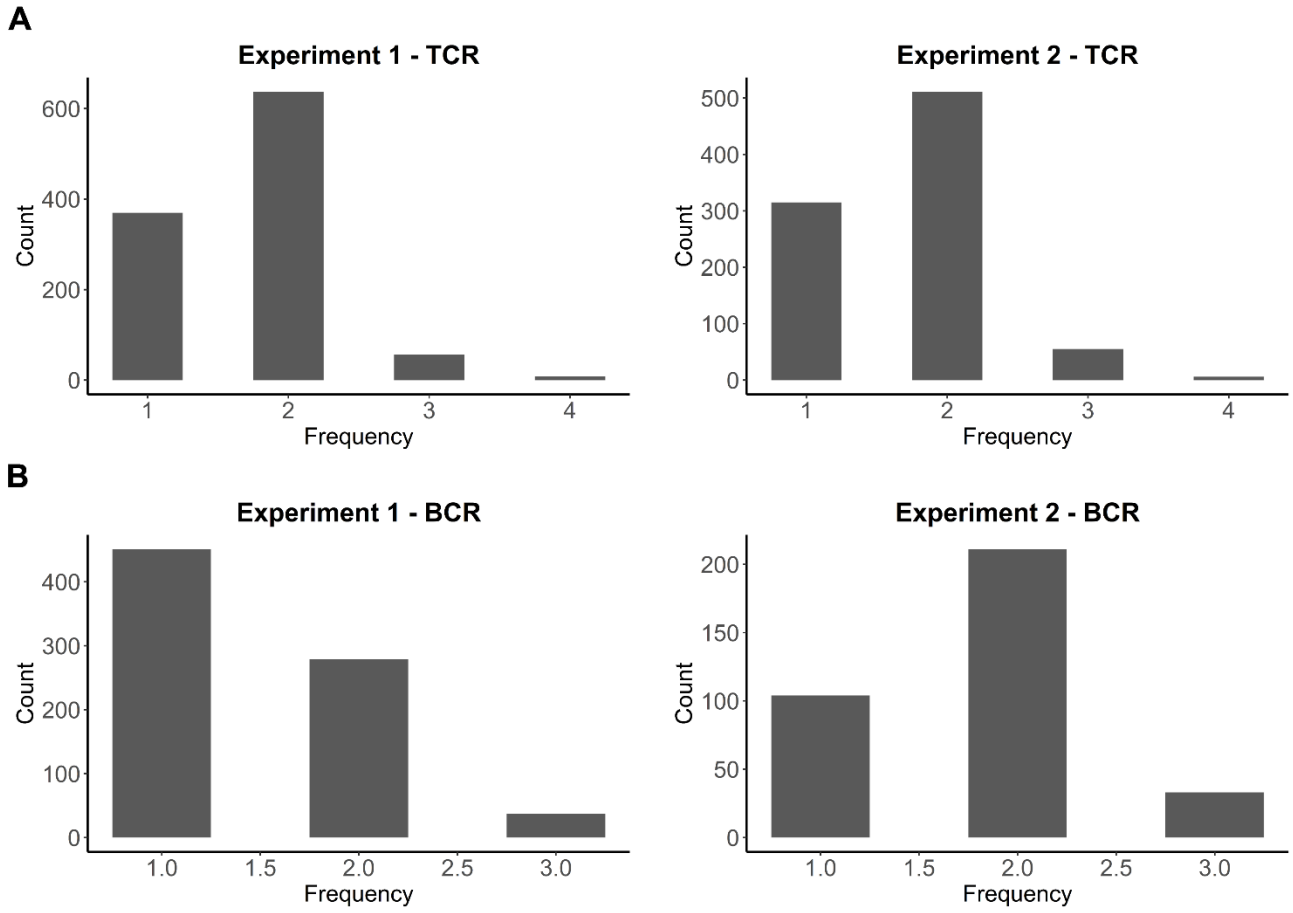

Supplementary figure 3: Preprocessing and quality control of scRNA TCR and BCR sequencing data. A Number of chains per TCR in experiment. Only TCRs with two chains were used for analysis. **B:** Number of chains per BCR in experiment. Only BCRs with two chains were used for analysis.

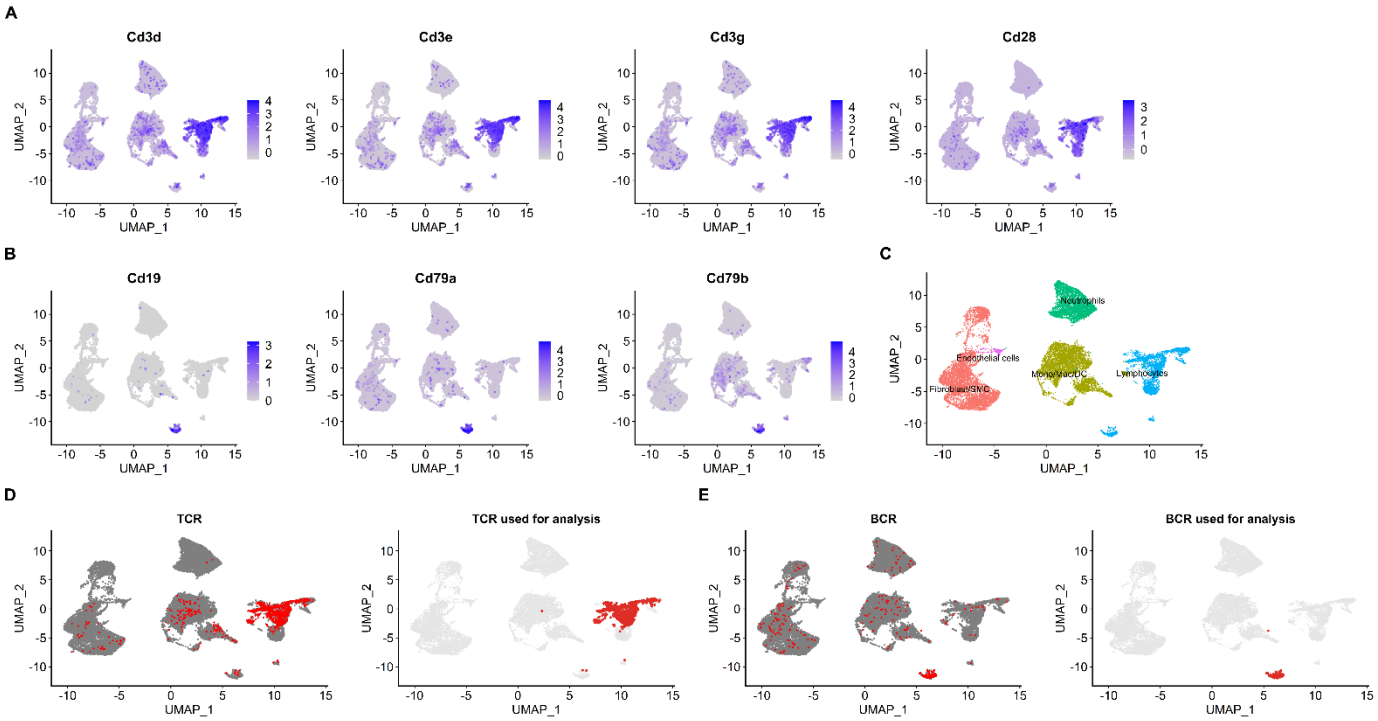

Supplementary figure 4: Identification of B and T cells expressing BCRs and TCRs

A: Featureplots indicating the expression of the T cell markers *Cd3d*, *Cd3e*, *Cd3g* and *Cd28* **B:** Featureplots displaying the expression of the B cell markers *Cd19*, *Cd79a* and *Cd79b*. **C:** UMAP plot displaying main cell clusters in our scRNA sequencing data. Lymphocytes are indicated in blue. **D:** Assignment of TCRs to the corresponding cells in scRNA sequencing data reveals that 79% of TCRs is expressed on T cells (left). For analysis only TCRs expressed on T cells were used (right). Each TCR is indicated by a red dot. **E:** Assignment of BCRs to the corresponding cells in scRNA sequencing data reveals that 47 % of BCRs is expressed on B cells (left). Only BCRs that were expressed on B cells were analyzed (right). Each BCR is indicated by a red dot.

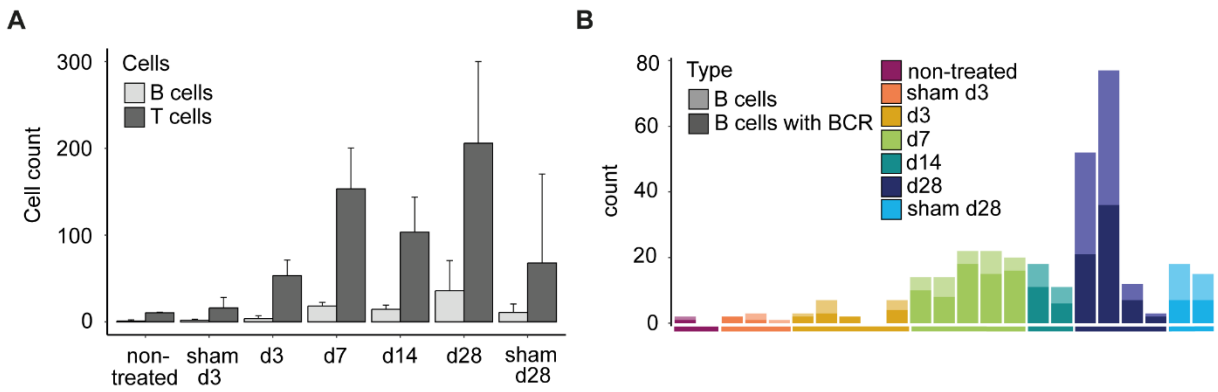

Supplementary figure 5: B cell numbers in AAA tissue increases over time.

A: Number of B and T cells in scRNA sequencing data from non-treated, sham operated (d3 and d28) and PPE-perfused (d3, d7, d14 and d28) aortic tissue. Displayed is the mean ± SD. The amount of B and T cells increases with AAA progression, with the highest amount of cells on day 28 after PPE-induced AAA formation. **B:** B cell numbers (light bar color) and counts of B cells exhibiting an intact BCR (dark bar color) in aortic tissue at different AAA disease stages computed from scRNA Seq data. An intact BCR could be sequenced in 55% of the B cells

Supplementary Table 7: Number of analyzed T cells, TCRs, B cells and BCRs per mouse

mouse	timepoint	T cells	TCRs	B cells	BCRs
#1	sham d28	45	9	18	7
#2	sham d28	196	66	15	7
#3	d28	188	52	52	21
#4	d28	340	84	77	36
#5	d14	75	26	18	11
#6	d14	132	45	11	6
#7	d7	88	39	14	10
#8	d7	128	48	14	8
#9	d3	58	19	3	2
#10	d3	67	23	7	3
#11	sham d3	30	9	2	2
#12	sham d3	11	5	3	1
#13	sham d28	1	1	0	0
#14	non-treated	11	4	2	1
#15	d28	120	33	12	7
#16	d28	176	43	3	2
#17	d7	169	80	22	18
#18	d7	170	77	22	15
#19	d7	212	81	20	16
#20	d3	48	16	2	2
#21	d3	25	9	0	0
#22	d3	69	19	7	4
#23	sham d3	7	3	1	0
#24	non-treated	10	5	0	0

Supplementary Table 8: Number of all TCRs, unique TCRs, expanded TCRs and the frequency of the expanded TCRs per mouse.

Mouse	All TCRs	Unique TCRs	Expanded TCRs	Frequency of expanded TCRs
#1	9	9	0	0
#2	66	37	4	25/4/2/2
#3	52	47	3	3/3/2
#4	84	77	4	5/2/2/2
#5	26	26	0	0
#6	45	40	3	3/3/2
#7	39	39	0	0
#8	48	47	1	2
#9	19	19	0	0
#10	23	22	1	2
#11	9	9	0	0
#12	5	5	0	0
#13	33	32	1	2
#14	43	42	1	2
#15	1	1	0	0
#16	80	78	1	3
#17	77	74	3	2/2/2
#18	81	78	3	2/2/2
#19	16	14	2	2/2
#20	9	9	0	0
#21	19	19	0	0
#22	3	3	0	0
#23	4	4	0	0
#24	5	5	0	0

Supplement

Supplementary Table 9: Frequencies, V-, D- and J-genes of alpha and beta chain, CDR3 nucleotide and amino acid sequences of the expanded TCRs per mouse.

mouse	time point	frequency	TRA_v_gene	TRA_d_gene	TRA_j_gene	TRA_cdr3	TRA_cdr3_nt	TRB_v_gene	TRB_d_gene	TRB_j_gene	TRB_cdr3	TRB_cdr3_nt
#2	sham d28	25	TRAV7-4		TRAJ6	CAASELPWGGNYKPTF	TGTGCAGCTAGTGAGCTCCCCTGGGGAGGAAACTACAAACCTACGTTT	TRBV13-1		TRBJ2-1	CASSGVNYAEQFF	TGTGCCAGCAGTGGGGTTAACTATGCTGAGCAGTTCTTC
#2	sham d28	4	TRAV7D-3		TRAJ27	CAVSPPTNTGKLTF	TGTGCAGTGAGCCCCCCCACCAATACAGGCAAATTAACCTTT	TRBV26		TRBJ1-2	CASSLVENSDYTF	TGTGCCAGCAGTCTGGTGGAAAACTCCGACTACACCTTC
#2	sham d28	2	TRAV13-2		TRAJ37	CAIDRGGNTGKLIF	TGTGCTATAGATCGAGGAGGCAATACCGGAAAACTCATCTTT	TRBV1	TRBD1	TRBJ2-2	CTCSGGTGPNTGQLYF	TGCACCTGCAGTGGGGGGACAGGGCCAAACACCGGGCAGCTCTACTTT
#2	sham d28	2	TRAV1		TRAJ33	CAVTDSNYQLIW	TGTGCTGTGACGGATAGCAACTATCAGTTGATCTGG	TRBV5	TRBD2	TRBJ2-7	CASSQDTGGGYEQYF	TGTGCCAGCAGCCAAGATACTGGGGGGGGCTATGAACAGTACTTC
#3	d28	3	TRAV7D-2		TRAJ53	CAASEGGSNYKLTF	TGTGCAGCAAGCGAAGGAGGCAGCAATTACAAACTGACATTT	TRBV19		TRBJ2-3	CASSIWGGAGAETLYF	TGTGCCAGCAGTATTTGGGGGGGCGCTGGTGCAGAAACGCTGTATTTT
#3	d28	3	TRAV13-2		TRAJ37	CAIGGTGNTGKLIF	TGTGCTATAGGAGGGACAGGCAATACCGGAAAACTCATCTTT	TRBV3		TRBJ1-2	CASSLAGGDSDYTF	TGTGCCAGCAGCTTGGCGGGGGGGGACTCCGACTACACCTTC
#3	d28	2	TRAV7D-2		TRAJ21	CAAGTPNYNVLYF	TGTGCAGCCGGGACCCCTAATTACAACGTGCTTTACTTC	TRBV13-3	TRBD1	TRBJ2-7	CASSPGGSYEQYF	TGTGCCAGCAGTCCAGGGGGCTCCTATGAACAGTACTTC
#4	d28	5	TRAV13-2		TRAJ37	CAIGGTGNTGKLIF	TGTGCTATAGGGGGAACAGGCAATACCGGAAAACTCATCTTT	TRBV3		TRBJ1-2	CASSLAGGDSDYTF	TGTGCCAGCAGCTTAGCAGGGGGCGACTCCGACTACACCTTC
#4	d28	2	TRAV14D-1		TRAJ9	CAASARNMGYKLTF	TGTGCAGCAAGTGCACGCAACATGGGCTACAAACTTACCTTC	TRBV16		TRBJ2-1	CASSFQGNNYAEQFF	TGTGCAAGCAGCTTTCAGGGTAATAACTATGCTGAGCAGTTCTTC
#4	d28	2	TRAV6N-7		TRAJ6	CALGPASGGNYKPTF	TGTGCTCTGGGCCCCGCCTCAGGAGGAAACTACAAACCTACGTTT	TRBV20		TRBJ2-2	CGAIIRNTGQLYF	TGTGGTGCTATAATACGGAACACCGGGCAGCTCTACTTT
#4	d28	2	TRAV5-4		TRAJ56	CAASAGGNNKLTF	TGTGCTGCAAGTGCTGGAGGCAATAATAAGCTGACTTTT	TRBV12-2		TRBJ2-5	CASSLDWGDDTQYF	TGTGCCAGCTCTCTTGACTGGGGGGATGACACCCAGTACTTT
#6	d14	3	TRAV13-4-DV7		TRAJ52	CAMEPGANTGKLTF	TGTGCTATGGAACCTGGAGCTAACACTGGAAAGCTCACGTTT	TRBV13-1		TRBJ2-2	CASSEDNTGQLYF	TGTGCCAGCAGTGAGGACAACACCGGGCAGCTCTACTTT
#6	d14	3	TRAV14-2		TRAJ34	CAASATSNTNKVVF	TGTGCAGCAAGTGCGACTTCCAATACCAACAAAGTCGTCTTT	TRBV13-1	TRBD1	TRBJ1-2	CASSGDRRSDYTF	TGTGCCAGCAGTGGGGACAGGAGGTCCGACTACACCTTC
#6	d14	2	TRAV7-6		TRAJ52	CAVSIEAGANTGKLTF	TGTGCAGTGAGCATTGAGGCGGGAGCTAACACTGGAAAGCTCACGTTT	TRBV2	TRBD2	TRBJ2-7	CASSQDVTGGAFEQYF	TGTGCCAGCAGCCAAGACGTGACTGGGGGGGCGTTTGAACAGTACTTC
#8	d7	2	TRAV4-3		TRAJ39	CAALNNNAGAKLTF	TGTGCTGCCCTGAATAATAATGCAGGTGCCAAGCTCACATTC	TRBV29		TRBJ1-5	CASRSQPNQAPLF	TGTGCTAGCAGGTCACAGCCCAACCAGGCTCCGCTTTTT
#10	d3	2	TRAV12-3		TRAJ40	CALSPNTGNYKYVF	TGTGCTCTGAGCCCTAATACAGGAAACTACAAATACGTCTTT	TRBV12-1		TRBJ2-1	CASSLRDWGYAEQFF	TGTGCCAGCTCTCTCCGGGGACTGGGGGTATGCTGAGCAGTTCTTC
#13	d28	2	TRAV6-6		TRAJ31	CALGDHSNNRIFF	TGTGCTCTGGGTGATCATAGCAATAACAGAATCTTCTTT	TRBV10	TRBD1	TRBJ2-1	CASRNRGHAEQFF	TGTGCCAGCAGGAACAGGGGGCATGCTGAGCAGTTCTTC
#14	d28	2	TRAV6-6		TRAJ37	CALVITGNTGKLIF	TGTGCTCTGGTCATAACAGGCAATACCGGAAAACTCATCTTT	TRBV29		TRBJ2-2	CASVRGTGQLYF	TGTGCTAGCGTCCGTGGCACCGGGCAGCTCTACTTT
#16	d7	3	TRAV7-3		TRAJ13	CAANSGTYQRF	TGTGCAGCAAATTCTGGGACTTACCAGAGGTTT	TRBV19		TRBJ1-1	CASSKTTNTEVFF	TGTGCCAGCAGTAAGACAACAAACACAGAAGTCTTCTTT
#17	d7	2	TRAV7N-4		TRAJ23	CAVSEQ2GYNQGKLIF	TGTGCAGTTAGTGAGCAGGGGTATAACCAGGGGAAGCTTATCTTT	TRBV19		TRBJ2-5	CASSRDRFNQDTQYF	TGTGCCAGCAGTCGGGACAGGTTTAACCAAGACACCCAGTACTTT
#17	d7	2	TRAV14D-2		TRAJ21	CAASRVSNYNVLYF	TGTGCAGCAAGTAGGGTGTCTAATTACAACGTGCTTTACTTC	TRBV12-2+TRBV13-2		TRBJ2-3	CASGNWGPSAETLYF	TGTGCCAGCGGTAACTGGGGCCCTAGTGCAGAAACGCTGTATTTT
#17	d7	2	TRAV5D-4		TRAJ26	CAARSYAQGLTF	TGTGCTGCGAGGAGCTATGCCCAGGGATTAACCTTC	TRBV20		TRBJ2-5	CGARDRGDQDTQYF	TGTGGTGCTAGGGACAGGGGCGACCAAGACACCCAGTACTTT
#18	d7	2	TRAV13D-2		TRAJ2	CAIVQNTGGLSGKLTF	TGTGCTATAGTCCAGAATACTGGAGGACTAAGTGGTAAATTAACATTC	TRBV10		TRBJ2-1	CASRRDYNYAEQFF	TGTGCCAGCAGGCGGGACTATAACTATGCTGAGCAGTTCTTC
#18	d7	2	TRAV6-5		TRAJ17	CALRPNSAGNKLTF	TGTGCTCTGAGGCCCAACAGTGCAGGGAACAAGCTAACTTTT	TRBV19		TRBJ2-5	CASSIAGGAQDTQYF	TGTGCCAGCAGTATAGCTGGGGGGGCCCAAGACACCCAGTACTTT
#18	d7	2	TRAV14-3		TRAJ50	CAASATSSSFSKLVF	TGTGCAGCAAGTGCAACATCCTCCTCCTTCAGCAAGCTGGTGTTT	TRBV19		TRBJ2-2	CASSIDSTNTGQLYF	TGTGCCAGCAGTATTGACAGCACAAACACCGGGCAGCTCTACTTT
#19	d3	2	TRAV7D-2		TRAJ42	CAASRGGGSNAKLTF	TGTGCAGCAAGCAGGGGTGGAGGAAGCAATGCAAAGCTAACCTTC	TRBV2		TRBJ1-5	CASSQGEAPLF	TGTGCCAGCAGCCAGGGGGAGGCTCCGCTTTTT
#19	d3	2	TRAV7D-2		TRAJ21	CAGQGANYNVLYF	TGTGCAGGACAAGGGGCTAATTACAACGTGCTTTACTTC	TRBV13-3		TRBJ1-2	CASTGGNSDYTF	TGTGCCAGCACCGGGGGAAACTCCGACTACACCTTC

Supplementary Table 10: Number of murine TCR sequences per disease/pathogen of the McPASTCR database that were used for comparison with the AAA data set.

disease/pathogen	Number of TCR sequences
Allograft rejection	16
Chronic obstructive pulmonary disease (COPD)	30
Collagen type II(Col II)-induced arthritis	20
Diabetes type 1	385
Experimental autoimmune encephalomyelitis (EAE)	97
Graft vs host disease (GVD)	67
Herpes simplex virus 1 (HSV1)	25
Human immunodeficiency virus (HIV) related	16
Influenza	1831
Lupus nephritis	16
Lymphocytic choriomeningitis virus (LCMV)	15
Lymphoma	79
Murine cytomegalovirus (MCMV)	529
Melanoma	30
Murine leukemia virus (MuLV)	8
Systemic Lupus Erythematosus (SLE)	75
Tick-borne encephalitis	12
Tumor	161
Vesicular stomatitis virus (VSV)	10
West Nile virus	70
Plasmodium Berghei	38

Supplementary Table 11: Results from Fisher exact test for each disease in the two public databases.

Disease	not in AAA data and not in disease	in AAA data but not in disease	not in AAA data but in disease	in AAA data and in disease	p-value	adjusted p-value (Bonferroni)	adjusted p-value (Hochberg)
Allograft rejection	4272	55	4	0	1	1	1
ColII-induced arthritis	4264	55	12	0	1	1	1
EAE	4181	55	95	0	1	1	1
GVD	4236	55	40	0	1	1	1
HIV related	4261	55	15	0	1	1	1
Influenza	3109	51	1167	4	1	1	1
Lupus nephritis	4260	55	16	0	1	1	1
MCMV	3326	34	950	21	0.006	0.13	0.12
MuLV	4272	55	4	0	1	1	1
Plasmodium Berghei	4066	52	210	3	0.51	1	1
Tick-borne encephalitis	4270	55	6	0	1	1	1
VSV	4227	54	49	1	0.47	1	1
COPD	4261	55	15	0	1	1	1
Diabetes Type 1	3971	50	305	5	0.36	1	1
HSV1	4251	55	25	0	1	1	1
LCMV	4132	49	144	6	0.01	0.25	0.12
Lymphoma	4226	55	50	0	1	1	1
Melanoma	4246	55	30	0	1	1	1
RSV	4152	55	124	0	1	1	1
SLE	4202	55	74	0	1	1	1
Tumor	4182	54	94	1	0.71	1	1
West Nile virus	4241	55	35	0	1	1	1

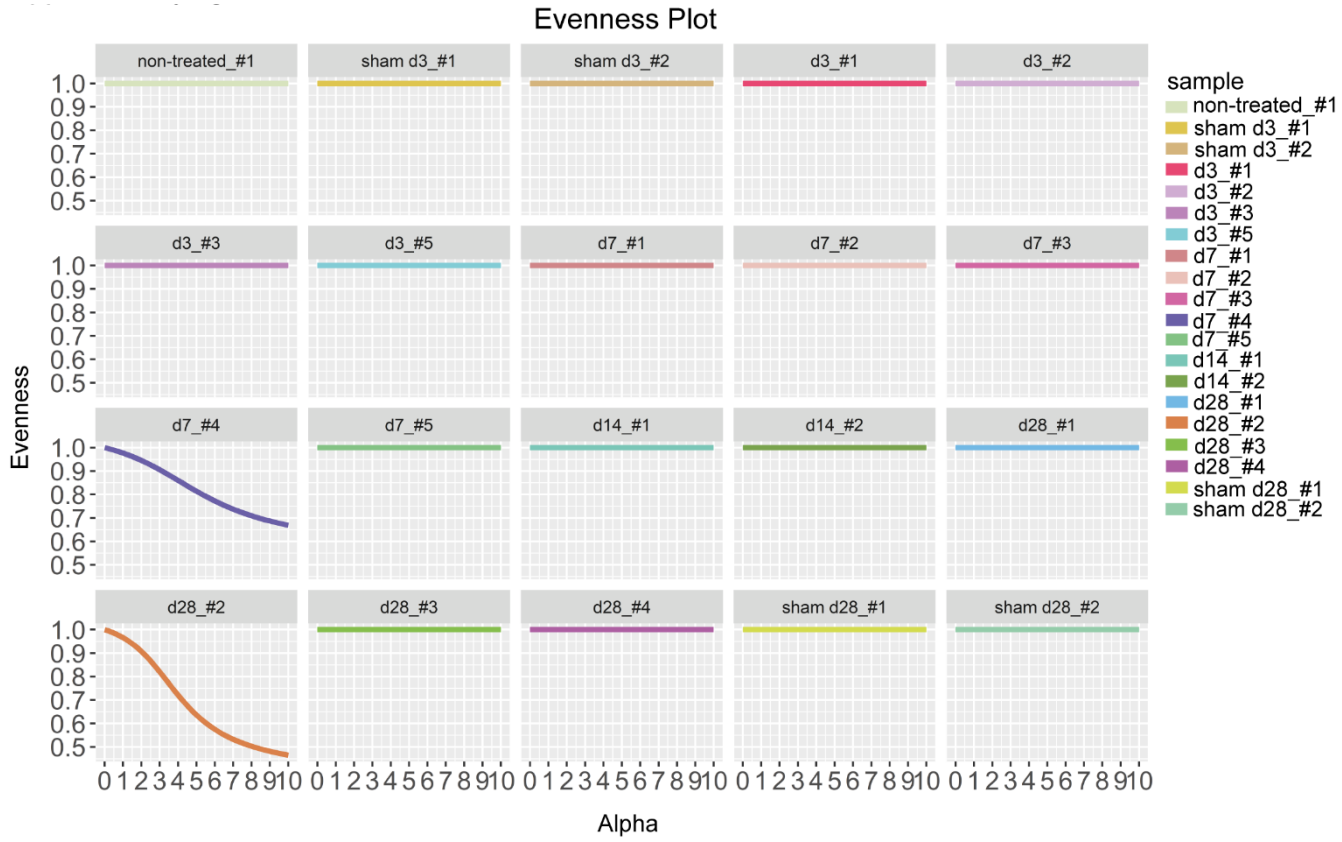

Supplementary figure 6: BCR receptor clonality was detected in 2 out of 20 samples.

Evenness profiles of BCR repertoire showing the extent of clonal expansion for every sample. One AAA sample at d7 and one AAA sample at d28 after PPE-perfusion shows higher receptor clonality, whereas all other samples exhibit no clonal expansion.

9 Acknowledgements

Mit dieser Danksagung schließt sich ein großes und wichtiges Kapitel meines Lebens. Die Promotion war eine spannende und aufregende Zeit, in der ich sehr viel gelernt habe, über mich hinausgewachsen bin und gute Freundschaften entstanden sind. Hätte mir vor vier Jahren jemand gesagt, dass meine Doktorarbeit zum Großteil aus Bioinformatik bestehen wird, hätte ich das nicht geglaubt. Dies hat mir jedoch gezeigt, dass man alles schaffen kann (wenn man will). Zu meinem Glück hat mir Programmieren dann nach einiger Zeit auch tatsächlich Spaß gemacht. Dennoch gab es Höhen und Tiefen und zwischendrin auch mal viel Frustration. Doch jetzt am Ende bin ich glücklich und stolz auf das, was ich geschafft habe. Auf meinem Weg haben mich viele Personen begleitet und unterstützt, bei denen ich mich im Folgenden bedanken möchte.

Zuallererst möchte ich mich ganz besonders bei meinem Doktorvater **Prof. Dr. Norbert Gerdes** bedanken. Vielen Dank für deine Betreuung und Unterstützung während meiner Promotion. Du hattest immer ein offenes Ohr für alle Ideen, Fragen und Probleme. Ich bin sehr dankbar dafür, dass du mich gefördert und ermutigt hast nach der Promotion eine wissenschaftliche Karriere anzustreben und bin sehr gespannt, wo dieser Weg mich hinführt.

Des Weiteren danke ich dem Direktor der Klinik für Kardiologie, Pneumologie und Angiologie **Prof. Dr. Malte Kelm** dafür, dass ich meine Forschung und Promotion im kardiovaskulären Forschungslabor durchführen konnte. Dem **TRR259** danke ich für die Finanzierung meines Forschungsprojektes.

Ich danke allen Personen und Kooperationspartnern, die zu meinem Projekt beigetragen haben, insbesondere **Miriam**, **Alex** und **Susi**. Danke, dass ihr mir immer mit Rat und Tat zur Seite gestanden habt und ich mich immer auf euch verlassen konnte. **Alex**, ohne deine Hilfe hätte ich das Programmieren bestimmt schon nach ein paar Monaten wieder aufgegeben und beim brainstormen mit dir sind mir oft gute Ideen für mein Projekt gekommen. **Susi**, du bist immer zur Stelle, wenn Hilfe benötigt wird, und findest für jedes Problem eine Lösung. Vielen Dank dafür! Ein großes Dankeschön auch an **Steffi und Julia**, ohne deren Hilfe bei den OPs es diese Arbeit nicht geben würde. Ich bedanke mich bei der gesamten **AG Gerdes** und den Studenten, die ich während meiner Promotion betreuen durfte, **Milena**, **Marius**, **Noura** und **Mara**. Durch euch habe ich viel gelernt. Ein ganz besonderer Dank geht an **Sven**, **Isabella**, **Viti**, **Ashley**, **Miriam** und **Cami**, die mich teilweise die gesamte Zeit oder einen Teil meiner Promotion begleitet haben und gute Freunde geworden sind. Ihr habt einen großen Teil dazu beigetragen, dass ich jeden Tag gerne ins Labor gekommen bin. Danke, dass ich immer auf euch zählen konnte. Natürlich möchte ich mich beim gesamten **CVRL** für die schöne Zeit und den Zusammenhalt bedanken.

Während meiner Promotion hatte ich die Chance einen 3-monatigen Forschungsaufenthalt in Oslo zu machen, wofür ich ebenfalls sehr dankbar bin. Denn das war eine wirklich schöne Zeit, in der ich nicht nur wissenschaftlich viel gelernt habe, sondern ein wunderschönes Land kennen lernen durfte, Freunde gefunden und die Freude am Wandern entdeckt habe. Ich danke **Prof. Dr. Norbert Gerdes** für die Unterstützung dabei und **Prof. Dr. Victor Greiff** für die wissenschaftliche Betreuung in Oslo.

Da bekanntermaßen das Beste zum Schluss kommt, möchte ich mich im Folgenden bei **Freunden und Familie** bedanken. Ich danke **meinen Freundinnen**, die mich größtenteils seit meiner Kindheit begleiten, für ihre emotionale Unterstützung und diverse Süßigkeiten-Wellness-Überlebenspakete, die ich in der stressigen Schreibphase per Post bekommen habe. Ich danke **meinem Bruder** und **meiner gesamten Familie** für die emotionale Unterstützung und dafür, dass ihr immer hinter mir steht. Ein besonderer Dank geht an **meine Eltern**, die immer sehr interessiert an meinem Forschungsprojekt waren, auch wenn sie nicht immer alles verstanden haben. Danke für eure Unterstützung, euer Vertrauen und eure Liebe und vor allem danke, dass ihr immer an mich geglaubt habt. Zu guter Letzt möchte ich der wichtigsten Person in meinem Leben danken. Danke **Patrick**, dass du immer für mich da bist, mich in allem unterstützt und mir den Rücken freihältst.

10 Eidesstattliche Erklärung

Ich versichere an Eides Statt, dass die Dissertation von mir selbstständig und ohne unzulässige fremde Hilfe unter Beachtung der „Grundsätze zur Sicherung guter wissenschaftlicher Praxis an der Heinrich-Heine-Universität Düsseldorf“ erstellt worden ist.

Während der Anfertigung dieser Arbeit habe ich teilweise KI-gestützte Sprachverarbeitungsprogramme verwendet, und zwar DeepL und ChatGPT (OpenAI), um die englische Sprache und Lesbarkeit zu verbessern. Nach der Verwendung dieser Tools habe ich den Inhalt und die Formulierungen überprüft und bearbeitet und übernehme die volle Verantwortung für den Inhalt der Arbeit.

Die aufgeführten Versuche und Analysen wurden selbstständig durchgeführt. Mit Ausnahme der folgenden Versuche und Ergebnisse, welche von Dritten bzw. in Kooperation mit Dritten erstellt wurden:

- Die PPE-Operationen und I/R-Operationen wurden von Julia Odendahl und Stefanie Becher durchgeführt.
- Immunfluoreszenzfärbungen wurden von Bachelorstudentin Kea Mara Tönnißen unter meiner Betreuung durchgeführt.
- Die Etablierung des FACS-Panels für IFNICs wurde von Masterstudentin Noura Kharrat unter meiner Betreuung durchgeführt.
- RNA-Scope® Färbungen wurden von Dr. Susanne Pfeiler durchgeführt.
- Die Sortierung der Zellen für Einzelzellsequenzierungsexperimente wurde in Kooperation mit Dr. Katharina Raba vom Durchflusszytometrischem Labor am Institut für Transplantationsdiagnostik und Zelltherapeutika des Universitätsklinikum Düsseldorfs durchgeführt.
- Die Einzelzellsequenzierungsexperimente wurden in Kooperation mit Dr. Tobias Lautwein vom Genomics & Transcriptomics Labor der Heinrich-Heine-Universität Düsseldorf durchgeführt.
- Die Sortierung von IFNIC Makrophagen wurde in Kooperation mit Dr. Stefanie Lichtenberg und Dennis Müller von der Core Facility Flow Cytometry durchgeführt.

Teile dieser Dissertation wurden bereits in einer wissenschaftlichen Zeitschrift veröffentlicht.

Diese Dissertation wurde weder in gleicher noch in ähnlicher Form in einem anderen Prüfungsverfahren vorgelegt. Außerdem erkläre ich, dass ich bisher noch keine weiteren akademischen Grade erworben oder zu erworben versucht habe.

Düsseldorf, den 27.05.2025

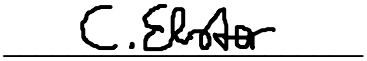

Unterschrift

11 Author contribution to the publication used in this dissertation:

Scientific Paper published in Frontiers in Cardiovascular Medicine, 2023

Application and challenges of TCR and BCR sequencing to investigate T- and B-cell clonality in elastase-induced experimental murine abdominal aortic aneurysm

Christin Elster, Miriam Ommer-Bläsius, Alexander Lang, Tanja Vajen, Susanne Pfeiler, Milena Feige, Tin Yau Pang, Marius Böttenberg, Sarah Verheyen, Khang Lê Quý, Maria Chernigovskaya, Malte Kelm, Holger Winkels, Susanne V Schmidt, Victor Greiff, Norbert Gerdes

Contribution:

The author of this dissertation, Christin Elster, contributed approximately 85% to the data and manuscript completion. The author performed most of the experiments, analyzed the data and wrote the manuscript.

Confirmation of the supervisor:

I hereby confirm the above-mentioned contributions of Christin Elster to the completion of the publication used in this dissertation.

Prof. Dr. rer. nat. Norbert Gerdes